KU LEUVEN

ARENBERG DOCTORAL SCHOOL
Faculty of Engineering Science

Polymer-based Dry Electrodes for Biopotential Measurements

Yun-Hsuan CHEN

Supervisor:

Prof. Dr. Ir. Chris Van Hoof

Dissertation presented in partial fulfilment of the requirements for the degree of Doctor of Engineering Science (PhD): Electrical Engineering

November 2016

Polymer-based Dry Electrodes for Biopotential Measurements

Yun-Hsuan CHEN

Examination Committee:

Prof. Dr. Ir. Hugo Hens, chair
Prof. Dr. Ir. Chris Van Hoof, supervisor
Dr. Ir. Maaike Op de Beeck, co-supervisor
(imec, Leuven & Universiteit Gent, Gent)
Prof. Dr. Ir. Jan Van Humbeeck
Prof. Dr. Lieven Lagae
Prof. Dr. Ir. Robert Puers
Prof. Dr. Ir. Dominiek Reynaerts
Prof. Dr. Kristl Vonck
(UZ Gent, Gent)
Dr. Luc Vanderheyden
(Datwyler Pharma Packaging International NV, Alken)

Dissertation presented in partial fulfilment of the requirements for the degree of Doctor of Engineering Science (PhD): Electrical Engineering

In collaboration with imec
Kapeldreef 75
B-3001 Heverlee, Belgium

November 2016

Uitgegeven in eigen beheer, Yun-Hsuan CHEN, Kasteelpark Arenberg 10, B-3001 Heverlee (Belgium)

Acknowledgements

In the past 5 years, working at imec as a PhD researcher has been a very fruitful experience. There were enjoyable moments as well as moments of doubt. I would like to thank all those who have accompanied me through thick and thin. Without your support, I would not have been able to overcome those and reach my goal.

First and foremost, I would like to thank my promoter, Prof. Chris Van Hoof. Thank you for giving me the opportunity to join imec, a place I once dreamt of joining because of its reputation and cutting edge research. I appreciate very much your guidance and support throughout my PhD studies. Thank you for giving me the freedom to explore the various possibilities in my research topic and encouraging me to interact with colleagues who can have input on my research topic. I will never forget those carpooling rides, departing early morning from Leuven to Holst center and the different sceneries we enjoyed on the way as one season gave way to another. I enjoyed very much the conversations we had and the stories behind each pair of cufflinks during those trips. I am lucky to have had such an easygoing and supportive promoter.

The second person I would like to thank is my daily supervisor, Dr. Maaike Op de Beeck. From the moment I arrived at imec for my interview, you became as it were my second mother in Belgium who was concerned for both my private and working life. Thanks for guiding me and letting me know how to be a good scientist and how to make professional and organized presentations and posters. I appreciate the time and effort you spent on correcting my English, and teaching me how to explain things in a more logical structure. Thanks also for the constructive criticisms, all of which have resulted in a better outcome. Thanks for arranging the cooperation with Datwyler and the hospitals (UZ Gent and UZ Leuven), and for including me in the project. Thanks for encouraging me when the going was tough during the PhD studies. It was really a great pleasure to have worked with you and to have had you as my daily supervisor.

I also would like to thank the members of my PhD examination committee: Prof. Lieven Lagae, Prof. Robert Puers, Prof. Jan Van Humbeeck, Prof. Dominiek Reynaerts, Prof. Kristl Vonck, Dr. Luc Vanderheyden, and Prof. Hugo Hens. Thank you very much for being part of the jury and for your time and effort in providing feedback regarding the thesis. Your valuable suggestions have improved the quality and comprehensiveness of the thesis, for which I owe you all a debt of gratitude.

I also want to express my sincere appreciation to Luc and his colleagues at Datwyler for the cooperation on the dry electrode project. Thank you for helping to improve the electrodes' fabrication yield and sharing your experiences regarding the fabrication of electrodes. Thank you Luc for the valuable discussions and suggestions regarding the optimization of polymer materials and shape of the electrodes.

I also want to thank Prof. Vonck and Prof. Lagae for welcoming and allowing me to carry out measurements with their patients at UZ Gent and UZ Leuven. I also want to thank their

colleagues in those hospitals for their assistance with those measurements, using our dry electrodes with their patients. Thank you to Evelien and Stefanie in UZ Gent for recruiting the participants and arranging my appointments with them. Thanks to both of you for the assistance during the measurements and the suggestions regarding improvement of the recording system. Thanks Jan for the assistance with measurements at the UZ Leuven.

Next, I want to express my gratitude to the colleagues and collaborators I met during the PhD studies. I want to thank my old HIM-HCI colleagues: John, Lei, Ben, Paolo, Akif, Karen, Hieda-san, Tom, Larissa, and Andrea. Although this team does not exist anymore, I will always remember your warm welcome and patience especially when I encountered problems as a brand new imec researcher. In particular, I wish to thank John in a special way for teaching me plenty of experimental skills and suggestions, all of which were very helpful for my PhD. John was willing to help me even when I had problems in the bio labs in the later years of my research. Thanks Filip Vanlerberghe for sharing your knowledge on dry electrodes and helping me to get on track at the start of the project.

I also thank my colleagues in my current team, MEDIC, which I joined at the end of my 1st year of PhD studies. Thank you Nick and Firat for your support as team leaders and for the technical discussions we had. Thank you Marion for the help regarding all the administration stuff and helping me secure a date for my defense, which was more difficult than anticipated. Thank you Tom and Jan for the training in using tools in the lab, and also for the valuable discussions regarding my experiments and results. I am lucky to have shared the office with Elena and Neide over the past 2 years. Thanks for your support regardless of whether I was sharing good news or complaints. I did enjoy very much the girl talks in office 02.01. Thank you Rachit, Bogdan and Rajesh for sharing information during the PhD studies. Thanks Marco, Carolina, Kasra, Shuang, Shiwei, Eric, Ivan, Diana, Joonsung, Ho Sung, Srinjoy, Hyejung, my former colleagues who have moved on and all the colleagues mentioned above for the happy moments during lunch time and team events. Thanks Vladimir for the suggestions regarding the biopotential measurements, and the experiences regarding the experiments you shared with me.

Besides the colleagues in my group, I also would like to express my gratitude to other imec colleagues who assisted me during my PhD studies. Special thanks to Frank Gijbels who taught me a lot about electronics, especially when I was making those active electrodes and designing my experiments. Thanks also to Silke Musa who assisted me with the electrochemical experiments and generously spent her time discussing my results. Thanks to Kris Vanstreels who helped me with the experiments regarding mechanical properties of my electrodes, and trained me on how to use the tool. In addition, thank you Kris for all the discussions and suggestions regarding the experimental methods and the results of the mechanical properties tests. Thanks to Sebastien Moitzheim who read that part of my thesis regarding electrochemistry, and gave valuable suggestions on how to improve it.

Besides the colleagues in Leuven, I also want express my deep appreciation to colleagues in Holst who closely collaborated with me. Thanks Bernard and Vojkan for the support on the project, the assistance on the arrangement of the equipment for my measurements, and the valuable discussions before, during, and after my experiments, as well as the suggestions on

my reports and publications. Thanks Shrishail, Jaiwei and Paruthi for the assistance and discussions regarding recording devices. Thanks Marcel for the assistance on the electrochemical experiments on the electrodes and the valuable discussions with me over my results.

Thanks to the PenO students, internship students, and masters' students who either cooperated with me or joined the exercise sessions I gave. Thanks for giving me a chance to guide you and explain things to you, all of which allowed me to understand my weak points in terms of being a mentor or teaching assistant, and in the end helped me to improve.

This thesis would not have been completed without the participation of those volunteers for the measurements. I want to express my heartfelt appreciation to all the people who allowed themselves to become test subjects in my experiments. Thank you very much for spending your time with me and for your willingness to put up with certain inconveniences during those experiments.

Needless to say, the support from friends is very important during any PhD studies. Thanks Vikas, Tomislav, Cheng-Hsueh and Cheng-Yen for the chats during coffee breaks. Thanks to all other friends at imec who always gave me a warm greeting when we crossed paths at the corridors. Those chats often cheered me up. Thanks to all my Taiwanese friends I met in these 5 years in Leuven. Special thanks to Tian-Li, Michael and Mark – it was great to have had some overlap period with your PhD studies at imec. I enjoyed the lunch we had every Thursday at imec and all the activities organized by the Taiwanese students association. Thanks to all my other friends who shared both happy and unhappy moments with me. Thank you especially to Wan-Yu, Chin-Yin, Jia, Nisi, Scheling, Chia-Hsin, Ko-Hui, Ya-Chien, Melody, Chia-Yang, Joy, Wan-Ling, Ya-Ling, Alice, Debby, Yun-An, Ting-Wei and Cheng-Ming for making my life in Leuven not so boring. Thank you also to those who have obtained their PhD degrees, including Frank Kao, Wei-Jhih Tseng, Chen-Yi Su, Hsin-Yi Chou, Wan-Chih Wang, Fu-Kang Wang, Chin-Fu Kao, Hemmings Wu, Yi-Shiang Huang, Li-Gang Lin, and Tung-Huei Ke – your suggestions and encouragement during my PhD studies were very helpful and supportive. Thanks also to my dear friends at the MONABIPHOT masters' program: Rafaël, Xiaoxue, and Meaw. It was always a happy occasion to get your greeting cards and emails. Thanks to all the aforementioned and those I could not list your names here for accompanying me at imec, in Leuven, in Belgium, in Europe, in Taiwan and around the world.

A very special person I cannot overlook is my boyfriend, Li Weng. Your suggestions were always very helpful, especially when I was very frustrated or faced with difficult decisions. You see only the positives in me during these 5 years, including the best and the worst moments. Thanks for always putting up with me when I was bad-tempered or trying to encourage me not to give up. Thanks for always reminding me to do things step-by-step in order to reach the goal and not let other non-related and trivial issues interfere with the original plan. Although you always complain that I do not see you as a senior at KUL, I hope that my graduation as a junior will make you proud.

Last but not least, I want to thank my family members, especially my parents. Thanks for your support in my decision to pursue PhD studies in a country far away from home. Thanks

for your understanding and for being patient when things did not happen as planned. Thanks for your love and being the ones that I can always lean on for protection and encouragement. I appreciate the way you have raised and educated me on how to deal with all the difficulties in life and to be a person surrounded by plenty of supportive people during my PhD studies. Besides my parents, I also would like to thank my grandparents for their support and concern. It is such a pity that it is a little too late to tell you that the thesis is finally completed.

There were other people who also played a role in my PhD studies, but space would not allow me to list all your names in this acknowledgement. Please accept my humble apologies and thank you for your support during these years. This thesis would not have been completed without you.

Yun-Hsuan Chen

November 2016

Leuven, Belgium

Abstract

Monitoring biopotential signals such as electrocardiography (ECG) and electroencephalography (EEG) provides important information about certain health-related conditions which open up a broad range of applications. The electrical and mechanical properties of electrodes used for the measurements have a great impact on the quality of the signals. Conventional wet electrodes, which contain conductive gel to hydrate the skin and lower the electrode/skin impedance, are widely used. Furthermore, the flexible gel stays in good contact with the skin during movement, hence the impedance also remains low when the subject is moving. However, the gel's various drawbacks are also well-known. For example, before an EEG monitoring, the setup of wet electrodes is not only often time-consuming but also ought to be done by an expert. During EEG monitoring, signal degradation occurs due to the gel drying out, and skin irritation due to the glue used to fix the electrodes on the scalp are often observed. After EEG recording, removing the glue to detach the electrode is difficult and can mess up the hairstyle.

To avoid these drawbacks of the wet electrodes, various types of dry electrodes have been introduced. In this thesis, dry electrodes fabricated from a flexible conductive polymer are presented. The elastic properties -especially the flexibility- of the conductive polymer ensure higher user comfort than obtained by rigid metal electrodes. The conductivity of the polymer does away with the need for any extra conductive coating layer, which often flakes off during use. Electrodes with various pin-shapes (length, width, density) are fabricated for different applications. Various additives have also been added to the polymer, and additive type and quantity are optimized to obtain low contact impedance and good mechanical properties for better comfort and skin contact.

Impedance measurements on phantoms and human skin are carried out for impedance characterization. The electrodes with optimal material composition, i.e. polymer containing 43% of carbon, show only ~10 times higher electrode/skin impedance than that of wet electrodes. Applying abrasive gel or lotion with the polymer dry electrodes and producing sweat before the measurements reduce the impedance of polymer electrodes. However, the impedance does not remain low because the agents reducing the impedance (gel, lotion or sweat) disappear with time. The influences of these skin pretreatments and sweat processes on the electrode/skin impedance with time are investigated by modelling the recorded impedance with the equivalent electrical circuits.

To investigate the mechanical properties of the polymer dry electrodes, compression tests are carried out for elastic modulus and compliance characterization. The elastic modulus of polymer materials increases with growing carbon content and electrodes made from polymer with a higher carbon content show to be less compliant. Also the electrode shape is influencing the mechanical properties: the electrodes with more pins, thicker pins and shorter pins are less compliant. The compliance of the pin-shaped electrodes can be predicted rather well using the elastic moduli of the polymer materials and the shapes of the electrodes.

Polymer electrodes with optimal material composition are directly capable of recording strong biopotential signals such as ECG. The ECG signals recorded using polymer dry electrodes show a high similarity to those recorded by the neighboring wet electrodes when the subjects sit still and avoid movements. Pin-shaped polymer electrodes are sensitive to motion artifacts when applied on non-hairy skin. This proves that the shape of the electrode should depend on the applications.

To record low amplitude signals such as EEG, polymer electrodes need to be coupled with active circuits. In this thesis, our own active circuits are fabricated, and their compatibility with commercial EEG recording systems is investigated. The EEG signals recorded by polymer dry electrodes are compared with those of their adjacent wet electrodes. Polymer dry electrodes are capable of recording good quality EEG signals however they are more sensitive to pick up power line interferences (50 Hz signals) and they show more baseline drift (low frequency signals). Both of the 50 Hz signals and the baseline drift can easily be filtered out and the baseline drift reduced while polymer electrodes are becoming stabilized. The signals containing baseline drift still have sufficient good quality for interpretation by an experienced medical staff. However, it has to be noted that the baseline drift in the raw signals might result in misinterpretation of EEG signals distributed at low frequency (< 2 Hz). Besides using the commercial EEG recording systems, the signals of polymer dry electrodes are compared with those of wet electrodes and AgCl-coated polymer electrodes using imec's EEG recording system. Polymer electrodes show higher impedance and slightly lower signal quality than the other 2 types of electrodes, which might be improved after they are stabilized. A stabilized electrode shows fewer impedance variation and baseline drift resulting in better signals.

Besides the electrical and mechanical properties of the polymer electrodes, biocompatibility and user comfort are also important criteria of good electrodes. The polymer material used in this thesis is non-cytotoxic. No skin irritation is found after applying the polymer electrodes up to a few days. In addition, no participants report any skin discomfort during and after measurements. As to the user comfort of EEG monitoring, only a few participants with a larger head-size experience local pressure from the one-size electrode fixation device. Furthermore, all participants report that the application and removal of polymer dry electrodes are much more convenient than conventional wet electrodes.

To conclude, our polymer dry electrodes show high user comfort and are able to record good quality ECG and EEG signals. Therefore, combining polymer electrodes with the proper fixation devices may be seen as promising alternatives to either the commercially available devices equipped with dry electrodes or the conventional wet electrodes.

Beknopte samenvatting

Biopotentiaalsignalen zoals electrocardiografie (ECG) en electro-encefalografie (EEG) geven belangrijke informatie over bepaalde aspecten van iemands gezondheid, waardoor ECG/EEG metingen een brede waaier aan medische toepassingen hebben. Zowel de elektrische als de mechanische eigenschappen van de elektroden die gebruikt worden om biopotentiaalmetingen te doen, hebben een belangrijke impact op de kwaliteit van de gemeten signalen. De traditioneel gebruikte natte gel-elektroden bevatten een geleidende gel die de huid hydrateert en hierdoor de huid/elektrode impedantie drastisch verlaagt. De gel zorgt ook voor uitstekend contact met de huid, zelfs bij beweging van de huid, waardoor een lage impedantie behouden blijft. Nochtans heeft het gebruik van deze gel-elektroden ook belangrijke nadelen. Het plaatsen van de gel-elektroden alvorens de EEG meting kan starten, moet gebeuren door een expert ter zake en neemt ook dan nog een hele tijd in beslag. Verder zal de gel van de elektroden uitdrogen tijdens de EEG meting, en vaak veroorzaakt de gel en/of de lijm nodig voor de elektrodebevestiging ook huidirritatie. Tot slot is het wegnemen van de gel-elektroden en de bevestigingslijm na de EEG meting een zeer lastige zaak en in de meeste gevallen verlaat de patiënt het hospitaal met een nog vuile en erg verwarde haardos.

Om de nadelen van het gebruik van natte gel-elektroden te vermijden, zijn er al een reeks alternatieve elektrodesoorten bedacht en uitgetest. In deze thesis worden droge elektroden bestudeerd die gefabriceerd zijn uit een flexibel geleidend polymeer. De elastische eigenschappen - in het bijzonder de flexibiliteit - van dit polymeer vormen een belangrijk pluspunt met betrekking tot het gebruikscomfort, zeker in vergelijking met metalen droge elektrodes. De geleidbaarheid van het polymeer vermijdt dat er nog een geleidend laagje op het zachtere materiaal moet worden aangebracht, wat een voordeel is gezien het snelle afpellen van zo'n harder laagje aangebracht op een flexibel materiaal. De vorm van de elektroden (met name pinlengte, breedte en densiteit) kan aangepast worden naargelang de toepassing. Additieven die aan het basispolymeer worden toegevoegd zijn geoptimaliseerd om zowel een lage huid/elektrode impedantie te bekomen als om de geschikte mechanische eigenschappen te verkrijgen die bijdragen tot een hoger gebruikscomfort en een beter huidcontact.

De impedantie van deze polymeer-elektroden is uitvoerig gekarakteriseerd op relevante surrogaat-substraten en op menselijke huid. De optimale polymeersamenstelling (43% koolstof als additief) is hieruit bepaald, en deze blijkt een huid/elektrode impedantie te hebben die slechts een factor 10 hoger is dan die van natte gel-elektroden. Deze impedantie kan nog extra verlaagd worden door het gebruik van een licht schurende gel (scrub) op de huid, een hydraterende huidlotion, of gewoon door lokale transpiratie, maar de bereikte impedantie-verlaging houdt slechts tijdelijk aan.

De mechanische eigenschappen van droge elektroden zijn uitvoerig geëvalueerd, voornamelijk via samendrukkingstesten gebruikt om de hardheid (via elastische modulus) van de polymeren te bepalen als functie van de hoeveelheid koolstof in het polymeer. De flexibiliteit van de elektroden zelf, mede bepaald door de vorm en densiteit van de pinnen op de elektrode, is ook uitgetest via samendrukkingstesten. Deze testen toonden dat de

elektroden minder samendrukbaar waren indien de elektrode meer koolstof bevat, kortere en/of dikkere pinnen heeft, of een hogere pindichtheid heeft. Via de gemeten elastische modulus van het gebruikte elektrodemateriaal, gecombineerd met de afmetingen van de elektroden, kan de hardheid van de uiteindelijke elektrode vrij goed voorspeld worden.

De polymeer-elektroden met optimale polymeersamenstelling zijn dadelijk geschikt om sterkere biopotentiaalsignalen te registreren, zoals het geval bij een ECG. Testen tonen aan dat ECG signalen opgemeten met polymeer-elektroden bij een testpersoon in rust, een zeer sterke gelijkenis vertonen met signalen simultaan opgemeten met de klassieke natte gel-elektroden. De pinvormige polymeer-elektroden zijn echter minder geschikt voor een ECG, zij zijn gevoelig aan signaalstoringen tgv. beweging indien gebruikt op onbehaarde huid, wat bewijst dat de elektrodevorm moet gekozen worden naargelang het gebruik.

Om signalen op te meten die eerder zwak zijn, zoals EEG signalen, moeten de polymeer-elektroden aan een actief elektronisch circuit worden gekoppeld. Zo'n actief circuit is in deze thesis geoptimaliseerd, en de compatibiliteit met de bestaande klinische EEG systemen is geëvalueerd. De EEG signalen opgemeten met polymeer-elektroden is uitvoerig vergeleken met signalen bekomen via natte gel-elektroden. De polymeer-elektroden leverden goede signalen op, maar ze waren gevoeliger voor ruis en storingen (zoals 50Hz ruis van het net), en voor drift van het nulniveau van de meting (zeer laagfrequente signaalstoring). 50Hz ruis kan zeer eenvoudig weggefilterd worden, waardoor het EEG signaal –ondanks de drift van het nulniveau- zeer vlot interpreteerbaar is door ervaren medisch personeel. Indien toch gewenst kan trouwens het nulniveau gestabiliseerd worden door de laagste frequenties weg te filteren. Dit moet echter met de nodige voorzichtigheid gebeuren, om een mogelijke foutieve interpretatie te vermijden van laagfrequente signaalcomponenten (< 2Hz). De polymeer-elektroden werden in dit werk ook vergeleken met andere 'droge' alternatieven van natte gel-elektroden, zoals AgCl elektroden en polymeer-elektroden met een AgCl-coating. Voor deze vergelijking werd imec's EEG systeem gebruikt. De flexibele polymeerelektroden vertoonden initieel een hogere huid/elektrode impedantie dan de alternatieven, maar na een zekere stabilisatietijd verlaagt en stabiliseert de impedantie, en wordt ook de drift van het nulniveau kleiner.

Biocompatibiliteit en gebruikscomfort zijn ook belangrijke eigenschappen van elektroden. Het basispolymeer dat gebruikt wordt voor de droge elektroden is niet cytotoxisch, en er is ook geen huidirritatie waargenomen na langdurig (enkele dagen) gebruik van de elektroden. Ook de vele testpersonen hebben geen huidirritatie gemeld tijdens of na de kortere testen. Tijdens de EEG metingen is door een beperkt aantal testpersonen (met wat groter hoofd) wel een verhoogde druk opgemerkt ter hoogte van sommige elektroden. Voor deze metingen werd dan ook een bevestigingsmethode voor de elektroden gebruikt die maar beperkt aanpasbaar was aan verschillende hoofdmaten. Het aanbrengen en wegnemen van de droge elektroden werd door alle EEG-testpersonen als veel praktischer ervaren.

We kunnen besluiten dat onze polymeer-elektroden hoogkwalitatieve ECG en EEG signalen opnemen. Indien polymeerelektroden gecombineerd worden met een optimale bevestigingsmethode op de huid, dan vormen zij een veelbelovend alternatief voor natte elektroden of voor harde droge elektroden.

List of abbreviations/symbols:

Abbreviations	Descriptions (units)
C_{dl}	double layer capacitance (F)
CE	counter electrode
C_{GC}	Goüy - Chapman capacitance (F)
C_H	Helmholtz layer capacitance (F)
CNT	carbon nanotube
CPE (Q)	constant phase element ($F \cdot S^{a-1}$)
CR64	Polymer electrodes with material composition number 64
CR95	Polymer electrodes with material composition number 95
CV	cyclic voltammetry
E	elastic modulus (Pa)
ECG	electrocardiography
EEG	electroencephalography
E_{hc}	half-cell potential (V)
$E_{hc}°$	standard reduction potential (V)
EPDM	ethylene propylene diene monomer
f	frequency (Hz)
GND	ground electrode
H	hardness (Pa)
HPF	high pass filter
IHP	inner Helmholtz plane
K_{sp}	Solubility product constant (M^2)
LPF	low pass filter
OCP	open circuit potential (V)
OHP	outer Helmholtz plane
op-amp	operational amplifier
PBS	phosphate-buffered saline
PDMS	polydimethylsiloxane
PSD	power spectrum density ($\mu V^2/Hz$)
R_{ct}	charge transfer resistor (ohm)
RE/ REF	reference electrode

Abbreviations	Descriptions (units)
S	sense electrode
SC	stratum corneum
SHE	standard hydrogen electrode
SNR	signal to noise ratio
SS	stainless steel fibers
SSVEP	steady state visually evoked potentials
WE	working electrode
Z	impedance (ohm)
ω	angular frequency (Hz)

Contents

Chapter 1. Introduction

The aim of this thesis is to develop a conductive polymer dry electrode for biopotential measurements on the human body with high user-comfort. The conductive polymer electrodes fabricated in this thesis overcome some important disadvantages of conventional wet electrodes and existing dry electrodes for biopotential measurements which are discussed in section 1.2. The materials and shape of the polymer electrodes are optimized based on their electrical and mechanical properties as is discussed in Chapter 3. The electrocardiography (ECG) and electroencephalography (EEG) signals recorded using the optimized polymer dry electrodes are compared with those recorded using conventional wet electrodes.

1.1 Biopotential signals

Biopotential signals are the result of electrochemical activity in certain cells of the nervous, muscular or glandular tissue. When one cell is triggered, ion exchange occurs through the membrane of this cell, creating a so-called action potential. When the action potential reaches the end of the cell, another adjacent cell will be activated after receiving the neurotransmitters, released from the first cell, at the postsynaptic membrane [1]. This activity in between the two cells causes more ion exchange compared to the action potential propagating in single cell and results in a postsynaptic potential. Extracellular ions flow due to the postsynaptic potentials and the superposition of all ionic currents are measurable using electrodes, called biopotential signals [1-4]. An example of the ionic currents resulted from the activated neuron cells can be found in Figure 1.1 [5]. The biopotential signals we are interested in this thesis are the summation of the electrical activity of a group of cells, and such signal can be monitored in various locations throughout the human body [6-8]. The average activity of the brain cells can be monitored on the scalp, and this signal is called electroencephalography (EEG). On the other hand, the electrical activity of the heart cells is monitored by electrocardiography (ECG).

The amplitude and frequency distributions of some typical biopotential signals are shown in Figure 1.2. The amplitude of EEG signals ranges from a few to hundreds of micro-volts. EEG signals are weak because the bioelectricity signals generated from the brain cells have to pass through tissues acting as a propagation barrier (e.g. bone and cerebral spinal fluid) before reaching the surface of the scalp. These obstacles reduce the amplitude as well as the spatial resolution of the EEG signals. ECG signals have larger amplitudes than EEG signals, varying from a few hundred micro-volts to a few millivolts. Signal interference from power lines are around a few tens of micro-volts to few tens of volts [9, 10], hence these ECG and EEG biopotential signals are rather weak and prone to noise [11]. As a consequence,, proper electrodes and compatible recording amplifiers are required for high-quality biopotential recordings [12, 13].

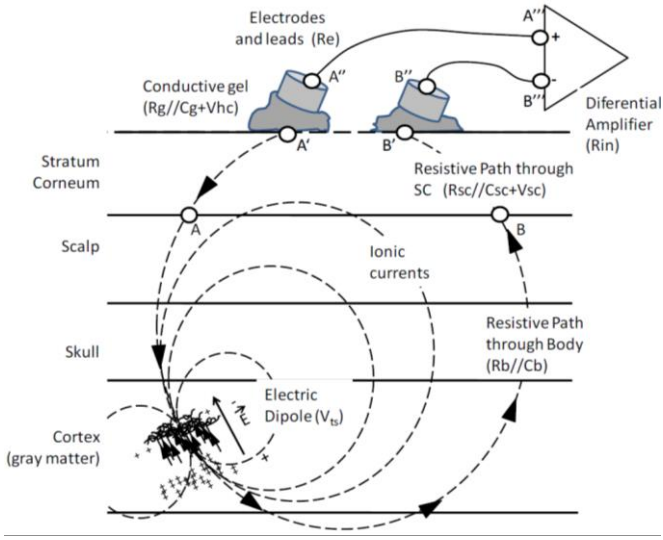

Figure 1.1: The ionic currents flow in the brain tissue due to the postsynaptic potentials generated by actived neuron cells. The summation of the currents resulted from a group of actived cells can be measured by placing two electrodes and a recording device on the scalp. This figure is copied from [5].

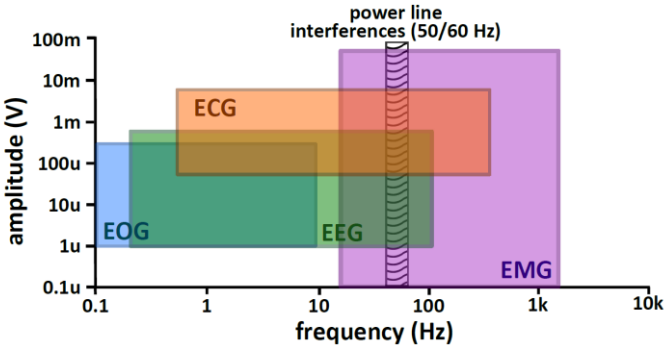

Figure 1.2: Frequency and amplitude distribution of biopotential signals.

Monitoring biopotential signals, such as ECG and EEG, can provide important information on certain health-related conditions, thereby opening up a broad range of applications [14, 15]. Wearable devices can monitor ECG to trace the heart rate during exercising. The heart rate can provide information on stress levels in a working environment and daily life as well. During clinical ECG monitoring, the biopotential signals are studied in greater detail in order to diagnose cardiovascular diseases. EEG monitoring among patients suffering from epilepsy is applied to register seizures; it is also essential for diagnosing during workup and for seizure classification [16]. Besides seizure classification, EEG signals are also used to evaluate sleep disorders, mental confusion, head injuries or to confirm brain death among comatose patients [17]. Moreover, EEG neurofeedback training is applied to attention deficit hyperactivity

disorder (ADHD) patients and elderly people in order to achieve cognitive enhancement. EEG monitoring also offers interesting possibilities for brain computer interface (BCI) applications [18]. Motion-disabled patients are able to control their wheelchairs, while communication-disabled patients can spell words via BCI techniques based on EEG signal recording [19].

1.2 Electrodes for biopotential measurements

In this thesis, electrodes used for ECG/EEG measurements are the subject of investigation. An important criterion for such electrodes is a low impedance so as to limit the noise generated during signal recording, which could jeopardize the accuracy of the obtained biopotential signals. The top layer of the skin, the so-called stratum corneum (SC), has a high impedance [6]. The water content and the concentration of conductive ions transmitting the biopotential signals in the SC is lower than that in deeper part of skin [20]. Therefore, wet electrodes containing conductive gel are very interesting: the gel hydrates the SC and conductive gel provides conductive ions, thus creating an easier ionic path between the metal part of the electrode and the skin below the SC layer, thereby making the transduction of ionic current into electric current easier [5]. Therefore, the gel lowers the skin-electrode's impedance. Furthermore, the flexible and viscous gel stays in good contact with the skin during movement because the gel is limited in a space, such as in the center of the adhesive pad surrounding an ECG electrode or of an EEG cup electrode, hence the level of impedance also remains low when the subject is moving. As such, gel electrodes provide high-quality signal recording with limited motion artifact disturbances, which makes them very popular for biopotential recording. Widely-used wet ECG electrodes are shown in Figure 1.3a. These ECG electrodes consist of a metal snap, a silver/silver chloride (Ag/AgCl) coated sensor, a conductive and adhesive hydrogel, and an adhesive foam. The EEG electrodes used for clinical EEG monitoring are shown in Figure 1.3b and Figure 1.3c. Figure 1.3b depicts a so-called 'bridge electrode'. It consists of an Ag/AgCl contact and a felt pad. Before placing the bridge electrode on the scalp, the electrode is immersed in a saline solution, and conductive gel is added to the felt pad. In Figure 1.3c, cup electrodes are shown. They are available in a wide range of materials, such as gold (Au), silver (Ag), and Ag/AgCl. These electrodes are glued onto the scalp and then the cups are filled with conductive gel. An often-used glue to fix the cup electrodes is Collodion, which contains nitrocellulose, ethyl ether, and ethanol. In this thesis, these three electrodes will be called 'wet electrodes'.

(a) (b) (c)

Figure 1.3: (a) ECG electrodes; (b) EEG bridge electrode; (c) EEG cup electrodes.

Although these wet gel electrodes are widely used in clinical environments, the use of gel-based electrodes has various well-known drawbacks [5, 21]. Before biopotential monitoring can start, skin preparation is often needed to improve electrode signal quality: abrasive gel and cleaning alcohol are used to remove some part of the SC layer. For long-term EEG recording, electrodes have to be glued onto a well-defined position on the scalp. Then, the electrodes are filled with conductive gel. This time-consuming EEG setup has to be precisely done by an expert. During the EEG monitoring, signal degradation will occur due to the gel drying out, and skin irritation may often be observed. After the EEG recording, electrode removal is difficult and time-consuming. If electrodes are glued onto the scalp, the removal is often even painful. For short-period monitoring, electrodes can be clamped onto the scalp by a cap, and while it may require shorter setup and removal times, it is uncomfortable to wear. To avoid these drawbacks regarding wet electrodes, various types of dry electrodes have been introduced, which will be discussed in the next section.

1.2.1 Various types of dry electrodes

Contact and non-contact electrodes are the two main categories of dry electrodes [22]. Non-contact electrodes shown in Figure 1.4a are capacitively coupled to the skin. The capacitance of these electrodes is typically 1-100 nF resulting a high electrode/skin impedance. Therefore, these electrodes give a very small signal amplitude. In addition, these electrodes are highly sensitive to motion artifacts since motion changes the distance in between the electrode and skin resulting variation of skin-electrode capacitance [23, 24]. It is reported in [25] that if the electrode moves 100 μm vertically away from being on the surface of the skin, the capacitance changes by a factor of 10. Two types of direct contact electrodes exist: electrodes with microscale needles on the surface that penetrate only the SC, and electrodes that are in direct contact with the skin but without penetration, see Figure 1.4b and Figure 1.4c, respectively. The microscale needles are conductive (conductive bulk material or coating), and they bypass part of the highly resistive SC barrier, so they will lower the overall electrode–skin impedance. In order to function well on hairy skin, contact electrodes are often equipped with macroscale pins (an example is shown in Figure 1.4c), hence the hair can be positioned in the space in-between the pins which results in an improved electrode-skin contact.

Various authors have reported their work on contact dry electrodes. Regarding penetrating, contact electrodes, nanoscale needles made of carbon nanotubes are reported in [26], while microscale tips have been fabricated using a silicon wafer with conductive coating [27, 28]. Microscale tips could also be realized using polymer which is coated with a conductive metal [29]. Nano- and microscale electrodes for SC penetration are expensive due to the fabrication process. Furthermore, they might cause irritation and infections, especially in case of breached skin [30]. Moreover, additional requirements regarding material biocompatibility have to be respected since the needles can easily break during use. Therefore, contact electrodes for SC penetration are not popular for use in commercially available EEG systems. In this thesis, the contact dry electrodes without penetration will be the subject of investigation. The state of the art in this type of dry electrodes will be discussed in the next section.

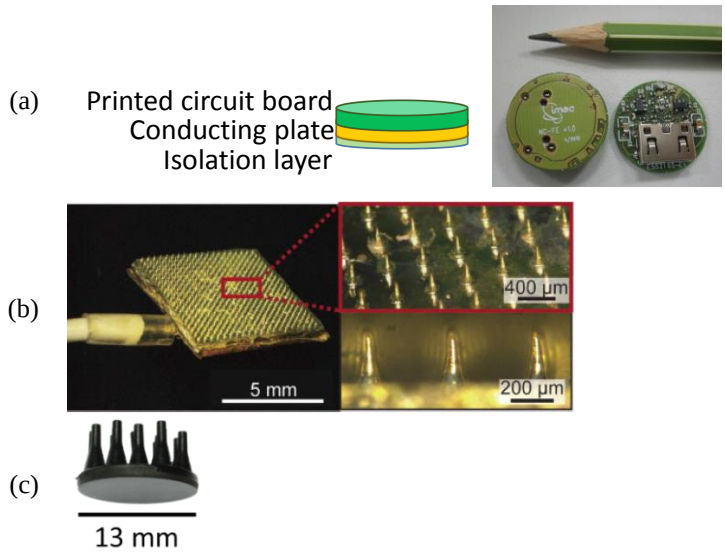

Figure 1.4: (a) non-contact electrodes[31]; (b) microscale electrodes [29]; (c) macroscale pin-shaped electrodes.

1.2.2 Various types of contact dry electrodes

To overcome the disadvantages of wet electrodes, the so-called "semi-dry" electrodes are developed for EEG monitoring; such electrodes release an electrolyte for skin hydration during use. These electrodes contain a reservoir or felt pad to store the electrolyte [32, 33]. This electrolyte provides a conductive channel and hence promotes the conversion of ionic signals to electronic ones. The amount of conductive electrolyte is small compared to that of conventional wet gel EEG electrodes. This causes fewer electrolyte (gel) smearing and cross talk problems. However, it is time-consuming to fill each of the reservoir of electrodes with the electrolyte. As to the electrodes with felt pads, the electrolyte needs to be re-applied during every hour of wearing to maintain a good signal quality [34].

Semi-dry electrodes do not solve the signal degradation issue entirely. The ideal improvement is still the development of a completely dry electrode. Various types of dry electrodes without any extra conductive fluid have been presented in a number of publications, see Figure 1.5. According to their form factor, the electrodes are categorized into the following groups:

textile electrodes

Due to the ease of wearing and capacity for long-term use, electrodes integrated in textile are developed for physiological signal sensing [35-37]. Conductive thread, rubber or ink are the main materials applied to increase the conductivity of the textile [38, 39]. Stainless steel yarn is the most popular type of conductive material for textile electrodes. Besides stainless steel yarn, Ag coated nylon (AgNy) [40] and graphene-clad textile prepared with a graphene layer coated on nylon fabric are popular materials for cardiac monitoring textile electrodes [41]. In

addition, conductive rubber, composed of silicone rubber and conductive additives, is also used as a textile electrode. These conductive rubber materials are integrated with the textile by means of printing. Stencil-printed conductive rubber electrodes are fabricated on a woven textile for ECG, EOG, and EMG monitoring [42]. Screen-printing is the technique applied to disperse conductive inks on the textile substrate. An active electrode fabricated by this technique is used for ECG monitoring [43]. Such an active electrode is a combination of an electrode and an impedance transforming electronic circuit placed close to the electrode. The circuit often includes an operational amplifier (op-amp) with both a high input and low output impedance. The high input impedance of the op-amp ensures a low signal attenuation while its low output impedance reduces the environmental noises induced by the cables connecting the electrode and recording device [44]. In contrast, an electrode not combined with an active circuit is called a passive electrode. Textile electrodes are applied in EEG monitoring as well. However, it has been reported in another paper that the signal quality of EEG signals acquired from passive dry electrodes is low. A saline solution or conductive gel needs to be added to passive textile electrodes for high quality EEG measurements [45]. This is because a flat textile electrode mounted on hairy skin behaves like a capacitive electrode. The conductive fluid creates a conductive channel for the ions to transmit current from the skin to the electrodes. To summarize, textile dry electrodes are flexible and can be fixed onto the human body quite easily. However, the flat surface limits their applications for biopotential measurements on hairy skin.

flexible film electrodes

Another type of flexible dry electrode is fabricated on polymeric substrates, whose flexibility enhances the electrode-skin contact. A tattoo-like epidermal sensor-system is a good example [46]. This tattoo-like system consists of dry electrodes in the shape of a stretchable metal mesh on a very thin silicone which is tightly attached to the skin. Due to the stretchability of this ultrathin sensor, high-quality electrode-skin contact is obtained on non-hairy skin. This electrode is successfully mounted on areas of the auricle and mastoid for BCI applications [47]. Yet another type of flexible film electrode is composed of carbon nanotubes (CNT) embedded in adhesive polydimethylsiloxane (aPDMS). An ECG patch using this type of electrode shows similar quality ECG recordings to that of conventional gel electrodes [48]. Ag balls can also be embedded into a PDMS substrate, forming electrodes which have been used for forehead EEG monitoring [49]. Another popular polymer material used for flexible film electrodes is poly (3,4- ethylenedioxythiophene) (PEDOT). PEDOT is often coated on metal surfaces of electrodes to improve their electrochemical performance [50]. No matter how extraordinary the skin contact that these dry film electrodes can offer, such contact is always limited when applied on hairy skin.

bulk electrodes

Apart from textile and flexible film electrodes, flat-shaped bulk dry electrodes are also developed for biopotential measurements, e.g. a wristband fabricated by patterned gold in PDMS on a base structure [51] or an ECG patch composed of three Au contact pads on a PDMS substrate [52]. Other realizations include polymer foam electrodes with metal coating or conductive textile and polymer electrodes for non-hairy locations, or a urethane polymer

foam surrounded by conductive textile to be mounted on the scalp for EEG signals recording [53]. Bulk electrodes made of conductive elements and a polymeric base (e.g. CNT/PDMS-mixed material) are developed for EEG monitoring using the ears instead of the forehead area [54]. Bulk electrodes should be fabricated from sufficiently flexible materials, so that their shape will adapt to an irregular body surface to ensure a good skin contact.

pin-shaped electrodes

Most electrodes discussed above are only applicable in ECG monitoring, since their flat surface has difficulty achieving good electrode/skin contact on hairy skin. Therefore, electrodes with macroscale pins are developed to extend the contact area of electrodes and skin, especially on the scalp. One type of pin-shaped electrodes is fabricated using non-conductive materials with conductive coating. 3D-printed pin-shaped electrodes coated with Au are applied in both ECG and EEG monitoring [55]. Electrodes made from polyurethane (PU) pins and then coated with titanium nitride (TiN) or Ag/AgCl are fabricated for EEG signal acquisition [56, 57]. A bristle electrode, with thinner but non-penetrating pins fabricated by a polymer coated with Ag, is used for BCI application [58]. Other types of pin-shaped electrodes are made from metal. Electrodes consisting of Au-coated probes and springs to control the force on the scalp are produced, too [59]. From all these types of pin-shaped dry electrodes, full metal electrodes have the lowest impedance but due to their rigidity combined with the pressure essential for good skin contact, they can be painful during use [60]. Softer non-conductive polymer electrodes coated with a metal layer are more comfortable, but the coating easily flakes off, resulting in the electrode's high resistivity [61].

Considering the pros and cons for all types of dry electrodes, only dry electrodes fabricated from a flexible conductive polymer are considered in this thesis. Such electrodes overcome the drawbacks of wet gel electrodes and of the various types of dry electrodes mentioned above. The elastic properties of the conductive polymer ensure user comfort, while the conductivity of the polymer avoids any layers from flaking off during use. To my knowledge, except for the polymer electrodes presented in this thesis, the only pin-shaped conductive polymer electrode for EEG monitoring is described in [61], a recent paper published in 2015, which is a considerable time from the first publications related to this thesis. The electrodes described in [61] consist of a molded silicone-based material mixed with Ag. The authors of [61] report that the life cycle of their electrodes is limited because the oxidation of Ag may have reduced the conductivity.

In the next section, the commercialized dry electrodes together with the mounting devices for EEG applications will be reviewed. However, electrodes for the commercially available ECG recording device will not be addressed, because the polymer electrodes evaluated in this thesis are especially useful in EEG recording devices. There exists already a large number of well-functioning ECG devices equipped with other dry electrodes. In contrast, only a small number of companies offer EEG recording devices equipped with dry electrodes, and improvement made to these devices is still very useful.

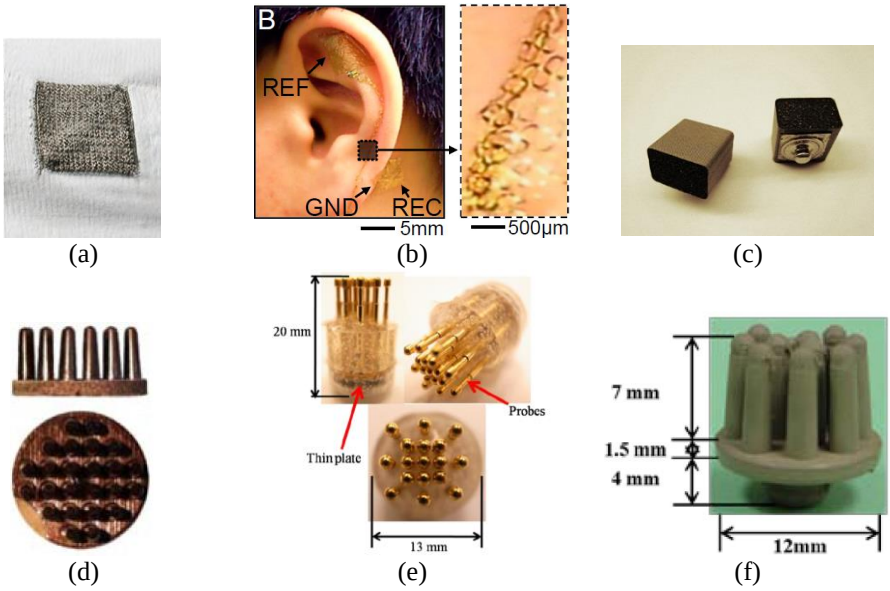

Figure 1.5: (a) textile electrode made of conductive fibres [62]; (b) flexible film electrode fabricated by Au wires on flexible polymer substrate [47]; (c) bulk electrodes formed by polymer bulk and conductive outer layer [53]; (d) pin-shaped non-conductive polymer electrode coated with TiN [56]; (e) pin-shaped metal electrode with spring loaded pins [59]; (f) pin-shaped conductive polymer electrode [61].

1.2.3 Mounting of (semi)-dry electrodes for EEG monitoring

Wet ECG and EEG electrodes are mounted on the human body using adhesive foam, glue, or a dedicated cap. The fixation approaches of dry electrodes need to be taken into account when designing dry electrodes, especially for EEG electrodes. In the evaluation of dry electrodes in academic research, simple fixation methods were applied such as elastic bands or a cap. However, once the dry electrodes are commercialized, a superior fixation is needed. A proper fixation maintains a high signal quality while also providing considerable comfort to the user. User comfort depends on the combination of the electrode material, its shape, and the fixation technique used. Loading the appropriate pressure from the device to the electrodes ensures good electrode/skin contact and results in no pain due to the local pressure from long-term measurements. Many EEG monitoring devices have been developed and sold for reasons of research and/or entertainment [63]. In this section, commercially available devices that are equipped with dry electrodes and mounted on electrodes in hairy locations will be discussed. Devices with forehead-only electrodes will not be investigated in this section since they have limited functionality. In Table 1.1, the fixation approaches of devices capable of EEG monitoring at hairy locations are shown. In addition, the design and material of the dry electrodes are also listed.

Emotiv headset is the only device in Table 1.1 equipped with bulk and semi-dry electrodes. To be more specific, the electrodes are 10 mm in diameter and soaked in saline solution. These saline-soaked electrodes can only guarantee a good signal quality for a few hours since

they dry out after only as many hours [64]. More electrolytes need to be added to maintain signal quality. Although the headset is available in only one size, the producer claims that this will fit on most users' head due to the flexibility of the headset material. However, some users have felt pain after only one hour of wearing it [65]. The second type of electrode is g.SAHARA, which is a rigid metal-pin electrode produced by g.tec. Together with the electrode, a clip containing the active circuit (resulting in an active electrode) is sold in order to connect the electrode and recording device. The clip is also used to fix the electrode on a cap, which is called g.GAMMAcap. This cap offers 160 pre-cut holes according to the positions of the 10-20 international system. Users can mount the electrode on their location of choice. The g.SAHARA electrodes have two pin-lengths (7 mm and 16 mm) for users with various hairstyles. Besides the length of the electrode, the user can also choose from three different cap sizes. In a paper published by g.tec, none of the 23 subjects who used the g.SAHARA electrodes reported any discomfort [66]. However, in another publication that compared the usability of g.SAHARA to two other devices, two participants with larger head-sizes experienced discomfort due to the pressure from the g.SAHARA electrodes [67]. The third device in this overview, which offers up to 21 channels, is made by QUASAR. With somewhat larger electrode sizes (around 25 mm in diameter), the number of electrodes that can be fitted in the headset is limited. Moreover, the weight of both the electrodes and headset, more than 500 g in total, can lead to discomfort when wearing it [60]. The fourth device, Mindo-64 Coral from Mindo, is equipped with metal-pin electrodes that have springs. Several versions of the headset exist, the one which has the most recording channels is armed with 64 channels. The spring-loaded electrodes have a smaller size and less weight compared to electrodes in the QUASAR headset [68]. This increases the spatial resolution. Although the total weight of the device is around 200g, the headset looks bulky. The fifth headset, developed by Cognionics, offers up to 72 recording channels. It is equipped with 3D-printing flexible electrodes coated with Ag/AgCl. The flexible legs of the electrodes penetrate through hair and become flattened when accepting pressure. However, the author of publication [69] reports that the coating layer of the electrodes fades and the flexibility of the electrodes reduces after certain time of use [70].The headset of Cognionics consists of soft fabric, allowing for multiple degrees of freedom to adjust the size. The whole system weighs 350 g [71]. From the demonstration video on their website, it is obvious that it takes some time to adjust all the mechanical joints to ensure good contact between the electrodes and skin after putting the headset on the head. User comfort evaluations on a large number of subjects are yet to be published. The last commercially available headset is ENOBIO 32, fabricated by Neuroelectrics. This headset is equipped with electrodes that are coated with Ag/AgCl. The ENOBIO device is capable to monitor and stimulate brain activities, which gives the possibility for neurofeedback applications [72]. No evaluation regarding the user comfort of ENOBIO 32 and dry electrodes has been reported.

To the best of my knowledge, no systematic evaluation of the EEG signal quality and user comfort of these commercially available EEG headsets has been published. However, publications providing a comparison of one or two of these devices and conventional wet devices do exist. Some publications describe the discomfort of wearing certain devices [60], while others conclude that certain devices are not suitable for clinical applications due to the limited number and location of electrodes [67, 73]. Although the use of dry electrodes

removes the disadvantage of using wet ones, the challenge of achieving high EEG signal quality and high user comfort is still not met, and so room for further improvement still exists.

1.3 Overview of this thesis

The aim of this thesis is to optimize and characterize a novel type of cylindrical-shaped and pin-shaped conductive polymer electrode for biopotential measurements on the human body with high user-comfort.

In Chapter 2, the design and material selection of the conductive polymer electrodes will be explained. Electrodes with various pin shapes (in terms of length, width, density) were fabricated for different applications. Various additives were added into the polymer, while the additive type and quantity were optimized in order to obtain low contact impedance and good mechanical properties for better comfort and skin contact.

In Chapter 3, an evaluation of electrodes regarding their electrical and mechanical properties will be made. Impedance measurements of various types of conductive polymer electrodes in electrolyte on phantoms and human skin were carried out for impedance characterization. Besides, the electrochemical model of the electrode/skin interface will be discussed. Regarding the mechanical properties of polymer electrodes, compression tests are used for the elastic modulus characterization of the polymer materials as well as the compliance characterization of the pin-shaped electrodes.

Finally, the optimized conductive polymer electrodes were used for ECG and EEG recording, while the obtained biopotential signals were compared to those obtained using conventional wet electrodes. The experimental setup, protocol and results of ECG and EEG monitoring will be presented in Chapters 4 and 5, respectively.

In Chapter 6, the user comfort and skin biocompatibility of these conductive polymer electrodes will be evaluated.

Chapter 7 brings this thesis to a close, and proposes possible paths for future research.

Device Name/ Company	Fixation Type	Electrode Shape			Electrode Material	Number of Channels
		Base diameter (mm)	Pin length (mm)	Pin number		
Emotiv EPOC/ Emotiv	headset 	Bulk: felt pads 			Saline soaked felt pads	14
		10	10	NA		
g.SAHARA/ g.tec	Cap 	Pin shaped 			special golden alloy	Up to 160 for g.GAMMA cap
		19	7 or 16	8 (circular arrangement)		
DSI-10/20/ Quasar	headset 	Pin-shaped 			Conductive metal	21
		25	~ 5	30		
Mindo-64 Coral/ Mindo	headset 	Pin-shaped: spring loaded metal pins 			Au coated	64
		16 or 20	3	16		
Cognionics	headset 	Pin-shaped: flexible legs flattened under hard pressure 			Ag/AgCl coated 3D printed conductive polymer	Up to 72
		15.24	11.43	8, 10, 12		
Enobio 32/ Neuroelectrics	headset 	Pin-shaped 			Ag/AgCl coated	32
				10		

Table 1.1: Commercially available devices equipped with (semi-)dry electrodes for EEG monitoring.

Chapter 2.
Materials and Designs of Conductive Polymer Electrodes

The conductive polymer electrodes presented in this thesis are composed of ethylene propylene diene monomer (EPDM) rubber as a base matrix, with various additives that are fabricated by compression molding. Various pin configuration and button shapes are fabricated using various polymer compositions to optimize the electrical and mechanical properties and to increase the feasibility of recording systems' integration. The properties of these polymer electrodes were evaluated, and then a new batch of polymer electrodes with improved shape designs and materials was fabricated. This optimization process will be discussed in Chapter 3 in terms of the electrical properties' evaluation and the mechanical properties' evaluation. In section 2.1, the designs of the polymer electrodes used in this thesis are summarized. In section 2.2, the additives added in the polymer electrodes are listed. In section 2.3, the fabrication process of polymer electrodes in Datwyler is introduced. In section 0, the materials and designs of the polymer electrodes used for ECG and EEG monitoring in this thesis are listed. These are the optimal materials and designs based on the results discussed in Chapter 3.

2.1 Electrode designs

2.1.1 Prototype electrodes with metal coating

Before the conductive polymer electrodes were fabricated, metal-coated prototypes had been manufactured using stereolithography. Stereolithography is a technique to create models and prototypes in a layer by layer fashion using photopolymerization, a process by which light causes chains of molecules to link together, forming polymers. This is a rather cheap and efficient technique for fabricating electrode prototypes. This kind of electrode was used mainly to optimize the electrode design for a minimum impedance on hairy skin: influences of pin number, pin shape and pin gap size had been studied. The fabrication processes of the non-conductive polymer electrodes are shown in Figure 2.1.

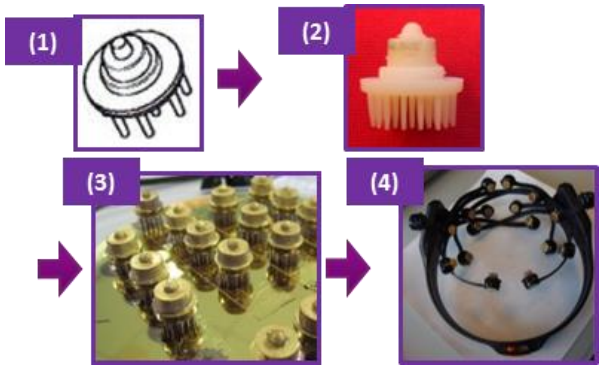

Figure 2.1: The fabrication of non-conductive polymer electrodes with metal coating for conductivity using stereo lithography. The non-conductive polymer electrodes were: (1) designed by software (2), prototyped by stereolithography, (3) coated with conductive layers, (4) mounted into an EEG headset.

First, the electrode shapes were designed in a 3D design software, Solid Edge (Siemens PLM Software, Plano, TX, USA). Second, they were then fabricated by stereo lithography using Verowhite as material. Third, a four-layer metal stack (TiW/copper/TiW/gold) was coated onto the Verowhite material to make the electrodes conductive. Finally, the electrodes were mounted into the Emotiv EEG headset for EEG monitoring, as shown in Table 1.1.

Various designs of prototype electrodes are shown in Table 2.1. These electrodes are labelled as designs 3×3, 5×5, 7×7 and 11×11. The base planes of designs 3×3, 5×5, 7×7 are circles with a diameter of 10 mm. The base plane of design 11×11 is a circle with a 13-mm diameter. 3×3 indicates that there are 3 pins on both vertical and horizontal axes of the base plane. Other pins are distributed equally on the base plane of the electrode. The pin lengths of these designs vary from 3 mm to 5 mm. The electrode/skin contact and user comfort of these electrodes are evaluated by mounting them into an EEG headset. 16 electrodes are mounted in the headset and the contact quality of the electrode/skin is evaluated using the headset's companion software. In the software, 5 colors are used to indicate the contact quality, see Figure 2.2a. Figure 2.2b shows the contact quality of each electrode when placing electrodes with designs 11×11 and 5×5 on one male with hair style shown in this figure. The total contact quality of other designs, calculated as the sum of the scores of 16 electrodes, is shown in Table 2.1. It is found that electrodes with too few pins (3×3) generate a high local pressure that results in pain. On the other hand, electrodes with too many pins (11×11) result in bad electrode/skin contact because the pins cannot penetrate through the hair and make contact with the skin. Besides the number of pins, their length is also a key parameter of electrode design. A proper pin-length ensures a good electrode/skin contact. From our experiences, it is found that 5×5 and 7×7 electrodes with 3 mm or 4 mm pin length show no difficulty in contacting the hairy skin. These preliminary results using prototype electrodes suggest a specification for designing conductive polymer electrodes.

Name	3×3	5×5		7×7		11×11
Pin length	5mm	3mm	4mm	3mm	4mm	3mm
Base diameter	10 mm	10 mm	10 mm	10 mm	10 mm	13 mm
Schematic						
picture						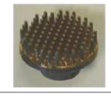
contact quality	51	65	72	68	61	40
remarks	too few pins→ High local pressure → painful					too dense pins → cannot penetrate hair

Table 2.1: Various designs of the metal-coated prototype electrodes.

Colors	contact quality	score
black	No signal	1
red	Very poor signal	2
orange	Poor signal	3
yellow	Fair signal	4
green	Good signal	5

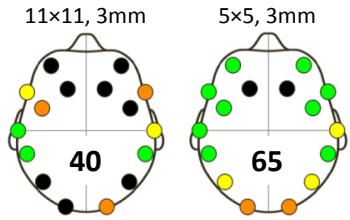

(a) (b)

Figure 2.2: (a) The contact quality is indicated using 5 colors in Emotiv EEG headset's companion software. Scores are given to each color to calculate the sum of contact quality of the 16 electrodes in the headset. (b) The contact quality of prototype electrodes 11×11, 3mm and 5×5, 3mm on one male with hair style shown in the picture. The contact quality of other designs on the same person can be found in Table 2.1.

2.1.2 Conductive polymer electrodes

When fabricating conductive polymer electrodes, Solid Edge was again applied to design the shapes of these electrodes. For the top side of the electrode, being the side in contact with the skin, both flat and pin-shaped electrodes were designed. For the bottom side of the electrodes, various shapes were designed to integrate the electrodes with different types of ECG/EEG recording systems. The designs were used to make the electrode molds. The various material mixtures, which are described in the next subsection, underwent compression molding in order to form the electrodes, as shown in Figure 2.3. The detailed molding process is introduced in section 2.3. The base plane diameter of these electrodes ranges from 10 to 13 mm, and pin lengths are ranging from 2 to 10 mm. These base plane dimensions were chosen because they are similar to the size of conventional cup and bridge electrodes (Figure 1.2b and c). These pin lengths and density were decided based on the evaluation of the contact quality of prototype electrodes with various designs (section 2.1.1). Cylindrical-shaped electrodes with a diameter of 13 mm and height of 5 mm were also fabricated for each material mixture so as to test their mechanical properties and to perform other material characterization tests; these electrodes are further called "bulk electrodes". The type of electrode used for each particular test will be mentioned throughout this thesis.

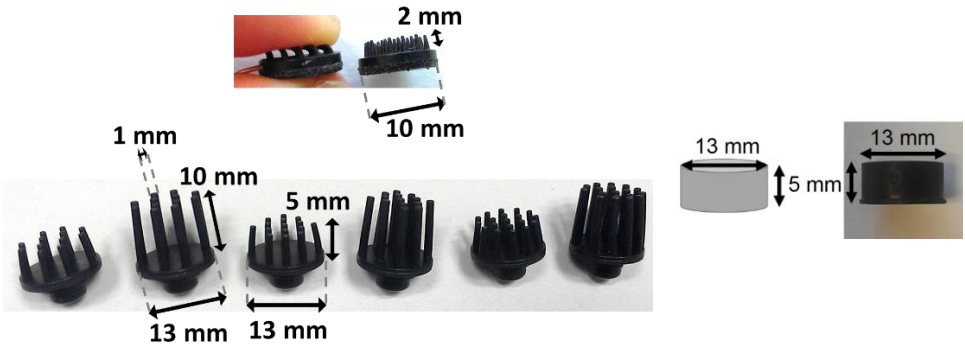

(a) (b)

Figure 2.3: (a) pin-shaped and (b) cylinder-shaped conductive polymer dry electrodes.

2.2 Material composition of polymer electrodes

In order to obtain the optimum properties regarding material conductivity, hardness, flexibility and ease of fabrication, various additives were mixed in an ethylene propylene diene monomer (EPDM) matrix, with the resulting polymer being tested as electrode material. Several types of conductive additives, e.g. carbon, stainless steel fibres, and carbon nanotubes (CNTs), were tested. These additives were chosen due to their reported use for biomedical sensing in other publications.

carbon

Electrodes with carbon added to increase their conductivity have been fabricated by other researchers. A film composite with carbon black powder mixed with salt and visco-elastic polymeric adhesive was applied in ECG monitoring [74]. Carbon-loaded rubber electrodes, integrated in a chest band, were used to record the ECG signals [43]. Electrodes made of 3000 carbon fiber filaments, each with 7 μm in diameter, were fabricated and used to record the EEG signals [75]. Carbon has high stiffness, elevated tensile strength, and good conductivity. Consequently, carbon was chosen as one of the additives for the polymer electrodes. The optimization of the carbon content in polymer electrodes regarding their electrical and mechanical properties is discussed in Chapter 3.

stainless steel

Several examples of using stainless steel as sensors are introduced in other publications. Stainless metal cans were used to measure the myoelectric signals [76]. Stainless steel foil, glued onto a foam substrate, was used to acquire the ECG signals [77]. A textile electrode surface made of stainless steel strands twisted around a viscose yarn was applied in ECG monitoring [78]. Besides these non-invasive applications, stainless steel is a popular material for biomedical implants. The biocompatibility of stainless steel has been well documented

thanks to the wide use of stainless steel for biomedical implants. Therefore, stainless steel fibers were added in the conductive polymer electrodes to increase conductivity.

In this thesis, 2 mm stainless steel fibers were added in the polymer electrodes. The impedance of these electrodes can be found in Chapter 3, section 3.2.3 and section 3.2.4. It is concluded that stainless steel fiber is not a suitable additive for the polymer electrodes because of the following reasons: (1) The impedance of polymer electrodes containing ~10% of stainless steel is still high. (2) The use of polymer with high load stainless steel fibers (>20%) is not feasible for mixing and filling in molds with thin pins. (3) Polymer with high load stainless steel fibers would scratch the mold during processing. (4) Some small quantities of stainless steel residues in the tools would contaminate other polymer formulations (risk of defects and customer complaints) in the regular production of Datwyler.

carbon nanotube (CNT)

CNTs are good conductors that have gained lots of attention in terms of biomedical applications in recent years. Some electrodes introduced by other research groups are also introduced here. The CNT/polydimethylsiloxane (PDMS) composite-based dry electrode was presented for biosignal monitoring [48, 54]. Multi wall carbon nanotube (MWCNT) containing thin film was developed to record EEG signals during computed tomography (CT) and magnetic resonance imaging (MRI) scan [79]. The CNT array, grown on a conductive substrate, was applied in ECG and EEG monitoring [26]. These publications have all proven that CNT has excellent mechanical and electrical properties; therefore, CNTs were chosen as one of the additives in our polymer electrodes.

The impedance of polymer electrodes containing CNT measured on skin phantoms is shown in Chapter 3, section 3.2.4. Althought the impedance value of them is low, CNT is not considered anymore as interesting additive in polymer electrodes becuase there still exist controversial opinions about the use of CNT containing samples on humans.

In this thesis, the conductive polymer electrodes, fabricated for biopotential measurements, contain one or more of the additives mentioned. The additives' quantity varies for each batch of conductive polymer electrodes and their weight percent will be mentioned in the following chapters. Other additives not mentioned here were added for the optimization of mechanical and electrical properties.

2.3 Compression molding of conductive polymer electrodes

The conductive polymer electrodes are fabricated by Datwyler using compression molding technique. The fabrication process includes mixing the polymer formulations and shaping the polymer formulations into polymer electrodes.

2.3.1 Mixing of the polymer formulations

For the initial trials the rubber ingredients were mixed on a small 2 roll lab mill at Datwyler Alken. This lab mill is using small quantities of the different ingredients for a typical total weight of about 180-200 g. Rubber formulations are expressed in parts per hundred meaning

each ingredient is expressed in a weight (in g) compared to 100 g of the elastomer (in these formulations an EPDM elastomer).

Later the rubber was mixed in the Datwyler pilot plant in Switzerland because the carbon black caused too much contamination of other products in the pilot plant. Datwyler Alken is typically producing only light colored formulations with white silicate fillers.

Because in the course of the project also the demand for samples increased, the mixing was done in a mixer with a typical batch yield of 7 kg. The mixer used is a small internal mixer with intermeshing rotors. After mixing, the rubber was milled on a lab mill, preformed in sheets, cooled and packed and sent to Datwyler Alken where the rubber was shaped into the electrodes by compression molding. Each mixing batch has been checked at Datwyler Alken for its proper curing behaviour by taking a rheograph.

2.3.2 Shaping of the polymer formulation into polymer electrodes

Based on product drawings obtained from imec, a trial mold was built by the tool shop of Datwyler, see Figure 2.4. Initially a number of cavities were made with 2 mm short targeted for impedance measurement on non hairy skin and for ECG monitoring. Later additional cavities with pins with variable pin distribution and length were added to the same trial mold.

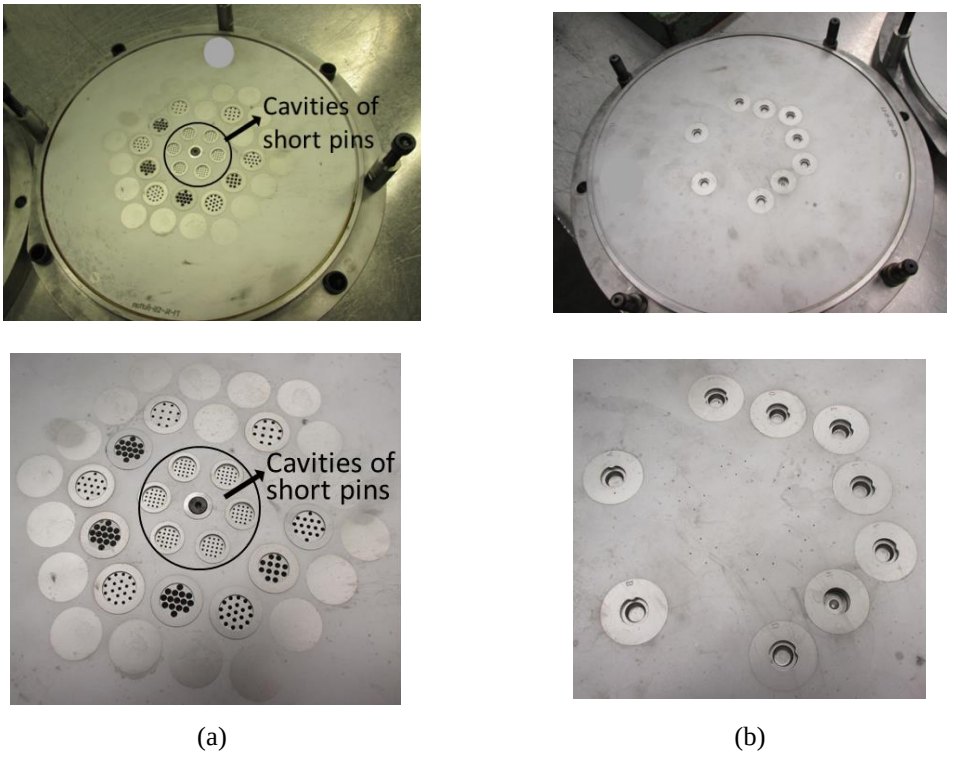

Figure 2.4: (a) The trial mold on the side of pin cavities. (b) The trial mold on the side of the connecting cavity (for the connection with the electronic system).

The initial pins with longer legs for biopotential measurements on hairy skin had a straight cylindrical design. These straight legs resulted in some breaking of the pins when the rubber was released from the mold. As a consequence the broken pieces of rubber were left in the cavity of the mold. Because the pins are quite thin it is difficult to remove this stuck rubber. Another drawback of the electrodes with straight pins was that the position of the pins on the head was not stable enough. The pins showed too much deformation when they were put under pressure to get a good contact with the skin. The mechanical properties of these electrodes can be found in Chapter 3. To solve these problems the pins were redesigned into a conical shape. These new designs were added to the same trial mold.

An exact weight of the uncured rubber was added to fill the mold and then the rubber was cured for a fixed time and temperature (proprietary to Datwyler). The product obtained after molding was a rubber sheet with the different electrodes, see Figure 2.5.

(a) (b)

Figure 2.5: (a) The molded sheet on the pin side. (b) The molded sheet on the connector side.

After the molding steps the electrodes were punched out from the sheet becoming the electrodes shown in Figure 2.3a. These electrodes underwent heat treatment to remove some of the volatile traces of the rubber and were rinsed for 5 minutes in demineralized water of 60°C before being sent to imec.

2.4 Materials and designs of the polymer electrodes used for ECG and EEG monitoring

Among the conductive additives discussed in section 2.2, only conductive carbon is selected for the final formulations that were tested in this thesis: formulations CR64 and CR95. The details of the formulations are proprietary to Datwyler and cannot be revealed in this thesis.

The designs of polymer electrodes used for ECG and EEG monitoring in this thesis are shown in Table 2.2.

ECG	EEG
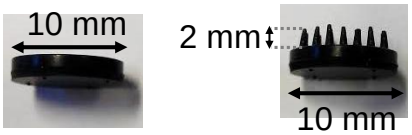	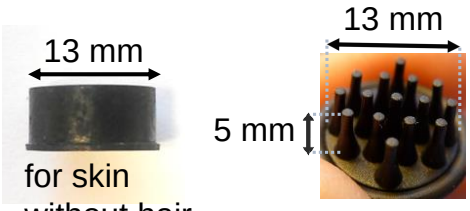

Table 2.2: Shapes of the electrodes used for ECG and EEG monitoring in this thesis.

Chapter 3.
Basic electrode evaluation: Electrical and Mechanical Properties

It has been mentioned in Chapter 1 that the ionic current in the body has to be transformed to electrical current by the electrodes, in order to result in measurable biopotential signals. The fluids containing conductive ions are generally referred to as electrolyte. Current is carried by conductive ions in the electrolyte while carried by electrons in the electrode. When currents pass through the interface of electrode and electrolyte, electrochemical reactions can happen at the interface to convert ionic currents to electronic currents or vice versa. Three main evaluation tests are often used to characterize the properties of this electrode/electrolyte interface: measurement of the open circuit potential (OCP), cyclic voltammetry (CV) and impedance measurements. The properties of the electrode/electrolyte interface and its link with electrochemistry measurements results are explained in section 3.1. In section 3.2.1, the polymer electrodes with various design and material composition are characterized, after paying attention to the experimental setup and protocol applied for the OCP and CV measurements. Among the three characterization tests, impedance measurements get most attention since the electrode/skin impedance is strongly influencing the quality of biopotential measurements. Lower impedance results in stronger signals as well as less noise disturbance [80]. The setup for impedance measurements is explained in section 3.2.2. The following section shows the measured impedance of cylindrical shaped and pin shaped polymer electrodes and a further discussion of these results can be found in section 3.2.3 and section 3.2.4. In addition, the influence of skin pretreatment techniques on impedance is presented in section 3.2.5. In order to obtain a better understanding of the obtained impedance results, a mathematic equivalent circuit of the electrode/skin is modelled, as shown in section 3.3. Besides the electrical properties, the mechanical properties of the polymer electrodes are also investigated since they had an impact on the fabrication yield, biopotential signal quality, and user comfort. The techniques used to measure the mechanical properties of materials are introduced in section 3.4. In the same section, the test protocols and the results are discussed. In section 3.5, several polymer material compositions and shape designs are selected for further biopotential evaluations according to all the results regarding electrical and mechanical properties. The overview of material compositions and shapes of polymer electrodes are summarized in section 2.4 already.

3.1 Interface of electrode/ electrolyte

As shown in Figure 3.1, when a metal electrode consisting of metal atoms labelled C comes into contact with an electrolyte solution containing the cations of the same metal (C^{n+}) and some anions (A^{m-}) to preserve the neutrality of the electrolyte, oxidation and reduction reactions (redox reactions) can occur at the interface, where the interchange of ions and electrons takes place [81, 82]. Metal atoms can become oxidized to form a cation and one or more free electrons. The cation is discharged into the electrolyte while the electrons remain in the electrode. Anions reaching the electrode can be oxidized to neutral atoms, giving one or more free electrons to the electrode. When these oxidation reactions happen, the current flows through the interface from the electrode to the electrolyte as shown in Figure 3.1a. It is to be noted that both oxidation reactions are often reversible, resulting in the reduction reactions and reversed current direction as shown in Figure 3.1b. The cations in the electrolyte can be reduced by accepting one or more electrons from the electrode. The atom also receives electrons from the electrode and then becomes an anion in the electrolyte.

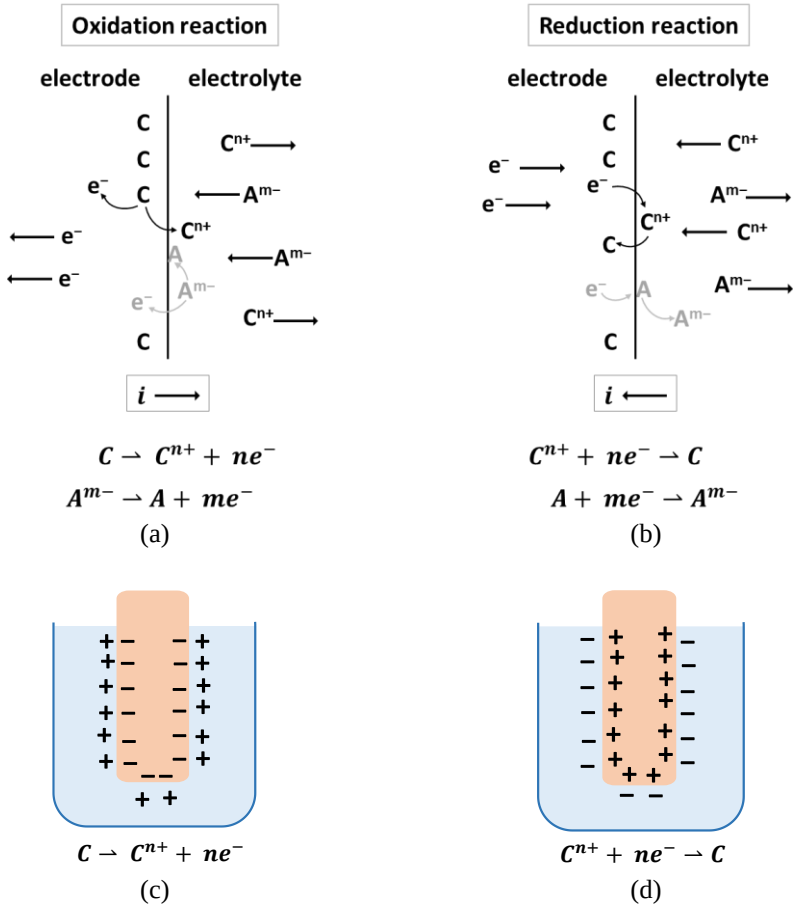

Figure 3.1: The (a) oxidation reactions and (b) reduction reactions occur at the interface of an electrode and the electrolyte containing the ions of the electrode and some anions. (c) When the metal atoms prefer to be oxidized, the metal electrode at the interface becomes negatively charged and the electrolyte at the interface becomes positively charged. (d) When the cations prefer to be reduced, the metal electrode at the interface becomes positively charged and the electrolyte at the interface becomes negatively charged.

Initially when the electrode contacts the electrolyte as shown in Figure 3.1, either the oxidation or the reduction reaction dominates depending on the chemical potential of the reactants, which is defined by thermodynamics [83, 84]. Regardless of whether oxidation or the reduction reaction is preferred, both reactions change the concentration of the cations in the electrolyte at the interface. The concentration of the cations of the electrolyte at the interface increases when metal atoms prefer to be oxidized as shown in Figure 3.1c. Excess cations in the electrolyte at the interface result in a positively charged plane. The free electrons in the metal electrode are attracted by the positive charges in the electrolyte and form a region of excess negative charges in the metal at the interface. The electrolyte at the interface can be negatively charged up when the cations prefer to be reduced, thus becoming metal atoms as shown in Figure 3.1d. In the metal electrode, the free electrons move away

from the interface resulting in a positively charged plane to neutralize the negative charges in the electrolyte. The positively charged and the negatively charged planes form a double layer structure at the interface, resulting in the potential difference across the interface. The electric field causes the rearrangement of the ions and orients the polar molecules in the electrolyte. Many models have been proposed to describe the structure and charge distribution near the metal interface. First the Helmholtz model is developed [85], followed by the Gouy-Chapman model [86], the Stern model [87], the Grahame model [88] and finally the Bockris, Devanathan and Muller (BDM) model [89]. The BDM model, which is a modification of all previous models, is now commonly used [90-93]. A detailed view of the BDM model will be explained using a Ag/AgCl electrode immersed in an electrolyte containing NaCl. If the excess charges in the electrode or in the electrolyte resulting from the electrochemical reactions are not removed by completing the current loop with another electrode in the electrolyte, the excess charges slow the electrochemical reaction down, which is preferred initially. When the rate of oxidation reaction is equal to the rate of reduction reaction, the electrochemical reactions reach equilibrium [94]. Under equilibrium, the net current through the interface is zero and the potential difference across the interface is defined as half-cell potential (E_{hc}).

The so-called standard reduction potential ($E°_{hc}$) is the half-cell potential across the interface which is measured under standard conditions, meaning solutions containing ions at unit activity (e.g. an electrode consisting of C atoms in an electrolyte containing C^+ ions at unit activity) at 25°C. The activity of an ion is equal to the activity coefficient (γ) times the ratio of its concentration and the standard concentration (1M) [95]. Activity and the activity coefficient are dimensionless. In a diluted solution, the activity of the ion is approximately equal to its concentration divided by the standard concentration (1M) [81, 96]. The $E°_{hc}$ of an electrode cannot be measured alone; another (reference) electrode is always needed to determine the potential difference between them. A standard hydrogen electrode (SHE) is an electrode scientists use for reference on all half-cell potentials. Its $E°_{hc}$ is defined as 0. The SHE is composed of a platinum electrode half immersed in a solution containing H^+ ion at unit activity and half exposed to pure H_2 gas at a pressure of 1 atm [84]. During the redox reactions, the H_2 gas oxidizes and becomes H^+ ions, while in the meantime, the H^+ ions reduce and become H_2 gas. The $E°_{hc}$ of some metal electrodes with respect to the SHE as a reference is shown in Table 3.1.

Electrode	Reaction	Standard reduction potential, $E°_{hc}$ (V)
Al	$Al^{3+}_{(aq)} + 3e^- \rightarrow Al_{(s)}$	-1.66
Zn	$Zn^{2+}_{(aq)} + 2e^- \rightarrow Zn_{(s)}$	-0.76
H_2	$2H^+_{(aq)} + 2e^- \rightarrow H_{2(s)}$	0.00
AgCl	$AgCl_{(s)} + e^- \rightarrow Ag_{(s)} + Cl^-_{(aq)}$	+0.22
Cu	$Cu^+_{(aq)} + e^- \rightarrow Cu_{(s)}$	+0.52
Ag	$Ag^+_{(aq)} + e^- \rightarrow Ag_{(s)}$	+0.80

Table 3.1: The standard reduction potential of various electrode materials.

Under non-standard conditions, the potential over the double layer E_{hc} of an electrode with respect to SHE can be determined using Nernst equation:

$$E_{hc} = E_{hc}^{\circ} + \frac{RT}{nF} ln\left(\frac{a_{O_x}}{a_{R_{ed}}}\right) \qquad \textit{Equation 3.1}$$

Where $E_{hc}°$ is the standard electrode potential against SHE, R is the universal gas constant, T is the absolute temperature, n is the number of electrons involved in the redox reactions, F is the Faraday constant, a_{Ox} is the activity of the oxidized ions, a_{Red} is the activity of the reduced ions.

The electrochemical reactions and double layer structure at the interface of a Ag/AgCl electrode and an electrolyte containing NaCl are discussed. When the Ag/AgCl electrode is immersed in the electrolyte containing Cl^- and Na^+ ions, electrochemical reactions happen, as shown in Figure 3.2 [97, 98]. The oxidation and reduction reactions happen at the interface of the Ag electrode and the AgCl coating layer resulting in excess Ag^+ ions in the AgCl coating layer. Since there are Frenkel defects in the AgCl crystal structure, the Ag^+ ions can move in AgCl by filling up the vacancies or by moving adjacent Ag^+ ions to an interstitial site [99, 100]. A Ag^+ ion diffusing to the interface of AgCl and the electrolyte interacts with the Cl^- ions in the electrolyte. Therefore, along with the oxidation and reduction reactions, the precipitation and dissolution of AgCl occur at the interface of the AgCl coating layer and the electrolyte [101].

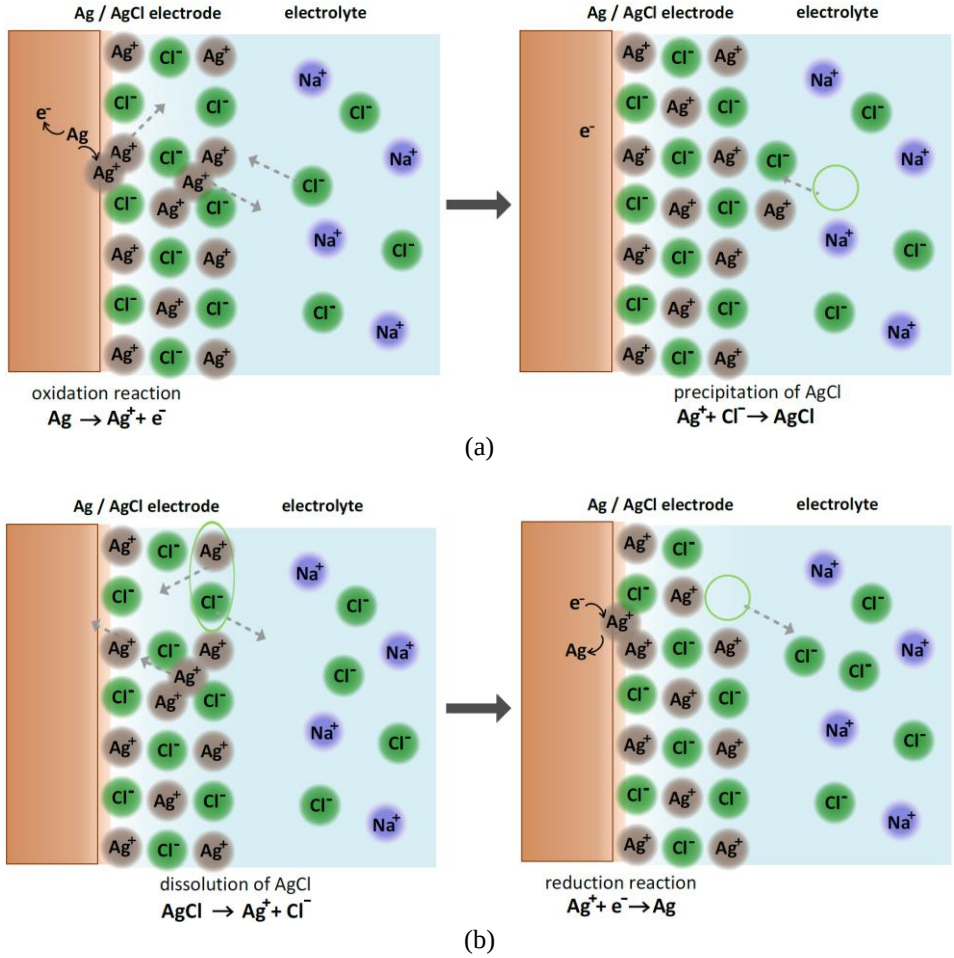

Figure 3.2: The (a) oxidation and (b) reduction reactions happen at the interface of a Ag electrode and a AgCl coated layer. The (a) precipitation and (b) dissolution of AgCl influences the rate of the oxidation and reduction reaction.

According to thermodynamics, the Ag^+ ions in AgCl prefer to be reduced, resulting in the dissolution of AgCl. The Cl^- ions are dissolved into the electrolyte, resulting in the concentration of Cl^- ions at the interface being higher than the concentration of another region in the electrolyte. The Ag electrode becomes positively charged at the interface to neutralize the negatively charged electrolyte at the interface. The separated positively charged and negatively charged planes result in a double layer structure and a potential difference across the electrolyte/electrolyte interface.

Figure 3.3 shows the BDM double layer model applied on the Ag/AgCl electrode placed in the electrolyte containing Cl^- and Na^+ ions. The potential difference across the interface

($\Phi_{Ag/AgCl} - \Phi_{electrolyte}$) causes the rearrangement of Cl^- ions and orientates the water molecules. At the AgCl/electrolyte interface, oriented water molecules align due to their dipolar character. Besides the water molecule, some partially dissolved Cl^- ions (due to dissolution of AgCl) are specifically adsorbed on the AgCl surface. The plane crossing the centers of the water molecules is defined as inner Helmholtz plane (IHP). Next to IHP, more Cl^- ions are electrostatically attracted by the positive charges of the Ag/AgCl electrode. They form an outer Helmholtz plane (OHP) which is the plane passing through the center of the aligned Cl^- ions. The positively charged plane in Ag/AgCl electrode and the negatively charged OHP behave like a capacitor and the combination of them is called 'Stern layer'. Other Cl^- ions in the electrolyte but outside the Stern layer are diffusing in all directions driven by thermal motion or by the attraction of the electrostatic field. From OHP, the concentration of the Cl^- ions decreases exponentially following the Boltzmann distribution. The region where gradients of electric field and ion concentration exist is defined as the diffuse layer. The thickness of the diffuse layer depends on the electrostatic field, the concentration of ions and the temperature [102]. Higher ion concentration or lower temperature results in a thinner diffusion layer. The diffusion layer extends until the bulk electrolyte, where no potential gradient exists. The potential difference from the Ag/AgCl electrode surface to the bulk solution is also depicted in Figure 3.3. From Ag/AgCl electrode surface to IHP and then to OHP, the potential decreases linearly while from the OHP to bulk electrolyte, the potential decreases exponentially. The combination of the Stern layer and the diffusion layer is defined as the double layer structure of the electrode/electrolyte interface. The capacitance of the double layer (C_{dl}) is often expressed as the capacitance of Helmholtz layer (C_H) and the capacitance of diffusion layer (C_{GC}) as if they are connected in series, see Equation 3.2.

$$\frac{1}{C_{dl}} = \frac{1}{C_H} + \frac{1}{C_{GC}} \qquad \textit{Equation 3.2}$$

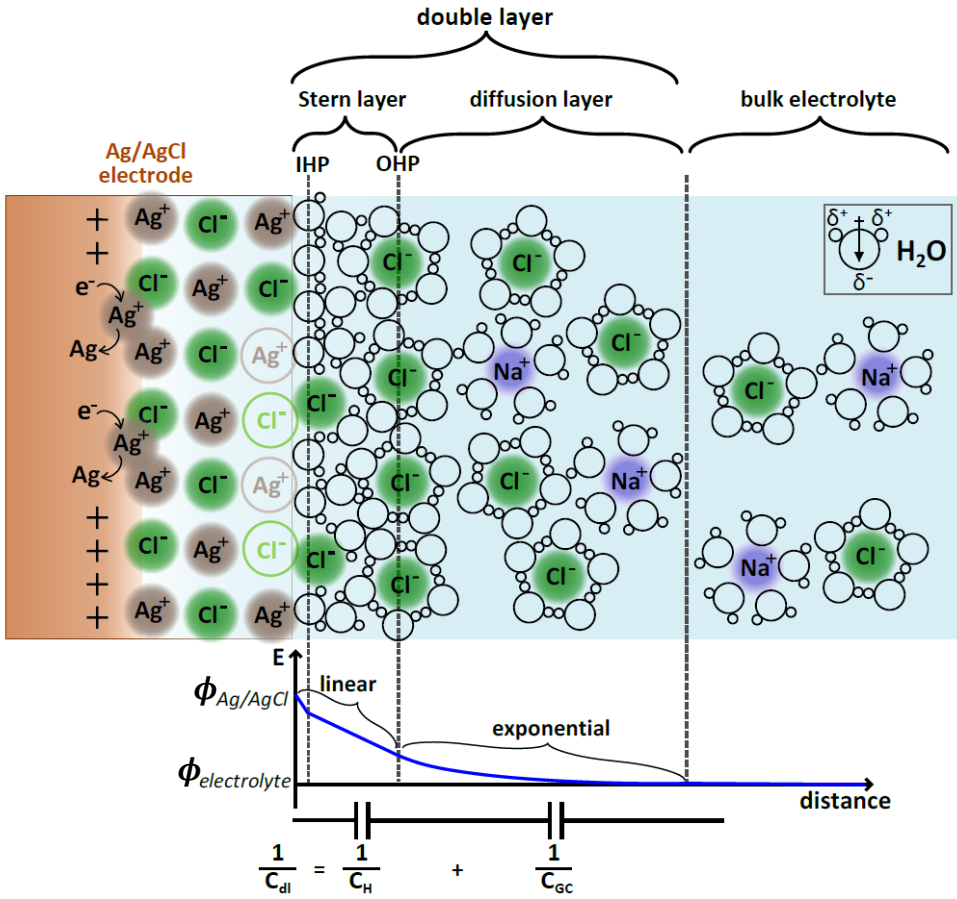

Figure 3.3: The double layer structure and electric field of the interface of a Ag/AgCl electrode and an electrolyte containing Cl^- ions. IHP: inner Helmholtz plane, OHP: outer Helmholtz plane, C_{dl}: double layer capacitance, C_H: Helmholtz layer capacitance, C_{GC}: diffusion layer capacitance, $\Phi_{Ag/AgCl}$: potential of Ag/AgCl electrode, $\Phi_{electrolyte}$: potential of electrolyte.

Assume the Ag/AgCl electrode is immersed in an electrolyte with 3M of Cl^- ions at 25 °C, the oxidation and reduction reactions happen at the interface of Ag electrode and AgCl coating layer (Ag^+ ions are reduced) are described in Equation 3.3. According to Equation 3.1, the E_{hc} across the Ag electrode and AgCl coating layer depends on the activity of Ag^+ ions. Noted that the precipitation and dissolution reactions of AgCl happening at the AgCl/electrolyte interface described in Equation 3.4 influence the oxidation and reduction reactions happening at the Ag/AgCl interface as well as influence the E_{hc} across the Ag/AgCl electrode and the electrolyte [84]. Solubility product constant (K_{sp}) reflects the ratio of the concentrations of Ag^+ ions and Cl^- ions when the reaction in Equation 3.4 is in equilibrium. Therefore, the concentration of Ag^+ ions can be determined by the concentration of Cl^- ions in the electrolyte according to the definition of K_{sp}.

The overall reaction when immersing a Ag/AgCl electrode in an electrolyte containing Cl^- ions can be expressed by Equation 3.5 as a result of combining Equation 3.3 and Equation 3.4 [97, 98]. It is known that the standard potential of the reaction shown in Equation 3.3 with respect to SHE is 0.8V and the K_{sp} of AgCl is $1.8E^{-10}$ M^2. Plugging in the parameters in Equation 3.1 and converting the natural logarithm (*ln*) to the logarithm to base 10 (*log*), Equation 3.6 reveals the E_{hc} of the reaction shown in Equation 3.5 respect to SHE. The negative sign of the potential means the reaction of Equation 3.5 (or we can say Equation 3.3) respect to a SHE electrode is in favor toward the left side. In other words, the Ag^+ ions are easier reduced than the H^+ ions in SHE are.

$$Ag^+ + e^- \leftrightharpoons Ag_{(S)} \qquad E^0 = 0.8\ V \qquad \textit{Equation 3.3}$$

$$Ag^+ + Cl^- \leftrightharpoons AgCl_{(S)} \qquad K_{sp} = 1.8\ E^{-10} M^2 = [Ag^+] \times [Cl^-] \qquad \textit{Equation 3.4}$$

The overall reaction can be written as:

$$Ag_{(S)} + Cl^- \leftrightharpoons AgCl_{(S)} + e^- \qquad \textit{Equation 3.5}$$

$$\begin{aligned} E_{hc} &= E_0 + \frac{RT}{nF} ln\left(\frac{a_{O_x}}{a_{R_{ed}}}\right) = -0.8\ volts + 0.0592\ log\left(\frac{1}{\frac{[Ag^+]}{1M}}\right) volts \\ &= -0.8\ volts + 0.0592\ log\left(\frac{1M \times [Cl^-]}{K_{SP}}\right) volts \\ &= -0.8\ volts + 0.0592\ log\left(\frac{1M \times 3M}{1.8E^{-10}\ M^2}\right) volts \\ &= -0.197\ volts \end{aligned} \qquad \textit{Equation 3.6}$$

To conclude, the E_{hc} of an electrode depends on the reference electrode, the electrode material, the temperature and the concentration of ions involved in the redox reactions. In this thesis, the potential measured across the test electrode and a reference electrode is called open-circuit potential (OCP). At equilibrium, the OCP equals to the combination of the E_{hc} of the test electrode and of the reference one.

Every interface of the two different phases has a double layer due to the unbalanced charge concentrations between them. If there are any electrochemical reactions at the interface, they happen in the double layer structure and result in a faradaic current. The double layer structure can be expressed as a capacitor, while the faradaic current flowing through the interface resulting from the electrochemistry reactions can be seen as leakage current of the capacitor. The feasibility of the faradaic current passing through the interface can be expressed as a resistor in parallel with the capacitor. Due to the double layer structure and the possible electrochemical reactions, forcing a current through the electrode/electrolyte interface results in a change of potential difference at the interface. The variation of this potential from the E_{hc} is defined as overpotential [81, 82]. Overpotential is related to the extra energy needed for a current to pass through the interface. Depending on the resulted

overpotentials, electrodes can be classified as non-polarizable and polarizable electrodes, see Figure 3.4. For an ideal non-polarizable electrode, the current can pass through the interface freely without any overpotential meaning the electrochemical reactions can happen easily at the interface. In contrast, no faradaic current can pass through an ideal polarizable electrode because of the unlimited overpotential meaning no electrochemical reactions happen at the interface. In reality, an electrode falls in between these two ideal categories. The resistivity for current passing through an electrode/electrolyte interface can be defined by the slope of injected current plotted versus the measured voltage. This is also called the 'charge transfer resistance (R_{ct})' of the electrode. The R_{ct} of an ideal non-polarizable electrode is zero while that of an ideal polarizable electrode is infinite large unlimited.

Based on the properties of the electrode/electrolyte interface introduced in the text above, a common equivalent circuit applied to represent this interface is composed of the half-cell potential (E_{hc}), a double layer capacitor (C_{dl}) and the charge transfer resistor (R_{ct}).

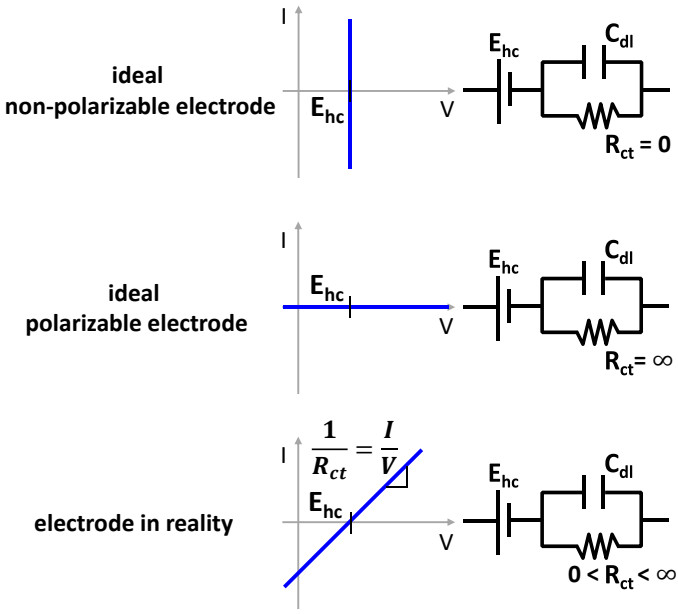

Figure 3.4: The current-voltage curves of an ideal non-polarized electrode, an ideal polarized electrode and an electrode in reality.

The value of C_{dl} can be determined using cyclic voltammetry tests (CV) [103]. During such CV measurements, a certain cyclic voltage signal is applied over the electrode and the current passing through the interface is recorded, see Figure 3.5. Starting from E_{hc}, the voltage is increased (E_{hc} + E') and then decreased (E_{hc} - E'). C_{dl} can be determined by the current recorded at E_{hc} and the scan rates of the applied voltages using Equation 3.7. The current measured at E_{hc} is used for calculation in order to eliminate the contribution of the current passing through the R_{ct}. For an electrode, different scan rates of the applied cyclic voltages result in the variations of the current-voltage (I-V) curves. The solid curve in Figure 3.5 is recorded using a higher scan rate than the dotted curve. In order to increase the accuracy of

the calculated C_{dl} value, the current values recorded using the voltage sweeps with various scan rates are used. When comparing the slopes of the I-V curves of difference electrodes, non-polarizable electrodes show steeper slopes of I-V curves while polarizable electrodes show flatter ones. Experimental results are shown in section 3.2.1.

$$I_{\,at\,E_{hc}} = C_{dl}\,\frac{dE}{dt} \qquad \textit{Equation 3.7}$$

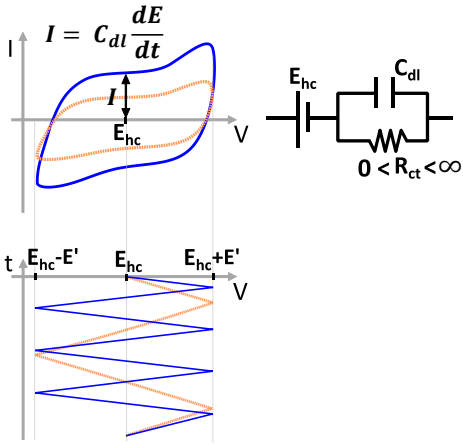

Figure 3.5: The cyclic voltammetry curves are used to determine the double layer capacitance (C_{dl}) of the electrode/electrolyte interface.

To determine the E_{hc}, R_{ct} and C_{dl} of an electrode, a reference electrode is used during the measurements to simplify the characterization. Since the preparation of the SHE electrode mentioned previously is complicated, a silver/ silver chloride (Ag/AgCl) electrode is a commonly used reference electrode. Ag/AgCl electrodes easy to fabricate and their E_{hc} is stable in electrolytes with large amounts of Cl^- ions. For a standard Ag/AgCl electrode, an Ag electrode coated with AgCl is placed in a tube filled in a 3M KCl solution. A porous plug at the bottom of the tube serves as a salt bridge in between the KCl solution and the solution outside. The redox reactions of this Ag/AgCl electrode can be expressed by Equation 3.3, Equation 3.4 and Equation 3.5 as well. Since the variation of the concentration of Cl^- ions near the electrode is limited, the E_{hc} of the Ag/AgCl electrode is stable. Besides its stable E_{hc}, an Ag/AgCl electrode is close to an ideal non-polarizable electrode [104]. Currents pass through the interface easily due to the conversion of ionic currents and electric currents (the redox reactions) at the interface of the Ag/AgCl electrode without generating a large overpotential. Besides being applied as reference electrodes, Ag/AgCl is also popular as the test electrode for biopotential measurements because the conversion of Ag+ ions and Ag atoms at the interface of the Ag electrode and AgCl coated layer is easy resulting in a fast response to the variations of the Cl^- ion concentration in the body. Therefore, the interface of the Ag/AgCl electrode returns to the equilibrium state quickly. Although the same redox reactions happen on an Ag electrode in an electrolyte containing Cl^- ions, a Ag electrode generates more noise than a Ag/AgCl electrode. This is because the process of AgCl

precipitation on the surface of the Ag electrode occurs when the Ag electrode contacts the electrolyte. The time needed for the interface to reach equilibrium is longer. Before equilibrium, disturbance of the concentration of Cl^- ions in the body influences the measured signals.

In real biopotential recording, the source of the signal is a fluctuating voltage. Therefore, the properties of the electrode/electrolyte interface when an AC voltage is passing through are also important, which is described by the impedance of the electrodes. The impedance is measured by applying an AC voltage determining the impedance magnitude and the phase changes of the interface as function of frequency.

In next section, the experimental setup, protocol of performing the OCP, CV and impedance measurements and the results are discussed.

3.2 Electrochemical measurements using IVIUM

3.2.1 Open circuit potential (OCP) and cyclic voltammetry (CV) tests using a potentiostat

Setup

An IVIUM potentiostat (Ivium Technologies B.V., Eindhoven, The Netherlands) is applied for the electrochemical measurements. The IVIUM is equipped with four electrodes: sense (S), working (WE), reference (RE) and counter (CE). The principle of a potentiostat is injecting current through WE and CE while measuring the voltage in between S and RE [105]. A 3-electrode configuration was applied for the OCP and CV tests, see Figure 3.6. In this configuration, the S and WE were shorted and connected with the electrodes under test. A Ag/AgCl electrode was selected as RE and a Platinum coated silicon wafer (around 5cm × 10cm) was used as CE. These tests were carried out when placing all the electrodes in a beaker filled with phosphate-buffered saline (PBS) solution, which is often used to prevent changes in the pH of the solution The RE was placed close to the WE while the CE was at ~5cm distance.

The OCP is the potential measured between RE and WE when there is no current passing through the CE and WE. For two electrode, the OCP is measured: a pin-shaped polymer electrode and a pin-shaped AgCl coated polymer electrode. The polymer compositions of the two electrodes were identical: both contained 43.6% of carbon. On one electrode, AgCl was coated on the tips of the pins. During the OCP measurements, not the total electrode but only 2-3 mm of the tips of the pins were immersed in the phosphate-buffered saline (PBS) solution. This depth was chosen to mimic the scenario when the electrode is contacting the skin. The OCP of both electrodes was recorded during one hour.

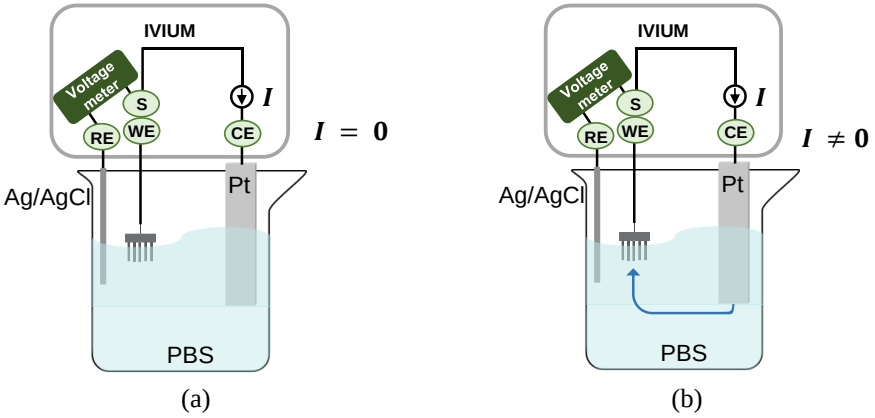

Figure 3.6: Setup to for (a) open circuit potential (OCP) measurements; (b) for cyclic voltammetry (CV) measurements.

Regarding the CV measurements, the same setup and electrodes were used but a current was forced through the WE and CE resulted a voltage across WE and RE. The voltage applied on the polymer electrode without AgCl coating was ±50 mV on top of the E_{hc}. However, the voltage applied on the polymer electrode with AgCl coating was only ±10 mV on top of the E_{hc}, because irreversible chemical reactions would occur if a large current passes through the AgCl coating layer. Eight different voltage scan rates were applied during the CV measurements: 1 mV/s, 2 mV/s, 5 mV/s, 10 mV/s, 20 mV/s, 30 mV/s, 40 mV/s and 50 mV/s. The capacitance of the interface was computed using Equation 3.7.

Results

The OCP of AgCl coated and non-coated electrodes versus the AgCl reference electrode (the RE) are shown in Figure 3.7. Some inevitable disturbances occurred during the OCP measurements, such as the vibrations of the setup due to the passage of people close to the test setup. Although the two measurements were not carried out simultaneously, they were placed in the same experimental environment. Thus, the frequency of the disturbances was similar. However, it is found that OCP of non-coated electrode contains more interferences. Its OCP is sensitive to the changes of the double layer structure of the electrode/electrolyte because the polymer material cannot provide Ag^+ ions to react with the Cl^- ions in the PBS as what happens on AgCl coated electrode. Although the recorded OCP contains these interferences, it is still found that the stabilization time of the OCP of the non-coated electrode is much longer than that of coated electrode. The AgCl coated electrode reaches the equilibrium OCP (variation < 0.1 mV/30s) in a short period while for the non-coated electrode takes around an hour to reach the same state (including some small disturbances).

The OCP of AgCl coated electrode reaches equilibrium (variation < 0.1 mV/30s) ~1 hour after immersing the electrode in the electrolyte. The OCP value, 76.76 mV, is corresponding to the value calculated by Equation 3.1. The reference Ag/AgCl applied in this test contains 3M of KCl and the PBS contains 150mM NaCl. Plugging in these parameters in Equation 3.1, results in Equation 3.8.

$$OCP = E_{hc,ref.} - E_{hc,test}$$
$$= (\mathrm{E}^0 + \frac{\mathrm{RT}}{\mathrm{nF}} ln \frac{1}{a_{Ag^+}})_{ref.} - (\mathrm{E}^0 + \frac{\mathrm{RT}}{\mathrm{nF}} ln \frac{1}{a_{Ag^+}})_{test} \quad \textit{Equation 3.8}$$
$$= \frac{RT}{nF} ln \left(\frac{[Cl^-]_{ref.}}{[Cl^-]_{test}}\right) = 0.0592\, log \left[\frac{3M}{150mM}\right] = 77\, mV$$

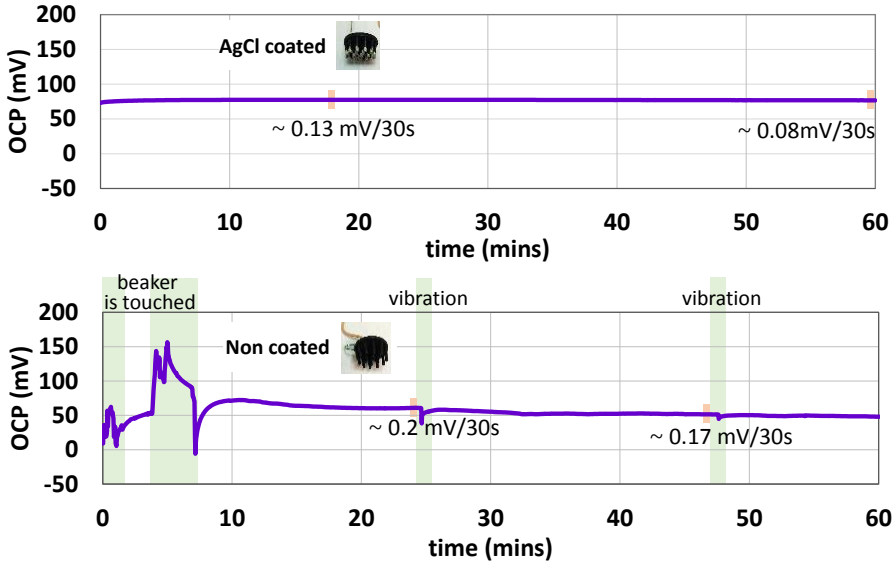

Figure 3.7: The OCP of pin-shaped electrodes with and without AgCl coating on the pins.

The CV results of the AgCl coated polymer electrode is shown in Figure 3.8. Comparing to the CV results of the non-coated electrode shown in Figure 3.9a, it is obvious that the current passes much more easily through the interface of coated electrode. It can be concluded that the AgCl coated electrode behaves more like a non-polarizable electrode while the non-coated one behaves like a polarizable electrode. A polarizable electrode reacts like a capacitor during the CV tests. The electrode is charged when the applied voltage increases (from E_{hc} - E' to E_{hc} + E', -2 to 98 mV in Figure 3.9a) and is then charged with opposite polarity when the applied voltage decreases (from E_{hc} + E' to E_{hc} - E', 98 to -2 mV in Figure 3.9a). The positive and negative charges distributed at the interface of the electrode/electrolyte result in the hysteresis effect shown in Figure 3.9a. The current does not change direction immediately at the voltage transients and the current is not constant because the non-coated electrode is not an ideal polarizable electrode, in other words, it is not an ideal capacitor [106]. The diffusion and rearrangement of ions in the electrolyte decelerate the reaction of the electrode/electrolyte system to the variation of the applied voltage. It is also found that a larger current is recorded using a faster scan rate, as described in Equation 3.7. This is because the amount of charge passing through per unit area of cross section per second (current) is larger with a faster scan rate. The C_{dl} of the coated electrode cannot be determined from

Figure 3.8 because conversion of the ionic current and electronic current at the interface is easy and the double layer structure cannot be well defined. The C_{dl} of the interface of the non-coated electrode and the electrolyte is derived using the current data recorded when applying different scan rates, see Figure 3.9b. The C_{dl} of the non-coated electrode is 28 nF. The value is not normalized to the surface area because it is hard to define the contact area of the pin-shaped electrode to the electrolyte. The small C_{dl} of the non-coated electrode, which is in the same range as the non-contact electrodes (1-100 nF) discussed in section 1.2.1, results in high impedance of the electrode/electrolyte interface. In the next section, the experimental method and the results of the impedance of polymer electrodes are discussed in detail.

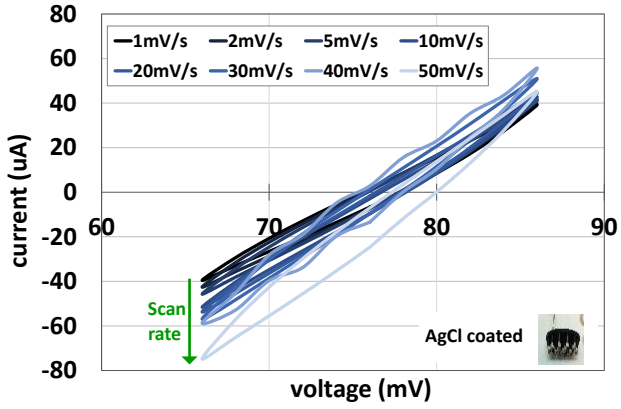

Figure 3.8: The current-voltage curves of the CV measurements of AgCl coated polymer electrode.

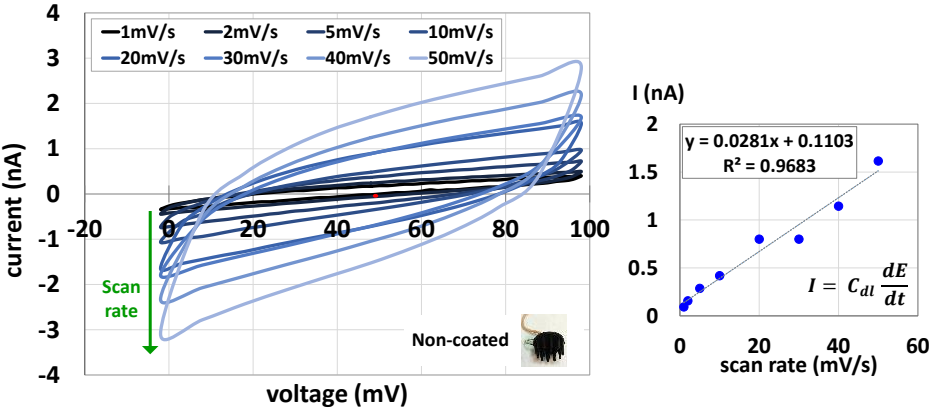

Figure 3.9: (a) The current-voltage curves of the CV measurements of non-coated polymer electrode. (b) The plot of current versus scan rate for C_{dl} calculation.

3.2.2 Principle and setup of impedance measurements using a potentiostat

The IVIUM coupled with an impedance analyzer is also used for the impedance measurements. As mentioned before, the IVIUM is equipped with S, WE, RE and CE electrodes. Besides the 3-electrode configuration applied for OCP and CV measurements can be used for impedance measurement, 2-electrodes and 4-electrodes configurations can be applied as well depending on the interested impedance. Figure 3.10 shows the schematics of applying these electrode configurations for impedance measurements on the skin. The impedance of the interface of electrode and skin is represented by a capacitor in parallel with a resistor as discussed in section 3.1.

A 2-electrodes setup is connecting WE and S together to one electrode; while connecting CE and RE together to the other electrode. This setup measures the voltage crossing the two electrodes and the current flowing through them. The impedance computed by the measured voltage and current reveals the impedance of electrode-skin interface and that of the tissue in between the two electrodes.

A 3-electrodes setup is connecting WE and S together to the electrode to be studied. In addition, the CE is connected to the counter electrode and RE is connected to the reference electrode. In this setup, the current goes through the CE and WE electrodes. The voltage is acquired in between the S and RE electrodes. Since no current is passing through the RE resulting no voltage drop, the measured voltage can be considered mainly attributed to the WE and the impedance of the skin beneath the WE. The impedance acquired in this setup indicates the electrode/skin impedance of the WE.

A 4-electrodes setup is connecting WE, CE, RE and S to four different electrodes. The WE is close to S while CE is close to RE. In this setup, the current only passes through CE and WE and the voltage across the S and RE is measured. This is a technique to acquire the impedance of the tissue of the inner layer of skin between the WE and CE [107, 108].

In this thesis, the 3-electrodes configuration is selected for characterizing the electrode/skin impedance of pin-shaped electrodes.

When using IVIUM for impedance measurement, an adjustable AC current is sent through WE and CE to maintain a 25 mV voltage across the RE and S. The schematic of the setup used for characterizing the electrode/skin impedance in this thesis is shown in Figure 3.10b. The impedance Z, being the impedance of the electrode/skin interface, is computed internally by the IVIUM. The impedance measurement is a continuous recording of electrode-skin impedance swept through a frequency range. Since every type of biopotential signal has it's own frequency distribution (Figure 1.2), recording the impedance value through a frequency range provides understanding of the characteristics of electrode during different biopotential recordings but it also allows to model the electrode-skin interface using electronic circuits. Therefore, impedance is measured through frequencies from 0.1 Hz up to 100 kHz in this thesis.

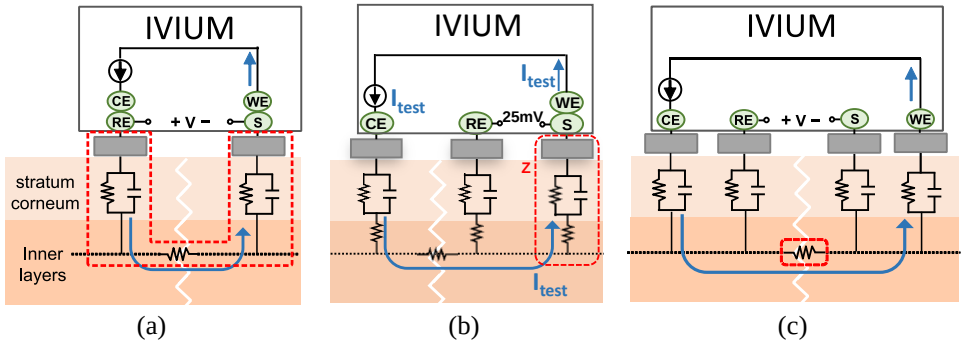

Figure 3.10: Electrode configurations for impedance measurements. The electrode/skin interface is typically modeled using a parallel RC circuit [109]. More studies of the equivalent model of electrode/skin interface will be introduced in section 3.3. (a) 2-electrodes configuration for electrode-tissue and inner tissue impedance measurements. (b) 3-electrodes configuration for electrode-tissue impedance measurement. (c) 4-electrodes configuration for inner tissue impedance measurement.

3.2.3 Impedance measurements of various polymer compositions of cylindrical shaped electrodes

Before the impedance of the polymer electrodes are measured on the phantoms and forearm, the impedance of the polymer materials themselves are characterized. The cylindrical shaped bulk electrodes (Figure 3.11) with various carbon contents in the polymer are used for the measurements. Two brass films were used to contact the right and left surface of each sample. A clamp was used to stabilize the bulk sample in between the two metal plates, see Figure 3.11. The RE and CE of IVIUM were shorted and connected with the first metal plate while the S and WE of IVIUM were shorted and connected with the other metal plate. Apart from the cylindrical shaped bulk electrodes, the impedance of conventional ECG wet electrodes (ARBO H124SG, Kendall, Mansfield, MA, USA) was measured for comparison. To do this, two wet gel electrodes were placed back to back (both gel parts sticking together) and the electrode snaps were used as connectors for the electrode input of the IVIUM tool [110].

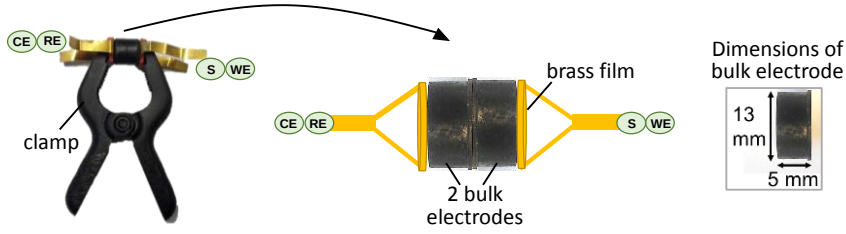

Figure 3.11: Setup and electrode configurations of impedance measurements of cylindrical shaped electrode.

A 25 mV signal across the RE and S was generated by the IVIUM potentiostat and impedances were measured when the signal swept through frequencies from 0.1 Hz up to 100 kHz. In this thesis, only the impedance at 10 Hz is shown in the graphs to reduce the obtained information down to the frequency band of interest for biopotential signals, which is a few to hundred Hz [8]. For correct comparison of various electrodes, the size of the electrode should be taken into account [110]. Obviously, a larger contact area results in a lower contact resistance. Since the surface area of wet electrode and the cylindrical shaped electrode is different, the measured electrode impedance is always normalized towards the surface area of the electrodes. As such, the normalized impedance is independent of the electrode geometry but is an intrinsic property of the material itself [111]. A study of non-normalized and normalized impedance of wet electrode will be discussed in section 3.2.4. The area used to normalize the impedance data recorded on phantoms and forearm is described in the same section.

The additives added in the cylindrical polymer electrodes are 2 mm stainless steel fibers (SS) and carbon. Electrodes containing only one or both of these additives were tested. Figure 3.12 shows the normalized impedance at a signal frequency of 10 Hz of cylindrical shape electrodes containing various amount of additives. The impedance of the electrodes containing SS or SS and ~20 % of carbon (SS+carbon) are shown in Figure 3.12a. With only SS, the impedance remains very high and is not influenced by the amount of SS. This might be because the quantity of stainless steel fibers added to the polymer is not sufficient to create a continuous connection between the stainless steel fibers in order to conduct electrical current. Other authors working also with polymer containing SS reported that the surface resistance of their EPDM polymer containing SS fibers reduces from 30 kohm to ~0 ohm when the amount of SS increases from 15% to 26% [112]. In our experiments, SS quantities are lower. Furthermore, when rubbers with additives are molded, it is known that often a ‘skin’ is present that is richer in polymer and less in filler (SS in this case) in almost all rubbers [113]. The uniformity of the SS fibers in the molded polymer was studied by scanning electron microscope (SEM) images, see Figure 3.13 for rubber with 13.2% of SS. The images show that the SS is present in high quantities at the cutting edge of electrodes, while no SS is found at the sidewalls (‘skin’) of the same electrode. This non-uniform distribution of SS in the polymer electrodes might be another contribution to the high impedance even though the total amount of SS increases from 3.5% to 10.8%. Further increasing the amount of SS in our polymer electrodes or using longer SS in our polymer electrodes is theoretically an option, but there are important practical reasons not to do this: it would reduce the feasibility of mixing SS with polymer and filling the mixed material into the mold with thin and 2 mm short pins shown in Figure 2.3a. In addition, materials with high SS loads scratch the (expensive) molding tool during electrode fabrication.

Adding ~20% carbon in the stainless steel containing polymer reduces the impedance, and when this this 20% of carbon is present, a larger amount of SS helps to reduce the impedance even more. Although the impedance decreases with the amount of SS, the impedance of electrodes containing around 10% of SS + 20% of carbon is still around 100 kΩ. Although these SS+carbon electrodes contain ~20% of carbon, their impedance is much higher than the electrode containing ~30% of carbon without SS, as shown in Figure 3.12b. This implies

that there is a synergistic effect when both SS and carbon are present. The high impedance of SS+carbon electrodes suggests that he SS and carbon easily attach to each other resulting in a non-uniform distribution of the carbon.

In contrast to the electrodes containing only SS, for electrodes containing only carbon, the impedance decreases with the increasing of carbon content. The impedance of the wet electrode, acquired by placing two wet electrodes back to back, is found to be higher than that of polymer electrodes containing carbon (see Figure 3.12b). These results show that adding carbon decreases the electrode impedance more effectively than adding SS. Since SS might scratch the molding tool and contaminate other rubber formulations prepared for regular products of Datwyler (risk of defects and complaint in Datwyler's regular production), we can conclude that carbon is a more interesting polymer additive then SS.

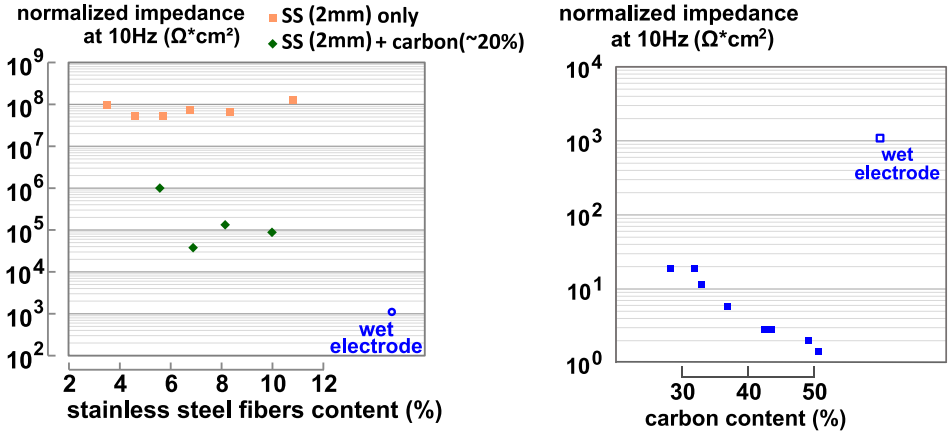

Figure 3.12: The impedance of cylindrical shape polymer electrodes containing various weight percentage of (a) stainless steel fibers (SS) only and SS with carbon; (b) carbon.

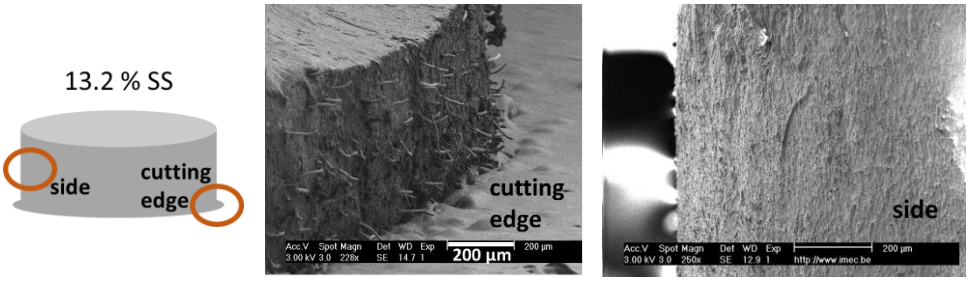

Figure 3.13: The SEM images of electrode with 13.2% of stainless steel fibers. The stainless steel fibers can be clearly seen at the cutting edge while they cannot be found at the side of electrode.

3.2.4 Impedance measurement of various polymer compositions of pin-shaped electrodes on phantoms and human skin

It has been reported that the impedance value will differ from subject to subject and even within time for the same subject [75, 76], the combination of the electrode with stable phantom surfaces is also evaluated, as a reference. A silicon wafer coated with platinum (Pt film) and a cloth soaked in silane solution (wet cloth) are used as phantoms to utilize well-controlled and stable conditions for impedance characterization. Besides the phantoms, the electrodes are placed on forearm skin of various subjects to characterize the electrode/skin impedance. The experimental setup of impedance measurements of bulk material and pin-shaped electrodes are discussed in this section.

A 3-electrodes configuration of the IVIUM potentiostat (see Figure 3.10b) was used to acquire the impedance of skin/phantom-electrode combination. Conventional wet electrodes were used as counter (CE) and reference (RE) electrodes for the IVIUM tool. They were placed 10 cm apart from each other on the skin/phantoms, and left in place for 30 min before starting the measurements, in order to allow impedance stabilization at the contact interface [114]. The electrode under test was connected with the working (WE) and sense (S) cables of IVIUM and placed next to the reference electrode (RE), see Figure 3.14a and b. As working electrodes, the polymer electrodes were used, but a wet gel electrode was also characterized in order to compare this result to the various polymer electrode results.

(a) (b)

Figure 3.14: Setup and electrode configurations of impedance measurements of pin-shaped electrodes on (a) phantoms and (b) skin.

As explained in section 3.2.3, impedances are evaluated over a range of frequencies, but only the impedance values corresponding to a 10 Hz input signal will be shown in this text in order to simplify the graphs. For a correct comparison of various electrodes, it is important to take also the electrode size into account. In case 2 electrodes consist of the same material, the larger electrode will have the lower impedance. Hence to compare various electrode materials or designs, the lateral electrode dimensions have to be taken into account. Therefore, the impedances are always normalized with respect to the skin area which is covered by the electrode, not with respect to the contact area of the skin and the pins of electrodes. In case the normalized impedance would be calculated using the real contact area between pins and skin, then the normalized impedances for pin shaped electrodes would be much lower and use of the polymer electrodes would look much more attractive. Nevertheless, the author of this work is not considering this approach correct, since if a certain area of the skin is covered by one electrode, no other electrode can be placed on the same area, that skin area is the occupied area when applying the electrode. The skin area of a conventional wet electrode is

equal to the gel area, while that of pin shaped electrode is the total base area, as is plotted in Figure 3.15. Mention that the base area is much larger than the pin-skin contact area for the pin shaped electrode, hence the normalization towards the base area will result in higher impedance values for the pin shaped electrode.

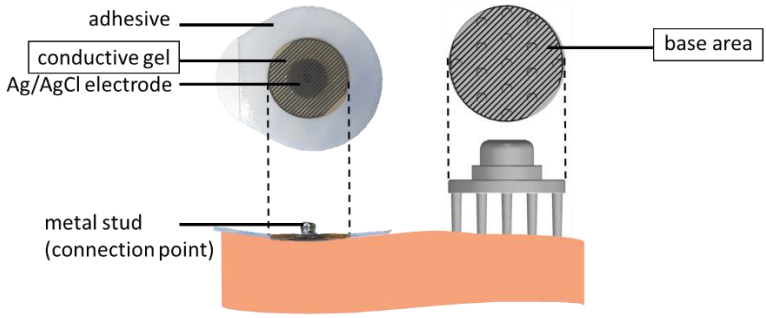

Figure 3.15: The area of wet electrode and pin-shaped polymer electrode used for normalized impedance calculation is the gel area and the base area, respectively.

This concept of normalization is tested by using wet electrodes with different contact areas. Figure 3.16a shows the non-normalized impedance of wet electrodes with different conductive gel contact area attached onto the skin via the adhesive pad surrounding the electrodes. The contact area means the area of the gel contacting the skin. As was expected, the impedance increases with the decreasing electrode/skin contact area. Figure 3.16b shows the data of Figure 3.16a multiplied by the contact area of each electrode, hence the so called normalized impedance. It is found that the normalized impedance of all tested gel electrodes is similar, in spite of their different contact area. Hence this normalized impedance is a good indication of the electrode material properties, and it is the scientific correct way to compare the impedance of electrodes with different skin contact area.

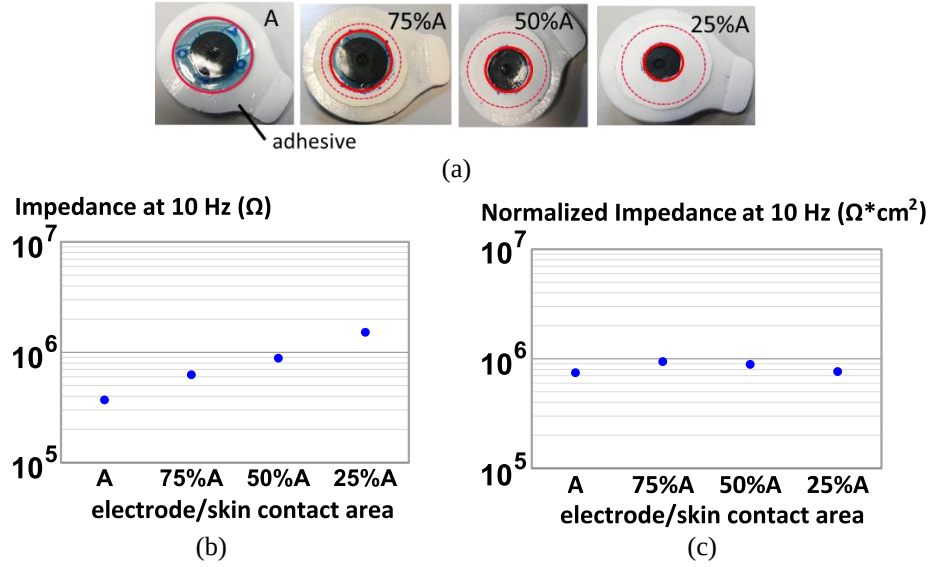

Figure 3.16: (a) Wet electrodes with different conductive gel contact area attached onto the skin via adhesive around the electrodes. (b)Non-normalized impedance of wet electrode with various contact area with the skin. (c) Normalized impedance of wet electrode with various contact area with the skin.

- Impedance of conventional gel electrodes

In order to verify the setup and measurement protocol mentioned in previous sections, the impedance of conventional gel electrodes was carried out first. It has been mentioned already that the impedance varies with time and between subjects. The results shown in the following section support this statement. In addition, the significant effect of the electrode size on impedance is discussed in this section as well.

Impedance variation through time on the same subject

Figure 3.17 shows the impedance of a wet electrode measured on different days on one subject. A lot of variation is seen, and this effect is known in the medical world [115]. The impedance variation might be caused by differences in temperature, humidity and the change of skin properties. This variability complicates the comparison of electrode materials and electrodes shapes, since the tests are never performed on exact the same skin position on exact the same time. Therefore, it is essential to perform additional measurements of the impedance of polymer dry electrodes on well-controlled phantoms, in order to study the impedance of material itself in a very reproducible way.

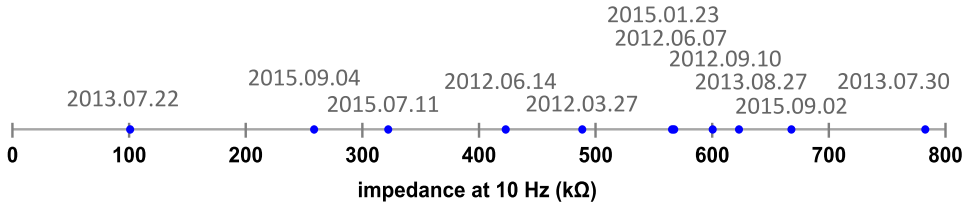

Figure 3.17: The impedance of wet electrode on the left forearm of the same subject on different days from 2012 to 2015.

- Impedance of electrodes containing various material compositions

In this section, the impedance of polymer electrodes containing various additives is shown and discussed. The additives added in the polymer electrodes were stainless steel fibers (SS), carbon nanotubes (CNT) and carbon. Only one additive or the combination of two additives was tested. For all the measurements during this additives optimization discussed in section 'various conductive additives', the electrodes with 2 mm pin length were used to mimic the scenario of using pin-shaped electrodes on the skin for biopotential measurements. Electrodes with pins longer than 2 mm are not used because it is more difficult to ensure proper electrode/skin contact when fixing the electrodes on forearm skin using medical tape.

Various conductive additives

Although it is known that SS is not a proper additive of polymer electrodes based on the results shown in Figure 3.12a, the impedance of the pin-shaped electrodes containing SS is still characterized on the phantoms and human skin to gain insight into the SS/electrolyte interactions. In Figure 3.18a, the impedance of polymer electrodes with SS only and with SS+carbon on Pt on cloth wetted by electrolyte is shown. The SS+carbon samples contain ~20% of carbon. With only SS, the impedance remains very high and is not influenced by the amount of SS. Adding ~20% carbon will reduce the impedance, again the amount of SS is not relevant. Figure 3.18b shows the impedance of polymer electrodes with SS only and SS+carbon, but this time measured on the forearm skin of one subject. The impedance of the 'SS only' samples is as high as on Pt and does not change with different amounts of SS. For SS+carbon samples, the impedance values are only slightly lower than 'SS only' samples. These tests are measuring both skin+electrode impedance, and the skin impedance is rather high. Hence obtaining higher impedance values on skin than on Pt and on cloth, is not surprising. So ~20% of carbon helps to reduce the impedance of SS sample material itself, but the reduction is not obvious on human skin. Besides the disadvantages of adding SS in the polymer as discussed in section 3.2.3, the impedance of electrodes containing SS only or SS + carbon measured on the skin is also high, which is confirmed by other literature measuring the impedance of stainless steel electrodes [116, 117]. Again it can be concluded that SS is not an interesting additive for polymer dry electrodes.

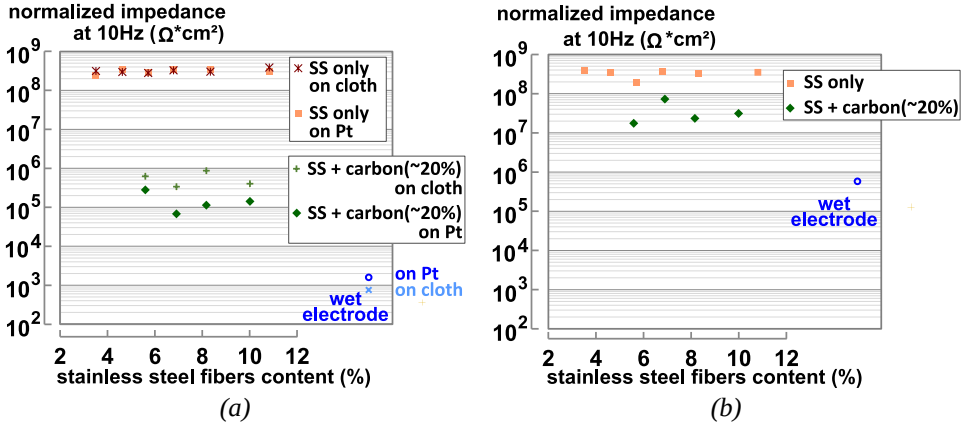

Figure 3.18: The impedance of electrodes with stainless steel fibers and carbon (a) on Pt and on the cloth wetted by electrolyte, (b) on skin.

Another good conductor gaining lots of attention last years are CNTs. Figure 3.19 shows the impedance of CNT+carbon sample compared to carbon only samples, all measured on phantoms. The impedance of carbon only samples decreases clearly with increasing carbon content ratio. Furthermore, when mixing ~9% of CNT with ~15% of carbon, the impedance value approaches that of the sample with ~30% carbon only, hence CNT is strongly reducing the impedance. However, there still exist controversial opinions about the use of CNT containing samples on humans. At this moment, it is not proven yet under which conditions the use of CNTs is safe. Moreover, the impedance can be easily lowered by increasing the carbon content, without any risk for the human using the electrodes. Therefore, CNT was not used in any further test and not considered anymore as interesting additive in polymer dry electrodes. It should be noted however that adding carbon will result in hardening of the polymer, hence the amount of carbon should remain limited, as discussed in next paragraph.

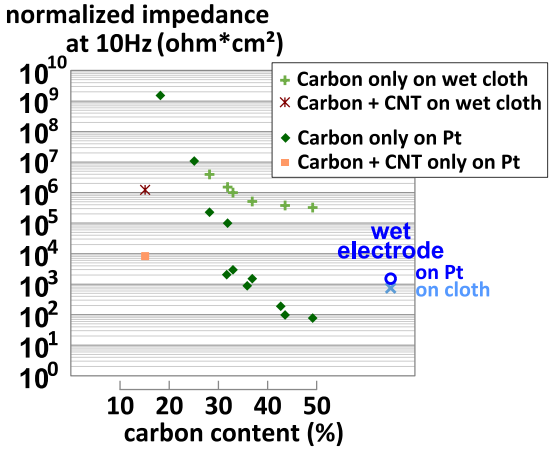

Figure 3.19: Normalized impedance of conductive polymer electrodes with carbon only and with carbon + CNT on Platinum film and wet cloth.

The impedance of these carbon only samples is also measured on the forearm skin of four different subjects, see Figure 3.20 and Figure 3.21. In Figure 3.20, the impedance of electrodes containing various amounts of carbon on Pt, on wet cloth, and on the skin are shown. The data points labelled with "on human skin" is the averaged impedance of the data from 4 subjects. The impedance of individual subjects is presented in Figure 3.21. Though the variations of different subjects is around 5-10 times magnitude, the trend of impedance decreasing with increasing carbon content ratio can be clearly seen and is similar for all substrates. When comparing the measurement on human skin with those of cylindrical shaped electrodes, the impedance is increased by the order of 10^6 Ω for all rubber material compositions. It is reported that the impedance of skin, mainly contributed by the SC layer, is around a few hundred KΩ to 1 MΩ per square centimeter at 10 Hz input signal frequency [114, 118, 119]. This explains why the impedance of dry electrodes on human skin increases approximately by the order of 10^6 Ω. For wet electrodes, the impedance variation between measurements on human skin with those of back-to-back assembly is rather small because of the skin hydration effect of the gel, which reduces the impedance of SC layer. The impedances of the wet electrode obtained by back-to-back measurements, on Pt and on wet cloth phantoms have all similar values, since this impedance is generated by the gel electrode itself, instead of the interface of the gel to the measurement surface. The trend of impedance on Pt is not as well correlated as it is on other surface. This might be because the Pt metal film has a rather flat and rigid surface. Though the force of placing the electrodes on Pt is well controlled, it is hard to estimate the bending direction and amount of contact area when the pins contact the Pt surface. A small non-uniform force can cause an important change of contact area. This might explain the nonlinear decreasing of impedance when increasing the carbon content on Pt.

The impedance of the highest carbon content ratio (49.2%) is around 10 times larger than conventional wet electrode. More carbon can be added in polymer electrodes but this will increase the hardness and reduce the elasticity, which has a negative effect on user comfort and processability. More details regarding the elastic molulus of the polymer electrodes will be discussed in section 3.4.

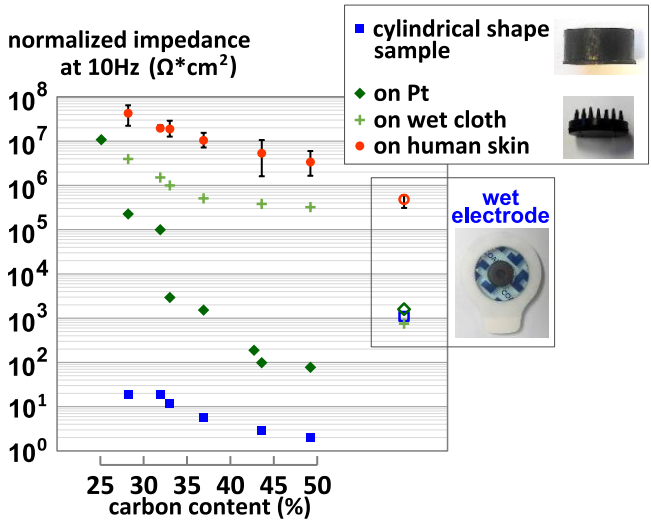

Figure 3.20: *The impedance of cylindrical and pin-shaped electrode with carbon only on phantoms and human skin. The error bars reveal the variation between the different subjects.*

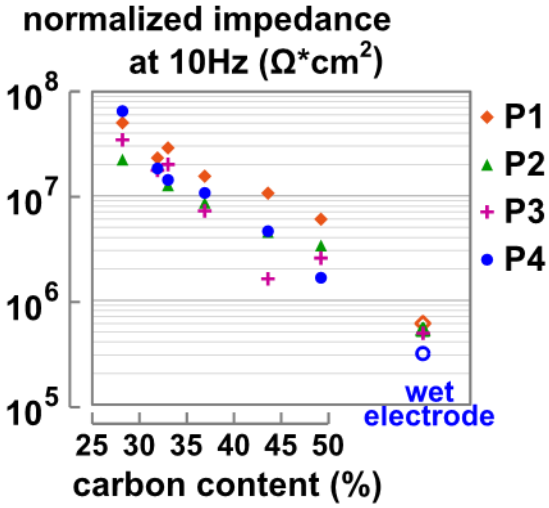

Figure 3.21: The impedance of electrode with carbon black only on human skin of 4 subjects.

- Various polymer electrode designs (pin configurations)

Until now, only the impedance of cylindrical shaped electrodes and electrodes with 2 mm pins is discussed. In this section, the impedance is evaluated of electrodes with longer pins on the forearm skin. Three designs with different pin configurations containing various carbon content are compared. All these electrodes have a 13 mm diameter round base with

pins on it. The amount of pins on the bases is 12, 15 and 19. The length of all the pins is 5 mm because only the electrodes with 5 mm pin length, designed for EEG measurements, are fabricated in various pin designs. The top of the pins is flat and the top area of each pin is the same. The configurations of these three types of electrode and their impedance on the forearm of one subject are shown in Figure 3.22. For all three designs, the impedance decreases with the increasing of carbon content. It is also found that the impedance of the electrode with 19 pins is slightly lower than that of other two configurations. The larger contact area of the pins and skin of the electrode with 19 pins results in the lower impedance. Although electrodes with 19 pins show the lowest impedance, they might not be suitable for certain hairstyle. It can be concluded that the optimal pin number of the electrode is not strongly related with impedance, but rather defined by the application of the electrodes: 19 pins are too dense for hair penetration while 12 pins are too sparse to withstand the force from the fixation device, resulting in severs pin bowing. Therefore, further in this thesis, the electrode with 15 pins will be applied for the EEG monitoring.

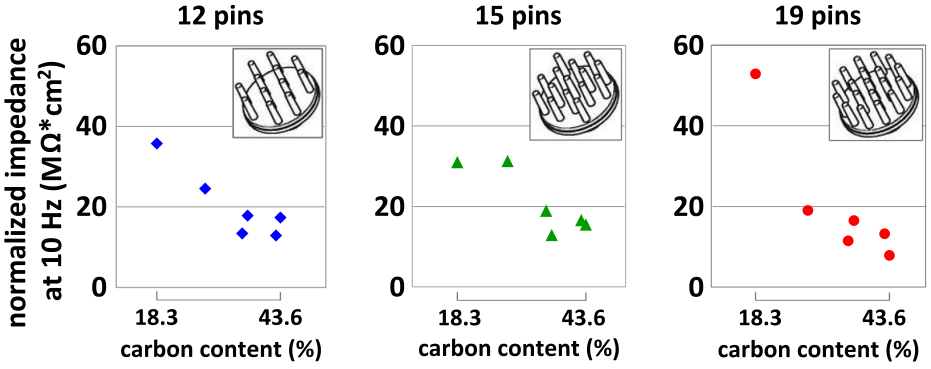

Figure 3.22: *The impedance of electrodes with three pin configurations on one subject's forearm. The y-axis has unit of MΩ*cm².*

3.2.5 Improvement of the skin/electrode contact

According to the results presented in section 3.2.4, it is know that the SC layer of the skin has a high impedance. It is reported in [22] that the impedance of SC layer can be represented by a 1M Ω resistor and a 10 nF capacitor connected in parallel. In order to decrease the impedance, the resistance of SC layer can be reduced by thinning the SC layer while the capacitance value of the SC layer can be increased by also thinning the SC layer and increasing the water content in it [120]. Therefore, the skin is often abraded by abrasive gel before the electrodes are mounted on the body for clinical measurements, especially in case of non-hairy skin [121]. In, addition, hydrating the skin with lotion or other types of ionic fluids reduces the impedance. This is because the dielectric constant of water (80) is about 20-40 times higher than of SC layer (2-5) [120]. It is reported in [122] that the resistance of SC layer is 14 times lower and the capacitance is 1.5 times higher when the outermost SC is exposed to hydrating conditions as compared to the case of more dehydrating conditions. The water content of the SC layer depends on (1) water permeability of the epidermis, where the water content of the deepest layer of epidermis (stratum basale layer) is higher than that of

SC layer [20, 123]; (2) water-retaining properties of the SC layer and (3) the rate of evaporative water loss from the skin surface [124]. The SC layer consists of dead flattened keratin filled corneocyte cells. In between the corneocyte cells, there is lipid lamellae where conductive ions need to pass through from the deeper layer of skin to the electrodes on the skin surface during biopotential measurements. The corneocyte cells and the surrounded lipid are arranged in a "bricks and mortar" structure, which forms a permeability barrier of water and small molecules. It is presented in [125] that the permeability of water and small molecules increases when more solid lipids are transformed to liquid lipid. The fluidity of lipids in the SC layer increases when temperature and relative humidity (RH) of the environment increase or when the water content in the SC layer increases. This explains that moisturizers which are increasing the water content of the skin, result also in higher water and conductive ions permeability [126]. The water-retaining properties of SC layer depend on the size of corneocyte cells. Water swollen corneocyte cells expand which results in a longer transmission path for water and small molecules, hence in less water loss [127].

As mentioned before, the usage of skin pretreatments such as skin abrasion and skin hydration is reducing the electrode/skin impedance, which will lead to a higher quality of biopotential recording, as illustrated in publications [128, 129], describing the reduction of artifacts of ECG signals due to skin treatments. Therefore, the skin-electrode impedance after various skin pretreatment techniques is also investigated in this section.

- Abrasive gel

For this study, the polymer dry electrodes contained 43.6% of carbon and had 2 mm pins, and four tests subjects were involved. The electrodes were placed on forearm using medical tape. The impedance was measured immediately after the electrode was mounted. Then the electrode was removed and abrasive gel (Nuprep Skin Prep Gel from Weaver and Company, USA) was applied on the electrode location. The gel contains water and Aluminum oxide, which is used for microdermabrasion. The skin was gently rubbed for 30 seconds, then cleaned first by wet tissue paper and then by dry tissue paper. The polymer electrode was placed back on the treated location and the impedance was measured continuously during 1 hour.

The impedance results are shown in Figure 3.23. It is found that the electrode/skin impedance is reduced 5-10 times by using abrasive gel. It is comparable with the values shown in publication [130], in which is reported that the electrode/skin impedance decreases from 200 kΩ to 10 kΩ after using the abrasive gel. This implies that the SC layer is thinned by the gel and the abrasive gel hydrates the skin, so the impedance of skin is reduced. However, the impedance does not stay low. The impedance recorded on all subjects increases with time. For one subject, only 30 minutes after applying the abrasive gel, the impedance was again equal to the one on untreated skin. It is know that the SC layer regenerates in about 24 hours [129]. Thus, this impedance increment is not caused by repair of the SC layer, but probably by moisture evaporation. In other words, it can be proved that the main cause of the impedance decrement is the water or the conductive ions in the abrasive gel. Also the authors of [131] claim that abrading the skin is an effective way to reduce the impedance for the first

half hour. Hence, it can be concluded that the abrasive gel indeed decreases the impedance of electrode/skin, but the effect is very short.

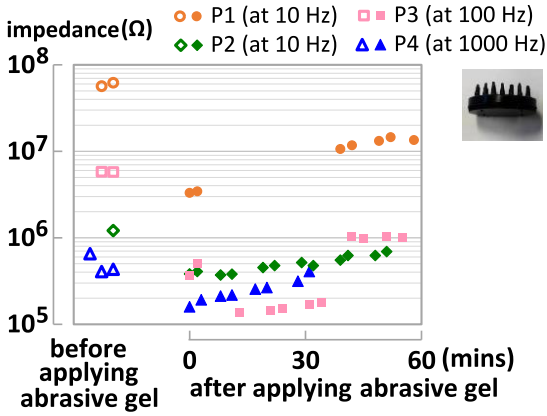

Figure 3.23: *The impedance of pin-shaped electrode before and after applying abrasive gel on the skin of 4 subjects.*

- Conductive cream

Highly conductive cream designed for routine use in electro-medical procedures contains mainly water and chloride ions to increase the water content of the skin and create conductive channels for chloride ions during biopotential measurements. The polymer electrode used to study the influences of hydration lotion on impedance of electrode/skin was the one with 19 5-mm length pins (see Figure 3.24). The carbon content of the electrode was 43.6%. The protocol of applying conductive cream was similar to applying abrasive gel. The impedance was measured immediately after mounting two identical polymer electrode on the forearm of one subject. These two electrodes were close to each other. Then the electrodes were removed and cream was applied. Two types of cream were used: EC33 (Grass Technologies) and Signa Cream (Parker Laboratories). The EC33 is a cream containing 0.5% of NaCl and is specially designed for skin resistivity measurements [132]. The Signa cream contains cetyl alcohol, potassium chloride (KCl) and reverse osmosis (RO) water. The cetyl alcohol forms a protective barrier on the skin that reduces water evaporation and hence locks in the moisture. A thin layer of each cream was applied on the locations of two electrodes respectively. The cream was not removed and the electrodes were placed back at the same skin locations. The impedance was measured immediately and after 30 and 60 minutes.

The impedance results are shown in Figure 3.24. The impedance decreases nearly 100 times after applying the EC33 cream and around 25 times after applying the Signa cream. This is because the chloride ions in both creams create conductive channels in between the electrodes and skin. The conductive channels result in an easier conversion of ionic currents and electronic currents. Similar to applying the abrasive gel, the impedance increases again after the treatment. However, the increase of the impedance is slow. Possible explanations is the

evaporation of the electrolyte of the cream or the cream is slowed down due to the effect of cetyl alcohol. To conclude, both creams reduce the impedance but this does not last long.

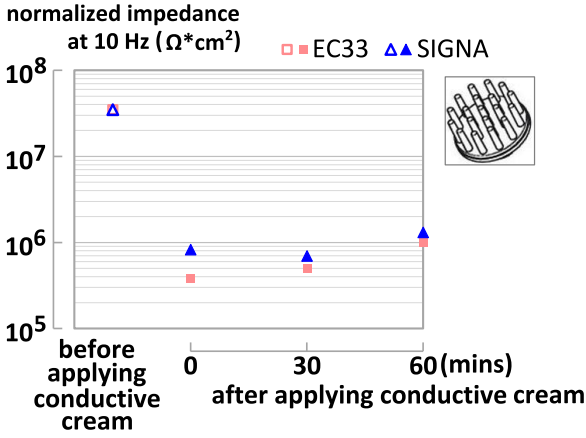

Figure 3.24: *The impedance of pin-shaped electrode before and after applying conductive gel on the skin of one subject. Two types of conductive gel were applied: EC33 cream and Signa cream.*

- Sweat

The cream applied in last section is a conductive agent with a constant concentration. In fact, sweat generated from human body can also be considered as a conductive agent for biopotential measurements. Since the composition of sweat and the sweat rate vary between persons, it is difficult to perform a well-controlled evaluation of the influence of sweat on the skin-electrode impedance. The electrode used for this test was the same as the one used for abrasive gel study. The impedance was measured initially as a reference. Then plastic film was wrapped around the forearm with all three (working, reference and counter) electrodes. The subjects biked 15 minutes to produce sweat. The plastic film speeded up the sweat process when the subjects exercised. After the exercise, the plastic film was removed and the measurement started immediately. The impedance was recorded continuously for 1 hour.

The results are shown in Figure 3.25. The impedance decreases around 10 times during the exercise and increases gradually with time after exercising. One hour after exercising, the impedance of three subjects returned to values similar to the impedance before exercising. It has been well studied that the sweat in the sweat ducts provides highly conductive channel for ions to pass through the SC layer [133, 134]. This results in reducing the impedance of the skin, but the impedance increases again when the sweat evaporates. It has to be noted as well that though sweat reduces the electrode/skin impedance, too much sweat resulting in sweat bridge in between electrodes will reduce the accuracy of recorded signals [135].

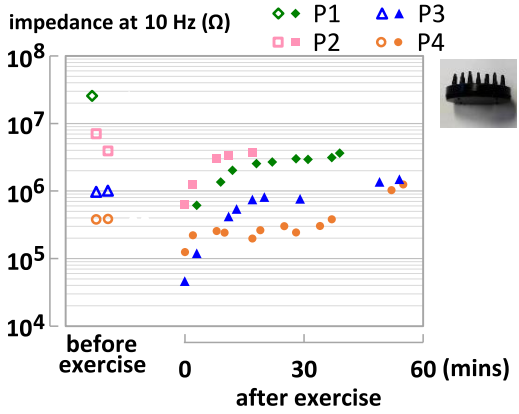

Figure 3.25: *The impedance of pin-shaped electrode before and after exercise on 4 different subjects.*

3.3 Equivalent circuit of electrode/skin interface

The interface of electrode and skin is a complex combination of voltage source, double layer capacitor and resistors as described in section 3.1. This combination results in the nonlinear behavior of the electrode/skin interface. Because of this, and as described in other publications, the electrode/skin interface introduces serious attenuation and distortion of the ECG signals [81, 119, 136, 137]. Consequently, characterizing the impedance of the skin-electrode interface provides essential information for the correct design of the amplifier for high accuracy biopotential measurements. In this section, modelling the equivalent circuit of polymer electrode/skin interface is investigated. In section 3.3.1, the elements used in electrochemistry systems modelling and the electrode/skin model as presented by other researchers are introduced. The software and protocol applied for the modelling and fitting are presented in section 3.3.2. Then, the models and fitted components of wet electrode, polymer dry electrode and polymer electrode on the skin underwent skin pretreatments are discussed in section 3.3.3, 3.3.4, and 3.3.5 respectively.

3.3.1 Equivalent circuits for electrode/skin impedance modelling

There are two methods to present the impedance of a circuit, see Figure 3.26. One is the Bode plot, showing the impedance magnitude and the phase variation versus frequency. The Bode plot is often used in electronics. The other representation is called the Nyquist plot. This plot shows the real part of impedance versus the imaginary part. The frequency of each data point is difficult to define when observing the plot. This plot is more popular for equivalent circuit modelling in electrochemistry studies since a semicircle shown in Nyquist plot corresponds to a double layer structure at the interface. A double layer is often expressed by a resistor and a capacitor in parallel as introduced in section 3.1. In the Nyquist plot of a system, often more than one semicircle exists. Most of the time, only partial semicircle can be seen. The

equivalent circuit of a system can be preliminarily determined by observing the shape of the Nyquist plot.

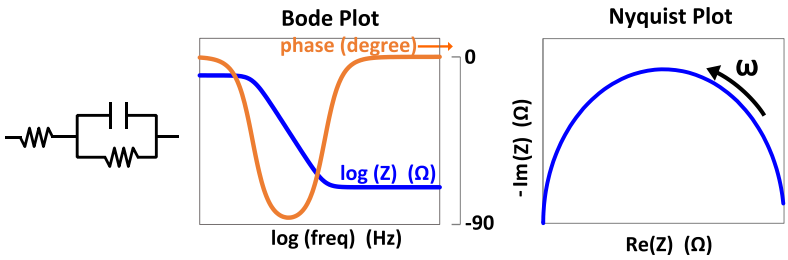

Figure 3.26: Both Bode plot and Nyquist plot are used to express the impedance of a circuit.

The elements commonly used to model an electrochemical system are shown in Figure 3.26. A resistor is used to present the resistance of the combination of the conducting wires, the gel, the electrode material and the inner skin tissue. A capacitor is used to model the double layer structure at the interface. Another element similar to a capacitor is a constant phase element (CPE). This is used to represent a capacitor with inhomogeneous and roughness surfaces. When modelling the impedance using a CPE, the Q and *a* value can be defined. The Q value is the capacitance of the CPE while *a* is a constant in between 0 and 1. When $= 1$, the CPE is the same as a pure capacitor. The last element introduced here is a Warburg diffusion element. This is representing the impedance of the semi-infinite diffusion of the conductive ions to or from the electrode. The Warburg element is more important at low frequencies.

Name	Symbol	Impedance	Nyquist plot	Parameter to be fitted (unit)
resistor	R	$Z(\omega) = R$	- Im(Z) Re(Z)	R (ohm)
capacitor	C	$Z(\omega) = \frac{1}{j\omega C}$	- Im(Z) ω Re(Z)	C (F)
constant phase element (CPE)	Q	$Z(\omega) = \frac{1}{(j\omega)^a Q}$	- Im(Z) ω $-a\frac{\pi}{2}$ Re(Z)	Q (F•s^(a-1)) a
Warburg element	W	$Z(\omega) = \frac{\sqrt{2}\,S}{\sqrt{j\omega}}$	- Im(Z) ω $-\frac{\pi}{4}$ Re(Z)	S (ohm•s^(-1/2))

Figure 3.27: The elements commonly used for equivalent circuits modelling in electrochemical systems.

As shown in Figure 3.27, each type of element has a different shape in the Nyquist plot. In Figure 3.28, three examples of the Nyquist plots of circuits combining two or three electrical components are shown. When a resistor and a capacitor are placed in parallel, the Nyquist plot is a semi-circle. If the capacitor in the first case is replaced by a CPE, the semi-circle is flatter. When a Warburg diffusion element is in series with the resistor, the 45 degrees tail is shown at the low frequency part of the Nyquist plot.

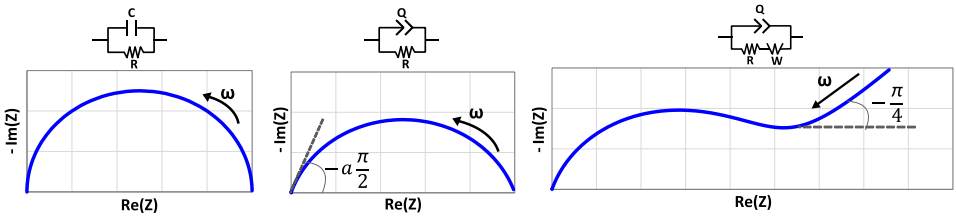

Figure 3.28: The Nyquist plots of the circuits combining two or three elements mentioned in Figure 3.27.

When applying an electrode on the skin for biopotential measurements, the properties of the interface is similar as placing an electrode in electrolyte solution. Therefore, a parallel RC circuit along with a voltage source is included in an equivalent circuit of electrode/skin interface. The skin itself is often represented by another parallel RC structure and voltage source, since the skin consists of a high impedant SC layer with below tissue, the epidermis and dermis, having lots of conductive ions. Due to the concentration difference of the conductive ions in the SC layer and the below tissue, ion transmission at the interface results in a potential difference and the double layer structure. The equivalent circuits of the interface of electrode and skin have been studied by lots of researchers [109]. A classical model used to represent the interface of wet electrode and the skin is shown in Figure 3.29 [81]. Two parallel RC circuits are used to represent the interface of electrode and the gel, and the interface of the SC layer and the skin below it. The researchers proposing this model also recommend that the sweat glands and ducts can be analogized as another parallel RC circuit in parallel with the elements representing the interface of the SC layer and the below tissue. In contrast to the wet electrode, the equivalent circuit of a dry electrode with pins penetrating the SC layer contains only one parallel RC element. The other RC element is discarded because there is no gel in between the electrode. Another reason is that the electrode bypasses the SC layer and accesses the conductive ions in the inner layer of the skin more easily.

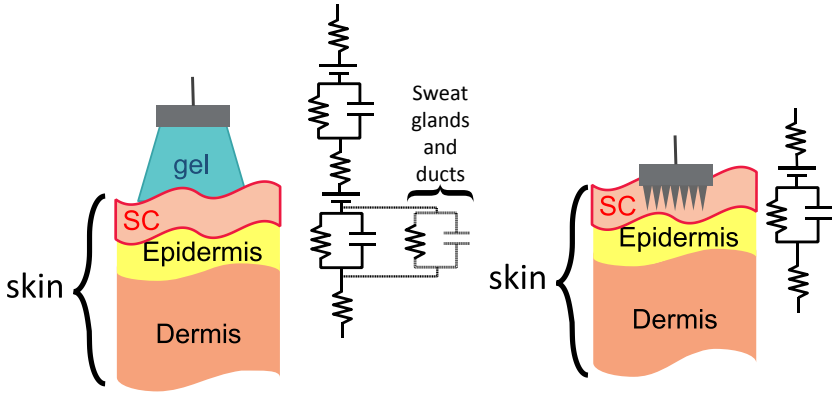

Figure 3.29: The schematic and equivalent circuits of wet electrode/skin interface and of dry electrode with pins penetrating the SC layer.

Regarding the polymer electrode evaluated in this thesis, the pins of the electrodes do not penetrate the SC layer. The ionic current transmits to the electrode through sweat or the conductive fluidic added to the interface, such as abrasive gel or lotion mentioned in section 3.2.5. Impedance modelling of the impedance of pin-shaped Ag and Au dry electrodes has been presented in a thesis [138]. Based on the results discussed in that thesis, the model shown in Figure 3.30 is applied for the impedance modelling of the data presented in section 3.2. The CPEs replace the capacitors in the model shown in Figure 3.29 because it is assumed that the interface of the electrode and the low amount of sweat is not homogeneous. Besides, a Warburg element is added in the circuit because there are very low amount of conductive ions at the interface of pure dry polymer electrode and the skin after the electrode is placed on the skin initially. It is believed that the ion diffusion from the skin to the electrode surface through conductive channels is necessary when applying polymer dry electrodes.

In the model shown in Figure 3.30, the $R1_a$ represents the resistance of the electrode material and the conductive wire while $R1_b$ represents the resistance of inner skin tissue, part of the epidermis below the SC layer and the dermis. Since it is difficult to distinguish the two resistors during modelling and fitting, R1 representing the combination of $R1_a$ and $R1_b$ will be used in signal analysis. The R2 and Q2 represent the double layer structure at the interface of the SC layer and the below tissue. Q3 represent the capacitance of the double layer at the interface of electrode and electrolyte. R3 models the charge transfer resistance and W3 models the diffusion impedance of the electrode/electrolyte interface.

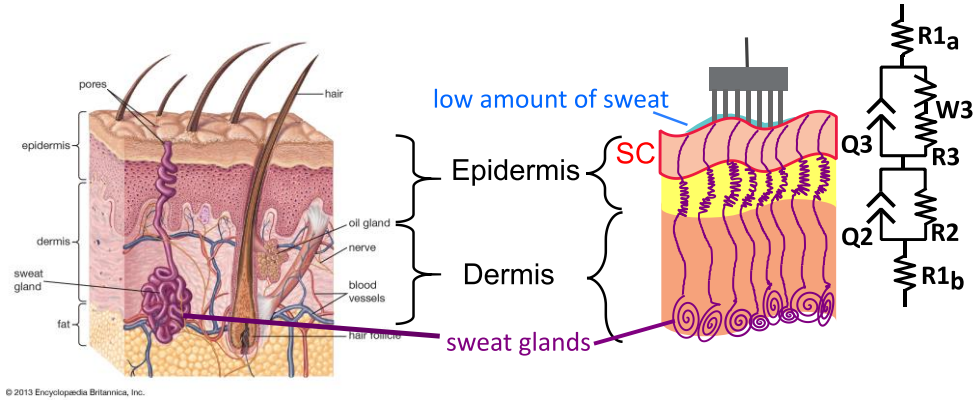

Figure 3.30: The skin structure [139] and the equivalent circuit applied in this thesis for electrode/skin impedance modelling.

3.3.2 Nyquist curves fitting using EC-Lab

EC-Lab software (Bio-Logic, Claix, France) is commercial available software for electrochemistry modelling. This software was used for fitting the measured electrode impedance data to the model shown in Figure 3.30. The 'downhill simplex algorithm' was selected to perform the fitting. During the process, the curves were fitted with weighting, which means dividing the variation of fitted data and experimental data by the standard deviation value. This will increase the accuracy of the fit at high frequencies, in other words, data with small impedance value.

3.3.3 Modelling of wet electrodes impedance along with time

The impedance modelling was first performed on the data of wet electrodes since the interface of wet electrode/ skin is better controlled comparing to that of dry electrode/ skin. The data was acquired using the protocol described in section 3.2.4. Two ECG wet electrodes were placed on the forearm with a distance of 10 cm as counter and reference electrodes. 30 minutes after placing these two wet electrodes, a third wet electrode was placed next to the reference electrode as working electrode. The impedance was measured every 10 minutes during 1 hour after the working electrode was mounted. This measurement was carried out on 7 subjects. In this section, only the data of one subject is discussed.

The Nyquist plots of all the measurements on this subject are shown in Figure 3.31. Each curve in the figure underwent the fitting procedure. In Figure 3.32, the variation of each fitted parameter with time is shown.

The wet electrodes are widely used for bio signal monitoring not only because the gel offers a stable contact interface, but also because the gel hydrates the skin and keeps the impedance low and constant. The impedance shown in Figure 3.31 and Figure 3.32 indeed decreases slightly with time in the first half hour and then remains almost constant. The element representing the impedance of inner tissues and the resistance of conducting wires, R1, remains constant. It is reported by the author of [120, 122] that the capacitance of the SC

layer increases with the increasing water content in the skin. Q2, the double layer capacitance of the SC layer, increases initially with time due to hydration, hence the corresponding impedance decreases. The charge transfer resistor of SC layer, R2, also decreases due to the conductive ions diffusing from the gel into the skin [140]. Both Q3 and R3, the elements representing the interface of the gel and electrode (the AgCl metal plate of the conventional ECG wet electrode) stay constant because this interface remains unchanged after the electrode is placed on the skin. The stable AgCl electrode/gel interface results in a homogeneous surface of the capacitor. In other words, it can be assumed that a3 equals to 1 and Q3 is a pure capacitor. The fitted data prove this assumption. Last, the diffusion element S3 decreases dramatically because the skin is being hydrated and hence less ion diffusion is needed for signal transmission. All these trends are not only corresponding to the data shown in Figure 3.32, but also to the data recorded from the other 6 subjects.

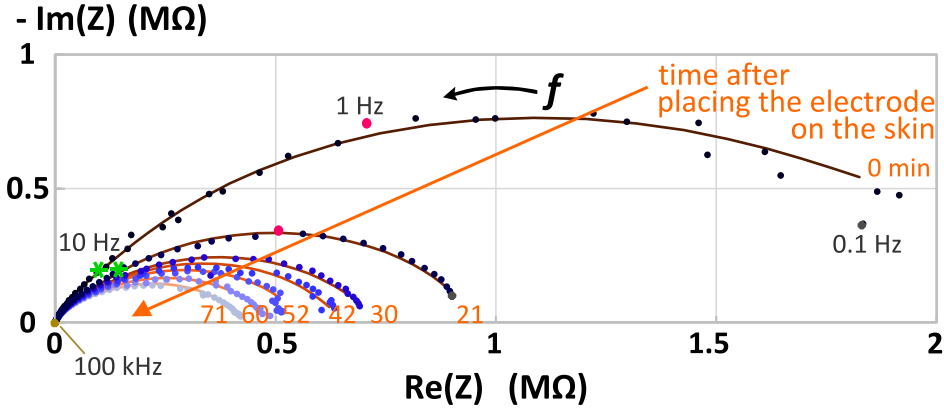

Figure 3.31: The Nyquist plots of the impedance of wet electrode. The impedance is recorded during 1 hour starting immediately after placing the working electrode on the skin. The impedance is swept from 100 kHz to 0.1 Hz. The dotted lines are experimental data while the solid lines are fitted data.

In summary, the impedance decreases slightly in the first half an hour for all subjects when placing a wet electrode on their skin. This is because the ions diffuse from the gel of electrode into the SC layer and the skin is been hydrated. This first half hour is defined as the stabilization period of the interface of wet electrode and skin, and due to this, one waits typically 30 minutes before starting with impedance measurements or EEG signal recording when wet electrodes are used.

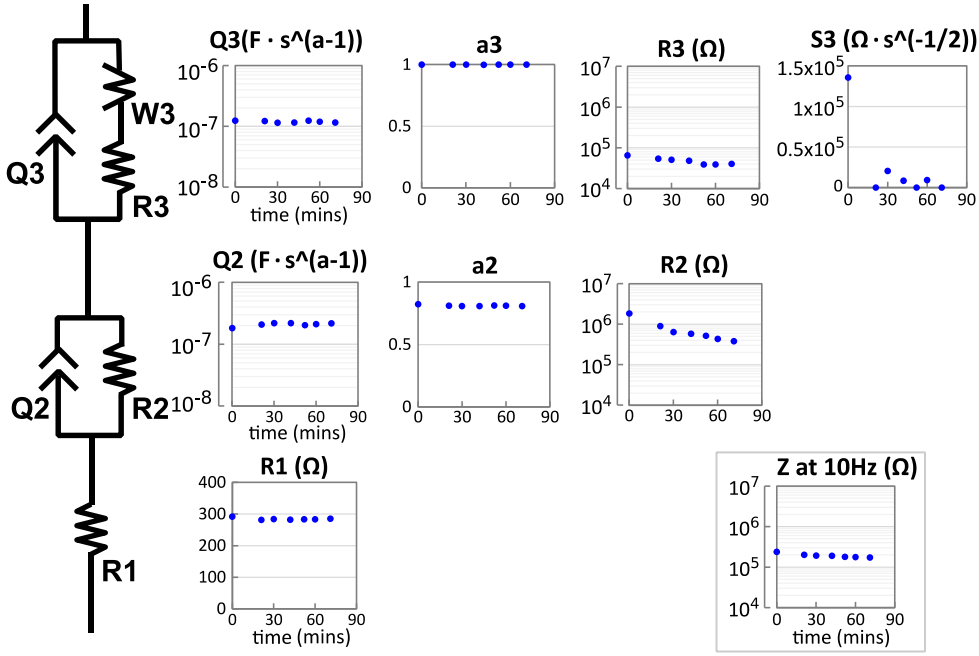

Figure 3.32: The fitted value of each parameters in the equivalent circuit model along with time. The data is recorded when a wet electrode is placed on the forearm of one subject.

3.3.4 Modelling of polymer dry electrode impedance

The same model as for wet electrodes is applied for fitting the impedance data recorded by polymer dry electrodes, to found out whether the wet electrode model can be extended to model also the dry electrode/ skin interface properly.

In contrast to wet electrode measurements, the impedance of dry electrodes is noisy at low frequency (below 10 Hz) on most subjects. A few times smooth data are recorded, typically in a warm and humid day, when the subject has a rather hydrated skin or when skin pretreatments mentioned in section 3.2.5 are applied. Regarding these noisy data, the impedance magnitude and the phase varies randomly along with frequency. As a result, all the impedance data reported in section 3.2 is the 10 Hz value of the fitted impedance data. Extrapolating the impedance magnitude in Bode plot is easier comparing to doing that for the resistance and reactance data in Nyquist plot. If the data is noisy at low frequency range as shown in Figure 3.33, the Nyquist curves are difficult to be fitted. This data becomes noisy when the frequency is smaller than 100 Hz. The data at high frequency range can still be fitted but the fitted parameters might not correctly represent the model of the impedance during biopotential monitoring. For example in Figure 3.33c, a Warburg element should be included in the model because the Nyquist curve contains a 45 degrees tail from 10Hz to 100Hz. If only the Nyquist curve from 100 Hz to 100 kHz as shown in Figure 3.33d is used for modelling and fitting, a Warburg element is not needed.

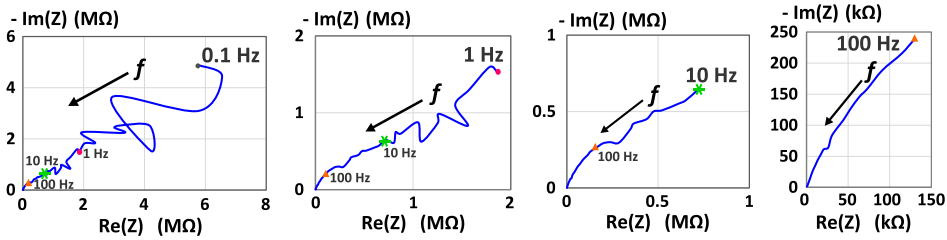

Figure 3.33: The Nyquist plots of noisy recorded impedance data plotted from (a) 0.1 Hz; (b) 1Hz; (c) 10 Hz and (d) 100 Hz to 100 kHz.

The instability of impedance curves when using polymer dry electrodes resulted from the drift of open circuit potential (OCP) with time. The OCP of polymer electrodes is sensitive to the change of the double layer structure as shown in Figure 3.7. The protocol used for all the impedance measurements is controlling a constant voltage of 25mV between working and reference electrodes. This 25mV is defined on top of the OCP. The drift of OCP causes the difficulty to control the voltage in between working and reference electrodes. This results in errors in the measured impedance value, especially at low frequency range. The drift of OCP is caused by the lack of conducting ions at the interface. The oxidation/reduction reactions at the interface of polymer are not clearly studied. A possible approach to improve the stability of OCP is coating a AgCl layer on the pins of polymer electrodes, as shown in Figure 3.7.

Among all the impedance measured immediately after the polymer dry electrodes are placed on the skin, around half of the data is noisy at low frequency and cannot not be modelled based on the data recorded in the frequency range from 0.1 Hz to 100 kHz. In the future, averaging the impedance curves recorded continuously might reduce the noisy parts at low frequency. However, the impedance of the polymer dry electrodes changes with time. Averaging the impedance data recorded in certain period, e.g. 10 minutes, instead of averaging those recorded in the entire measurement period, e.g. 1 hour, is optimal and can evaluate the evolution of impedance with time. Furthermore, analyzing the data acquired on more subjects help to optimize the polymer dry electrode/skin interface model.

Similar to the impedance of wet electrodes, it is found that the impedance signals become less noisy when there is conductive fluid on the skin or the SC layer is abraded. In section 3.3.5, the variation of each parameter in the model before and after the skin treatments is discussed.

3.3.5 Modelling of polymer dry electrode impedance after exercise

It has been discussed in section 3.2.5 that the impedance of polymer electrode decreases in the first 30 minutes after exercising. The experimental and fitted impedance data from one of the six subjects are shown in Figure 3.34. It can be found that the impedance measured before exercise and 0 min after exercise are noisy at low frequency. Therefore, only the data from 10 Hz to 100 kHz of these measurements are fitted. The variation of each elements in the equivalent circuit is shown in Figure 3.35.

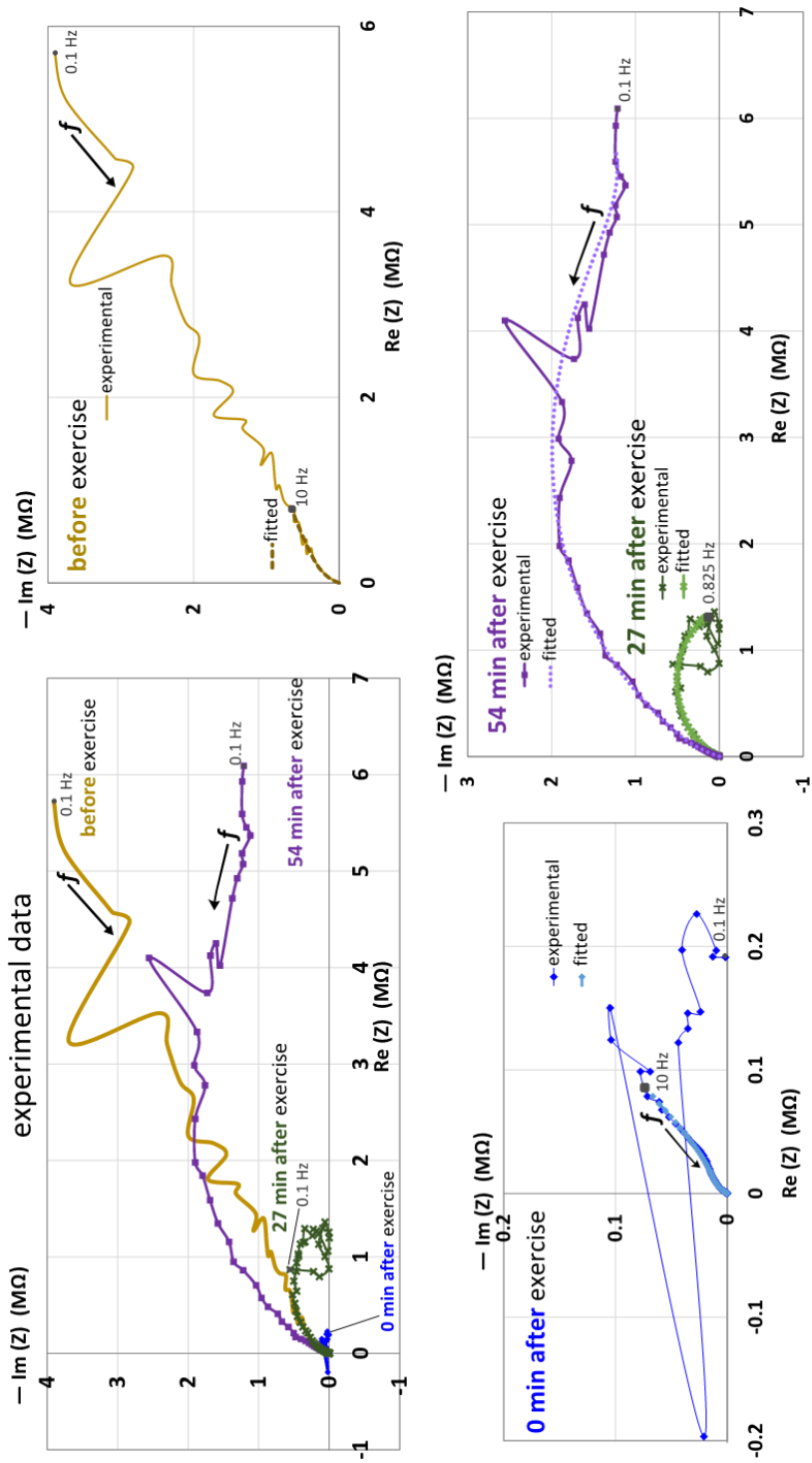

Figure 3.34: The Nyquist plots of the experimental data and the fitted data of polymer dry electrode/skin measured before and after exercise. All the experimental data are recorded from 0.1 Hz to 100kHz. However, the fitted data of the impedance measured before exercise and 0 min after exercise start from 10Hz to 100kHz; the fitted data of the impedance measured 27 min after exercise starts from 0.825 Hz to 100 kHz. In the figure of '0 min after exercise', the experimental signal is very noisy at low frequency resulting in a measurement error (negative value of resistance of a data point).

Similar to the previous skin pretreatment techniques, the resistance of inner tissue and the conducting wires, R1, is not influenced. During exercising, the sweat glands are filled with sweat and the skin becomes more conductive. It has been reported by other authors that the sweat ducts and glands in the skin can be represented by adding extra time constant elements (one capacitor and one resister connected in parallel) connect in parallel, see Figure 3.35. Thus in the model, the double layer capacitor, Q2, increases and the resistor, R2, decreases due to extra RC components connected in parallel. The fitted results are corresponded to the assumptions. Besides, it is also found that these variations resulted from the sweat does not last longer than 30 minutes. At interface of electrode/skin, Q3 increases and R3 decreases due to the existence of sweat. 30 minutes after exercising, the Q3 and R3 return to the values similar to the ones before exercise because the sweat evaporates. The a3 is not 1 as the cases of wet electrodes. This is because the sweat rate and its composition vary with time resulting in a non-uniform fluid layer at the electrode/skin interface. It is expected that the diffusion element (S3) will decrease dramatically after exercising. However, this trend is not found in this example, which might be because of the difficulties of fitting the data recorded before exercise and 0 min after exercise in low frequency ranges, where the Warburg element is the dominate component.

When evaluating the data recorded from the rest subjects, the trends concluded here are only found in half of the rest data. This is because the sweat composition and sweat rate vary in between each subject. It is more difficult to conclude a variation trend of the data recorded after exercising comparing to the data after applying skin lotion with constant concentration.

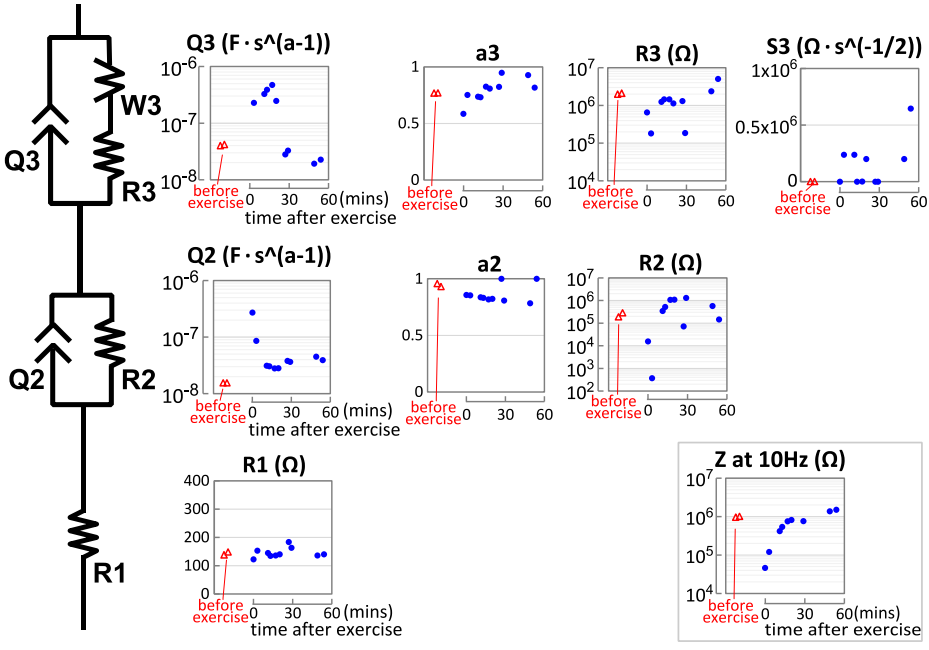

Figure 3.35: The fitted value of each parameters in the equivalent circuit model along with time. The data is recorded before and after the participate exercises.

3.4 Mechanical properties of polymer electrodes

The mechanical properties of the electrodes depend on the material composition and the electrode shape. These properties are important since they have an impact on crucial characteristics of the electrodes, such as the fabrication yield, biopotential signal quality, and user comfort. Though there is no specification regarding the essential mechanical properties of electrodes for biopotential measurements, we think it is still worth to quantify these properties since such an investigation can be used as references for future electrode development and optimization. The optimization of the material composition and shape-design of the polymer dry electrodes are partly based on the evaluation of the elasticity of cylindrical-shaped electrodes with various material composition and as well as based on the evaluation of the compliance of pin-shaped electrodes with various designs.

In section 3.4.1, the elastic moduli of the polymer materials are determined. The load-displacement curves of pin-shaped electrodes recorded during compression tests are shown in section 3.4.2. Next, the elastic moduli are combined with the geometric factors of the pin-shaped electrodes, more specific with the equivalent contact area and length of the pins, in order to predict the compliance of the pin-shaped electrodes with various designs. The comparison of the compliance calculated based on the measurements of pin-shaped electrodes and the predicted compliance is shown in section 3.4.3. The evaluation of the compliance of pin-shaped electrodes can be used for material or electrode shape optimization in the future. For example, if a certain compliance of a pin-shaped electrode with fixed shape is preferred, the minimum elastic modulus of a conductive rubber can be calculated, resulting in a more efficient material optimization. On the other hand, if the conductive material for the electrodes is fixed, one can predict which electrode shapes are desirable by measuring and calculating the elastic modulus of the selected conductive rubber. In section 3.4.4, the viscoelastic properties of the polymer electrodes are characterized. The influences of these viscoelastic properties on the real biopotential measurements are discussed.

3.4.1 The elastic modulus of various polymer materials

Elasticity is a material property, quantified by the elastic modulus [141]. The tendency of a material to deform along an axis when opposing forces are applied along that axis is described by its elastic modulus, also called Young's modulus. In this thesis, the elastic moduli of cylindrical-shaped electrodes with various materials as shown in Figure 3.36 are determined and they are used to predict the compliance of pin-shaped electrodes made from these materials but having various shape-designs. For the sake of simplicity, the cylindrical-shaped electrodes are called as test buttons in the following text in section 3.4.

Three techniques are used to determine the elastic modulus of various polymer materials in this thesis:

(1) calculating the elastic modulus using the measured Shore A hardness value;
(2) calculating the elastic modulus using nano-indentation measurements;
(3) calculating the elastic modulus using compression measurements.

The protocols and the obtained elastic moduli of various materials using each technique are discussed in this section.

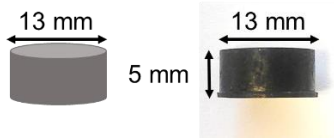

Figure 3.36: Cylindrical-shaped polymer electrodes are used in 3 techniques for elastic modulus calculation. These electrodes are called as test buttons in the following text in section 3.4.

(1) Calculating the elastic modulus using Shore A hardness

A hardness measurement is a simple way of obtaining a measure of the elasticity of a rubber by measuring its resistance to a rigid indentor to which is applied a force [142]. In standards ISO 48 and ISO R868, two techniques are explained to measure the hardness of a rubber [143]. In ISO 48, this hardness is measured using a rigid spherical indenter and the hardness is expressed using the International Rubber Hardness Degrees (IRHD) scale. The IRHD hardness has a range of 0 to 100, corresponding to a material with an elastic modulus of 0 (0) and infinite (100). In ISO R868, a Durometer with a rigid truncated cone indenter is used. Durometers contain also a hardened indenter and the penetration depth into the test material is measured and immediately converted to a hardness value shown on the Durometers, most often expressed in Shore A and Shore D units. Shore A is often used for softer materials while Shore D is used for harder materials. Both units range from 0 with full protrusion of the indenter to 100 for no protrusion. Other standards describing the hardness of a rubber measured using a durometer are ISO 7619-1 and ASTM D2240.

The relationship between the Shore A hardness of a rubber measured following ASTM D2240 and its elastic modulus is proposed by A. N. Gent as shown in Equation 3.9 [144]. Another relationship between these two parameters introduced in British Standard 903 is shown in Equation 3.10 [145].

$$E = \frac{0.981\,(56 + 7.62336\,H_{Shore\,A})}{0.137505\,(254 - 2.54\,H_{Shore\,A})}$$

Equation 3.9

(Gent's equation)

where E is the elastic modulus in units MPa and $H_{Shore\,A}$ is the ASTM D2240 Shore A hardness.

$$H_{Shore\,A} = 100\,erf\left(3.186 \times 10^{-4}\,E^{\frac{1}{2}}\right)$$

Equation 3.10

(equation in BS 903)

where *erf* is the error function, E is in units Pa and $H_{Shore\,A}$ is the ASTM D2240 Shore A hardness.

In this thesis, the Shore A hardness of 3 polymer materials with different carbon content is measured at Datwyler following standard ISO 7619-1, but with a 1-second indentation instead of the 15-second indentation duration as mentioned in the standard. This deviation from the standard is caused by the fact that the previous relevant ISO standard required this short indention period, and hence all previous measurements at Datwyler are performed with 1 sec. indentation time. Changing now to 15 sec. indentation according to the new ISO 7619-1 would result in Shore A values which can't be compared with previous work at Datwyler. Moreover, Datwyler obtained FDA approval for its material based on the 1 sec. indentation period, hence this particular test has still to be used to control all the rubber batches for medical applications. Finally it should be noted that in this thesis, limited data is available for elastic modulus calculation based on Shore A hardness tests, because the Shore A hardness is only measured on the three polymer materials which were the most interesting ones in the final phase of material optimization.

The elastic modulus calculated using Equation 3.9 and Equation 3.10 and Datwyler's Shore A hardness of 3 rubbers is shown in Figure 3.37. Not surprisingly, it is found that the elastic modulus increases with the increasing of carbon content. It has to be noted that the Shore A hardness used for elastic modulus calculation is not measured in accordance with ASTM D2240, although the formulas (Equation 3.9 and Equation 3.10) are based on this assumption. This fact jeopardizes the validity of our calculation of the elastic moduli using the measured Shore A hardness and the formulas. Moreover, the two formulas are not resulting in a similar Young's modulus for materials with a shore A value higher than 70 as shown in Figure 3.38. Another limitation of this technique is that only one elastic modulus value can be calculated while the Young's modulus is a function of stress/strain [146, 147]. Due to all these contributions to an uncertain Young's modulus, the obtained E values are probably not be suitable for the compliance prediction (see further). Due to these limitations, the other two techniques, nano-indentation tests and compression tests, are performed to compare if they are better techniques for elastic modulus determination.

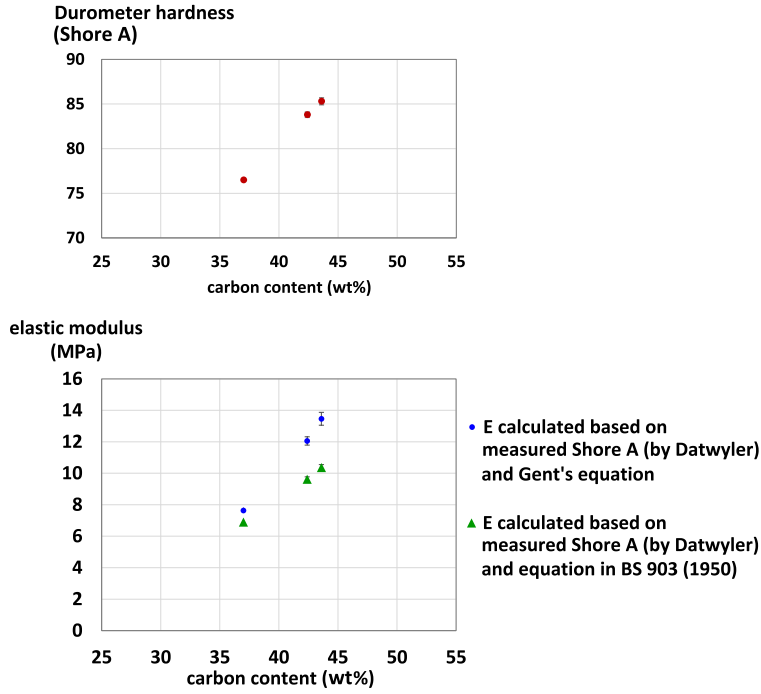

Figure 3.37: The Shore A hardness of various polymer materials and their elastic moduli calculated based on the measured Shore A hardness and Equation 3.9 (Gent's equation) and Equation 3.10 (equation in BS 903). The polymer materials have different carbon content in wt%.

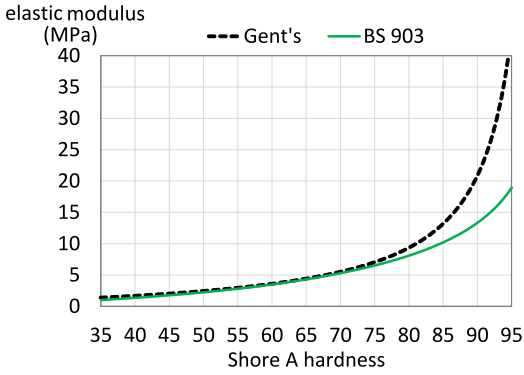

Figure 3.38: The elastic moduli versus the Shore A hardness based on Equation 3.9 (Gent's equation) and Equation 3.10 (equation in BS 903).

(2) Calculating the elastic modulus using nano-indentation tests

A nano-indentation tool is available in imec for hardness and elastic modulus measurements. The tests are carried out using a nano indenter XP system (MTS Systems

Corporation), equipped with a standard three-sided pyramid diamond indenter tip (Berkovich). The tool is especially useful for measuring the hardness and elastic modulus of rather hard materials, for which only small displacements are recorded in spite of a higher load. During the measurements of our rubber samples, the tool's maximum displacement of 20 µm and a constant strain rate of 0.05 s^{-1} are used. The nano-indentation tests are carried out on one sample of each material. For each material, multiple measurements (8 to 13) are performed. From the experimentally obtained load-displacement curves, the elastic moduli (E) are calculated based on the measured contact stiffness (S) and the contact area (A), based on the relationship indicated in Equation 3.11 [148]:

$$S = \beta \frac{2}{\sqrt{\pi}} \sqrt{A} \left[\frac{1-\nu^2}{E} + \frac{1-\nu_i^2}{E_i} \right]^{-1} \qquad \textit{Equation 3.11}$$

where β=1.034 is the geometry correction factor of a Berkovich indenter [149], ν is the poisson's ratio of the sample which is not determined in this thesis, so a value widely used for rubber materials is used: ν = 0.5. E_i (1140 GPa) and ν_i (0.07) are the elastic constants of the diamond indenter tip. The contact area (A) is the projected contact area of the indenter with the sample surface, which is determined from the indenter tip shape calibration, as described in [150].

The calculated elastic moduli for all tested materials are shown in Figure 3.39. As expected, the elastic modulus increases with increasing carbon content, however the values are around 7 times larger than the elastic moduli calculated based on Shore A hardness. This important difference is probably related to various conditions which should be fulfilled when performing a nano-indentation test. One condition is a very limited roughness of the test buttons. The roughness of the polymer electrodes is ~2-5 µm . The 20 µm penetration depth of the indentor is probably too shallow comparing to the roughness of the samples for an accurate measurement. Furthermore the test buttons are not perfectly homogenous: the molding process results in a 'skin' layer with different properties than the bulk material. Again the small penetration depth is probably causing that mainly the elastic properties of the skin are measured. Increasing the penetrate depth is impossible, and cutting the polymer buttons into half to measure on the bulk material, will result in a very rough surface. In addition, the elastic modulus values calculated using Equation 3.11 are supposing harder materials than the rubbers in this test, the formula is calibrated using fused silica having clearly different mechanical properties from the polymer materials. Detailed discussion of the nano-indentation tests and the results can be found in Appendix I.

To conclude, the elastic modulus of the polymers is strongly increasing with the increasing carbon content. The obtained Young values are much larger than the values obtained using the Shore A measurements (previous test method), especially for the harder materials. Although the nanoindentation results are certainly useful to compare the various polymer materials, it is doubtful if the calculated Young's modulus is correct, since various conditions for a correct nano-indentation test are not fulfilled when testing the polymer test buttons.

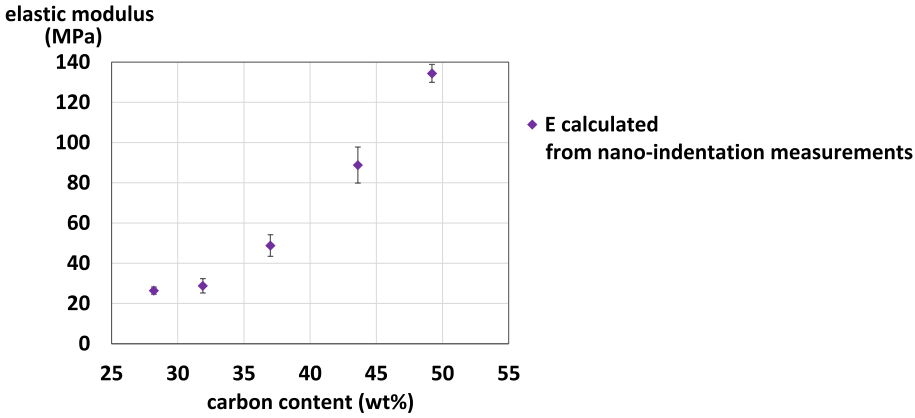

Figure 3.39: The elastic moduli of various polymer materials calculated during the nano-indentation tests.

(3) Calculating the elastic modulus using compression tests

The elastic modulus is defined by the relationship in between stress (force per unit area) and strain (proportional deformation) in a material as shown in Equation 3.12 [141]. Compressive force is applied on test material to obtain the stress (σ) versus strain (ε) curves. The elastic modulus is the slope of the stress versus strain curve during the period that the stress is proportional to the strain, in other words, when the material has elastic properties.

$$E = \frac{\sigma}{\varepsilon} = \frac{\frac{F}{A}}{\frac{\Delta L}{L_0}} \qquad \textit{Equation 3.12}$$

where σ is the force (F, in Newton) divided by the area (A, in m^2) that the force is acting on, ε is the difference between the final length of the sample and the original length of the sample (ΔL) divided by the original length of the sample (L_0). The unit of E is Pa.

The compression tests are performed using a high precision micro-mechanical test system with full computer control and data analysis. It includes an ultra-high-resolution linear actuator providing linear motion of up to 50 mm with a resolution 20 nm, see Figure 3.40. For these compression tests, the maximum applied load varies in different test sessions but a constant displacement of 25 μm/s is used. The detailed information for each test is mentioned further during the discussion of each test. The compression tests are carried out on 3 to 5 similar samples of each polymer material.

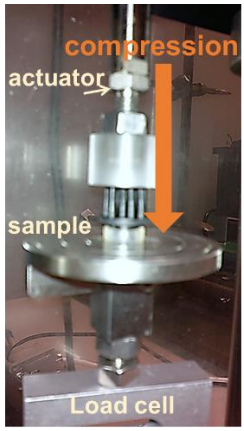

Figure 3.40: The compression tests characterize the elastic modulus of various materials and the compliance of pin-shaped polymer electrodes.

Figure 3.41a to Figure 3.41c show an example of the elastic modulus calculation based on the compression tests carried out on the polymer material containing 37 wt% of carbon. The load-displacement curves of three loading cycles are shown in Figure 3.41a. For the 2nd loading curve, the elastic modulus is calculated using Equation 3.12 for all positions of this curve, resulting in the data points in Figure 3.41b. Since the elastic modulus of a rubber is small, a small inaccuracy in the measured displacement or measured load results in a significant variation of the calculated elastic modulus. Therefore, a curve fitted to the scattered data points of elastic modulus is used to represent the elastic modulus calculated using the 2nd loading curve. It is found that the elastic modulus is not constant during the loading cycle. The fitted elastic modulus curves of the 1st to 3rd loading curves are shown in Figure 3.41c. Comparing the load-displacement curves or the corresponding elastic modulus curves for the three loading cycles, it is always seen (for all materials and all samples which have been tested), that the results of the 1st loading cycle deviates from that of the 2nd and 3rd loading cycles, while these latter cycles give always similar results. This is probably due to the placement of the test buttons. Some air particles in between the bottom of the test button and the compression tool are removed during the 1st loading cycle. This is also probably due to the mechanical conditioning happening during the 1st loading cycle. When the material is compressed for the 1st time, the structure of the fillers and polymer rearrange resulting in a different mechanical property from the rest loading cycles [151]. The elastic modulus curves of the 2nd and 3rd loading cycles are always similar. Therefore, the elastic modulus curve of the 2nd loading cycle is further in this thesis used to represent the curves performed after the 2nd loading cycle. In Figure 3.41d, the elastic modulus curves of the polymer materials containing various carbon content in weight percent are shown. As expected, the polymer materials containing more carbon have higher elastic modulus. Comparing the elastic modulus at low stress, the trend cannot not be found because the values at low stress are less accurate. This is because at the beginning of compression tests the surface of the sample does not contact firmly to the part of the compression tool that applies the load. Furthermore, at low loads, the load and displacement are too small to be measured accurately. The increase of elastic modulus is

not exactly proportional to the carbon content, which is indeed not expected because also some other additives are present in different quantities into the polymer materials (fillers, softeners,...). The elastic moduli calculated based on the compression measurements are ~ 7 times smaller than that recorded using nano-indentation tests and 2 times larger than that calculated based on the Shore A hardness.

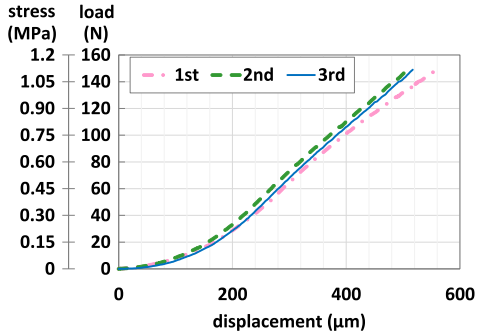

(a)

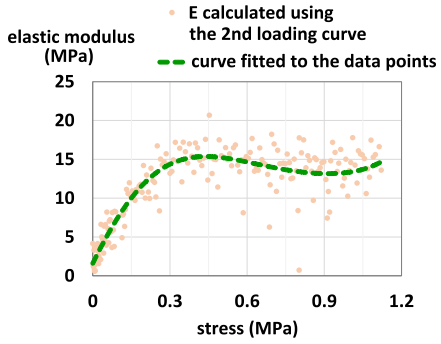

(b)

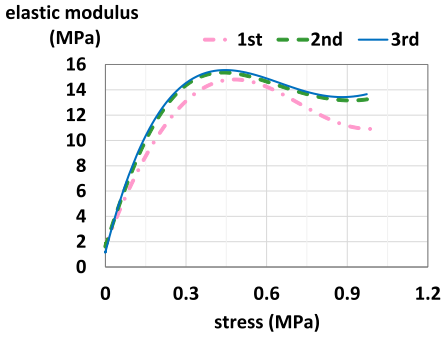

(c)

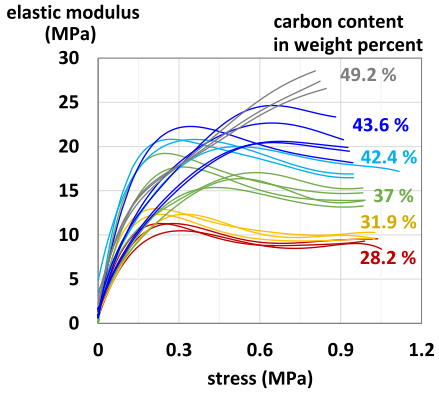

(d)

Figure 3.41: (a) The load-displacement curves of cylindrical-shaped electrode containing 37 % of carbon during 3 loading cycles. The maximum load is 150 N. (b) The elastic modulus (E) calculated using the 2nd loading curve shown in (a). The curve fitted to the data points showing that the E varies with stress. (c) The fitted E curves of the load-displacement curves shown in (a). The E curve of 1st loading cycle is slightly different from that of the 2nd and 3rd loading cycles. (d) The fitted E curves of the cylindrical-shaped electrode containing various carbon content. The E of the material containing more carbon is larger.

Discussions and Conclusions

Although the three techniques used to determine the elastic modulus are not resulting in the same E-values, one trend is very obvious for all three techniques: the elastic modulus of the materials under test is increasing with growing carbon content. This is not a surprise: carbon is a frequently used additive to EPDM polymer to reinforce the mechanical properties [152,

153]. Hence the observed increase of elastic modulus with increasing carbon content is expected and is in line with the results reported in [154-157].

Different E-values are obtained when different techniques are used to determine the elastic modulus. The accuracy of the elastic modulus calculated based on Shore A hardness and using Equation 3.9 and Equation 3.10 is uncertain because in this thesis the Shore A hardness is not measured according to the method which is required if Equation 3.9 and Equation 3.10 are used. For the nano-indentation measurements, the indent depth used in the measurements is not suitable for our polymer test button with a rough surface and a skin. Furthermore, the parameters used to calculate the elastic modulus based on the nano-indentation tests, are values derived for hard materials, they are less suitable for our softer polymer materials. Due to this, the obtained elastic moduli have to be considered as 'relative' E-values, only to be used to compare various rubbers. Finally, the nano-indentation tool can only be used by specialized personnel at imec, which limits the amount of tests which could be performed in the frame of this thesis. The third method used for E-modulus calculation is based on compression tests. The compression tool might be somewhat less accurate then the nano-indentation tool, but it has important advantages: the tool is easily accessible at imec, and can be used to test polymer test buttons as well as pin-shaped electrodes. The tool can be used myself, so more measurements on many different samples have been performed, which resulted in the determination of the elastic moduli versus load/stress of six different polymer materials, all tested using a multitude of similar test buttons to enhance the accuracy. Since the compliance of pin-shaped electrodes with various designs is also tested using the same compression tool, the elastic moduli resulting from the compression tests of the test buttons with various carbon content will be used for the compliance prediction of the pin-shaped electrodes as further discussed in 3.4.2.

3.4.2 The load-displacement curves of the electrodes with various pin shapes and selection of the boundaries of the load-of-interest for the predictive compliance calculation

In this section, the load-displacement curves of pin-shaped electrodes from various polymer materials or with different designs are obtained to characterize their compliance. The compression tests are carried out on pin-shaped electrodes using the test system shown in Figure 3.37. The displacement rate is always 25 μm/s for the measurements shown in section 3.4.2 and 3.4.3. During the compression test, a hard holder shown in Figure 3.42 is used at the backside of the electrodes resulting in a larger flat surface to support the load from compression tool. The holder does not cover the base plane of the electrodes completely but this does not result in a significant non-uniform load distribution during the compression tests, which is known by detailed observation of the deformation of the base plate and the pins during the compression. Even when load is applied on the electrode made from the material with the smallest elastic modulus (material containing 28.2 wt% of carbon), the base plate does not bend and the pins located at the center do not deform more than the ones located at the edge. These observations can be found in the pictures of Figure 3.43.

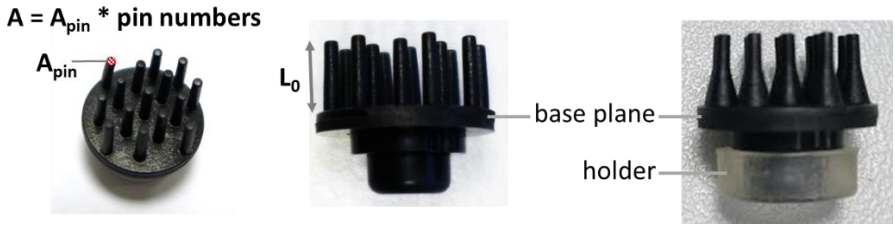

*Figure 3.42: A holder is connected the backside of a pin-shaped electrode resulting in a larger flat surface to support the force during the compression tests. During the compliance prediction, the L_0 is the length of the pins and the A is the sum of the tip area of all pins (A_{pin}*pin number).*

Stiffness (*S*) is the slope of a load and displacement curve and compliance is the inverse of stiffness (*S*). A more compliant electrode shows a shallower sloped load-displacement curve while a stiffer electrode shows a steeper load-displacement curve. The compliance of a pin-shaped electrode is related to the elastic modulus of the material and the geometry of the electrode as shown in Equation 3.13.

$$compliance = \frac{1}{S} = \frac{\Delta L}{F} = \frac{L_0}{E\,A} \qquad \textit{Equation 3.13}$$

where *S* is the stiffness of the shaped electrode, ΔL (m) is the difference between the final length of the sample and the original length of the sample, *F* (N) is the force applied of the sample, L_0 (m) is the original length of the sample, *E* (Pa) is the elastic modulus of the material and *A* (m^2) is the area on which the force is applied. *Compliance* has as unit of m/N, but in this thesis μm/N is used.

In this thesis, the electrode compliance based on the compression measurements is the inverse of the slope (or $\Delta L/F$) of the load-displacement curves. The electrode compliance can also be predicted since the shape of the electrode and the elastic modulus of the material is known, by calculating L_0/EA. For this calculation, L_0 is the length of the electrode pins and the *A* is the sum of the tip area of all pins of the electrode as shown in Figure 3.42. The base plane is not considered during the compliance prediction because the area is ~ 10 times larger than the area of the electrode pins and the height is ~ 30 % of that of the pins. The compliance of the total electrode is the sum of the compliance of both the base plane and the pins. But calculations show that the contribution of the base plane to the total electrode compliance is very small (< 3%) comparing to the compliance of the pins by the pins. Hence for the calculation of the predicted electrode compliance, only the contribution of the pins is considered.

The elastic modulus of the polymer materials is not a constant value but it varies with stress as shown in Figure 3.41d, hence the load/stress range of interest has to be defined, in order to know which elastic modulus range (*E* in Equation 3.13) should be considered for the predictive compliance calculation. The load range of interest is depending on the design of the pin-shaped electrodes. A load range is chosen based on the consideration that a minimal load is needed to ensure all pins of pin-shaped electrodes make good contact with the

compression part of compression tool and the maximum load is defined as the load for which the pins start to buckle due to too much load. As such, the boundaries of the load of interest range are determined for each pin-shaped electrode, converted to the stress boundary by dividing the load to the contact area with skin (the sum of the tip area of the pins). For this load range, the compliance of the shaped electrode can be predicted by combining the elastic modulus of the material with the geometric factors of the electrode.

In the following text, the experimentally obtained load-displacement curves are shown and discussed, as well as the determination of the load-of-interest-range, and this for electrodes containing various amounts of carbon, with various pin numbers, and with different pin thickness and pin length. The comparison between the electrode compliance calculated based on the compression measurements and the predicted value based on E-modulus and electrode shape, is discussed in section 3.4.3.

Comparison of electrodes with various polymer materials

The load-displacement curves of pin-shaped electrodes containing different amounts of carbon (28.2 %, 37 %, and 43.6 % in weight percent) are shown in Figure 3.43 to Figure 3.45. The deformation of the pins at various displacements is also shown in these figures. The load-of-interest-range is marked with a grey background.

Figure 3.43 shows the load-displacement curves of electrodes containing 28.2 wt% of carbon. Pictures in Figure 3.43 show that not all pins are standing straight even prior to the compression test, which is caused by the fact that the pins of this soft electrode bend very easy, and they were stored in a simple plastic bag for a long time before the compression test. Some pins were bended during storage, and these bended pins could not be straightened entirely prior to the compression tests. This results in a limited accuracy of the compliance result of these softer electrodes. The measurements are carried out on only two samples because no more samples are available. The pictures show that from ~ 250 μm displacement some pins start to buckle. For 300 μm displacement, the load-displacement curves is clearly flattening because of this buckling of the pins. Therefore, the load/stress when the displacement is 150-200 μm is defined as the load-of-interest-range.

The picture of 750 μm shows that even though the load is not applied uniformly over the entire base plane, the base plane does not deform and the pins located at the center do not buckle more severely than the ones at the edge. This shows that using the holder shown in Figure 3.42 during the compression tests causes no significant effects on the load distribution.

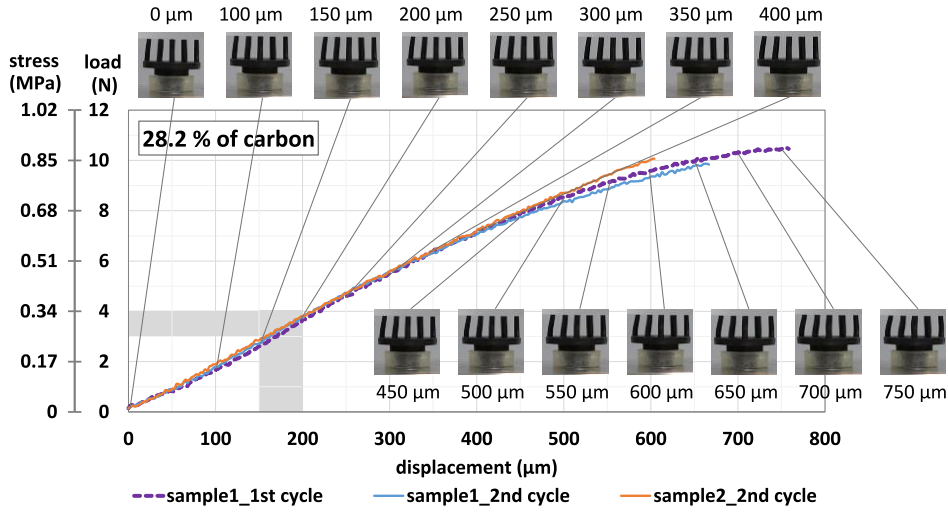

Figure 3.43: The load-displacement curves of pin-shaped electrodes containing 28.2 wt% of carbon. The deformation of the pins of one of the samples is shown in the pictures. The load/stress when the displacement is 150-200 µm is defined as the load-of-interest-range.

Figure 3.44 and Figure 3.45 show the load-displacement curves of electrodes containing 37 wt% and 46.3 wt% of carbon. It is found that the pins of the electrodes start to buckle at 250-300 µm displacement. Therefore, the load/stress when the displacement is varying between 150-200 µm is defined as the load-of-interest-range.

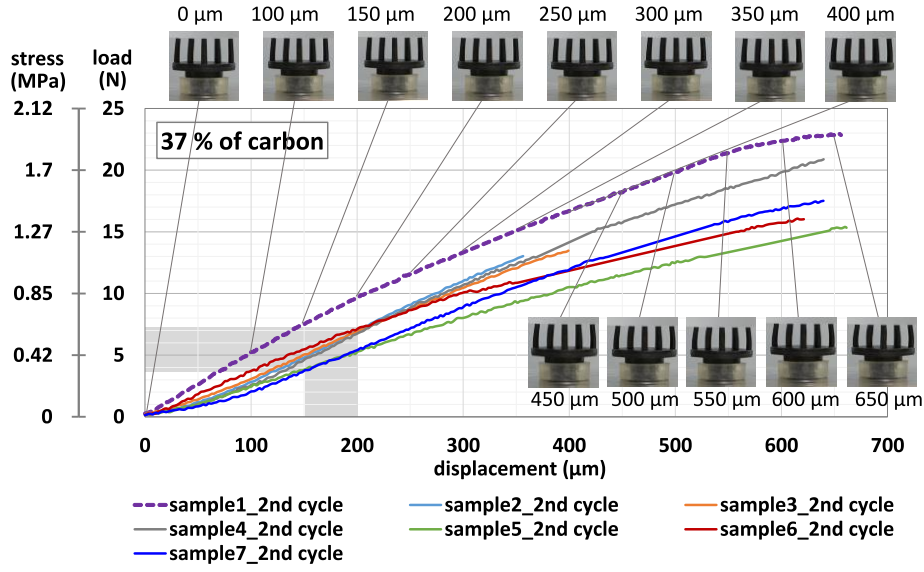

Figure 3.44: The load-displacement curves of pin-shaped electrodes containing 37 wt% of carbon. The deformation of the pins of one of the samples is shown in the pictures. The load/stress when the displacement is 150-200 µm is defined as the load-of-interest-range.

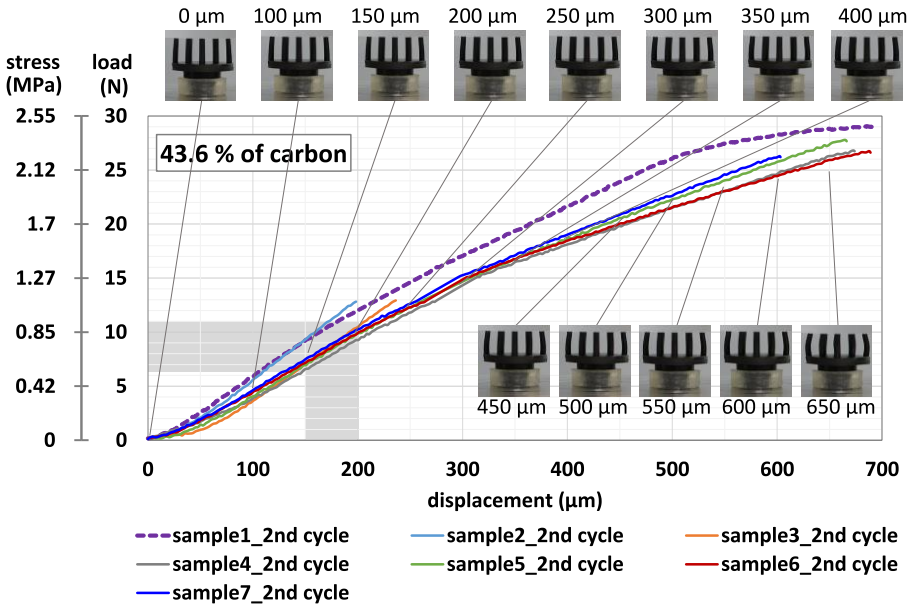

Figure 3.45: The load-displacement curves of pin-shaped electrodes containing 43.6 % of carbon. The deformation of the pins of one of the samples is shown in the pictures. The displacement at 150-200 µm is defined as the load-of-interest-range.

The load-of-interest-range indicated in the graphs above is essential to allow a predictive electrode compliance based on material properties and electrode shape, as is further discussed in section 3.4.3. It has to be noted that the load-of-interest-range marked in Figure 3.45 is according to load levels higher than the pain threshold of the skin of human beings. The pain threshold on the limb reported in [158] is around 0.5 MPa, which is 0.5 N/mm^2. On the forearm, the pain threshold is somewhat lower: around 0.4 MPa [159]. The pin area contacting the skin of our polymer electrode with 15 pins is 12 mm^2, hence the pain threshold is reached when a 4.8-6 N load is applied on the electrodes. This in line with our experience that the maximum load which the subjects experienced as non-painful is around 4 N when using our pin-shaped polymer electrodes containing 43 wt% of carbon. In Figure 3.45, the load/stress at around 4N is below the load-of-interest-range because not all of the pins of the electrodes make firm contact with the compression part of compression tool at this lower load level, resulting in the initial non-linear part of the load-displacement curves. Also for other electrodes, the load/stress of interest range is often higher than the pain threshold which is observed during biopotential measurements.

Comparison of electrodes with different pin numbers

The load-displacement curves of the pin-shaped electrodes with various pin numbers shown in Figure 3.46. All the electrodes are made from the polymer material containing 43.6 % carbon.

Figure 3.46: Pin-shaped electrodes with 12 pins, 15 pins and 19 pins.

Figure 3.47 shows the load-displacement curves of the electrodes with 12 pins. The pictures show that at 300 µm displacement the pins start to buckle and correspondingly the load-displacement curves start to flatten. The load/stress range at 150-200 µm displacement is defined as the load-of-interest-range.

The load-displacement curves of the electrodes with 15 pins are the ones shown in Figure 3.45.

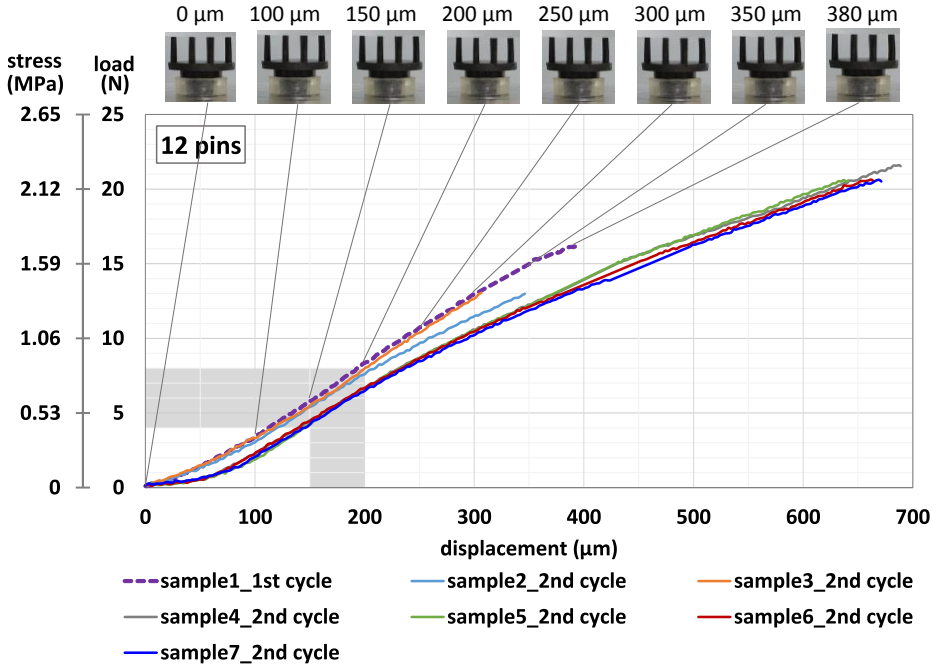

Figure 3.47: The load-displacement curves of pin-shaped electrodes with 12 pins. The deformation of the pins of one of the samples is shown in the pictures. The displacement at 150-200 µm is defined as the load-of-interest-range.

Figure 3.48 shows the load-displacement curves of the electrodes with 19 pins. The load/stress range at 150-200 µm displacement is defined as the load-of-interest-range.

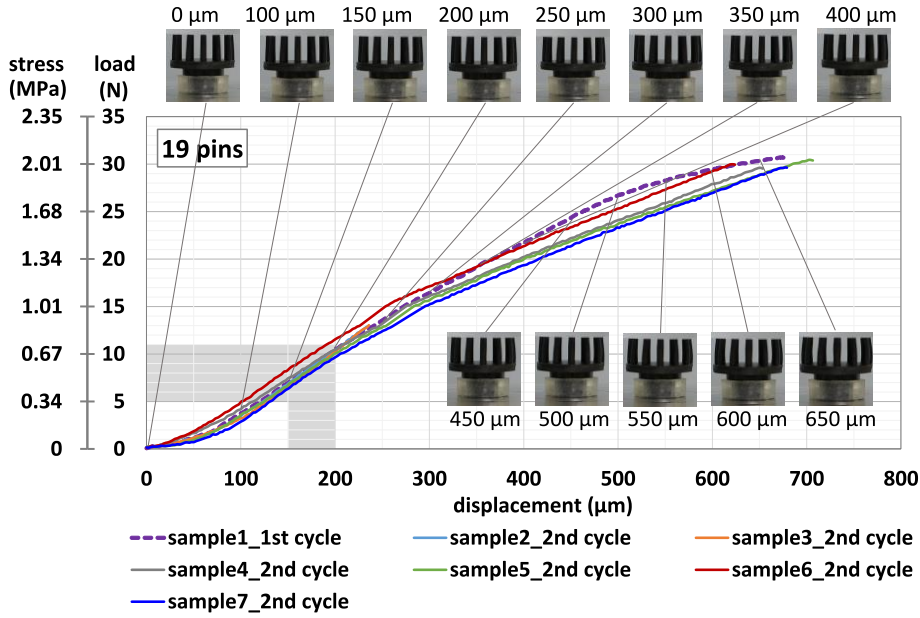

Figure 3.48: The load-displacement curves of pin-shaped electrodes with 19 pins. The deformation of the pins of one of the samples is shown in the pictures. The displacement at 150-200 µm is defined as the load-of-interest-range.

Comparison of electrodes with different pin thickness

The load-displacement curves of electrodes with the same material composition and pin numbers, but with different pin thickness, are shown in Figure 3.49.

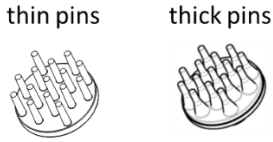

Figure 3.49: Pin-shaped electrodes with thin and thick pins.

The load-displacement curves of the electrodes with thin pins are shown already in Figure 3.45. Figure 3.50 shows the load-displacement curves of the electrodes with thick pins. The pictures show that from 300 µm displacement the thin part of the pins buckle much more than the thicker cone-shaped part. The load/stress range at 150-200 µm displacement is defined as the load-of-interest-range.

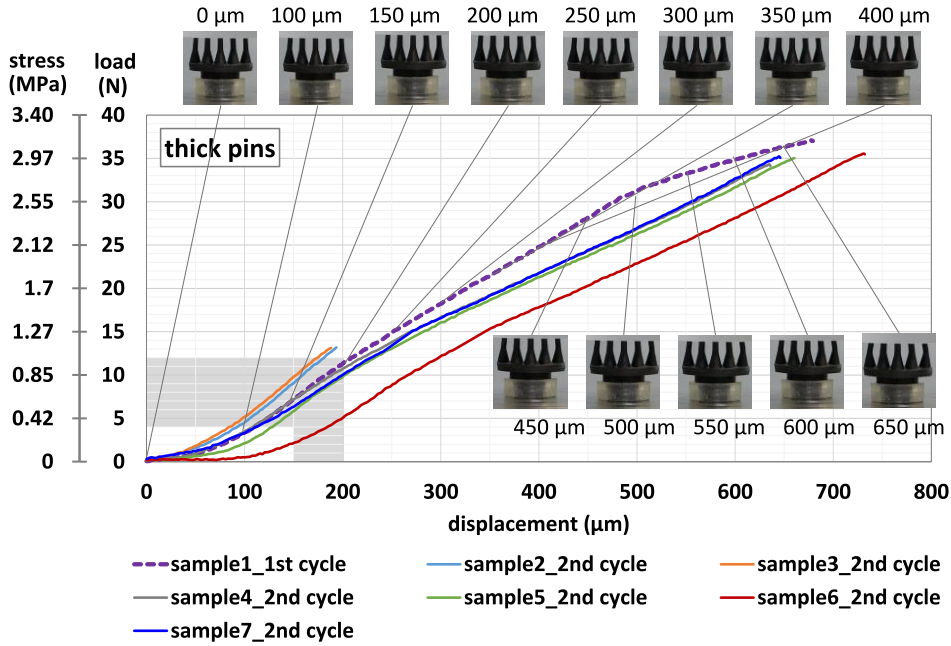

Figure 3.50: The load-displacement curves of pin-shaped electrodes with thick pins. The deformation of the pins of one of the samples is shown in the pictures. The displacement at 150-200 µm is defined as the load-of-interest-range.

Comparison of electrodes with different pin lengths

The load-displacement curves of electrodes with the same material composition and pin number, but with different pin lengths (5mm and 8mm), are shown in Figure 3.51.

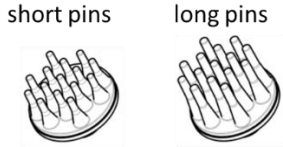

Figure 3.51: Pin-shaped electrodes with short and long pins.

The load-displacement curves of the electrodes with short pins are shown already in Figure 3.50. Figure 3.52 shows the load-displacement curves of the electrodes with long pins. The pictures show that from 250 µm displacement the cylindrical-shaped part of the pins start to buckle much more severe than the cone-shaped part. From this point, the load-displacement curves become more flat. The load/stress range at 130-180 µm displacement is defined as the load-of-interest-range.

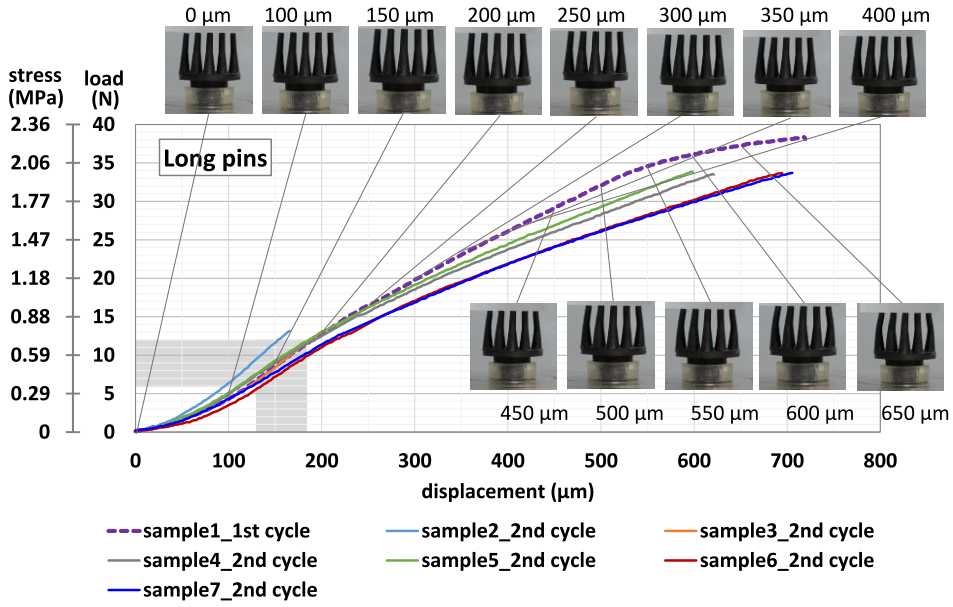

Figure 3.52: The load-displacement curves of pin-shaped electrodes with thick pins. The deformation of the pins of one of the samples is shown in the pictures. The displacement at 130-180 µm is defined as the load-of-interest-range.

3.4.3 Comparison of the compliance based on the electrode compression measurements and the predicted compliance

According to Equation 3.13, the compliance based on the electrode compression measurements is $\Delta L/F$ or the inverse of the slope of the load-displacement curves. Since this slope is varying over the curve, only the compliance in the load-of-interest-ranges is considered. The predicted compliance is calculated using L_0/EA as discussed in section 3.4.2. The E-values of the polymer materials are known from the compression tests, but also here E-values vary with load/stress. Hence the load-of-interest-ranges as defined for each electrode (shown in the figures in section 3.4.2) are used to calculate the relevant E-range for each material and electrode shape, this range is further called the E-of-interest-range.

The determination of the E-of-interest-range

During the compression tests, it was seen that the results can vary between test buttons made from the same material, or when the same test button was tested more than once. Hence it is considered essential to investigate the reproducibility of the compression measurements of the test buttons, before the determination of the E-of-interest-range. The test protocols and the test results are described as below.

(1) Measurements performed on the same test button for non-interrupted load/unload cycles.

As is discussed already in section 3.4.1, the load-displacement curve from the 1st loading cycle deviates from that of the 2nd and 3rd loading cycles applied on the same test button, while these latter cycles give always similar results. Therefore, the load-displacement curves of the 2nd cycle are always used in this thesis to represent the load-displacement behavior of a test button.

(2) Repeated compression measurements performed on the same test button but with a short interrupt in order to remove the sample from the compression tool and place it back.

Six load-displacement curves of one test button containing 37 wt% of carbon are measured in three sessions, called session A, B and C. In each session, 2 load-unload cycles are performed, the corresponding fitted elastic modulus curves of the 2nd cycles are shown in Figure 3.53a. In between each session, the sample is removed from the compression tool and then placed back. The maximum applied load is always kept sufficiently small to avoid settling of the material which would influence the compression test in the next cycle. It is found in the figure that especially for the higher stress/load values, clear variations in E-modulus are seen for the same test sample, showing clearly that some non-reproducibility exists. Similar tests are performed on test buttons from polymer material containing 28.2 wt% and 43.6 wt% of carbon, and similar variations in elastic modulus curves are obtained.

(3) Measurements performed on the same test button during various days.

Every day, a test sample containing 37 wt % of carbon is placed in the compression tool, two loading cycles are performed and the sample is removed. The test is performed on the same sample for three continuous days. The fitted elastic modulus curves of the 2nd cycles measured each day are shown in Figure 3.53b. The resulting curves are not identical. These tests over days showed a larger variation compared to the tests doing repeated measurements on the same day (curves in Figure 3.53a.) The same trend is also seen for other test buttons with the same and with different carbon content.

(4) Measurements performed on several test buttons made from the same polymer material.

Five ‘similar’ test buttons all containing 37 wt % of carbon underwent the compression tests and their fitted elastic modulus curves of the 2nd loading cycles are shown Figure 3.53c. Although the test buttons should be very similar, the test results show clear differences between the buttons. The variations between ‘similar’ buttons are larger than the variations seen after repeated tests on the same button as shown in Figure 3.53a and b. The same trend is also found for other test buttons with different carbon content.

To conclude, the reproducibility tests discussed above indicate that the measured elastic modulus varies between samples of the same material, and from test to test on the same sample. Obviously this will has a negative contribution to the accuracy of the predicted

electrode compliance. Since the variations in between samples are larger than the variations from test to test, only the variations in between samples are taken into account during the determination of the E-of-interest-range. Hence the prediction will not be made for one E-value, nor for an E-range-of-interest for 1 button, but for a range of E-values corresponding with the test results of the compression tests on the various 'similar' samples.

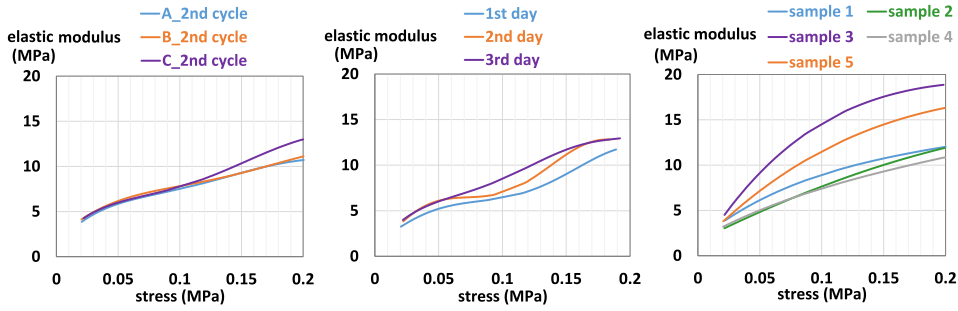

(a) (b) (c)

Figure 3.53: (a) The fitted elastic modulus curves of a test button containing 37 wt% of carbon measured during repeated tests interrupted to remove the sample from the compression tool and then place it back. (b) The fitted elastic modulus curves of a test button containing 37 wt% of carbon measured each day for 3 continuous days. (c) The fitted elastic modulus curves of 5 'similar' test buttons all containing 37 wt % of carbon. All curves are based on the 2nd loading cycles of the compression measurements.

Figure 3.54 shows an example of defining the elastic modulus in the stress-of-interest-range based on the measurements of five test buttons containing 37 wt% of carbon. Their fitted elastic modulus curves are shown in Figure 3.54a. The maximum, minimum and average value of the elastic modulus in the stress-of-interest-range (grey shade in Figure 3.54a) is determined for each sample and plotted in Figure 3.54b. Since variations between each sample are present, an average of all averages is calculated, and the general minimum and maximum E-values is determined and considered as the borders of the total E-range-of-interest (grey shade in Figure 3.54b) for a certain electrode shape and material.

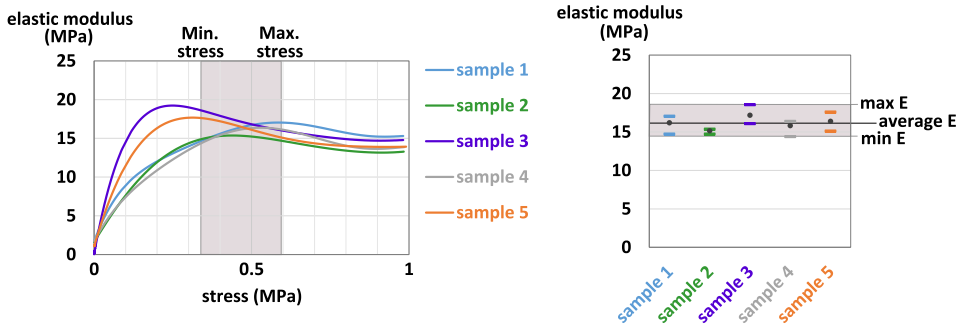

(a) (b)

Figure 3.54: (a) The fitted E curves of 5 samples of cylindrical-shaped electrode containing 37 wt% of carbon. For each sample, the maximum and minimum E values in the region of the stress-of-interest-range are obtained as shown in (b). The interest range is marked with grey background and is defined as when the stress of a cylindrical-shaped electrode is the same as the stress of the interest range applied on a pin-shaped electrodes made from the identical material. (b) The 'average E', 'max E' and 'min E' are used to calculate the predicted compliance of the pin-shaped electrodes.

Comparison of the compliance based on the electrode compression measurements and the predicted compliance

The compliance of the pin-shaped electrode measurements in the load-of-interest-range is calculated using Equation 3.13. The same equation is used for compliance prediction based on the E-range-of-interest of various materials and the geometric factors of the pin-shaped electrodes. The geometric factors (L_0 and A) of the pin-shaped electrodes are introduced already in section 3.4.2 and Figure 3.42.

Comparison of electrodes with various polymer materials

Figure 3.55 shows the compliance calculated based on the measurements (black dots) and the predicted compliance range of pin-shaped electrodes containing 28.2 wt%, 37 wt% and 43.6 wt% of carbon. All electrodes have the same shape as shown in Figure 3.55. The average and the range of predicted compliance are calculated using Equation 3.13 and using the 'average E' ,'max E' and 'min E' of the corresponding polymer materials as explained in previous section. The range of predicted compliance is marked with a grey shade in the graphs, and the average predicted compliance is marked with the dashed line. For each material, several similar electrodes are tested (amount of electrodes was dependent on availability). Each black dot corresponds with another similar electrode. The compliance of electrodes containing only 28.2 wt% of carbon deviate the most from the predicted region, probably because not all pins are standing straight prior the measurements which results in a limited accuracy of the compliance result of the softest electrodes as was discussed already in section 3.4.2.

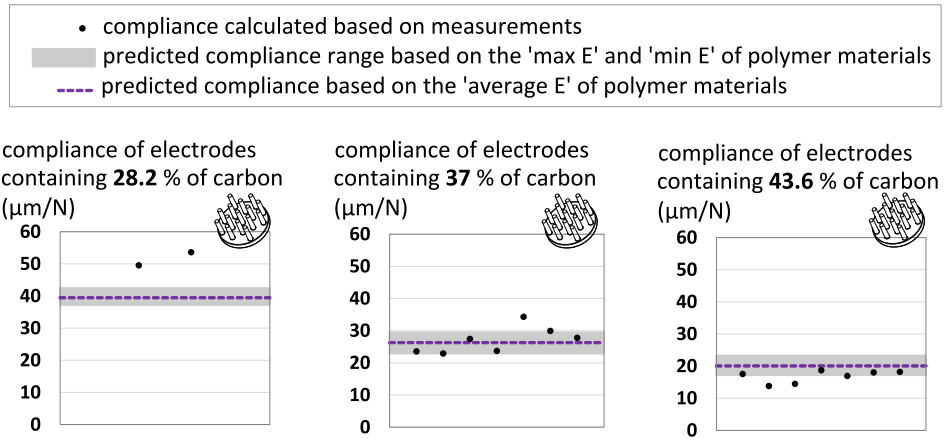

Figure 3.55: The comparison of the compliance calculated based on the pin-shaped electrode measurements (the black dots) and the predicted compliance of the electrodes, for 3 materials with different carbon content. The predicted compliance range based on the 'max E' and 'min E' of polymer materials is marked as a grey shade. The predicted compliance based on the 'average E' of polymer materials is marked with a dashed lines.

Comparison of electrodes with different pin numbers

Figure 3.56 shows the compliance calculated based on the measurements and the predicted compliance range of the pin-shaped electrodes with 12, 15 and 19 pins.

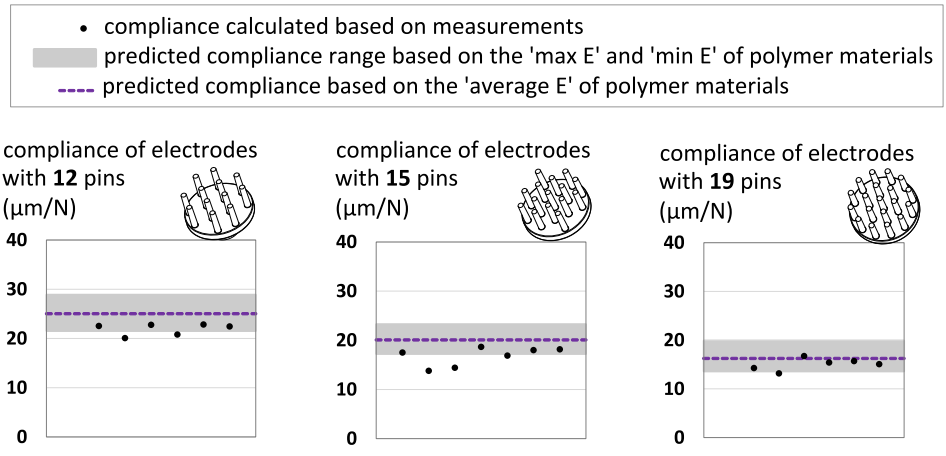

Figure 3.56: The comparison of the compliance calculated based on the pin-shaped electrode measurements (the black dots) and the predicted compliance of the electrodes, for pin-shaped electrodes with different pin numbers. The predicted compliance range based on the 'max E' and 'min E' of polymer materials is marked as a grey shade. The predicted compliance based on the 'average E' of polymer materials is marked with a dashed lines.

Comparison of electrodes with different pin thickness

As shown in Figure 3.49, the thick pins are cone-shaped while the thin pins are cylinder-shaped. To obtain the equivalent geometric factors of the electrodes with thick pins for compliance prediction, the pins are separated into upper cylindrical-shaped part and lower cone-shaped part. The lower cone-shaped part is further separated into four conical frustums as shown in Figure 3.57. The area at the center of each conical frustum is used to represent the A of the conical frustum. The predicted compliance of the cone-shaped electrodes is the sum of the predicted compliance of each separated part. The thick pins of the electrodes were introduced in order to make the electrode pins more stiff. This is indeed what is obtained, as can be seen in Figure 3.57: the thicker pins show a lower electrode compliance, and also the predicted compliance is lower.

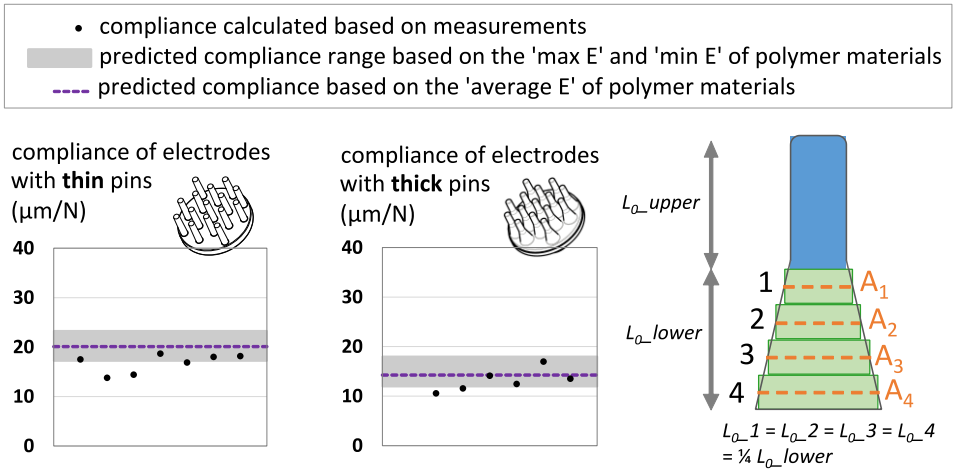

Figure 3.57: The comparison of the compliance calculated based on the pin-shaped electrode measurements (the black dots) and the predicted compliance of the electrodes, for pin-shaped electrodes with different pin thickness. The predicted compliance range based on the 'max E' and 'min E' of polymer materials is marked as a grey shade. The predicted compliance based on the 'average E' of polymer materials is marked with a dashed lines. The predicted compliance of electrodes with thicker pins is calculated by separating the con-shaped part of the pins into conical frustums.

Comparison of electrodes with different pin lengths

The compliance of the electrodes with the same material composition and the same number of pins, but with different pin lengths (5mm and 8mm) is characterized. The pins of both electrodes contain a cylindrical-shaped top part and a cone-shaped part at the bottom. Besides the differences of the pin lengths, the diameter of the cylindrical-shaped part of long pin electrode is 0.2 mm larger than that of short pin electrode. Also the diameters of the conical frustums of the long pin electrodes are slightly larger than that of the short pin electrodes. The calculation of the predicted compliance of the cone-shaped part of the pins is performed as discussed above (see also Fig. 3.22), the results are plotted in Figure 3.58. For the electrodes with design shown in Figure 3.51, the electrode with longer pins is more

compliant than that of the electrode with shorter pins, although the difference is small due to the fact that the longer pins are also slightly thicker.

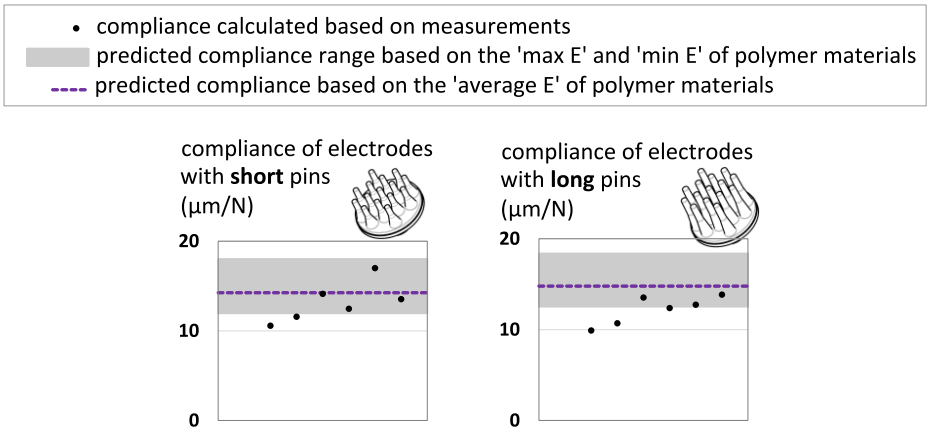

Figure 3.58: The comparison of the compliance calculated based on the pin-shaped electrode measurements (the black dots) and the predicted compliance of the electrodes, for pin-shaped electrodes with different pin lengths. The predicted compliance range based on the 'max E' and 'min E' of polymer materials is marked as a grey shade. The predicted compliance based on the 'average E' of polymer materials is marked with a dashed lines.

Discussions and conclusions

The first observation made when measuring the electrode compliance is that there is a lot of variation between 'similar' samples. This is in accordance with the observations made when the reproducibility of the compression test on the buttons was investigated.

When comparing the predicted compliance of the electrodes with the measured ones, ~71% of the measurement data points correspond with the prediction. However, the maximum deviation which is measured is less than 5 µm/N from the predicted range. The first possible reason of the deviation is the reproducibility issue when performing compression tests. Second, the elastic moduli of polymer materials are characterized on the test buttons where both the skin and bulk parts with different mechanical properties are taken into account. For the pin-shaped electrodes, the skin of each pin might result in different mechanical properties causing the deviation between the predicted and experimental compliance. Third, the lateral expansion of the pins during compression tests is not taken into account when the predicted compliance is calculated. In general, the Poisson's ratio of a rubber is considered to be ~0.5 indicating that the strain at the lateral direction is half of the strain at the vertical direction when a load is applied vertically. For the electrode with 15 pins shown in Figure 3.46, the predicted compliance decreases with 2.5 µm/N when the lateral expansion at 200 µm displacement is taken into account. These inaccuracies during the measurements and calculations result in the deviation in between the predicted and experimental compliance.

To conclude the influence of polymer materials on the compliance of the pin-shaped electrodes, the electrodes containing more carbon are less compliant. It is just this property

that limits the amount of carbon that can be added to the polymer matrix since regarding electrical properties a higher carbon content is desirable. The harder the polymer, the lower the user comfort and the greater problems related with polymer demolding and brittleness. Trial rubber formulations with higher carbon load resulted in more rejects in the molding process, since electrodes with very small pins or with long straight pins got easily stuck in the mold, resulting in missing pins on the final electrode. Obviously, if one of the pin-cavities of the electrode mold is partially filled with stuck rubber, the subsequent moldings will have defect electrodes. Hence, this problem should be prevented. Rubber formulations with a higher carbon load and hardness resulted in 50% or more rejects especially for the more difficult designs (very small thin pins or long straight pins), while for the optimized electrode designs (conical pins, shorter pins) the fabrication yield was 100%.

To conclude the influences of electrode shape designs on the compliance of polymer electrodes, the electrodes with thicker pins and higher pin density are less compliant or more stiff. Stiffer polymer electrodes can withstand more force from the fixation devices (e.g. EEG headset or cap) without bended pins. This ensures that the pins can penetrate the hair and touch the skin. For softer electrodes, the electrode pins bend to support the force from the headset, elastic bands or other mounting devices. A compromise need to be found: when the electrodes that are too compliant, they will not be able to penetrate the hair to reach the scalp, since they will not be able to support the weight and force of wearable devices without strongly bending pins.

The conclusion in last paragraph does not imply that the optimal electrodes are the ones with the shortest pins, thickest pins or higher pin density. The optimum electrode depends on the measurement situation: longer pins are only necessary if the body area has a significant amount of hair. The thicker and condensed pins of polymer electrodes reduce the space for hair, hence these electrodes are only suitable in case of a limited amount and/or short hair.

3.4.4 Viscoelastic properties of the pin-shaped polymer electrodes

In section 3.4.1 and 3.4.2, only the loading parts of the load-displacement curves are used for mechanical properties characterization. Figure 3.59 shows the entire load-displacement curves of both of the loading and unloading process of a pin-shaped electrode, and this for various subsequent load/unload cycles. The curve of the 1st cycle deviates significantly from the others. This is seen for all compression tests on all materials. Furthermore, load and unload curves are showing a clear hysteresis effect, again seen for all materials. This hysteresis effect indicates that the EPDM polymer materials have viscoelastic properties [160-163]. An elastic material stores 100% of energy due to deformation thus it recovers to its original shape after the applied load is removed; however, a viscoelastic material losses or dissipates part of the energy as heat during the deformation and recovery phase, resulting in the hysteresis loop.

The viscoelastic properties of the electrode materials will result in a 'recovery time': the time needed for the pins of the electrodes to recover to its original length. This is illustrated in Figure 3.59: 4 non-interrupted load/unload cycles are applied to a pin-shaped electrode. After a short interruption of 10 minutes, a 5th and 6th cycle are applied. The electrode deforms significantly after the 1st cycle and does not recover before the 2nd cycle starts. The 3rd to 4th

cycles are very similar to the 2nd. During the 10 minutes interruption, the deformation of the electrode recovers only slightly, as can be seen in Figure 3.59b. The 5th cycle is only slightly shifted towards the first one, and the 6th cycle is again similar to the 3rd and 4th cycle. Obviously total recovery of the pins will take much more time than 10 minutes.

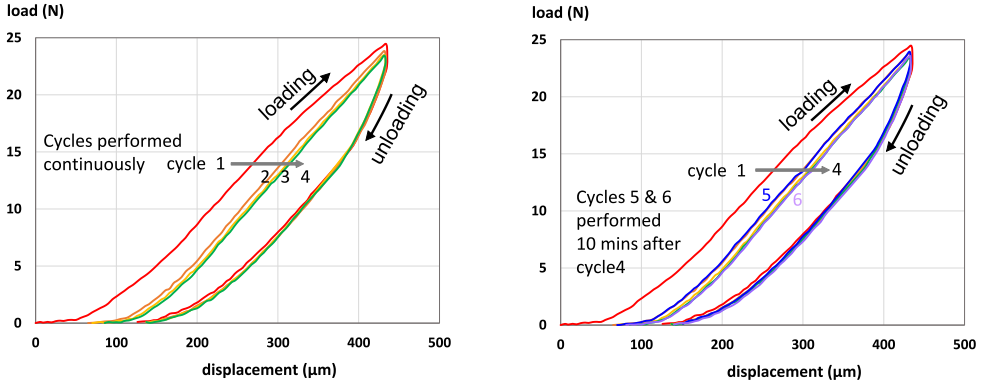

Figure 3.59: The load-displacement curves of repeated loadings on a pin-shaped polymer electrode. The curves shown in (a) is obtained after 4 continuous cycles. The curves obtained in cycles 5 and 6, which performed 10 minutes after cycle 4 are added in (b). The displacement rate of all cycles is 50 μm/s.

During real biopotential measurements, the polymer electrodes do not experience dynamic loadings as discussed in previous paragraph. A constant static load is used, with small 'dynamic' load variations. Hence a more relevant study is the deformation and the recovery time of a pin-shaped electrode after applying for a longer time a constant load, similar in magnitude to that of a real skin fixation device (i.e. headset). Therefore, a 0.42 N/mm^2 pressure being the pain threshold of human beings when using a pin-shaped electrode discussed in section 3.4.2 (i.e. 5 N on the pin-shaped electrode with a 12 mm^2 area contacting the skin) is applied on the electrode for 30 minutes being the time for a regular short-term EEG measurement. It is found that after the load is released, it takes 30 minutes for the pins of the electrode to recover to their original height.

Besides the hysteresis shown in the load-displacement curves and the 'recovery time' needed after the removal of the load, a viscoelastic material shows creep and stress relaxation when being deformed [164]. Creep describes the change of strain in a material with time, when a constant stress is applied. Stress relaxation means that the stress of a material changes with time when a constant strain is maintained. During the biopotential measurements, creep and stress relaxation of the electrodes might influence the electrode/skin contact when a fixation device gives a permanent pressure to the electrodes in order to maintain a good contact with the scalp. Both creep and stress relaxation show that the viscoelastic materials take time to response the load applied on it. The creep of the polymer materials cannot be characterized using the compression measurements. So, only the stress relaxation of the polymer materials is characterized using the compression tests.

In Figure 3.60a, stress relaxation of a pin-shaped electrode measured using a compression test is shown. During the test, the electrode is suddenly compressed till a 10N load (period 1) then the obtained displacement is maintained for 30 seconds while the load is measured (period 2), after which the compressive load is completely removed (period 3). Once the load is reduced to 0N, the displacement is kept constant again (period 4). Figure 3.60a shows the material relaxes during period 2, resulting in the decreasing of the load from 10N to 8N in 30 seconds. The compressed electrode recovers in period 4 resulting in an increasing load with time.

Stress relaxation of the polymer electrodes will have an influence during the real biopotential measurements. When the load from the fixation device (i.e. a headset) is suddenly applied on an electrode to obtain optimized location and pressure between the electrode and the scalp for a good electrode/skin contact, this pressure and position will not remain optimal after a short while since stress relaxation of the polymer electrodes might result in an insufficient pressure on the electrode, and an adjustment of the electrode position for a good electrode/skin contact is needed. Therefore, a proper headset should be equipped with an electrode holder with a spring function itself to compensate for this relaxation effect.

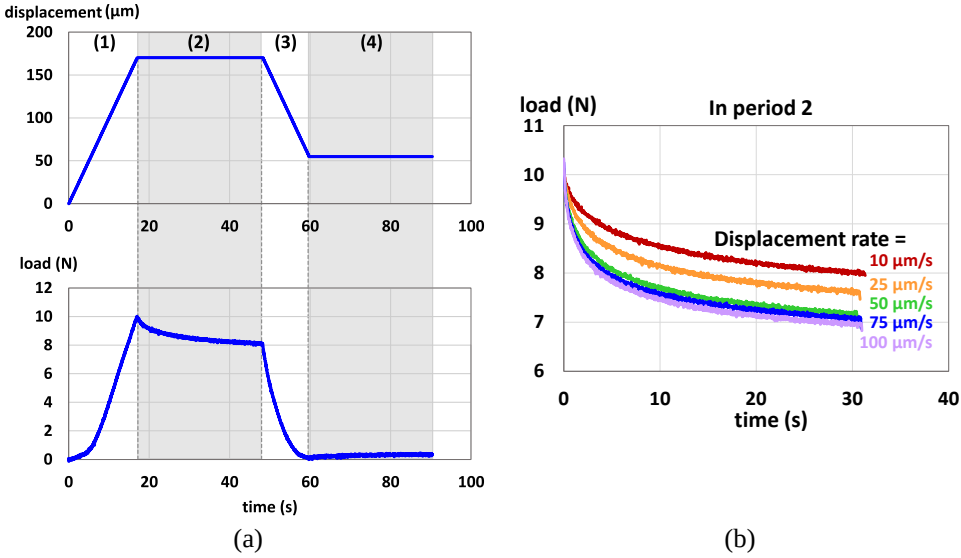

(a) (b)

Figure 3.60: (a) The stress relaxation property of a pin-shaped electrode. The curves are obtained using a compression test with a 10 µm/s displacement rate. (b) The load-time curves during stress relaxation after loaning a pin-shaped electrode using compression test with various displacement rates. The curves are recorded in period 2 of (a).

It is known that mechanical properties of a viscoelastic material vary when applying the load with various displacement rate [163, 165]. To test this for our electrode materials, the same experiment as before is repeated but with various displacement rates used in period 1. This results in various rates of stress relaxation as shown in Figure 3.60b. A faster displacement rate in period 1 results in a faster stress relaxation in period 2, which is in line with the results obtained from a polyether urethane-based rubber reported in [166]. For a faster displacement

rate, the material does not have sufficient time to relax during the load applied in period 1. Therefore, most of the stress relaxes in period 2 resulting in a more pronounced stress relaxation in this period. In case a slower displacement rate is used in period 1, the material has some time to response (relax) to the load already in period 1 while being deformed, so less stress relaxation is seen in period 2. In real applications, the load maximum load applied on the electrodes is ~ 5N (as discussed in section 3.4.2) and this load will result in a less pronounce variation of stress relaxation between different displacement rates. A proper headset with holders with a spring as mentioned in last paragraph will reduce this stress relaxation effect.

Conclusions

The results of the 'recovery time' and stress relaxation tests of the pin-shaped electrodes reveal the viscoelastic properties of the EPDM rubber. These properties will need to be taken into account when the electrodes are used in biopotential measurements, such as the design of the fixation devices and the usability of the electrodes over longer time periods.

3.5 Conclusions of the electrical and mechanical properties evaluations of polymer dry electrodes

Based on the results of the polymer electrode evaluation, including both electrical and mechanical properties, the polymer electrodes with material composition number 64 and 95 are used for the biopotential signals' validation in this thesis (They are labelled as CR64 and CR95 in the following chapters). Both materials containing 43.6 wt% of carbon show only ~10 times higher electrode/skin impedance than that of wet electrodes.

The mechanical properties of the polymer electrodes are characterized using compression tests. Experiments show a clear variation between tests on similar samples and smaller variations when the same sample is measured repeatedly. As expected, the elastic moduli of the polymer materials increase with increasing of carbon content, and electrodes made from polymer with a higher carbon content show to be less compliant. Regarding the shapes of the pin-shaped electrodes, the electrodes with more pins, thicker pins and shorter pins are less compliant. The compliance of the pin-shaped electrodes can be predicted rather well using the elastic moduli of the polymer materials and the shapes of the electrodes. The predicted values vary slightly (< 5 μm/N) from the compliance obtained by compression measurements on the electrodes.

The viscoelastic properties of the polymer electrodes, such as 'recovery time' and stress relaxation, are also evaluated. These properties are important regarding the design of the electrode fixation devices (ie. headset) and the usability of the electrodes over longer time periods, in order to ensure long term high quality biopotential measurements.

To conclude, the designs of the electrodes shown in Figure 3.61 are used in the ECG and EEG monitoring in this thesis. The polymer electrodes, both with and without pins, are applied in ECG monitoring. The pin-shaped electrodes have 2 mm pins. Other electrodes with 15 cone-shaped pins in 5 mm length are used in EEG monitoring on hairy locations. Sometimes when it is feasible to connect the cylinder-shaped electrodes to the electronic

devices, they are used on skin without hair (e.g. on bald scalp, on the forehead, and at the back of earlobes).

Figure 3.61: Electrodes that are applied in ECG and EEG monitoring in this thesis.

Chapter 4.
Polymer Electrode Validation 1: ECG monitoring

A standard 12-lead ECG signal is measured by placing ten conventional wet ECG electrodes on the chest. Each lead is formed by a pair of electrodes representing a vector along which the ECG signals are recorded. In other words, the lead represents the electrical potential difference between the two electrodes. This 12-lead ECG (including measurements along 12 different vectors) provides a thorough view of the heart's activities. A standard ECG signal is shown in Figure 4.1. It consists of a repeating cycle of a P wave, a QRS complex, a T wave, and a U wave, which represent different stages of the heart's activities. The shapes and amplitudes of these waves depend on the location of the electrodes (the leads).

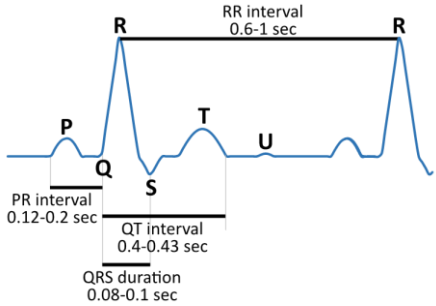

Figure 4.1: A standard ECG signal consisting of a repeating cycle of a P wave, a QRS complex, a T wave, and a U wave.

In this thesis, the aim is not to record a 12-lead ECG, but to compare the signals recorded by wet and dry electrodes using similar locations (similar leads). Therefore, a 1-lead ECG is recorded by placing two electrodes on the body. During the recordings, a bias electrode is also placed on the body to reduce interferences from the power lines. To validate the accuracy of signals recorded by polymer dry electrodes, ECG signals were recorded by polymer dry electrodes and compared with simultaneously recorded signals using conventional wet electrodes. The measurements were performed at two body locations: with electrodes placed on the chest and at the lower abdominal area. The experimental setup and protocol will be discussed in section 4.1. After which, the signal analysis of the recorded data is introduced in section 4.2. The results of ECG signals recorded from both body locations will be evaluated in section 4.3.1 and section 4.3.2. Last, section 4.4 reports about an additional series of electrical measurements carried out on selected polymer electrodes according to the "ANSI/AAMI EC12: Disposable ECG electrodes" standard, evaluating whether the polymer electrodes pass the EC standard established for commercial ECG electrodes.

4.1 Electrodes setup, recording system and protocol

Electrodes with the optimum conductive polymer containing ~50% of carbon and with 2 mm pin length and 10 mm base size were used for the ECG recordings. To connect the polymer dry electrode to the recording system and to place the dry electrode on the chest, a conventional wet gel ECG electrode (Meditrace 200 Series ECG Electrodes, Kendall) was taken, and the gel was removed leaving only the snap and skin adhesive part as attachment for the dry electrode. The backside of the dry electrode was attached to the snap using a double-sided copper tape, as shown in Figure 4.2a. In order to correctly compare the signal

of a dry electrode with that of a wet electrode, two conventional wet electrodes were placed next to two dry electrodes in order to obtain two very similar ECG signals (see Figure 4.2b). The distance between the centers of both electrodes was about 1.5 cm. Two such pairs of wet-dry electrodes were placed on the subject's chest or lower abdominal area, and then combined with one dry electrode as a bias signal. The locations will be described in detail in sections 4.1.1 and 4.1.2.

After placing the electrodes on the skin, cables were used to connect the electrodes to a recording amplifier. Since ECG signals are in the mV range, these signals are strong enough to be acquired directly without pre-amplifier between the dry electrodes and ECG recording system. An analog front-end ECG recording board designed at imec was used as a recording system [30]. This recording board is equipped with a programmable 4th order low pass filter (LPF). A 200 Hz LPF was used for the recordings in this work. The sampling rate is 256 Hz.

(a)

(b)

Figure 4.2: (a) Conductive polymer dry electrode mounted on an adhesive pad and electrically connected to the electrode snap; (b) A pair of wet and dry electrodes to be placed on the skin for signal comparison.

4.1.1 ECG recording from the chest

The locations of electrodes for ECG recordings on the chest are shown in Figure 4.3a. The subject performed the following movements during consecutive recording sessions: (1) sitting without moving; (2) opening/closing arms, turning left/right, opening/closing arms and then raising arms up and down; (3) standing, sitting, walking, and sitting while playing a chest game. Both wet and dry signals were recorded simultaneously, and the similarity between them is determined using correlation calculation which is going to be introduced in section 4.2. Since the lead of Ch1 and that of Ch2 in Figure 4.3a cannot be the same (the electrodes cannot be placed on top of each other), their signals are never identical. Conventional wet electrodes are considered as standard electrodes for ECG measurements for being able to record accurate signals. If dry electrodes are replaced by wet ones, resulting in the locations shown in Figure 4.3b, the similarity between the two signals represents the highest similarity of two standard electrodes placed in close proximity. Therefore, a so-called reference recording test was done in order to compare the similarity of this reference recording with that of the signals acquired by a pair of wet electrodes and a pair of polymer dry electrodes placed in close proximity to each other.

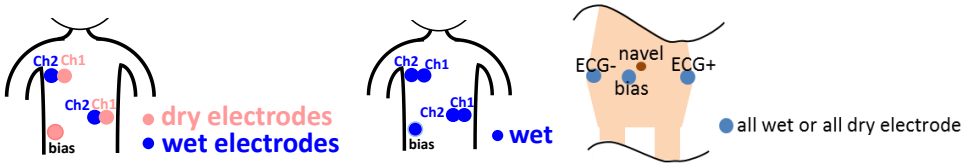

Figure 4.3: (a) Electrode locations for ECG measurements on the chest; (b) Electrode locations for reference recording test; (c) Electrode locations for ECG measurements at the lower abdominal area.

4.1.2 ECG recording at lower abdominal area

In order to mount the polymer dry electrodes on the chest, an extra fixation should always be used, as in the adhesive part in Figure 4.2a. Integration of the polymer dry electrodes in textile/clothes would lead to a more user-friendly ECG monitoring device. To evaluate if integration of dry electrodes in the elastic band of underpants would work well, the ECG signals acquired at the lower abdominal area using polymer dry electrodes were evaluated. A pair of channel electrodes and one bias electrode were placed at the location shown in Figure 4.3c for ECG recordings. During this recording, the signals of wet and dry electrodes were not simultaneously recorded. Wet electrodes were placed on the skin after the dry ones were removed to prevent the skin from being hydrated. During the recording, one subject sat on a chair and avoided any movements.

4.2 ECG signal processing

Filtering

After signal acquisition, disturbances can be present in the recorded signal, such as a 50 Hz power line interference or breathing muscle artifacts. Therefore, in order to remove both signal disturbances, signals acquired from the chest were filtered by a 50 Hz notch filter with a bandwidth of 0.25 Hz and then by a first order Butterworth high pass filter with a frequency of 0.5 Hz [31]. Signals recorded from the lower abdominal area are weaker (longer distance from the heart), hence these recordings were more sensitive to disturbances and more prone to breathing muscle artefacts. Thus, not only was a 50 Hz notch filter applied to those signals, but so was a high pass filter of 1 Hz. In addition, those signals were also filtered by a low pass filter of 60 Hz. The filters mentioned above were designed in Matlab.

Correlation

During the ECG recordings in Chapter 4 and EEG recordings in Chapter 5, a wet electrode is always placed next to a polymer dry electrode for signal comparison.

A so-called ‘Pearson correlation coefficient’ is calculated to compare the time coupling and waveform similarity of the two signals. If the two signals are linearly and positively correlated with each other, the correlation coefficient is 1, see Figure 4.4(1). In contrast, the correlation coefficient is -1 when those two signals are linearly and negatively correlated, see Figure 4.4(2). The closer the absolute correlation coefficient is to 1, the better the two signals

correlate with each other, i.e. the more similar are the two signals in terms of phase and waveform. The calculation is carried out using the *xcov (x, y, maxlag, 'coeff')* function in Matlab with the following parameters [167, 168]:

x and *y* : the two signals being compared

maxlag = 4**fs (sampling rate)*

If the two signals are identical except for a constant time shift over the total signal duration, their correlation might be (very) low even though the only difference is this constant time shift. Hence, the correlation coefficient will suggest a low relation between the signals even while they are strongly related. To avoid such situation, the correlation is also calculated for a series of possible time shifts (from -4**fs* over zero till +4**fs*, being the total 'lag window'). Hence, the maximum correlation over this total lag window is considered as 'the' correlation between the two signals. For most ECG recordings and all EEG recordings in this thesis, all the signals we want to compare are recorded using the same device so as to avoid any synchronization issue between these signals, and as a consequence the maximum correlation value is always obtained at zero delay. For a small number of ECG recordings in this thesis, the two signals are recorded using two different devices. In such cases, there is a time shift between the signals but then the maximum correlation coefficient calculated over the total lag window is reported.

Some examples of calculating the correlation coefficient of simplified signals are shown in Figure 4.4. (1) The correlation coefficient of two identical signals is 1. (2) The correlation coefficient of two identical signals but with opposite polarity is -1. This is very rare when analyzing the signals of the two electrodes mounted close to each other and referring to the same reference signal. Therefore, the scale of correlation shown in this thesis is from 0 to 1. (3) The correlation coefficient decreases when one of the two signals in (1) contains another signal (e.g. noise in ECG/EEG signals). However, the correlation coefficient is not sensitive to the difference in signal amplitudes, see (4). An important limitation of correlation calculations of the signals is that they are strongly affected by the baseline drifts in the signals. A baseline drift, superposed on the first signal but not on the second signal, will result in a decrease in the correlation coefficient. (5) On the contrary, suppose that 2 signals as shown in (5a) have a small correlation (i.e. 0.0035), and then a common signal (e.g. baseline drift recorded by reference electrode) is added to both signals as shown in (5b). The correlation between them increases significantly, which might result in a false positive interpretation.

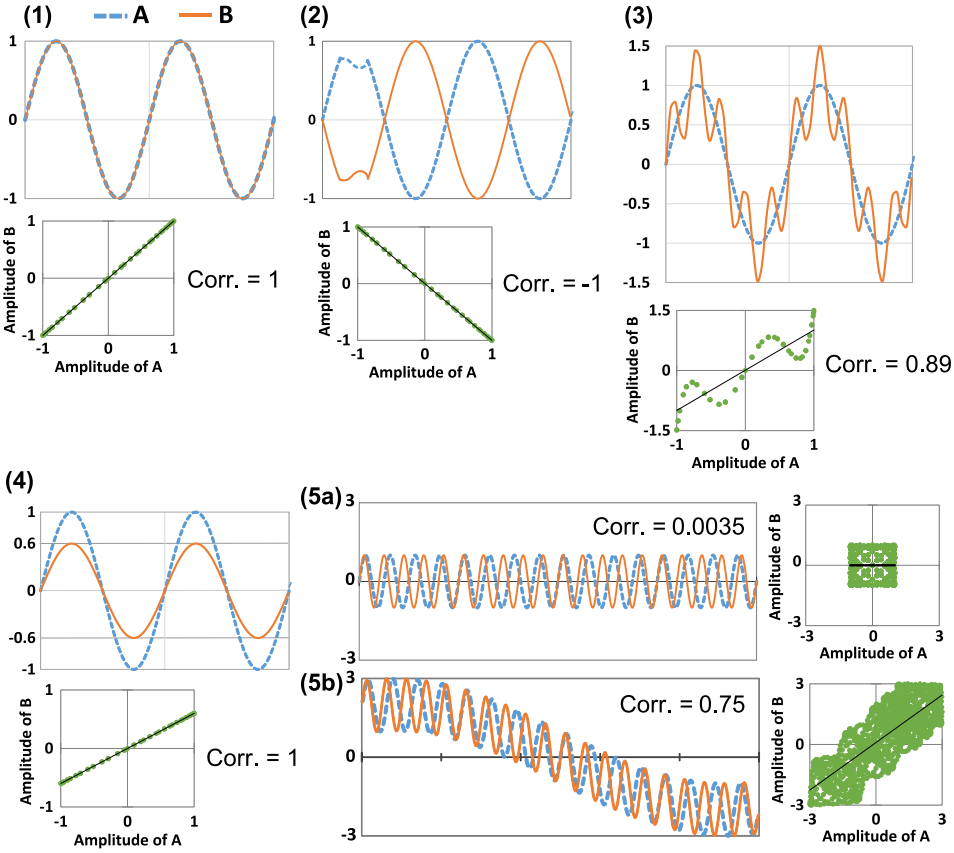

Figure 4.4: Examples of the correlation of a pair of signals.

4.3 ECG signals recorded using polymer dry electrodes

4.3.1 ECG recording from the chest

In this section, the results of the ECG measurements (as described in Section 4.1.1) are discussed. During the first recording session, the subject sat on a chair without moving. The signals recorded by both wet and dry electrodes are shown in Figure 4.5. In Figure 4.5a, it was found that polymer dry electrodes picked up more 50 Hz noise than conventional wet electrodes; however, these interferences could easily be filtered out. The filtered ECG signals acquired by conductive polymer dry electrodes and by conventional wet electrodes are also shown in Figure 4.5a.

The shapes of both signals have a high similarity, and the R peaks of both signals can be easily detected. T waves are also clearly seen. The correlation between both signals in Figure 4.5a is calculated, and a very high correlation (~0.99) is obtained. This high correlation between wet and dry electrodes could be achieved when the subject does not move

at all during monitoring. The correlation between the signals, recorded when the subjects made certain movements, will be discussed in the following paragraphs.

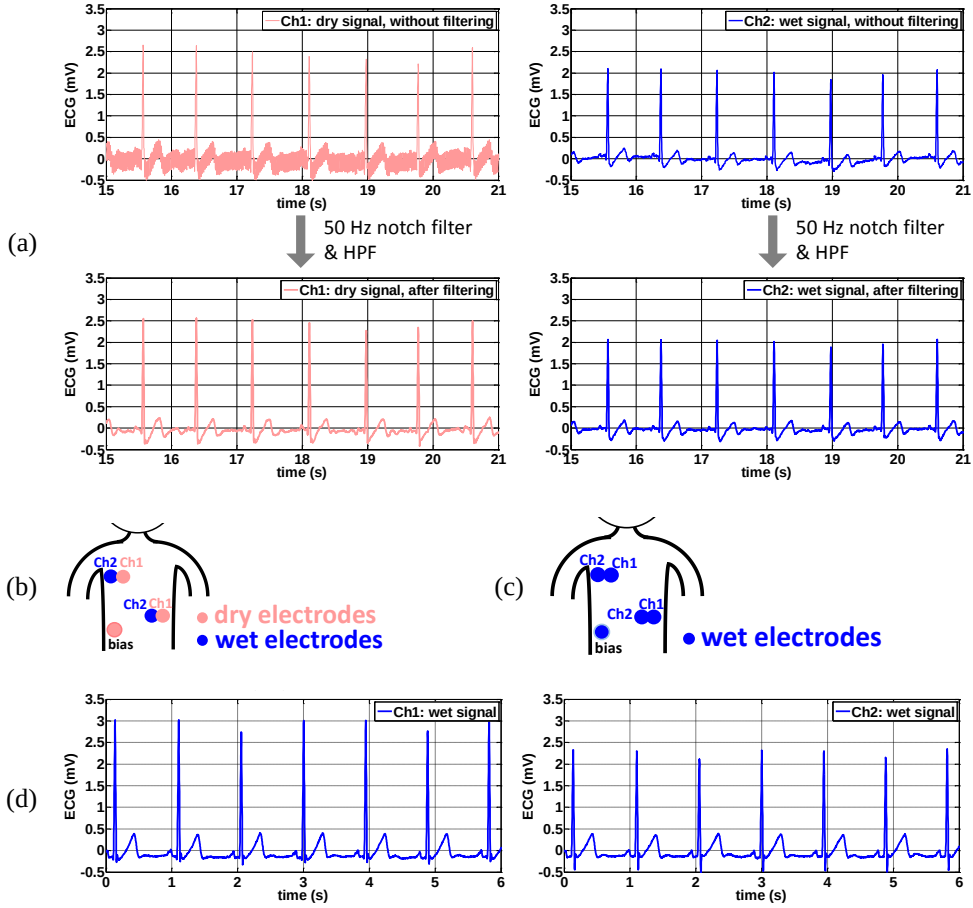

Figure 4.5: (a) ECG signals acquired by conductive polymer dry electrodes and by conventional wet electrodes before and after filtering; (b) Electrode locations using wet and dry electrodes; (c) Electrode locations using only wet electrodes; (d) Filtered ECG signals using only wet electrodes.

Note that for this recording, the amplitude of the R peaks of the dry electrode signal is ~0.6 mV higher than that of the wet ones, which is a direct consequence of the relative location of the electrodes. Even though the center of the wet and dry electrode is only 1.5 cm apart, as shown in Figure 4.2b, this difference in electrode location still affects the shape and amplitude of the ECG waves. This is easily observed in an ECG recording using only wet electrodes that are placed on exactly the same locations as the wet/dry electrodes of the previous test (see Figure 4.5b,c). The signals of the two wet channels were recorded simultaneously, as shown in Figure 4.5d. The amplitude of the R peaks recorded by both wet channels differs by ~0.5 mV, a variation which is only attributable to the small displacement between both sets of wet electrodes, and which is very close to the 0.6 mV variation observed for the dry/wet electrode pairs.

Motion artifacts in ECG signals

The same electrode locations shown in Figure 4.5b (with a dry bias) are applied for the second recording session. One of the signals recorded when the subject raised the arms up and down is shown in Figure 4.6. Both ECG signals were clearly affected by the muscle movements. However, the signal from wet electrodes was recovered faster than that from dry electrodes. To investigate whether the signal quality will improve by changing the dry bias electrode to a wet one, the correlation of wet and dry signals when applying both dry and wet bias electrodes is shown in Table 4.1. This table summarizes the signals from all recordings including with and without movements.

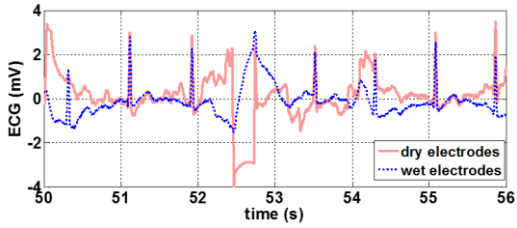

Figure 4.6: ECG recorded using dry and wet electrodes placed on the locations shown in Figure 4.5b. During the recording, the subject raised the arms up and down.

Recording sessions	Dry electrode as bias	Wet electrode as bias
Sit and avoid movement	0.91	0.95
Raise and lower arms	0.49	0.48
Open/close arms	0.41	0.46
Turn left/right	0.28	0.32

Table 4.1: The average correlation of signals recorded by wet and dry electrodes during each recording session is compared. The electrode locations are shown in Figure 4.5b. These signals are first recorded using a dry bias electrode and then using a wet bias electrode.

The correlation coefficient value in Table 4.1 shows that applying wet or dry bias electrode results in no significant difference in the recorded signals. In both cases, signals are disturbed when the muscles near the chest move. From Figure 4.6, it can be seen that the disturbances are mainly recorded by the dry electrodes. The pin-shaped dry electrodes are more prone to motion artifacts due to its higher electrode/skin impedance and the small electrode/skin contact area resulting a less strong skin contact compared to wet electrodes. This can be improved by increasing the contact surface and applying better skin attachment approaches.

To investigate the influence of the contact surface on signal quality, flat dry electrodes were also applied for the ECG recordings. The flat dry electrode was achieved by removing the pins of a 2 mm pin electrode. The measurement protocol was the same as that described in section 4.1.1. During the recordings, the subjects were asked to do a series of movements: stand without moving, sit, walk in a circle, sit and then play a chess game. Four male subjects participated in the monitoring using pin-shaped electrodes, and three other male subjects participated in the monitoring using flat electrodes. The average correlation of each recording

session with different movements is shown in Figure 4.7. By comparing the results acquired by 2 mm pin dry electrodes and flat dry electrodes, it is found that the correlation of wet and flat dry electrode is higher than the correlation of wet and pin-shaped dry electrode. The wet and dry signals recorded when subjects were walking showed the most variation between flat and pin-shaped electrodes. This is because the contact area of electrode pins with the skin is smaller compared to that of the flat electrode surface and skin, and this contact is less stable when subjects walked and moved. The amount of hair on the subjects' chest was small, hence there was no difficulty to place the flat electrodes with 1 cm in diameter on the participants' chest with good electrode/skin contact during the measurements. It can be concluded from the results in Figure 4.7 that flat electrodes can record ECG signals very well on skin with a small amount of hair, and the flat electrodes show better performance than pin-shaped electrodes because of the larger electrode/skin contact area resulting lower impedance and less contact area variations during motions. For subjects with a very hairy chest, the flat electrodes cannot contact the skin properly, hence the pin-shaped electrodes with 2 mm pin are more suitable since the pins of electrodes can penetrate the hair and ensure good contact with the skin.

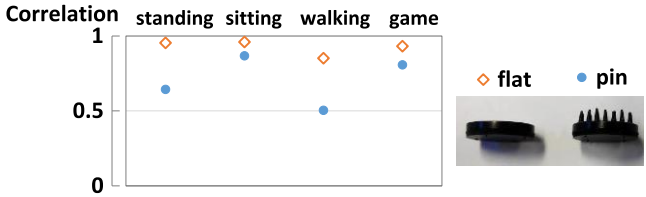

Figure 4.7: Comparison between flat polymer electrodes and pin-shaped polymer electrodes, regarding the correlation between wet gel electrodes and dry polymer electrodes, tested during various ECG recording sessions.

4.3.2 ECG recording at the lower abdominal area

Figure 4.8 shows the ECG signals recorded at the lower abdominal area, corresponding to electrodes integrated into the elastic band of the underwear. The signals were recorded when the subject sat on a chair without moving. It can be seen that both wet and dry signals were more sensitive to disturbances due to the longer distance between the electrodes and the heart. The 50 Hz noise could easily be filtered by a 50 Hz notch filter. Also, baseline drifting (mainly due to breathing) can be seen. Even though the dry signals show more pronounced drifting, a high pass filter (HPF) of 1 Hz can easily filter out this baseline drift (see pink curve in Figure 4.8). Heartbeat detection from the obtained recording can easily be achieved. T waves could also be identified.

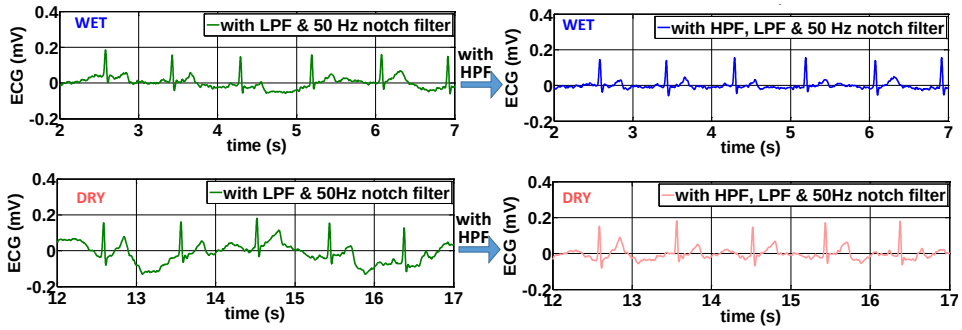

Figure 4.8: ECG signals recorded at the lower abdominal area using wet and dry electrodes. The signals were filtered by HPF, LPF and 50 Hz notch filter to remove disturbances.

4.4 Electrical requirements of electrodes according to "ANSI/AAMI EC12: Disposable ECG electrodes"

The standard "ANSI/AAMI EC12: Disposable ECG electrodes" is established to evaluate conventional ECG gel electrodes. The standard defined in the document ensures user comfort and safety and guarantees the compatibility of the electrodes with recording devices. Although some articles listed in the standard are not applicable on dry electrodes evaluation, our conductive polymer electrodes will still be inspected according to the standard if commercialization would be considered. Yet, the dry electrodes fulfilling the requirements do not promise a signal quality as good as the conventional ECG electrodes [82].

Two aspects of the requirements got our attention: electrical requirements and safety requirements. In this section, the electrical requirements will be discussed. 5 well-defined tests are mentioned in the standard and should be performed to evaluate the obligatory electrical requirements. For all these evaluation tests, the test sample is a pair of (wet) electrodes placed back to back. Hence for our tests, two cylindrical shaped polymer electrodes are clamped together (see 3.2.3) for the evaluation.

Test 1

Requirement: the average impedance for 10 Hz signals for at least 12 electrode pairs connected gel to gel shall not exceed 2 kΩ. A lower impedance is desired to reduce signal attenuation and distortion and to minimize the 50/60Hz interferences from the power line.

Result: The 10 Hz impedance of our polymer dry electrodes is lower than 2 kΩ. The impedance value of the polymer electrodes containing carbon can be found in Figure 3.12b.

Test 2

Requirement: after a 1 minute stabilization period, a pair of electrodes shall not exhibit an offset voltage greater than 100 mV. This requirement ensures that the offset voltage does not saturate the amplifier in the recording device. The offset voltage means the open circuit potential (OCP) resulting from the transmission of ions at the interface of electrode and electrolyte.

Result: Our polymer dry electrodes create no offset voltage when two cylindrical shaped pieces are contacting each other without any electrolyte in between.

Test 3

Requirement: after a 1 minute stabilization period, a pair of electrodes shall not generate a voltage over 150 µV peak to peak in the passband of 0.15 – 100 Hz for a period of 5 minutes. This requirement is added related to problems of baseline wandering which influences the accuracy of the recorded biopotential signals. In other words, this ensures that variations in offset and internal noise remain acceptable.

Result: When applying this evaluation on the polymer electrodes, the dominating signals are the 50 Hz signals with 20 µV amplitude. No other noise is recorded.

Test 4

Requirement: four defibrillation overloads are applied on the electrode pair under test. Five seconds after each defibrillation overload, the polarization potential of the electrode pair shall not exceed 100 mV. Besides, during the 30 seconds interval following the polarization potential measurement, the change of the residual polarization potential shall not be faster than ± 1 mV/sec. This requirement is needed to ensure electrodes are still functional and do not form any risk during and after a lifesaving defibrillation treatment. The clinical staff will have to judge the ECG signals only a few seconds after defibrillation and has to decide if more treatment is needed, hence the electrodes should function well.

Result: All the polymer electrodes containing over 25% of carbon pass this requirement. The one containing 43.6% of carbon shows 0.8 mV polarization potential and the potential remains almost constant during the 30 seconds measurement.

Test 5

Requirement: the dc voltage offset change across a pair of electrodes shall not exceed 100 mV when they are subjected to a continuous 200 nA dc current. The electrode might be polarized when a bias current from the recording device passes through it. This requirement is needed to avoid the polarized electrode generates a large offset voltage which is larger than the tolerated voltage range of the recording.

Results: When applying this protocol on the polymer electrode containing 43.6% of carbon, it is found that the averaged offset voltage is 0.02 mV during the 8 hours monitoring.

In summary, our polymer electrodes pass these standards, which is essential for commercialization. However, the standard is written for wet gel electrodes, and the prescribed tests are less relevant for our dry polymer electrodes, hence the tests will not guarantee that our dry polymer electrodes can record high quality biopotential signals. In addition, these requirements are established to evaluate two back to back connected ECG electrodes. This does not take into account the electrode/skin interface, which is a much more important property in biopotential measurements. A good understanding of dry electrode/skin interface properties provides better insight in their ability to provide good signal quality. Other researcher has evaluated their metal-loaded polymer electrodes using these requirements [169]. Although their electrodes pass the above requirements, low quality

signals are obtained using these electrodes. For our polymer dry electrodes, their impedance is evaluated in Chapter 3 and the ECG signals recorded using them are evaluated in this chapter. The evaluation of EEG signals using polymer dry electrodes is discussed in Chapter 5.

4.5 Conclusions of using polymer dry electrodes for ECG monitoring

The ECG signals recorded using polymer dry electrodes show a high similarity to those recorded by the neighboring wet electrodes when the subjects sit still and avoid movements. Regarding the selection of pin-shaped or flat electrodes for ECG monitoring, unless the subject has very hairy skin, flat electrodes are more suitable because the larger electrode/skin contact area results in a smaller impedance and a smaller impedance variation during motions, hence in less motion artifacts.

Chapter 5.
Polymer Electrode Validation 2: EEG Monitoring

EEG monitoring is typically performed using wet electrodes (Figure 1.3b and c), although for this application the adhesion of this kind of electrodes on the scalp, and the use of gel on the hairy skin is most difficult and disturbing. Hence for EEG monitoring, a dry and clean alternative as dry electrodes is most welcome. During the EEG recordings using polymer dry electrodes, active electrodes are always applied since the EEG signals have small amplitudes. The requirement and design of active front-end electrode and setup used for EEG monitoring are discussed in sections 5.1 and 5.2 respectively. Various signal analysis techniques are used to evaluate the obtained EEG signal quality and compare the signals acquired from wet and polymer dry electrodes. The analysis techniques themselves are discussed in section 5.3. The detailed EEG test protocol and results will be discussed in section 5.4 (EEG monitoring in UZ Gent), section 5.5 (EEG monitoring in UZ Leuven) and section 5.6 (EEG monitoring in Holst center, imec-NL).

5.1 The need for and requirements of active electrodes

The polymer dry electrodes successfully recorded ECG signals even though the recording systems are designed to be equipped with gel electrodes. This is due to the rather strong amplitude of ECG signals when comparing to the signal amplitude of other bio signals, see Figure 1.2. The EEG signals are 10 to 100 times weaker than ECG signals (few mV) because the signals generated by activated neurons need to penetrate various layers of brain tissue to reach the scalp as shown in Figure 5.1 [170, 171]. ECoG are signals recorded by placing the electrodes on the cortical surface and local field potentials (LFPs) and spikes are signals recorded by inserting electrode arrays into the cortex, both resulting in a signal amplitude 10 times larger than that of EEG signals. The weak EEG signals are very sensitive to signal disturbances. The high impedance of the dry electrode/skin interface is therefore disadvantageous, since it makes the recording highly sensitive to noise. As a consequence, many commercial EEG recording systems will check the electrodes-skin impedance before recording. If the impedance is too high, a warning is given, and some systems simply refuse to start the EEG recording. .

In order to overcome the problems related to the high impedance of polymer dry electrode and skin, active electrodes are needed [172]. Active electrodes are electrodes integrated with an active circuit. Active circuits include an operational amplifier (op-amp) to convert the output of the signals to a low impedance end, and they can additionally be used to amplify the biopotential signals from the human body. The signals passing through the active circuit resulting in a low output impedance are more resistive to the interference from the environment, such as 50 Hz power line interferences and signal disturbance caused by cable movements [44, 173, 174]. In addition, the low impedance end created by the op-amp will be seen by EEG recording systems as a low impedance skin/electrode system, and hence all recording systems will allow biopotential recording. Furthermore, signal amplification by the active circuit can result in a higher signal to noise ratio (SNR).

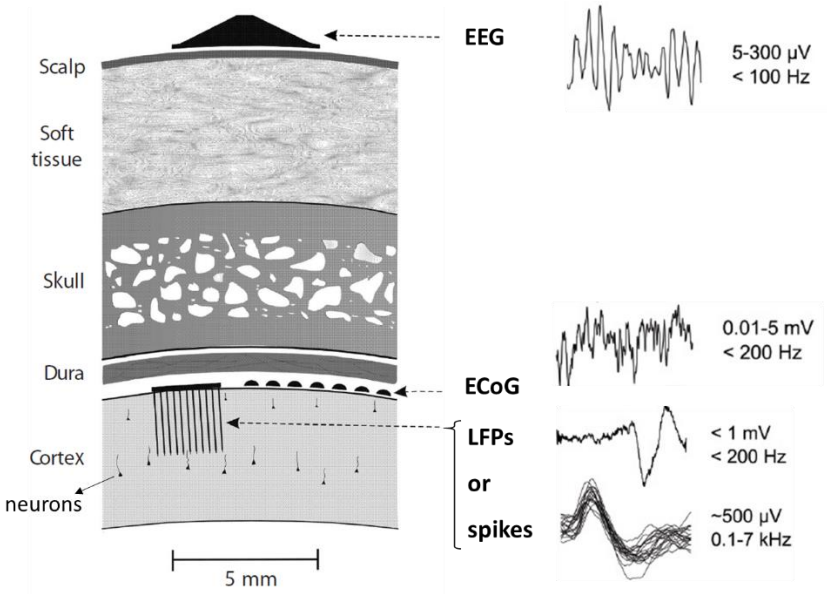

Figure 5.1: EEG is recorded by electrodes on the scalp; ECoG (Electrocorticography) is recorded by electrodes on cortical surface; LFPs (local field potentials) and spikes are recorded by electrode arrays inserted into the cortex. This figure is adapted from [170, 175].

In order to record EEG signals by using the polymer dry electrodes investigated in this thesis, an active electrode front-end system is designed and fabricated. It will be integrated with conventional recording systems in UZ Gent and UZ Leuven. The active circuit used for the EEG recordings in this thesis is a modification of one of the designs on *openEEG* website [176]. The criteria for the op-amp for active electrodes of bio potential monitoring are high input impedance, low noise, low bias current and unity-gain stability if a buffer circuit is going to be designed. During the fabrication and optimization of the active circuit, the recording system in UZ Gent is used to evaluate its compatibility. The optimization cycles of this active circuit are discussed in section 5.4.1.

The schematic of the final version of active circuit is shown in Figure 5.2a. The circuit contains an op-amp (LMP 7702), a body safety resistor (220 k ohm), a decoupling resistor (100 ohm) and a capacitor (100nF) next to the op-amp to stabilize the power supply. The backside of the PCBs shown in Figure 5.2b is coated with Au, enabling the connection with the conductive polymer electrodes as shown in Figure 5.2c. Each active electrode is further connected to an intermediate board through a 4-wire cable (04SUR-04SUR-32W300 from Farnell). This cable is not ideal since it does not have shielding and is quite fragile. However, this is the smallest and most flexible connector to our knowledge enabling an easy and patient friendly recording setup. Through two intermediate boards, up to 16 active electrodes could be connected to a terminal box, which provides the 9 V power supply to the op-amps and connects the signal of each electrode to the clinical EEG recording system, see Figure 5.2d. The setup shown in Figure 5.2d is further in this thesis referred to as ‘our own active electrodes’.

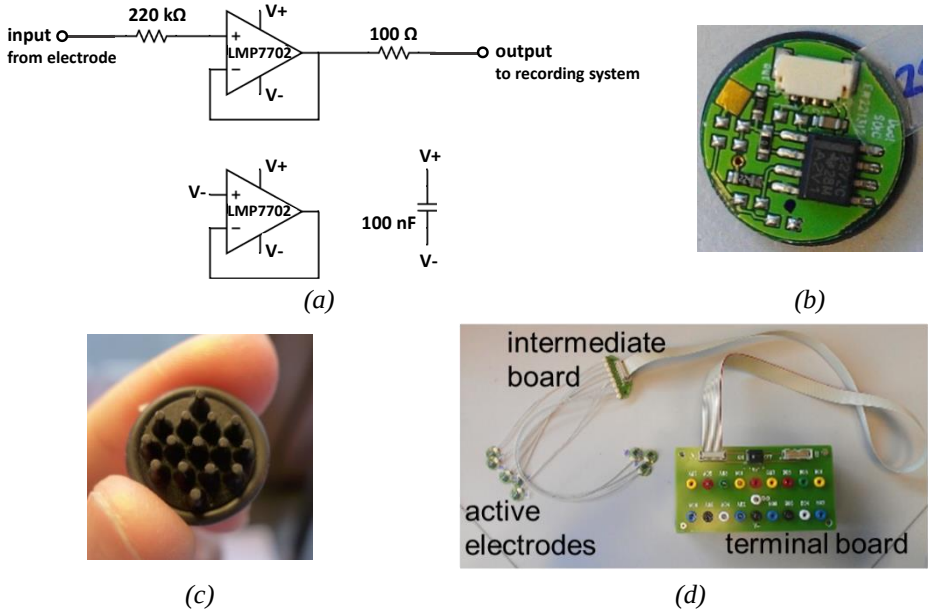

Figure 5.2: (a) Schematic of a unity gain active electrode. (b) PCB of the active circuit. (c) Polymer electrode coupled with its active circuit. (d) by the terminal board up to 16 active electrodes can be connected with the clinical recording device.

Two EEG recording systems are used in this thesis to evaluate the active dry electrodes. Besides the commercially available clinical EEG recoding system in UZ Gent (SD LTM 64 BS from Micromed), dedicated EEG recording system developed at imec is used. This electronic system combines also active front-end electrodes with a back-end EEG recording chip. Colleagues from imec-NL developed an EEG headset based on this electronic system combined with Bluetooth based wireless transmission electronics [177], see Figure 5.3. More details of this wireless EEG headset will be discussed in section 5.2.

Figure 5.3: The imec EEG headset equipped with active dry electrodes and dedicated EEG recording and transmission electronics designed at imec.

5.2 Electrodes fixation methods

For non-wireless recording e.g. when using the clinical EEG recording system, all system channel ports need to be connected individually to our own active electrodes via cables. The active electrodes themselves need to be fixed on the scalp by external fixation techniques. Therefore, a cap made by elastic bands is used, enabling the correct positioning of the electrodes on specific locations according to an international recognized method called 10-20 system to describe and apply the locations of electrodes on the scalp. The cap is similar to the functionality of the silicone elastic wires used in clinical environment and the elastic caps which are available on the market [178, 179]. The authors decide to make a cap using several strips of elastic bands since the existing fixation systems did not provide good and comfortable contact between the electrodes and the skin. The length of each elastic band as shown in Figure 5.4a is adjustable to enable a good fit on various head sizes. Comparing to the elastic cap generally used (see Figure 5.4b), the bands can more easy be adjusted, and they are also more comfortable since less skin area is covered, enabling perspiration to evaporate easy. Comparing to silicone elastic wires often used in hospitals in order to generate localized pressure to mount wet bridge electrodes (short term EEG recording, see Figure 5.4c), our elastic bands distribute the pressure to larger skull area. The silicone band setup is giving important discomfort even after only 30 minutes usage, while the elastic bands are more user friendly.

(a) (b) (c)

Figure 5.4: (a) The elastic bands used for the measurements in this research. (b) The silicone elastic wires used for short-term EEG monitoring in clinical environment [180]. (c)Elastic cap for EEG monitoring [181].

After both polymer and wet electrodes were placed on the scalp using the elastic bands, they are connected with the EEG recording amplifier through cables. Different recording systems are used to record the EEG signals in UZ Gent and UZ Leuven. The instruments will be introduced respectively in section 5.4 and section 5.5 together with the test setup and protocol.

When the imec EEG headset is used, the electrodes are positioned by the dedicated headset design and signals are transmitted wirelessly to a computer. No extra fixation of the electrodes is needed. The headset was originally designed to be equipped with AgCl rigid pin electrodes. Those AgCl electrodes are fixed in magnetic cups which are fitting in metal electrode holders of the headset. Springs inside the metal holders will adjust the pressure on the scalp, and the magnetic cups can freely rotate in the metal holders, both will improve the electrode/ skin contact. The active circuits are located very close to these metal holders. The reference and ground electrodes are located at the back of earlobes. There are four channel

electrodes in the imec headset, positioned around C3, Cz, C4 and Pz locations according to the international 10-20 EEG electrode location. The headset is available in one size only, but some size adjustment is possible by adjusting the length of a plastic strip at the back (adjustment of the pressure on Pz electrode). Due to this size adjustment, the electrodes are not always located at the exact 10-20 locations mentioned above. Due to the limited headset adjustability, not all electrodes achieve always good contact with the scalp, hence motion artifacts are introduced more easily when a subject is moving. In addition, this bulky headset often causes pain even after wearing it for a short period. Since the current design of this imec headset is not fully optimized yet, it is not ideal for electrode validation, hence another imec EEG system is used for EEG monitoring. This system has exactly the same electronics as those present in the headset, but they are not embedded in the headset resulting in more flexibility. The new system contains pieces of active circuit PCBs connected with a back-end chip through thin and flexible cables. The polymer dry electrodes are connected with the input of the active circuit PCB and then placed on the scalp using elastic bands. The details of the recording system will be introduced in section 5.6 together with the experimental setup and protocol.

5.3 Signal Analysis

EEG signals have smaller amplitudes compared to ECG signals. Hence interferences from the mainline and other sources might strongly disturb the EEG signals especially when the impedance of the skin/electrode is high. Therefore, filters are often applied to remove at least part of the noise and hence improve the signal quality of EEG signals. This filtering process will be discussed in section 5.3.1. Moreover, the frequency of EEG signals is not homogeneous and constant. EEG signals do not have a systematic curve pattern such as the PQRS peaks of ECG signals. Hence the quality of the signals can hardly be judged by non-experts just by looking at the raw signals. Therefore, a scientific relevant evaluation of the EEG signal quality from an engineering point of view is performed by using various analyzing techniques. The signals of wet electrodes are considered reference signals with high signal quality, to which the signals from dry electrode are compared. The power spectrum density (PSD) is calculated to inspect the signal strength as function of frequency. This is useful since it is known that during certain brain activities, signal patterns of certain frequencies will occur [182]. The PSD computing will be discussed in section 5.3.2. The signal to noise ratio (SNR) when eyes closed or during steady state visually evoked potential (SSVEP) is computed using formulas shown in 5.3.3. Correlation analysis is applied, which will be discussed in section 5.3.4, to compare the similarity of a dry and a wet EEG signal. Analyzing the similarity of the PSD of the wet and dry signals is further referred to as coherence calculation, which will be describe in section 5.3.5. The signal analysis techniques mentioned above are applied on all the EEG measurements discussed in this thesis, except when explicitly mentioned different.

5.3.1 Filtering

A 2–30 Hz Chebyshev type II bandpass filter is designed in Matlab. The frequency range is chosen to filter out the baseline drift (low frequencies) and 50 Hz signals (power line

interference) and its' harmonic interferences with the EEG signals [183]. The data is filtered backward and forward by this filter to eliminate expected distortion [184].

For signals recorded using the imec recording system, a 1–20 Hz Chebyshev type II bandpass filter is applied due to the interference of bluetooth transmission occurring at 20–30 Hz. More details will be discussed in section 5.6.

5.3.2 Power spectral density (PSD)

In order to compute the PSD of the EEG signals, the *pwelch(x,window,noverlap,f,fs)* function in Matlab is used with following parameters:

window = 2 seconds

noverlap = 1.8 seconds

fs = sampling rate, depending on the applied recording system

f = 10**fs* (*f* represents the number of discrete Fourier transforms and this setting results in a 0.1 Hz resolution of the spectrum)

- PSD of 50 Hz power line interference

It has been observed that higher skin/electrode impedance causes a higher sensitivity to interferences from power lines [30]. Hence the amount of 50Hz power line interference in the PSD of the signals contains information about the contact resistivity of electrode and skin. Therefore, the averaged power spectrum density of EEG signals within the frequency range of 48-52 Hz is computed and compared for wet and polymer dry electrodes.

5.3.3 Signal to noise ratio (SNR) when eyes closed or during the SSVEP

As mentioned above, certain frequencies of the EEG signals represent certain brain activities. Whether the EEG signals contain signals at a certain frequency range can be easily determined by studying the power spectrum. When someone is closing his eyes, typical and easily recognizable 'alpha waves', having a frequency between 8 and 13 Hz, are produced in the brain. A repeatable EEG signals at a certain frequency can also be evoked by an external stimulant, such as a cyclic visual or audio stimulant. When a person receives a visual stimuli generated at a specific frequency, the brain will often generate EEG signals with that frequency. These signals are called steady state visually evoked potential (SSVEP). In this thesis, EEG signals recorded when the subjects close their eyes ('alpha wave' evocation) and when they receive cyclic visual stimuli are not only studied by looking at the power spectrum, they are also analyzed by computing the signal to noise ratio (SNR). We define those signal expected to be seen in the EEG recordings during certain tasks as "signal" in the signal to noise ratio (SNR) calculation. On the other hand, recordings distributed outside the evoked frequency range are considered as "noise" in the SNR calculation. The value of SNR is the power of the "signal" divided by the power of the "noise". In fact, all frequency components of the total EEG signal have a certain origin and reflect a certain brain reaction, hence they are no 'noise' in the strict sense. In this thesis, this noise definition and following SNR calculation is only defined to quantify the ability of the electrode to record the signals that we are interested in. If one type of electrode picks up more "noise" than another electrode,

the SNR will be lower. As such, the higher SNR value reveals the ability of an electrode to pick up the signals with less disturbances.

In a mathematical way, the calculation of the SNR when eyes closed is expressed in Equation 5.1.

$$SNR = 10 \times log_{10}\left(\frac{PSD\ of\ 8{-}13Hz}{PSD\ of\ the\ 2{-}8Hz\ \&\ 13{-}30Hz}\right) \quad \textit{Equation 5.1}$$

Regarding the SSVEP using an 8 Hz stimulant, the signal frequency range corresponding to it is considered between 6 and 10 Hz. Hence the SNR of SSVEP is as expressed in Equation 5.2.

$$SNR_{SSVEP} = 10 \times log_{10}\left(\frac{PSD\ of\ 6{-}10Hz}{PSD\ of\ the\ 2{-}6Hz\ \&\ 10{-}30Hz}\right) \quad \textit{Equation 5.2}$$

In order to compute the SNR, the EEG recordings are first filtered by the 2-30 Hz bandpass filter and then the PSD was calculated using *pwelch* function in Matlab, see section 5.3.1 and 5.3.2. After this the SNR is calculated, the SNR value is expressed in dB units.

5.3.4 Correlation

The EEG signals recorded from a pair of wet and dry electrodes, which are mounted close to each other, are compared. The correlation coefficient of their signals is calculated using the technique introduced in Chapter 4, section 4.2.

5.3.5 Coherence

The coherence of 2 signals reveals information about the similarity of the dynamic behavior of both signals: the coherence expresses the similarity of the phase difference and amplitude difference between 2 signals in a series of analyzed periods. The coherence is determined for each frequency component of the signals. To calculate the coherence, the signals are cut into time segments (called 'epochs'). For each signal, the PSD of each epoch is calculated and PSD's of subsequent epochs are compared to determine the signal change. Then the PSD change of both signals are compared in order to obtain the coherence value, which is representing the similarity of the signals change (hence PSD change) in all the epochs. By definition, the coherence values of the two signals at each frequency component in first epoch are all 1 (no PSD change if only one epoch is considered). Depending on the phase and amplitude changes between the signals in the following epochs, the coherence has a value between 1 and 0.

To explain the concept of coherence value more clearly, some basic examples will be given using simplified signals. The signals amplitude and phase are shown in the amplitude versus time plots in Figure 5.5. These signals are all cut into epochs of 2 seconds.

- The correlation of 2 signals being both a pure 1 Hz sine wave is 1 because the phase and amplitude differences of these 1 Hz signals remain the same in all epochs

(graph 1). In EEG recordings, such a case corresponds to a perfect constant skin-electrode impedance for both signals in all epochs.

- If the amplitude of the 1 Hz EEG signals increases in the brain, and the two electrodes are able to record this amplitude change accurately and simultaneously (see graph 2), the coherence of both recorded signals at 1 Hz is 1, since both signals are changing is the same way.
- However, variation of the skin-electrode impedance during the measurements results in changes in phase and amplitudes of the signals as shown in graphs (3) and (4). Depending on changes of the phase or amplitude differences between the signals in epoch2 respecting to that in epoch1, the coherence of 1 Hz signals is shown in the tables below graphs (3) and (4).
- Graph (5) shows the scenario that a 5 Hz signal interferes with one of the signals. As long as the phase and amplitude differences of recorded 1 Hz signals are not affected by the interferences, the coherence of 1 Hz is 1. The coherence of 5 Hz is smaller than 1 because the 5 Hz signals only exist in epoch2. Considering the coherence of a frequency range, the coherence of each frequency component included in the range is averaged. In graph (5), the average coherence over the entire frequency band is 0.76.
- Suppose one signal exhibits a baseline drift without changing the phase and amplitude of the 1 Hz components (see graph 6), then the coherence of 1 Hz signal is 1. The coherence of the frequency of the baseline drift signals is 0.5. The overall coherence is again calculated by averaging the coherence values of each frequency components.
- In the recorded biopotential signals, the phase and amplitude difference between signals might change more than once or even constantly as shown in graph (7) and graph (8). Signals with sudden phase changes are shown in graph (7). The coherence of 1 Hz signals reduces to ~0 after a 180° phase change at 5s. At 10s, another 180° phase change converts the signals back to the same ones as the ones in 0-5s. This results in a slightly increasing of the coherence value. Since 10s, the phase difference between signals remains constant, so the epochs contain the same signals as the ones in epoch N1. The longer the signal period, more identical epochs are involved in the calculation. This results in the increasing of coherence of 1 Hz signal. In graph (8), the signals with subsequent phase changes are analyzed. Since the phase difference between the signals changes frequently, the similarity of the phase difference of all epochs included in the signal period is low. This results in the coherence of 1 Hz signal close to 0.

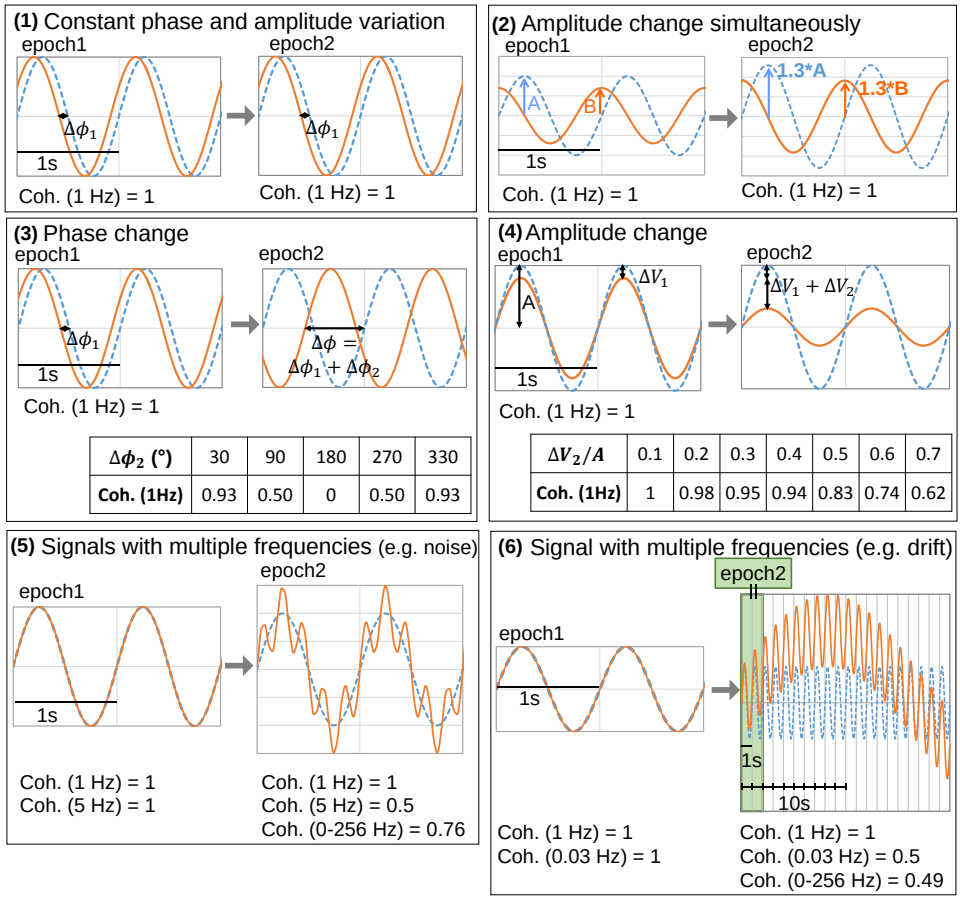

$\Delta\phi_2$ (°)	30	90	180	270	330
Coh. (1Hz)	0.93	0.50	0	0.50	0.93

$\Delta V_2/A$	0.1	0.2	0.3	0.4	0.5	0.6	0.7
Coh. (1Hz)	1	0.98	0.95	0.94	0.83	0.74	0.62

This figure continues on next page.

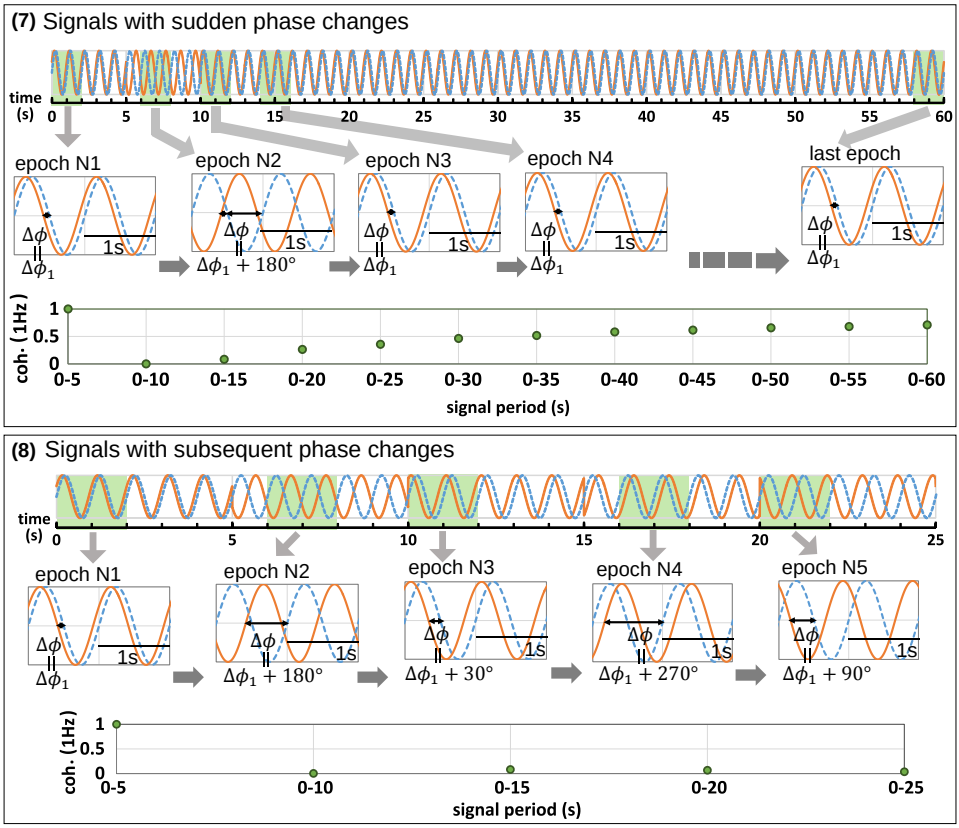

Figure 5.5: Examples of the coherence of a pair of signals. To calculate the coherence, the signals are cut into 2s epochs. The phase and amplitude of the signals are shown in the amplitude versus time epoch plots.

As the examples above are showing, the highest coherence value 1 indicates that both signals have similar changes in their amplitude or phase. The lowest coherence is 0, indicating that both signals have very different changes in amplitude or phase with time (hence in all epochs).

To calculate the coherence in this thesis, all frequency components in the frequency band of 2 to 30 Hz (after filtering) are considered, the coherence value is calculated using the *mscohere(x,y,window,noverlap,nfft,fs)* function in Matlab with the following parameters:

x and *y* = the two signals which are compared

window = 2**fs (sampling rate)* indicating the duration of the epochs

noverlap = 1.8* *fs*

The epochs overlap with 1.8* *fs* period to increase the sensitivity of the amplitude or phase changes.

nfft = *fs*

In this thesis, we are interested in the coherence of two signals in the entire frequency range (2-30 Hz) and in the alpha waves frequency range (8-13 Hz). For both frequency ranges, all

the calculated coherence values are averaged and these average coherence values are further used as signal evaluation criteria.

In the following sections, the EEG recordings using the recording amplifiers in UZ Gent, UZ Leuven and imec will be presented. The signal analysis approaches discussed in this section (section 5.3) are applied on the obtained signals.

5.4 EEG measurements in UZ Gent

In this section, the results of polymer electrode validation using EEG monitoring in UZ Gent will be shown and discussed. When developing the active circuit for the polymer dry electrodes, one important concern is the compatibility of the active chips with the recording amplifier. The validation was taken place in UZ Gent using their recording amplifier: SAM 32 FOFC 1. The process of the active chip optimization will be described in section 5.4.1. Before starting the measurements, the locations of reference (REF) and ground (GND) electrodes need to be determined according to the influence of their location on the signal quality. This decision process will be discussed in section 5.4.2. The optimized locations of reference and ground electrodes were applied for all following EEG monitoring. In order to evaluate the signal quality of conductive polymer electrodes, the EEG signals of polymer dry electrodes, bridge electrodes and cup electrodes were compared. This evaluation was first carried out on healthy participants, later on epilepsy patients. These results will be shown in section 5.4.3 and 5.4.4 respectively.

Two types of EEG recording amplifiers are available in UZ Gent: SAM 32 FOFC 1 and SD LTM 64 BS (both from Micromed, Italy). The first one is used for routine EEG monitoring and is located in the standard patient examination room. The second system is used for research purposes and is located in the offices of the medical staff. During the active circuit optimization, both of the devices were used. Later on, when comparing the different types of electrodes, only the routine EEG device was used.

5.4.1 Phase 1: Electronics and system optimization

In this section, the process of active chip optimization will be described. This includes choosing the optimal op-amp which is compatible with the recording amplifier as well as the design and layout of the active circuit.

- 1st version of active circuit

The preliminary version of the active circuit was designed by a colleague [55]. During his work, this active circuit was connected with a 3D printed dry electrode and validated using the standard EEG monitoring equipment in UZ Gent. The circuit with unity gain buffer included an op-amp (OPA 140) and a voltage converter (TL 7660), see the schematic in Figure 5.6a. The active circuit was connected with a 9 V battery and the voltage converter transmits -9V and +9V to the op-amp. The polymer electrode was connected with the input of the active circuit (a larger piece of metal on the PCB) using Ten20 EEG conductive gel (Weaver and Company, USA), see Figure 5.6b and Figure 5.6c. The output of the active circuit was connected with a signal wire of the EEG recording amplifier of UZ Gent.

For active circuit testing, the polymer dry electrode made from material composition number 64 (the optimal polymer material of the electrical and mechanical properties evaluation, see Chapter 3 and Chapter 4) was used, having 4 mm pin length. The polymer dry electrode was placed at the left side of the C4 location while a wet electrode was placed at C4. Two wet electrodes were used as reference and ground electrodes, placed at the middle of forehead and at the back of left earlobe respectively.

(a) (b) (c)

Figure 5.6: The 1st version of active circuit for polymer electrodes.(a) The schematic. (b) the PCB with components. (c) the polymer dry electrode was connected with the input of the PCB, a metal connection at the backside of the PCB carrying the active circuit.

When comparing the recorded signals, it is observed that the polymer dry electrodes contain noise distributed in the range of 60-110 Hz (See Figure 5.7). The noise frequency pattern varies through time, and the amplitude of the noise was around 100 mV peak to peak. When the active circuit was inspected in a lab environment afterwards, it was found that the voltage converter itself generates this noise.

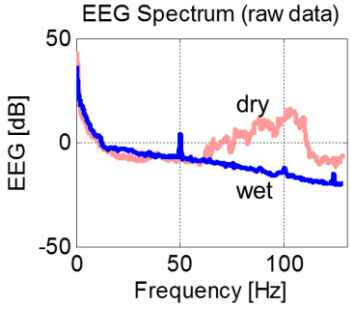

Figure 5.7: The PSD of EEG signals recorded using wet and polymer dry electrodes.

- 2nd version of active circuit

To avoid the noise from the voltage converter, it was removed and +9V and -9V voltage was provided to the op-amp directly through capacitors, hence two 9V batteries need to be connected with one active circuit. Recording was performed using wet electrodes as reference electrode and ground electrode, located at the back of right and left earlobes respectively. The signal wet electrode was placed at C4 while a polymer dry electrode connected with the 2nd version of the active circuit was placed at C3. The EEG signals were recorded using the recording amplifiers of UZ Gent. The EEG spectra of signals before and after passing the

2-30 Hz notch filter are plotted in Figure 5.8, showing a period when the subject closed the eyes, so the alpha waves were detected by both wet and polymer dry electrodes. This version of active circuit seemed to work well and is compatible with both recording amplifiers, the routine and research device. However, during the EEG recording, the temperature of two active circuit PCBs increased. It was assumed that the active circuit oscillated and then generated heat. The PCB was immediately replaced by another one during the EEG monitoring to avoid any discomfort for the subject.

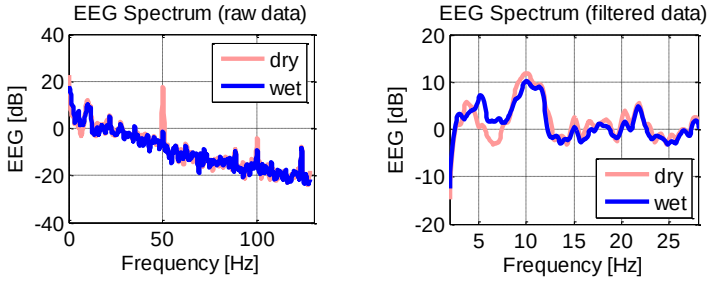

Figure 5.8: The spectrum of the signals recorded by wet and polymer dry electrode before and after filtered by 2-30 Hz notch filter.

Afterwards in the lab environment, noise detection setup was applied on the 2nd version of the active circuit to further investigate and identify the oscillating problem. Two approaches were carried out to determine the origin of the oscillation (See Table 5.1) [185, 186]. One was forming a low pass filter at the output of active circuit to decouple the noise resulted from the power lines of other electronic devices and picked up by the long cables. The second approach consists in stabilizing the power supply by reducing the capacitance values of the bypass capacitors. However, these actions did not solve the oscillating problem because OPA 140 op-amp itself is not unity gain stable. In other words, it generates oscillations easily in unity gain condition. Therefore, this opamp needs to be replaced. The criteria of the new op- amp are unity gain stability, narrower bandwidth to avoid oscillation, low noise and high input impedance.

aims	actions
Add a low pass filter to the output of active circuit to decouple the load of the long cables	Add 50 Ω resistor to the output
	Add 1 kΩ resistor and 10nF to the output
	Add 10 kΩ resistor and 10nF to the output
Increase stability of the power supply to the op-amp	Replace bypass capacitors from 10 µF to 10 nF
	Add 100 nF capacitors in parallel to the bypass capacitors

Table 5.1: The actions carried out to determine the origin of noise of the active circuits.

- 3rd version of active circuit

A new PCB chip was designed since a better type of connection wires and different op-amp was selected. A dual supply op-amp was chosen because the battery ground can be easy connected with the ground electrode on the human body. Three new active circuits with

op- amp TLC 2272 and amplification factors 1, 2 and 3 were made. The schematic is shown in Figure 5.9. The functionalities of each component are described in section 5.1.

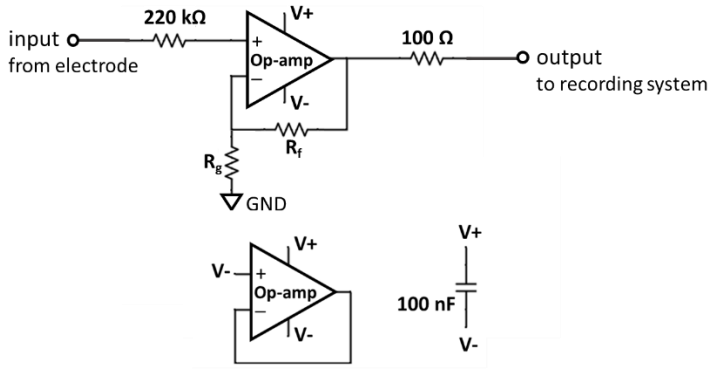

Figure 5.9: The schematic of 3rd version of active circuit.

During the EEG monitoring, the polymer electrodes connected to the active circuits were placed at C4 location while a wet electrode was placed at C3 location. Both wet reference and ground electrodes were placed at occipital region of the scalp. The active electrode with amplification factors of one, two and three were placed at C4 sequentially. The EEG signals were recorded when the subject closed the eyes.

The signals passing through the active circuits are affected less by environmental noise. In theory, the larger the gain, the less the signals are affected by environmental noise. However, this does not always results in less noise in the final recorded signals (hence higher signal quality), since the noise can also be produced from the interface of electrode/skin. Such noise will be amplified together with the signals by the amplifier. Moreover, if the amplification factors of the signal and reference active electrodes are not perfectly matched, the common- mode rejection ratio (CMRR) of the recording device will not function optimal, resulting in a lower signal quality.

Signals which are recorded using our active circuits with various amplification factors are analyzed to determine the optimum amplification factor for our application. EEG signals are acquired by one dry electrode coupled subsequently to an active circuit with amplification factor of 1, 2 and 3 respectively. During the total recording, an EEG signal using a wet electrode is recorded too. Wet electrodes are considered as standard electrodes for EEG monitoring which can record accurate EEG signals. The subject was asked to close the eyes in order to measure alpha waves. The obtained EEG spectra are shown in Figure 5.10. All 3 recordings show clear alpha waves. The SNRs of these signals are plotted in Figure 5.11a (see the definition of SNR in section 5.3.3). Remark that the SNR of the wet electrode signal decreased with time, which is not expected. A possible explanation is more 'noise' distributed in the frequency range of 16-20 Hz was recorded with time (see Figure 5.10). Hence ideally, the SNR the polymer dry electrodes with active circuit are similar to the SNR of the wet electrode. However, the SNR of the dry signals is higher, which is again not expected. The EEG spectra show that the wet electrode picks up distinct signals distributed in the frequency range of 16-20 Hz, signals less clearly visible in the dry spectra. These signals –if real–

disturb the SNR calculation. Beside the SNR, the correlation and coherence of the signals recorded by the wet and dry electrode are also computed to compare the similarity of wet and dry signals, see Figure 5.11b. It reveals that correlation decreases with the increasing of the amplification factors. The same trend is visible for coherence, both in the 8-13 Hz and 2- 30Hz frequency range. To conclude, the active circuit with gain 1 shows the most accurate signal recording. Therefore, it was decided that the active circuit with unity gain buffer will be applied for all further EEG monitoring.

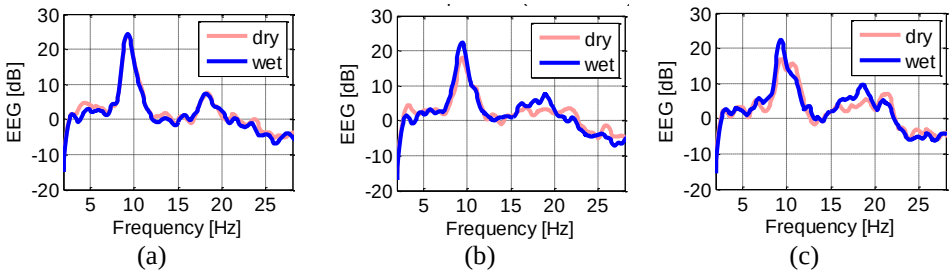

Figure 5.10: The spectra of EEG signals when using wet and polymer dry electrodes. The active circuits connected with polymer dry electrodes were (a) amplification factor 1, (b) amplification factor 2 and (c) amplification factor 3.

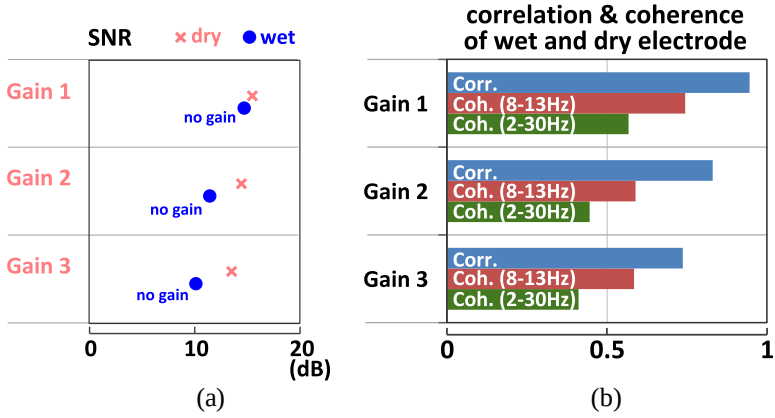

Figure 5.11: Comparison of (a) signal to noise ratio and (b) correlation, coherence of the EEG signals recorded by wet and polymer dry electrodes when using active circuits with amplification factor (or gain) of 1, 2 and 3. The signals were recorded when the subject closed the eyes.

When measuring EEG signals with dry electrodes, the reference (REF) and ground (GND) electrode can be wet or dry electrodes. To test which combination of electrode types is optimal, three electrode configurations listed in Table 5.2 were tested.

	signal	REF	GND
1	dry active electrode	wet electrode	wet electrode
2	dry active electrode	dry active electrode	wet electrode
3	dry active electrode	dry active electrode	dry passive electrode

Table 5.2: The electrode configurations used to optimize the combination of electrode types.

Dry active electrodes were polymer electrode combined with Gain 1 active circuit. In configuration 3, the GND is a dry passive electrode. For all 3 the configurations, the dry signal electrode was placed at C4 and a wet signal electrode was at C3 location to record both EEG signals simultaneously for comparison. The data analyzed and shown here was recorded when the subject closed the eyes. Figure 5.12a shows the SNR of the individual recording. Figure 5.12b shows the correlation and coherence of the signals recorded by wet and dry electrodes. The results reveal that the signal quality of using three different electrode configurations is similar. This suggests that applying polymer dry electrodes as signal, REF and GND electrodes is compatible with the recording amplifier in UZ Gent.

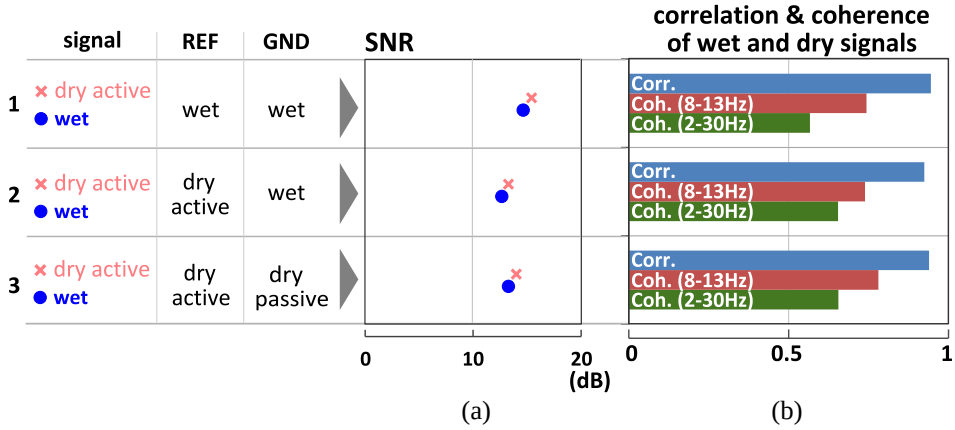

Figure 5.12: Comparison of (a) signal to noise ratio; (b) correlation and coherence of the EEG signals recorded by wet and polymer dry electrodes in three different electrode configurations. The signals were recorded when subject closed the eyes.

During the optimization of the amplification factor of the active circuit as described above, it was also found that the active circuits generated a noise peak around 41 Hz, see Figure 5.13. This noise was also detected when dedicated noise measurements were carried out on the same active electrode in the lab environment. The combination of the op-amp, the components and the PCB generated this noise. To solve this, the TLC 2272 was replaces with another op-amp in the next version of the active circuit.

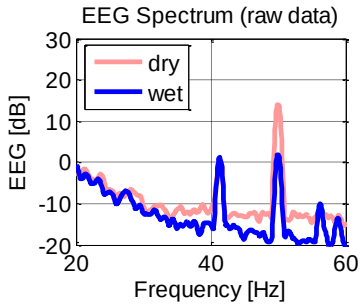

Figure 5.13: The spectra of EEG signals recorded by wet electrode and dry electrode connected with active circuit consisting of TLC 2272 op-amp.

- 4th version of active circuit

Finally, op-amp LMP 7702 was selected as the replacement op-amp. The active PCBs with amplification factor one using these op-amps were fabricated (see the schematic in Figure 5.2a). The circuits were evaluated in the lab using simulated signals and no specific noise was detected during the tests, hence these circuits are used for all further dry electrode recordings.

5.4.2 Phase 2: Optimization of REF electrode location and limitation of SNR calculation

Goal 1

The optimum location of REF electrode is determined by studying the influence of the **reference electrode location** on the signals.

Electrode types and locations

The electrodes were placed as listed in Table 5.3 (see also Figure 5.14).

Signals	two wet electrodes were placed on the left part of the head while the other two were placed on the right part
GND	one wet electrode was placed at the occipital region (back of the head)
REF	wet electrode was placed at occipital region, frontal region (forehead), back of right ear and back of left ear sequentially

Table 5.3: The types and locations of electrodes used in this test.

Signal analysis

During EEG recording, the subject was asked to close the eyes. The SNR of the 4 signals recorded by each wet signal electrode was calculated and averaged.

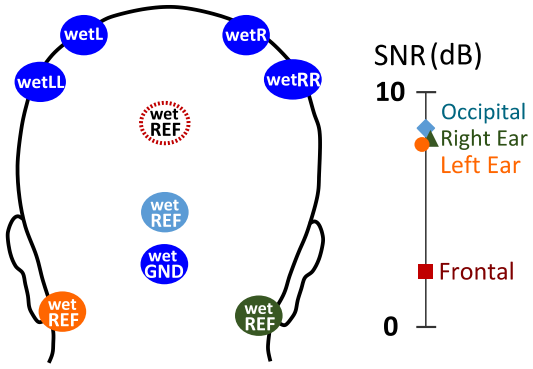

Figure 5.14: The locations of the electrodes when optimizing the location of reference (REF) electrode. The REF electrode was mounted on occipital area, frontal area (forehead), behind right ear and behind left ear sequentially. The SNR of the four wet signal electrodes is averaged and presented.

Results and discussions

The SNR values of mounting the REF electrode on various locations were compared, see Figure 5.14. It is shown that the weakest alpha waves were detected when REF electrode was placed at frontal area. This is due to the fact that alpha waves are mostly generated from the occipital lobe, hence the voltage difference between the REF and signal electrodes show less alpha waves when both electrodes are located at a distance from the occipital lobe. Moreover, artifacts related to blinking of the eyes were picked up most easily by the REF electrode when placed at the frontal area. Hence the frontal area is not an ideal location for the REF electrode. Figure 5.14 also reveals that placing reference electrode behind right or left ear or at the occipital region did not cause significant difference. For the following EEG measurements performed in UZ Gent, elastic bands (Figure 5.4a) were applied for electrodes fixation. There were no elastic bands covering the area behind both ears, so placing the REF electrode at occipital area is more feasible.

Conclusions

To record high quality EEG signals using the elastic bands, the reference electrode was placed at occipital area for the all the following measurements performed in UZ Gent.

Goal 2

The **SNR** of the signals recorded from **three subjects** is compared.

Electrode types and locations

The setup as in Figure 5.15 was applied, regarding placing the four wet signal electrodes and the REF wet electrode at occipital region.

Results and discussions

The SNR of the recordings is shown in Figure 5.15. It is found that subject 1 had the strongest alpha waves no matter where the signal electrodes were located. Subject 3 had no detectable alpha waves. These results reveal that not all subjects generate clear alpha

waves when they close the eyes. Besides, the frequency range of the alpha waves varies in between subjects. Figure 5.16 shows the spectra of the EEG signals recorded from all 3 subjects. The alpha waves of subject 1 are distributed between 8-11 Hz while those of subject 2 are distributed between 10-13 Hz. No obvious peaks are found in the spectra of the EEG signals recorded from subject 3.

Conclusions

Comparing the SNR of the signals recorded from different subjects is not the correct way to determine the signal quality of the applied electrodes. The SNR of the signals can only be compared when recorded on the same subject.

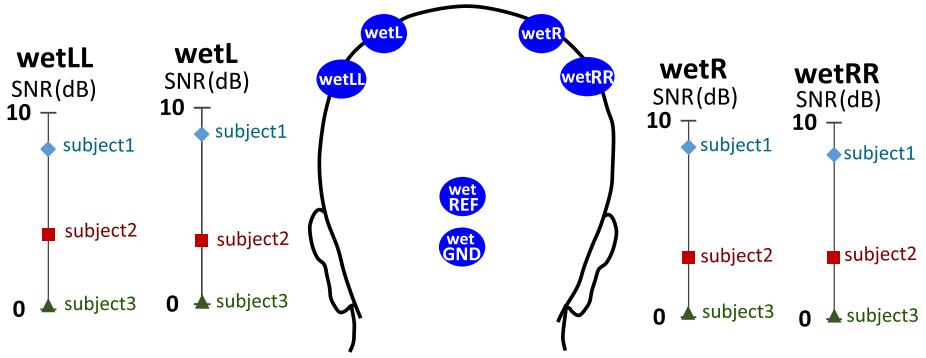

Figure 5.15: The SNR of the four wet electrodes when the subjects closed the eyes.

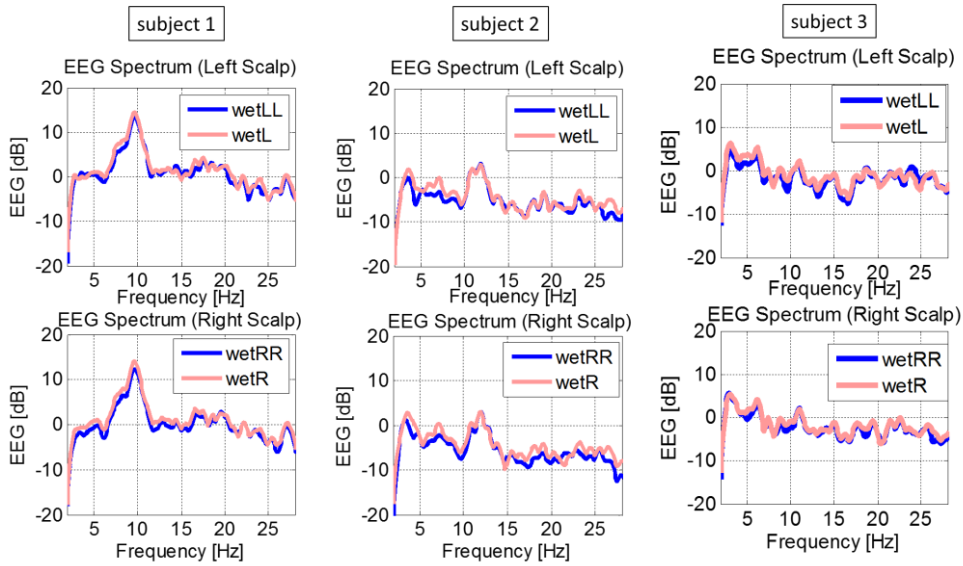

Figure 5.16: The spectra of EEG recorded from the four wet electrodes when subject 1, subject 2 and subject 3 closing their eyes.

5.4.3 Phase 3: EEG monitoring on healthy participants using dry, bridge and cup electrodes

To evaluate the quality of the EEG signals recorded using polymer dry electrodes, the EEG signals recorded by wet and dry electrodes were compared. The ideal scenario is using two identical recording systems. One of the recording systems connects with wet signal, REF and GND electrodes, while the other one connects with dry signal, REF and GND electrodes. However, synchronization of such signals recorded by two separate systems would be challenging. Besides, no two perfect identical systems are available in UZ Gent, hence the evaluation protocol has to be adjusted. There is always discussion about how to compare two EEG signals when recorded with one system only. Two approaches are possible: two electrodes located in close proximity which are measuring simultaneously using a common ground and reference electrode, or two electrodes located at the same position but measured consequentially, each recording with its own ground and reference electrode. For both approaches, the signals are not expected to be exactly equal, related to a difference in head position or timing [5]. In phase 1 and phase 2 of the polymer electrode validation, the first approach was applied. In phase 3 described below, the second approach was used.

Goal

In phase 3, a comparison is made between EEG signals recorded by **polymer dry**, **bridge** and **cup** electrodes.

In clinical EEG monitoring, bridge electrodes are used for short-term monitoring while cup electrodes are used for long-term recording. Both electrode types (Figure 1.4) are considered as standard electrodes with high accuracy, hence both of them provide a good reference for our polymer dry electrode evaluation.

Electrodes types and locations

Polymer **dry** electrodes were always tested first to ensure the scalp was dry, followed by EEG recording using wet **bridge** electrodes and finally Ten20 gel filled **cup** electrodes are used. During each recording period, six electrodes of the same type were placed on the scalp as signal, REF and GND with the locations listed in Table 5.4. Four EEG signals were simultaneously recorded.

4 signals	at C3, C4, P3 and P4 according to the international 10-20 system
GND	at the occipital region (back of the head)
REF	at the occipital region (back of the head)

Table 5.4: The locations of the electrodes for this test.

Protocol

During the recording period of each type of electrode, the subject was asked to alternate between open and close eyes. Each of such task segment lasted 30 seconds and this open/close eyes cycle was repeated 5 times, resulting in 5 minutes total test time. This protocol is approved by the ethical committee of UZ Gent and applied on four subjects in this phase.

Signal analysis

The signals recorded by different electrodes were filtered and their SNR when eyes closed was compared. As discussed in section 5.4.2, only the SNR values of the signals recorded on the same subject can be compared.

Results and discussions

The SNRs of all five 'eyes closed segments' using the various types of electrodes are shown in Figure 5.17. Results are plotted in a separate graph for each subject since SNR's can only be compared for the same subject.

A first observation is that only subject 1 and 3 have good SNR's, for subject 2 and 4 the SNR values are very low. This is related with the difference in frequency and strength of the alpha waves for each subject. Subject 1 and 3 have clear alpha waves between 8 and 13Hz. The situation is different for subjects 2 and 4. When inspecting the EEG spectra of subject 2, it was found that the alpha waves are present at a frequency range of 6-8 Hz, see Figure 5.18a. Hence the conventional SNR calculation for alpha waves at 8-13Hz will not result in a meaningful value. Thus, the SNR was recalculated by defining signals at frequency range of 5-10 Hz as "signal" and at the rest range as "noise". The re-computed SNR can be found in Figure 5.18b, obviously higher SNR's are obtained except for one recording segment of the dry electrodes. This can be explained by looking at the raw signal in Figure 5.19. During this recording segment artifacts occurred, probably a disturbance at the reference electrode since all signal electrodes show the artifacts, resulting in a very low SNR ratio for this one time segment. In general, for subject 2, the SNR's for polymer dry electrodes are just slightly lower than cup electrodes. The low SNR's for subject 4 have a very different origin: the EEG spectra of subject 4 show no obvious peak, hence no clear alpha waves were produced. In such case, analyzing the SNR value is not a proper approach for signal quality evaluation.

Both subject 1 and 3 produce clear alpha waves distributed around 8-13Hz, hence the standard SNR calculation is valid. The first graph in Figure 5.17, representing SNRs for subject 1, shows that the SNRs of all electrode types are similar. This suggests that polymer dry electrodes have a similar ability to acquire alpha waves as the other two wet electrodes. Same result is found for subject 3, except the polymer dry electrode signal on position P3. This dry electrode suffered from baseline drift, see Figure 5.20, resulting in worse signal quality and lower SNR. Baseline drift results from the bad electrode/skin contact.

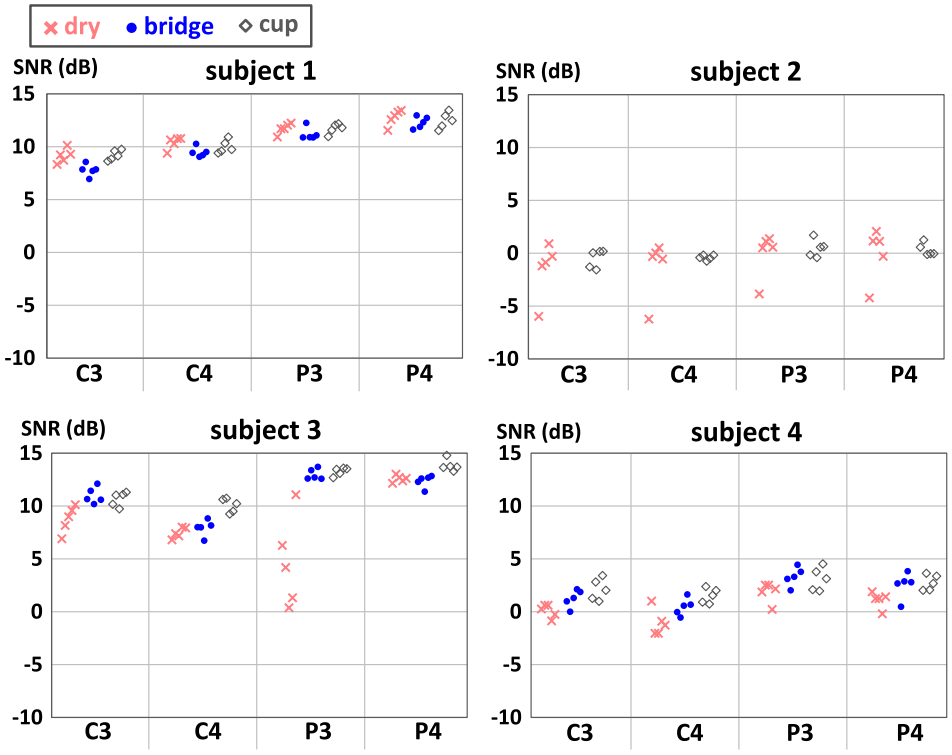

Figure 5.17: The SNR of three types of electrodes located at 4 different locations tested on 4 subjects. The SNR were calculated from EEG signals recorded when the subjects closed their eyes.

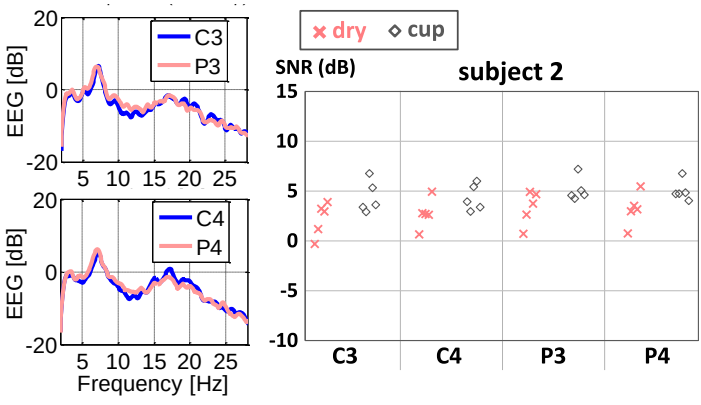

Figure 5.18: (a) The spectra of EEG signals recorded by cup electrode on subject 2 when the eyes were closed. (b) The re-calculated SNR when defining signals distributed at 5-10Hz are "signal" for SNR calculation.

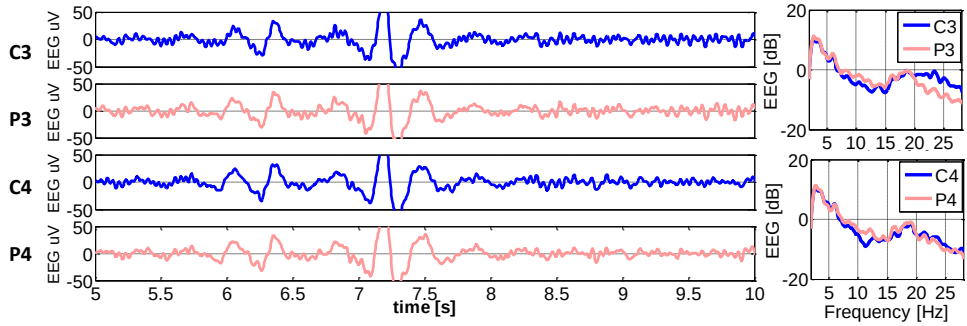

Figure 5.19: There were artifacts in the signals recorded using polymer dry electrodes on subject 2. These artifacts were low frequency signals.

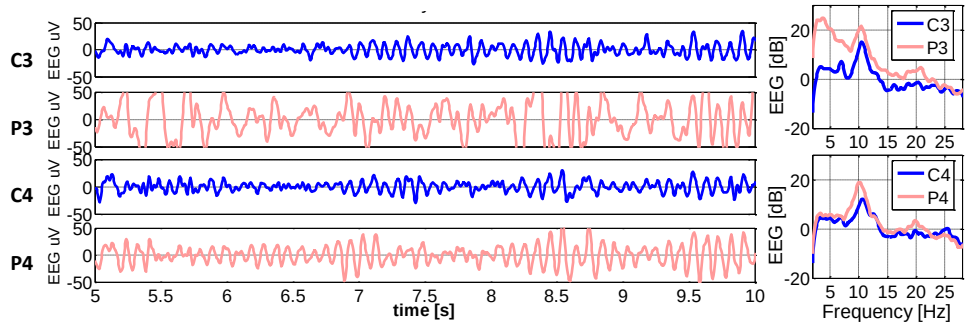

Figure 5.20: Partial EEG signals recorded by polymer dry electrodes on subject 3. The baseline of signal at P3 drifted severely so the intensity of signals at low frequencies was high in its spectrum.

Conclusions

The experimental setup and protocol described in section 5.4.3 were validated on healthy subjects without any adverse effect. Besides, our own active electrodes are compatible with the recording amplifier in UZ Gent and the signal quality of the signals recorded by them is similar to the conventional wet EEG electrodes.

5.4.4 Phase 4: EEG monitoring on epilepsy patients using dry, bridge and cup electrodes

Goal

In this phase, the EEG measurements are carried out on three **epilepsy patients** recruited from the patients of the department of neurology in UZ Gent.

EEG recordings are one of the best tools to diagnose epilepsy and to monitor the evolution of epileptic patients during treatment [187]. High quality EEG recordings are essential for this purpose, hence dry electrode recordings on epilepsy patients, delivering EEG patterns judged by a very experienced medical staff, is a good way to analyze the obtained recording quality. Furthermore, the group of epilepsy patients is a target group when developing comfortable polymer dry electrodes, because of the following: the EEG monitoring on

epilepsy patients often lasts a few days to one week and takes place in an epilepsy monitoring unit in a hospital. Mounting the conventional wet electrodes on the scalp by medical staff is time-consuming as discussed already in section 1.2.1. The staff needs to refill conductive gel into the electrodes frequently during the monitoring to ensure good signal quality [188]. Replacing conventional wet electrodes to polymer dry electrodes for EEG monitoring reduces the time of mounting the electrodes on the scalp, refilling the conductive gel and removing the electrodes after the monitoring. Moreover, using dry electrodes also reduce the discomfort of the patient during electrode removal using acetone. Therefore, the feasibility of using polymer dry electrodes to record EEG signals for seizure diagnosis on epilepsy patients is investigated in this thesis.

Electrodes locations and types

The electrode setup was the same as the one applied on healthy participants (section 5.4.3), except that the signal electrodes were placed on the locations where epileptic EEG signals occur according to the history of the patient. Figure 5.21 shows the electrode locations on patient 1. This patient had epileptic activities on the right part of brain. Hence 3 electrodes were placed at T4, T6 and P4 locations. To compare the signals recorded from the symmetrical sites of the previous electrodes, 3 more electrodes were placed at T3, T5 and P3 locations (on the left part of brain). Still one other signal is recorded from Fz using cup electrodes during all the recordings. This is to check the compatibility of the system when using dry and bridge REF and GND electrodes. The REF and GND electrodes were mounted at occipital location. Again, polymer dry, bridge and cup electrodes were mounted sequentially.

Results and conclusions

The EEG spectra of each type of electrode during one of the eyes closed segments are plotted in Figure 5.21. Since the signals of different electrode types were not recorded simultaneously, the spectra of them were not expected to be the same. However, similar patterns are shown in the signals using three different types of electrodes. It is found that all types of electrodes acquired similar intensity of signal distributed at 5-9Hz. However, dry electrodes picked up more low frequency noise than the other two did.

All the signals recorded using three types of electrodes on three subject are evaluated by a medical doctor. To conclude, although the signals recorded by dry electrodes contain more baseline drift (low frequency), the signal quality is sufficient for correct medical interpretation.

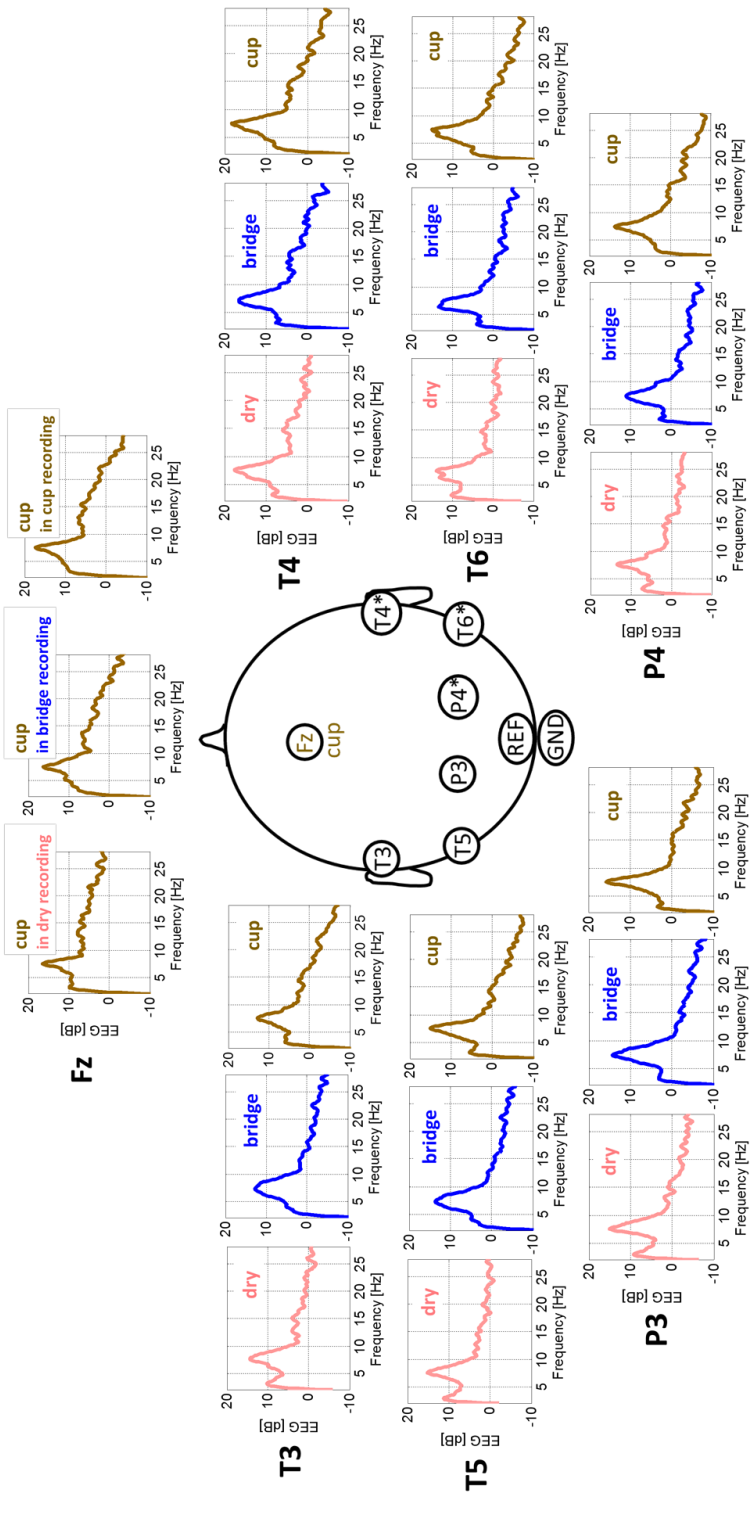

Figure 5.21: The spectra of the signals recorded by all types of electrodes at various locations. T4, T6 and P4 locations are where epileptic EEG signals have been recorded on this subject before. T3, T5 and P3 are mounted to record the signals from the symmetrical sites of previous electrodes. The signals were recorded when the subject closed the eyes.

5.5 EEG measurement in UZ Leuven

Besides the validation of polymer dry electrodes using the recording device in UZ Gent, the validation using another recording device in UZ Leuven was carried out. The recording amplifier used in UZ Leuven is from Schwarzer PSG (Natus, USA). Similar to the measurements in UZ Gent, the setup and protocol were first validated on healthy adults in a standard patient examination room and then performed on epilepsy patients in the hospital ward.

5.5.1 EEG measurements on healthy subjects

Goals

The aims of validating the test setup and protocol on healthy subjects are all related with the use of a EEG recording device never combined before with dry electrodes:

1. Evaluate the compatibility of the active polymer electrodes (with circuits as shown in Figure 5.2) with the clinical recording device in UZ Leuven.
2. Investigate the effects of applying wet and polymer dry electrodes as REF and GND.
3. Investigate the effects of REF and GND electrodes locations.

These goals and the corresponding tests are rather similar to the tests which were performed before with the clinical EEG recording system in UZ Gent. Therefore in this main part of the thesis text only limited experimental results will be shown, in order to illustrate the conclusions of these experiments. A full description of the experimental work including results and discussion can be found in Appendix II.

Electrodes types and locations

During the recordings, signals from **6** channel electrodes were evaluated. The locations of the electrodes are shown in Figure 5.22. The test is separated into 2 parts: dry GND and REF electrodes (Test 1a), and wet GND and REF electrodes (Test 1b). Dry electrodes are polymer electrodes with material composition number 95 (CR95) combined with our own active circuit (see section 5.1 and Figure 5.2).

Protocol

During the monitoring, the subjects repeated the open/close eyes tasks for three or four time periods. This test protocol has been approved upfront by the ethical committee of UZ Gent.

Signal analysis

- SNR when eyes closed
- Correlation and coherence of two adjacent wet electrodes and of a pair of wet and dry electrodes

Results and discussions

The signal spectra for these recordings when the subject closed his eyes are shown in Figure 5.22. Very clear alpha waves are seen. The spectra of wet2 and wet3 are very similar

and that of wet5 and wet6 are rather similar, although a slightly higher alpha peak is visible in wet6, this proves that the small difference in electrode location will not cause important changes in the signals. Also signal dry1 in both tests, and dry4 in Test 1a, are producing very similar signals as their neighboring wet electrodes, proving that these dry electrodes give high quality recording. There is however a disadvantage of the dry electrodes clearly visible in the graphs: the high intensity of signals of low frequency is typical for baseline drift. In Test 1a, the reference electrode suffers from baseline drift, hence all signal electrodes show this high intensity of low frequency signals. In Test 1b, the wet REF electrode is fine, but dry4 suffers from baseline drift.

The quality of REF signal can be improved by using cylindrical-shaped electrode instead of pin-shaped one in this test. Since there is no hair behind the earlobe, a cylindrical-shaped electrode has larger and more consistent electrode/skin contact area. Due to the more stable electrode/skin contact area, the cylindrical-shaped electrode is less sensitive to motion artifacts as discussed in section 4.5. Besides using an electrode with proper shape as REF electrode, mounting the REF electrode 15 minutes before the monitoring starts because the baseline drift decreases when the electrode/skin interface becomes stabilized.

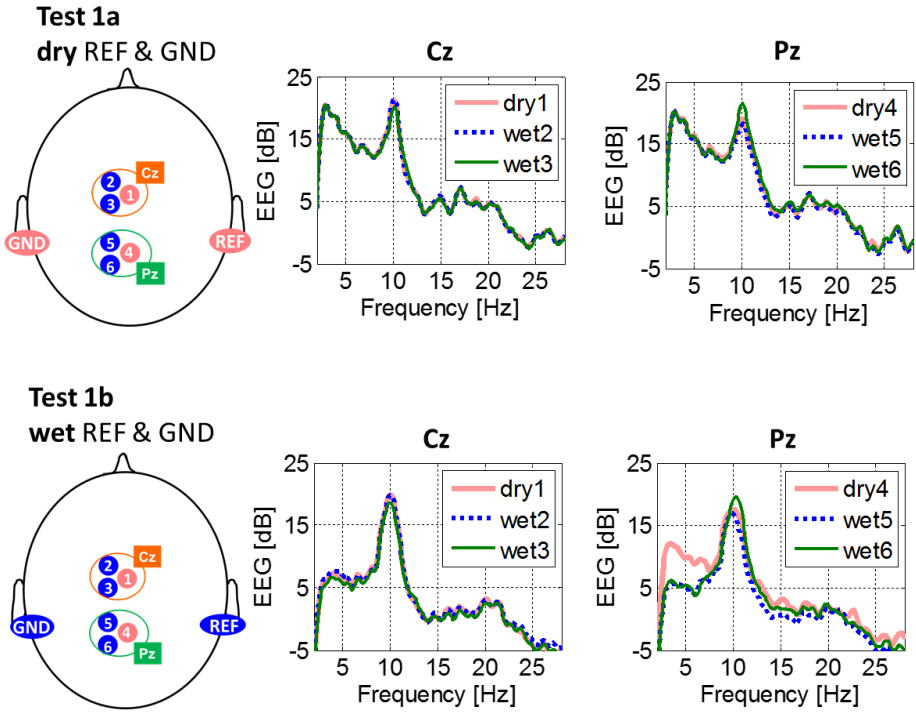

Figure 5.22: The PSD of the signals recorded in Test 1a and Test 1b.

When calculating the SNR for the signals of Tests 1a and 1b, the baseline drift becomes even more visible. Since the low frequency signal components are defined as 'noise' in SNR calculations, a lower SNR is calculated when baseline drift is present. The SNRs of all the recordings are shown in Figure 5.23. Each data point in the figure represents the

SNR value of that recording session, hence 3 SNRs per signal electrode for this Test 1. Without surprise, the SNR of the signals recorded in Test 1a is low because of the baseline drifts of the dry REF electrode. In Test 1b, all wet electrodes show high SNR except dry4, again due to baseline drift. In Test 1b, the SNR of wet6 is slightly higher than that of wet5, which might be related to the wet6 location: stronger alpha waves are present in the occipital region (hence larger alpha peak in wet6 signal, as already seen in Figure 5.22).

While a baseline drift of a REF electrode will show a low SNR for all related signal electrodes, the correlation and coherence of 2-30 Hz of such signals are just very high, since the baseline drift is a clear common signal. Hence for Test 1a, false positive results are obtained for the correlation and coherence. In Test 1b, the coherence and correlation of signals is lower, especially that of dry4_wet5 and dry4_wet6. But also for wet5_wet6, the correlation and coherence is less good than wet2_wet3, related to the larger spatial variability of the signals recorded at Pz location.

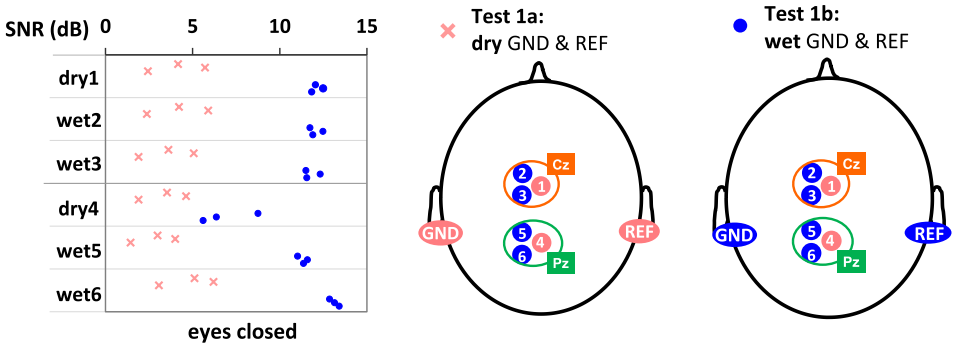

Figure 5.23: SNR of the signals recorded by wet and dry electrodes when placing the ground and reference electrodes behind the earlobes (Test 1a and Test 1b). Each data points represent the SNR of each recording sessions.

Interpretation of raw / filtered signals by medical staff

Figure 5.24 to Figure 5.28 show the eyes closed signals recorded during Test 1a. In Figure 5.24 the raw EEG signals are plotted. 50 Hz signals due to power line interference and baseline drift from dry REF electrode are clearly seen in all signals. Figure 5.25 shows the signals filtered by a 50 Hz notch filter. After the removal of the 50 Hz signals, the alpha waves can be clearly seen. However, baseline drift still exists. In Figure 5.25, period A contains 0.25 Hz signals, period B contains 0.85 Hz signals and period C contains 1.25 Hz signals. From Figure 5.26 to Figure 5.28, the signals in each of these figures are filtered by different bandpass filters with 0.5 Hz, 1 Hz or 2 Hz lower passband edges and 45 Hz higher passband edge. Figure 5.26 shows signals filtered by a 0.5-45 Hz bandpass filter, hence the 0.25 Hz waves are filtered out. Figure 5.27 shows signals filtered by a 1-45 Hz bandpass filter, hence both 0.25 Hz and 0.85 Hz waves are filtered out. Figure 5.28 shows signals filtered by a 2-45 Hz bandpass filter, filtering out all 0.25 Hz, 0.85 Hz and 1.25 Hz waves. Filtering with 2 Hz lower passband edge can be used to remove the baseline drift, however, EEG signals of low frequency (< 2Hz) which might be interesting for clinical interpretation are filtered out as well. In addition, it is noted that the filters used in this thesis are not ideal,

so they might slightly distort the signals distributed at the frequencies of the filters' passband edges. Therefore, the passband edges of the filters need to be selected depending on the frequency band of interested signals during interpretation.

Figure 5.29 to Figure 5.32 show the eyes open signals recorded during Test 1a. Figure 5.29 and Figure 5.31 are signals underwent only a 50 Hz notch filter. The baseline drift can again be filtered using a 2-45 Hz bandpass filter resulting the signals shown in Figure 5.30 and Figure 5.32. Even large amplitude peaks, such as the signals at 1 to 4 second in Figure 5.31, can be easily removed by the bandpass filter. Good quality signals result after this noise filtering. Theoretically, signals with extreme baseline drift might have the risk to reach the saturation value of the recording amplifier, which will result in a flat line locally in the raw and filtered signals, but it never happened in this evaluation.

In spite of the baseline drift, the quality of the raw signals is good and they can be used for interpretation by experienced medical staff. However, it has to be noted that the baseline drift in the raw signals might result in misinterpretation of EEG signals distributed at low frequency (< 2 Hz). Filtering the baseline drift using 2-45 Hz bandpass filter results in an easier interpretation of the signals distributed in 2-45 Hz, but this removes the low frequency EEG signals as well. This implies that polymer electrodes with material composition number 95 (CR95) are not optimal for the clinical applications focusing on signals of low frequency. For example, delta waves distributing at 1-4 Hz are crucial during deep sleep monitoring. 3 Hz spike and wave complexes are often seen in childhood absence epilepsy. Event-related potential (ERP) measuring the brain response which is the direct result of a specific sensory, cognitive, or motor event has a specific EEG waveform shown immediately up to 500 millisecond after the stimuli.

Conclusions

The results prove that our polymer active electrodes are also compatible with the clinical recording system in UZ Leuven. Furthermore, signal recordings from the dry electrodes are from good quality, although these dry electrodes are clearly more prone to baseline drift compared to wet electrodes. This baseline drift causes problems when performing mathematical signal analyses: it is resulting systematically in very low SNR values and might result in false positive correlation and coherence values. Trained medical staff is satisfied with the signal quality of alpha waves recorded during Test 1a. The staff is perfectly capable in giving correct interpretation to the signals, which are not interfered by low frequency baseline drift. The baseline drift might result in misinterpretation of EEG signals distributed at low frequency (<2Hz). To conclude, the recorded signals using polymer electrodes with material composition number 95 (CR95) show good quality but contain baseline drift, thus these electrodes are suitable for clinical applications for which low frequencies signals (< 2 Hz) are not the main interest.

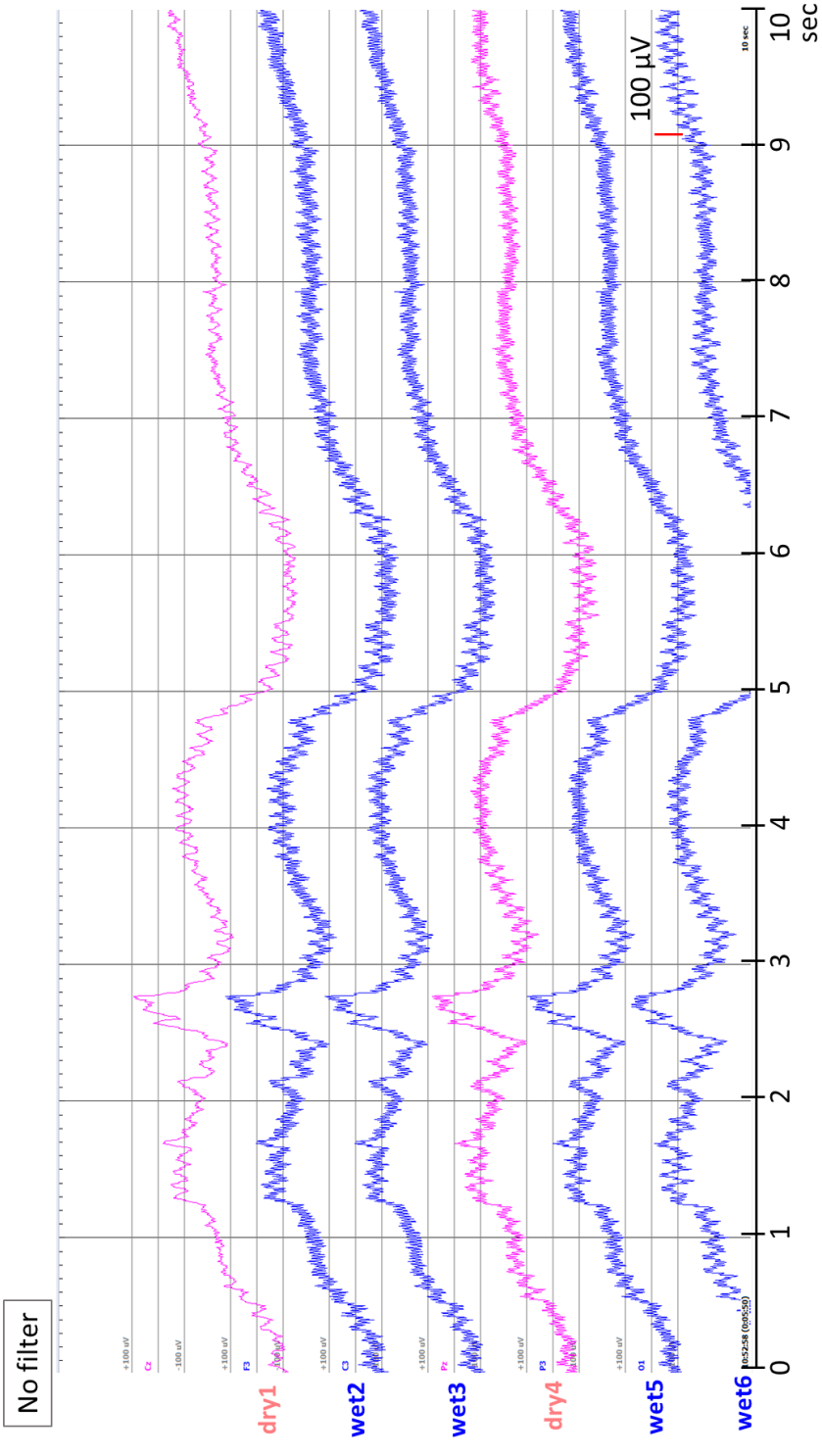

Figure 5.24: The signals recorded when eyes closed in Test 1a using dry GND and REF. The signals are raw signals.

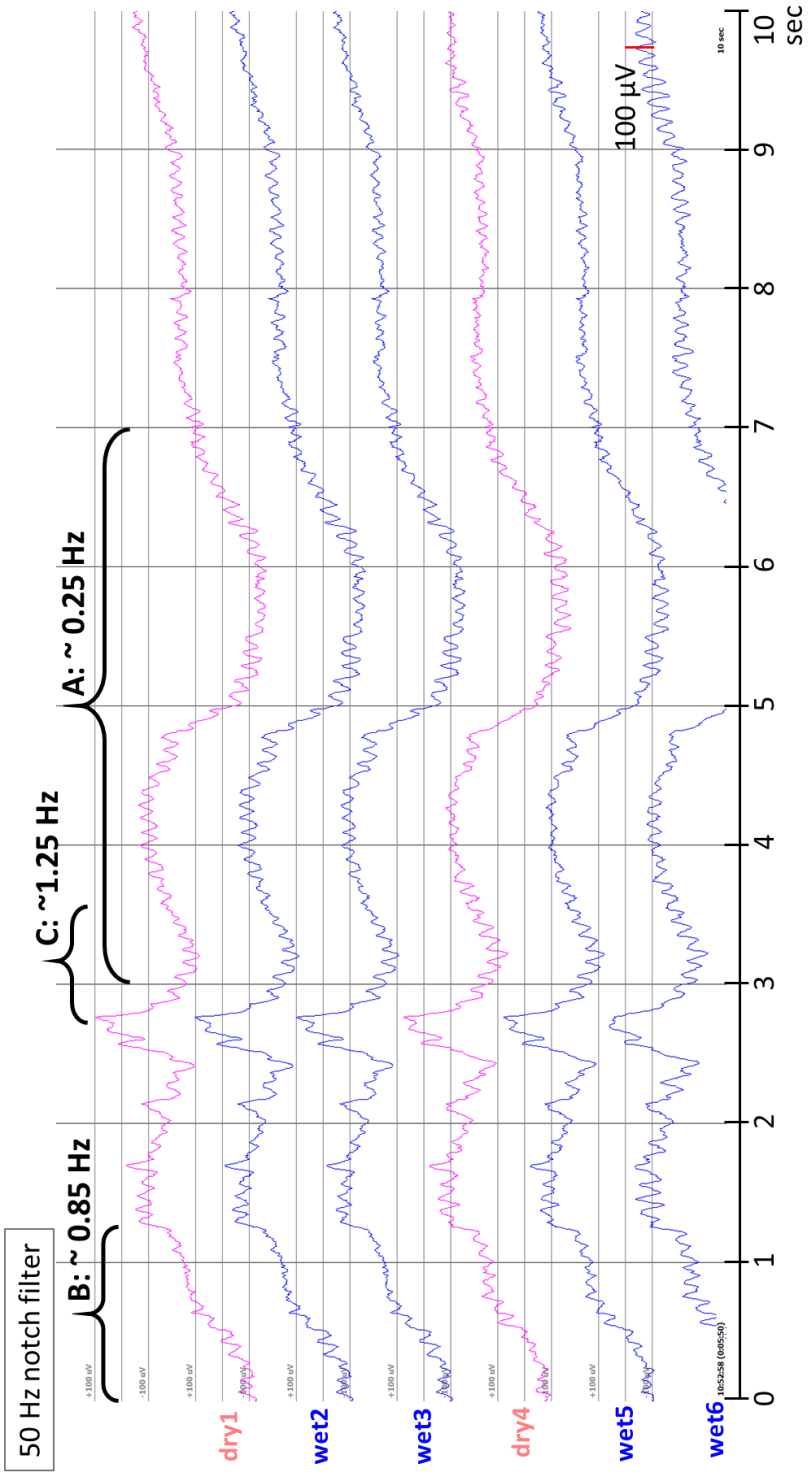

Figure 5.25: The signals recorded when eyes closed in Test 1a using dry GND and REF. The signals are filtered by a 50 Hz notch filter.

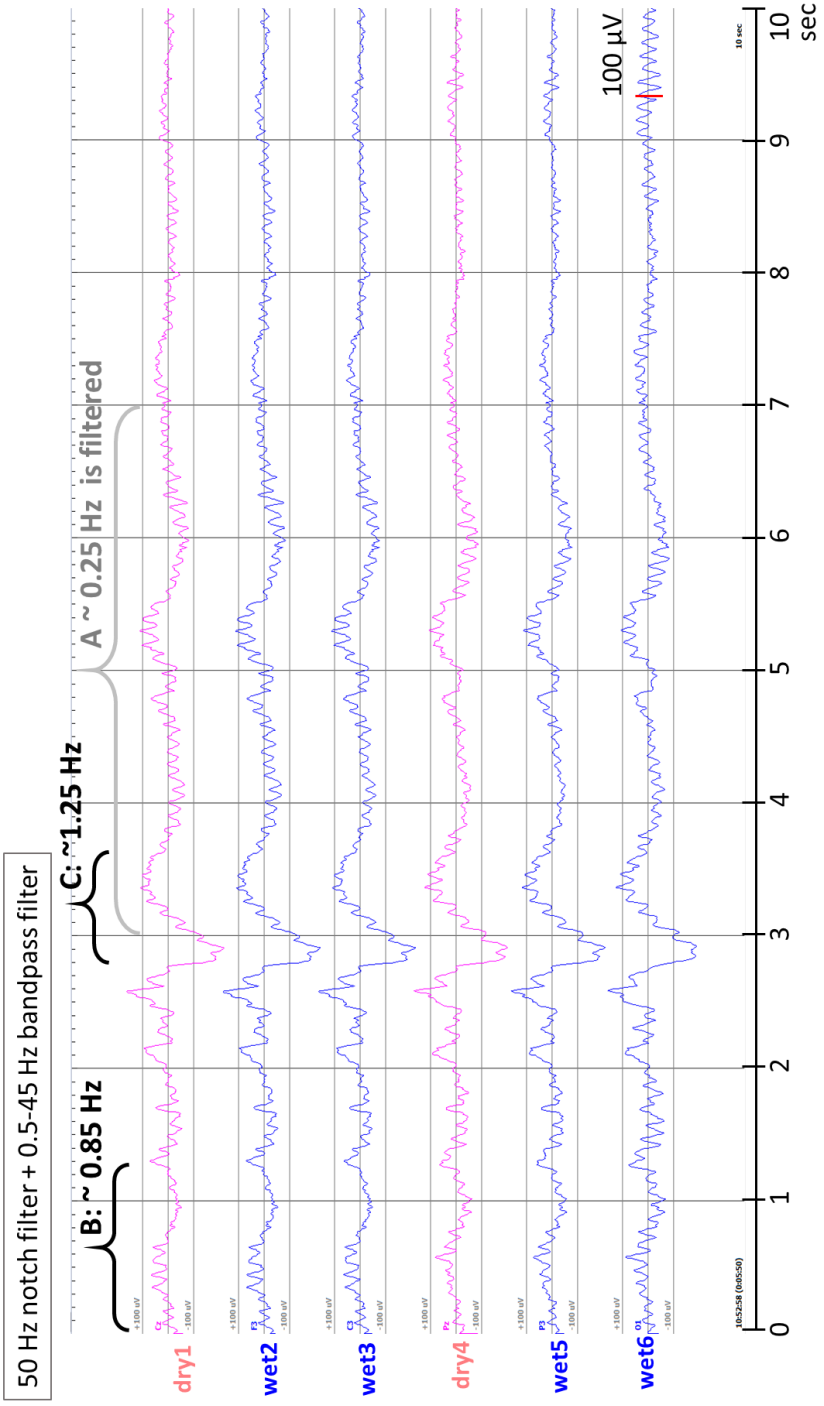

Figure 5.26: The signals recorded when eyes closed in Test 1a using dry GND and REF. The signals are filtered by a 50 Hz notch filter and a 0.5-45 Hz bandpass filter.

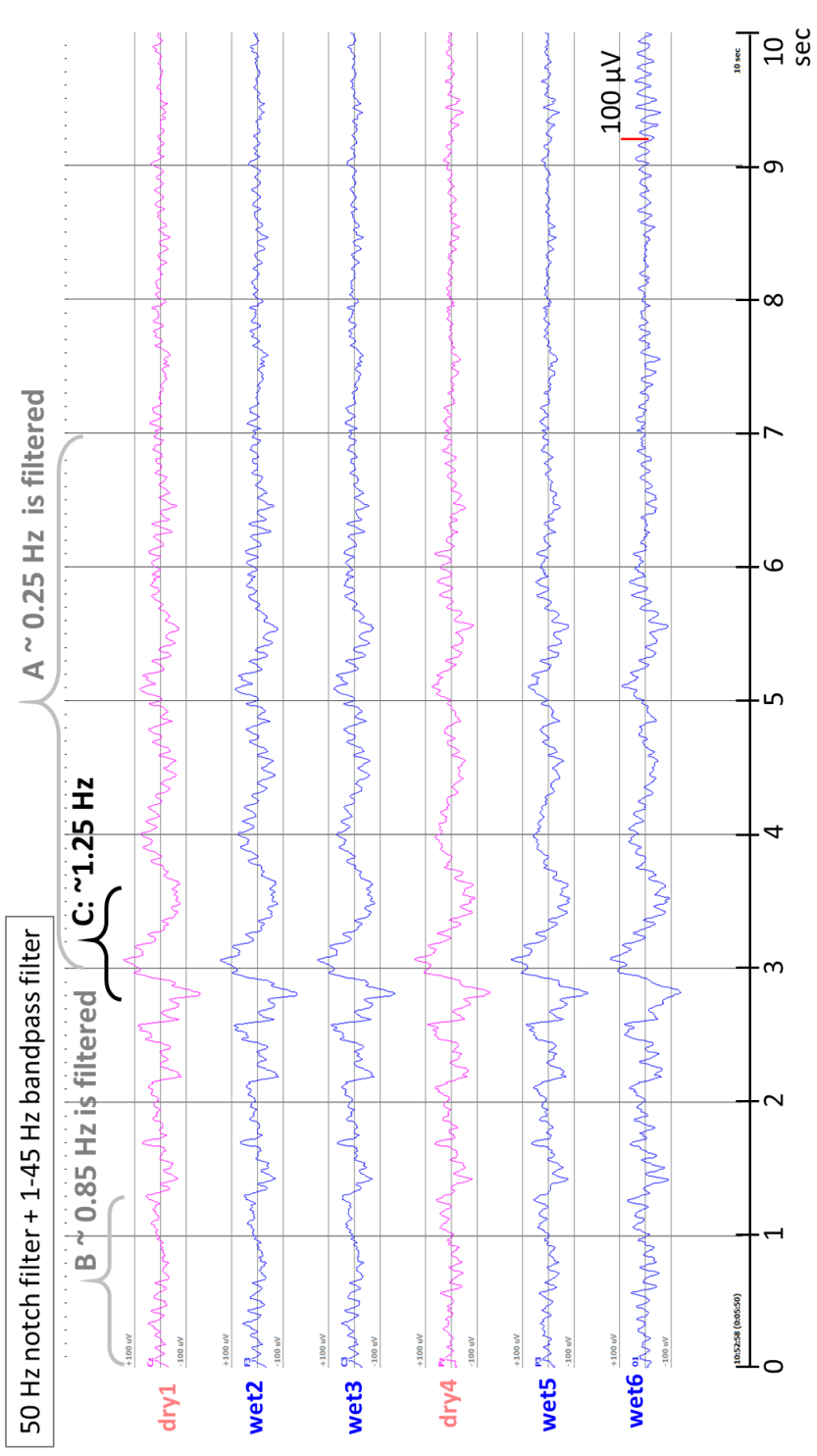

Figure 5.27: The signals recorded when eyes closed in Test 1a using dry GND and REF. The signals are filtered by a 50 Hz notch filter and a 1-45 Hz bandpass filter.

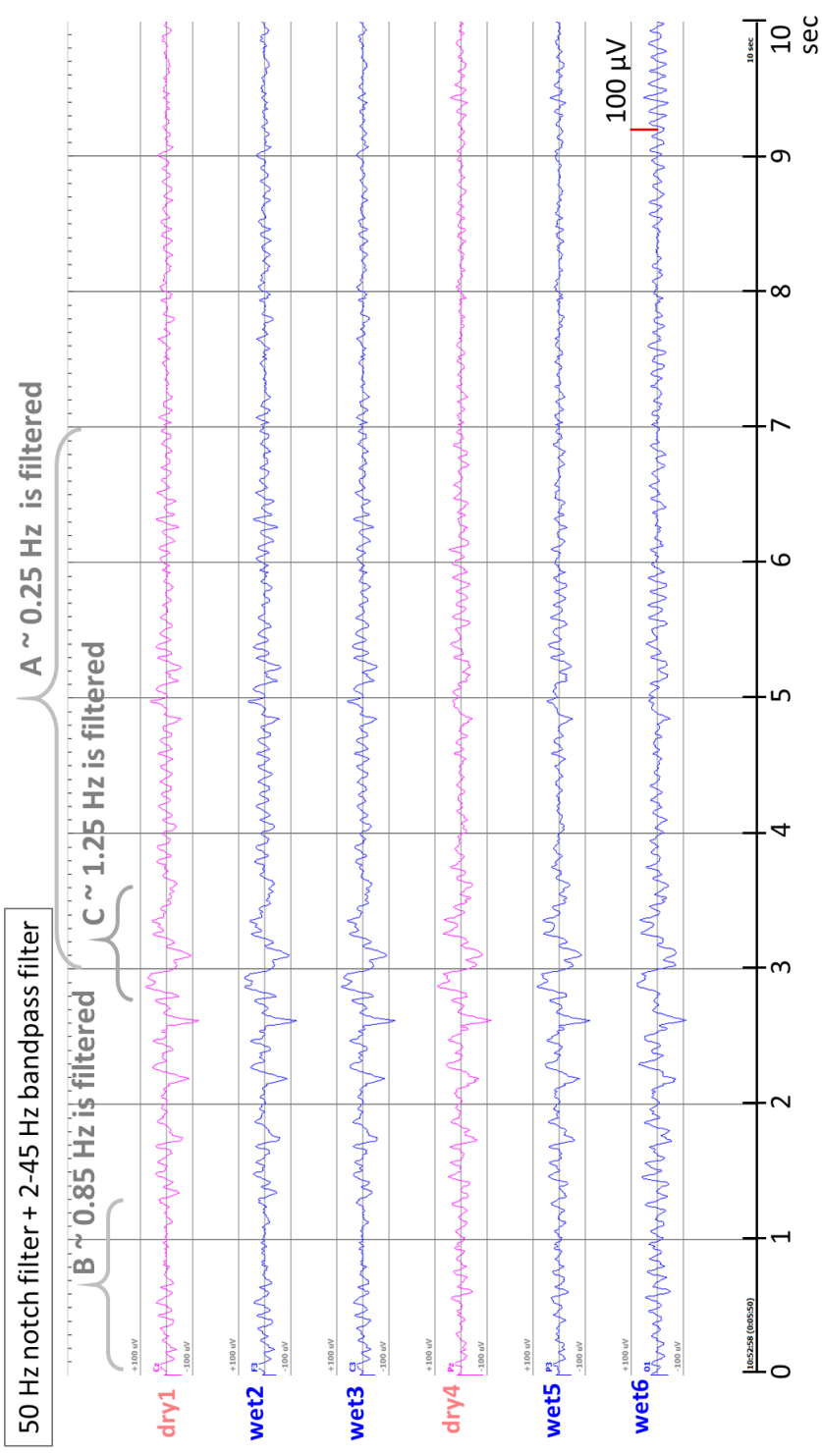

Figure 5.28: The signals recorded when eyes closed in Test 1a using dry GND and REF. The signals are filtered by a 50 Hz notch filter and a 2-45 Hz bandpass filter.

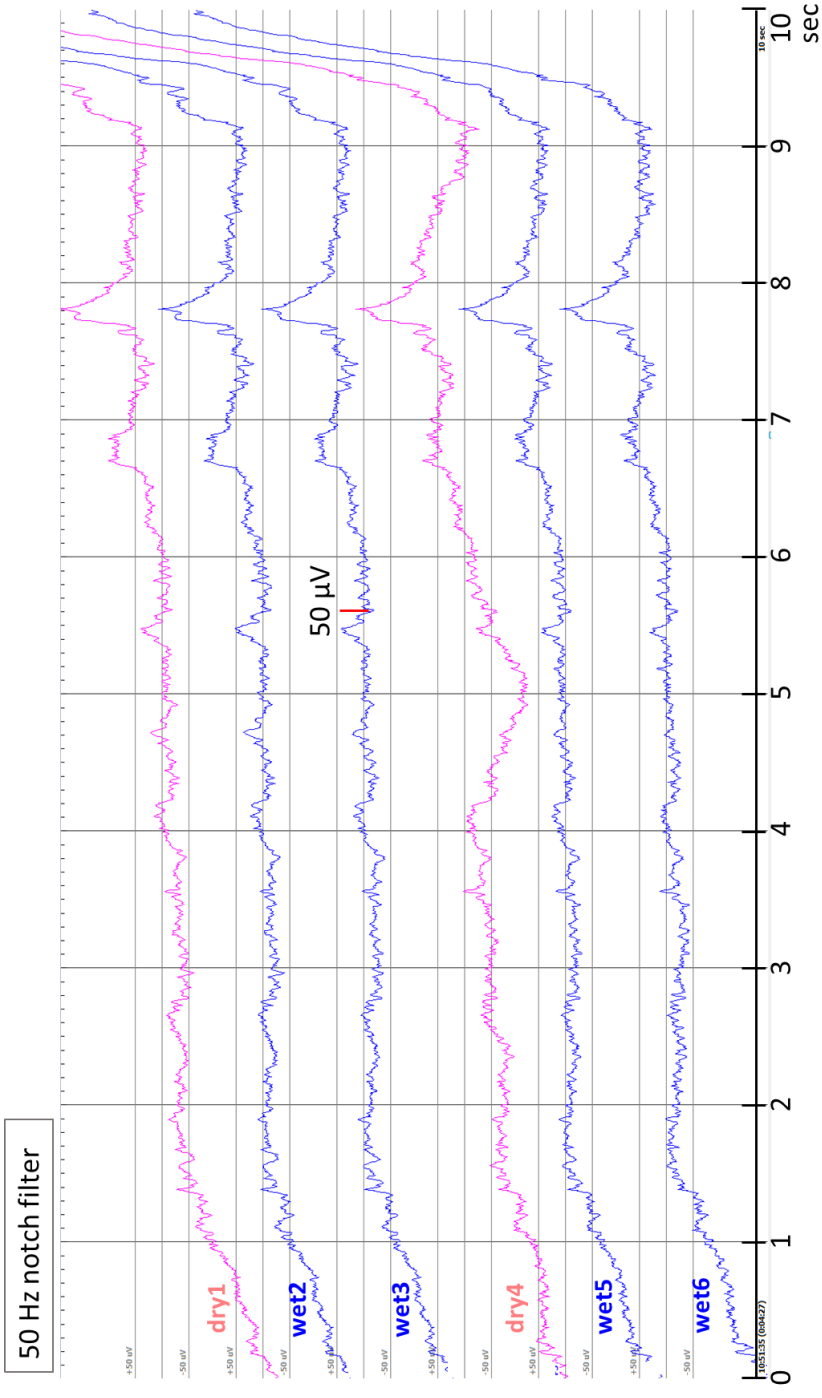

Figure 5.29: The signals recorded when eyes open in Test 1a using dry GND and REF. The signals are filtered by a 50 Hz notch filter.

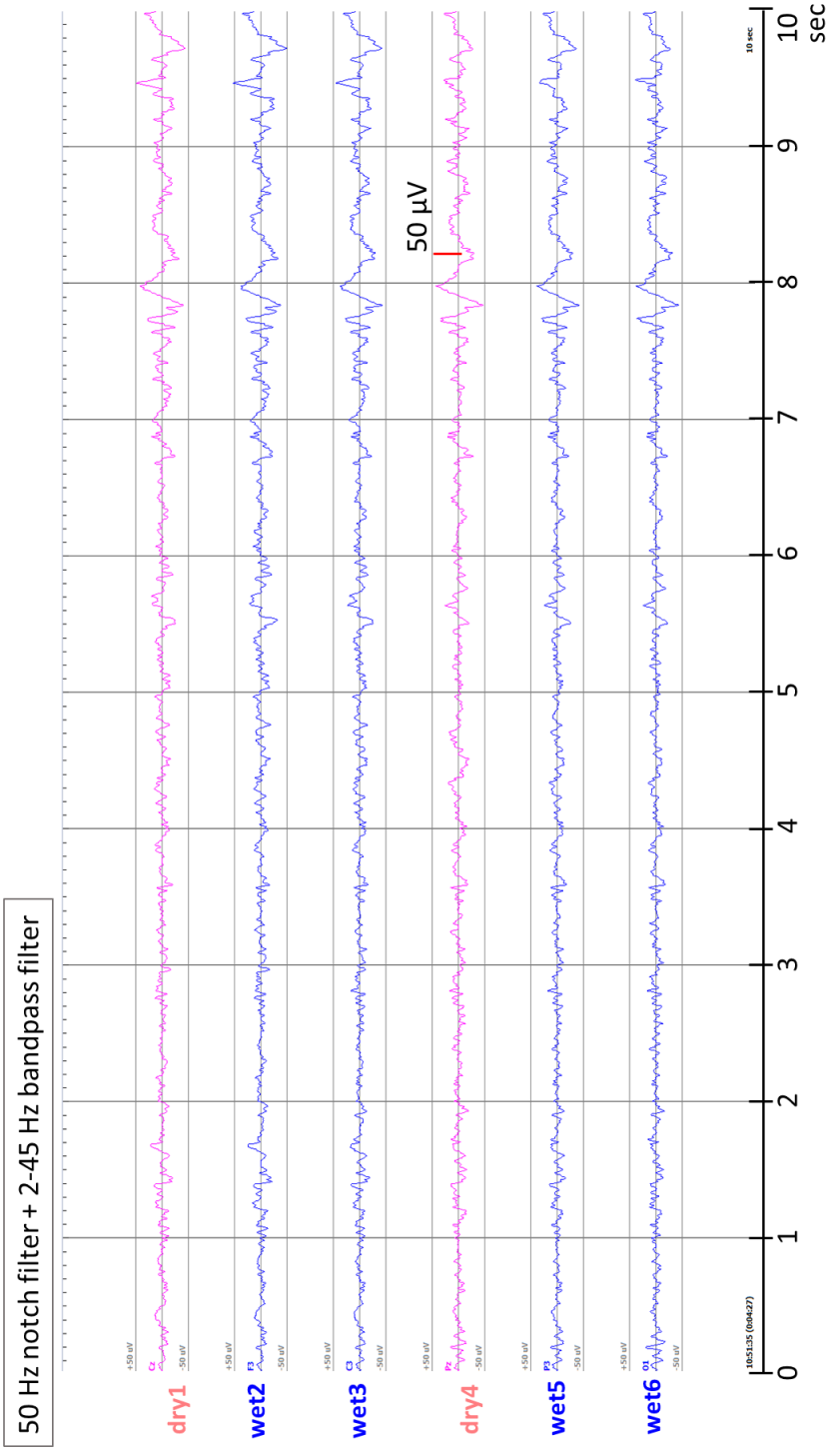

Figure 5.30: The signals recorded when eyes open in Test 1a using dry GND and REF. The signals are filtered by a 50 Hz notch filter and a 2-30 Hz bandpass filter.

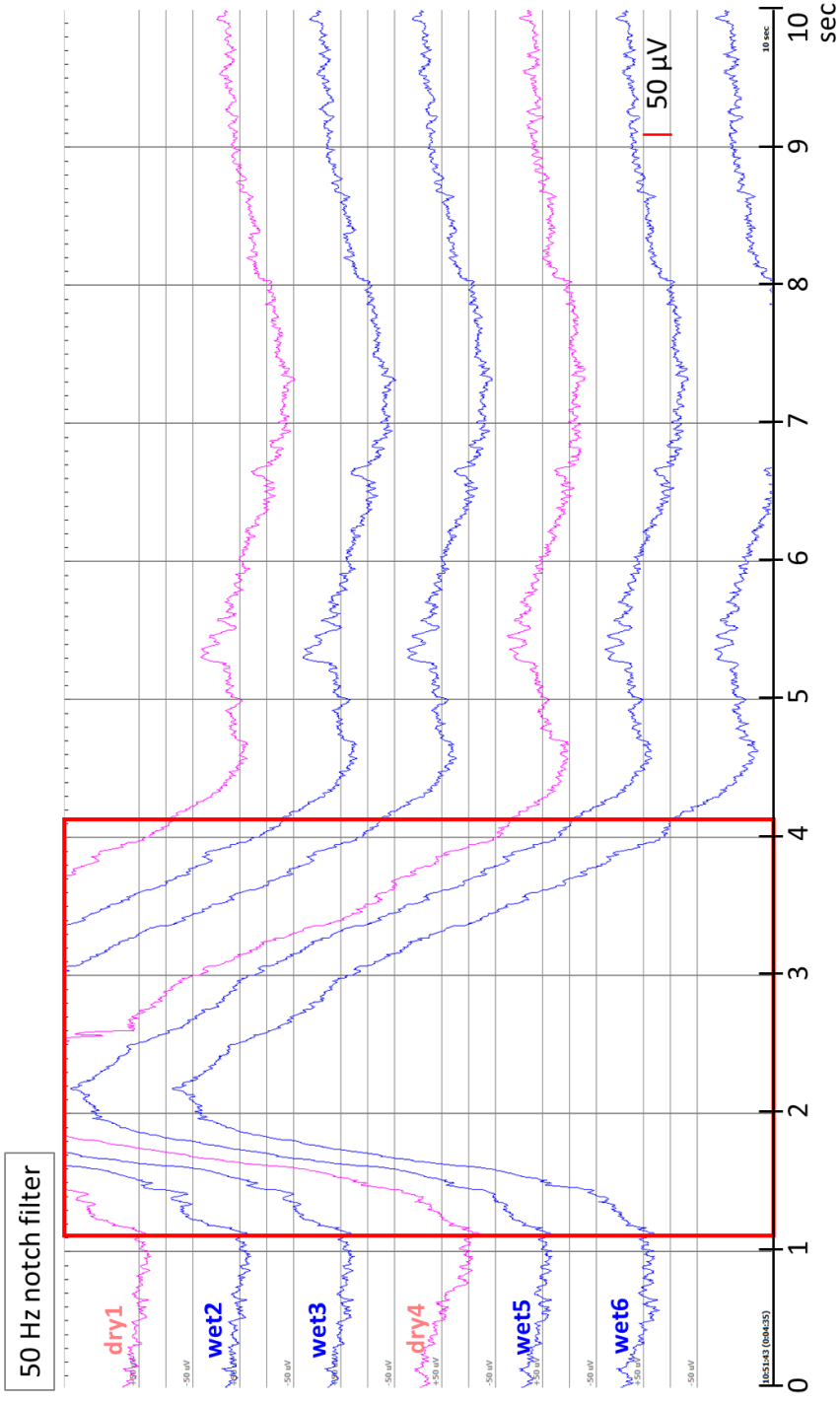

Figure 5.31: The signals recorded when eyes open in Test 1a using dry GND and REF. The signals are filtered by a 50 Hz notch filter. The red rectangular indicates the large amplitude signals at 1 to 4 second.

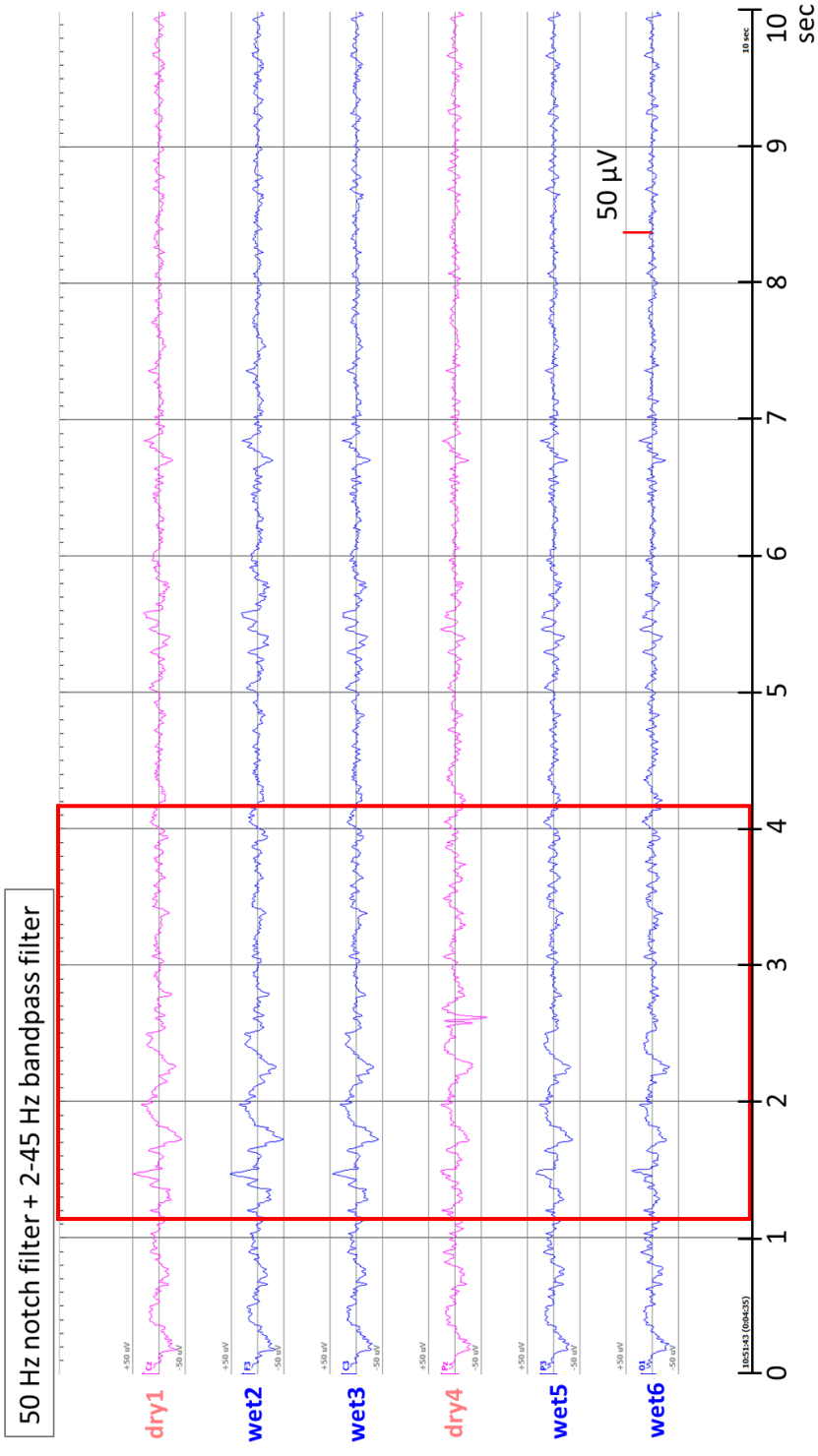

Figure 5.32: The signals recorded when eyes open in Test 1a using dry GND and REF. The signals are filtered by a 50 Hz notch filter and a 2-30 Hz bandpass filter. The red rectangular indicates the large amplitude signals at 1 to 4 second can be removed using the bandpass filter.

5.5.2 EEG measurements on children with epilepsy

Goal

The next goal is measuring EEG signals on two children with epilepsy using polymer dry electrodes and the recording amplifier of UZ Leuven.

The children were recruited from the patients of UZ Leuven. The potential participants and their parents were given a clear introduction of the goal and the procedure of this test before they decided to participate. Finally, 2 children volunteered for the EEG measurements. An informed consent was given to the participants before the measurements started.

Electrode types and locations

The dry electrodes with material composition number 95 (CR95) were mounted on the locations where epileptic discharges have been recorded according to the patients' history. Extra dry electrodes were mounted on the symmetrical locations of the ones selected because of epileptic seizures. The electrode locations for both patients are indicated in Figure 5.33. The GND electrode is placed close to nasion on patients. For patient 1, signals of 8 channels are recorded with the REF electrode placed on Cz. For patient 2, signals of 15 channels are recorded with the REF electrode placed behind left earlobe.

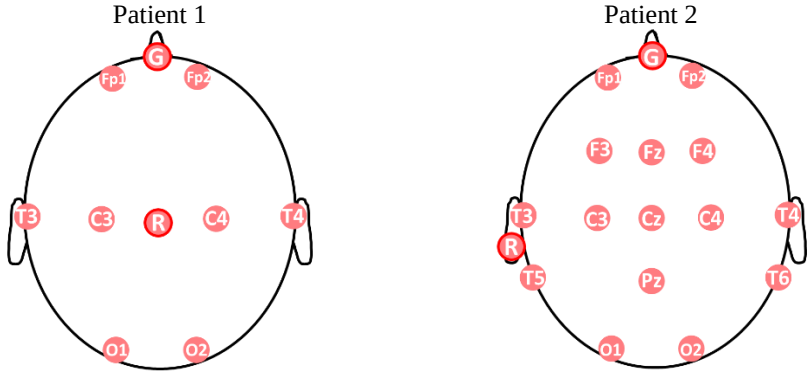

Figure 5.33: The locations of the electrodes on patient 1 and patient 2. There are 8 channel electrodes on patient 1 and 15 channel electrodes on patient 2. All the electrodes are polymer dry electrodes with material composition 95.

Protocol

Initially, the experimenters observed the signals and adjusted the electrodes to achieve better electrode/skin contact if that was necessary.

Signal analysis

SNR, correlation or coherence analyses are not applied on these signals. The signals are evaluated by an experienced medical staff during the recording.

Results and discussions

After the recording, the signals are readout and filtered by dedicated EEG software (EDFbrowser). The signals recorded from patient 1 are shown in Figure 5.34 and Figure 5.35 while those recorded from patient 2 are shown in Figure 5.36 and Figure 5.37, after filtering by a 50 Hz notch filter and 0.1-45 Hz, 4-order Chebyshev bandpass filter. Regarding the signals recorded from patient 1, no signals are recorded by 1 of the electrodes (Fp2). This might be because of improper connection of electrode and PCB or because of the failures of the components on PCB. It takes 4 minutes to manipulate the electrodes on patients before 85 % of all electrodes record signals with good quality. 1 of the 8 electrodes on patient 1 and 2 of the 15 electrodes on patient 2 suffer from severe baseline drift. Those signals containing severe baseline drift are labelled in green or grey color in Figure 5.34 to Figure 5.37.

The signals recorded in this test are not as stable as those measured on adult participants are. The signals shown in Figure 5.34 and Figure 5.36 are recorded in the periods when the signals contain fewer motion artifacts and other noise. Since the lower passband edge of the bandpass filter is 0.1 Hz, some baseline drift can be seen. During the monitoring, there are other segments of the signals with worse quality. Examples of these noisy segments can be seen in Figure 5.35 and Figure 5.37. The clinical interpretation of these signals with worse signal quality is more difficult. The artifacts and noise in the recorded signals are resulting from:

- Power line interferences [189]:
  The power line connected to electronic devices located in the monitoring unit produce electromagnetic fields around the patient. Besides, up to 15 active electrodes are connected with 30 cm long 4-wire cables transmitting power to the op-amp and signals to the recording system. Twisting the cables together to reduce the inductive loops created by them is difficult because of the different distances of each electrode to the back-end PCB. Therefore, the interactions of the inductive loops and the electromagnetic fields of other devices result in unwanted signal interference. In addition, the cables are very light so they can swing when someone passes by the subject or waves close to the cables. The movement of cables changed the size and the orientation of the inductive loops causing extra noise as well.

- Motion artifacts:
  When the subjects talked and moved the head or body, motion artifacts occurs at the interface of electrode and skin. Moreover, movements of the body cause the changes of interferences of the electromagnetic fields on the cables.

- Electrostatic interferences [8, 173]:
  When the patient is capacitively coupled with power line and earth ground, the patient body has a voltage resulting from the displacement current and the capacitances. This voltage combined with the mismatch of the impedance of electrodes affect the accuracy of the recording amplifier. During the monitoring, it is found that the signals become less noisy when the patient is touched by another person. This person may have better grounding than the patient does. This interference can be reduced by

switching the dry GND electrode to a wet one. This approach was tested during the recording session, the signals improve after swapping to the lower impedance and more stable wet GND electrode.

Furthermore, children might have lower tolerance to the discomfort resulted from the combination of the elastic bands (used to mounted the electrodes) and dry electrodes. The elastic bands are used on more than 20 adult participants before this test. Although this fixation approach is not optimized, complain regarding the comfortability of the elastic bands from adult participants is fewer. During the measurements, the children become less patient when they feel the discomfort of the electrodes and the elastic bands. Thus, the measurements could not last long and they are stopped after the low quality EEG signals due to the issues mentioned above are found.

Future improvements

No more EEG measurements are carried on patients in UZ Leuven after the monitoring on these 2 patients due to frequent artifacts and noises recorded using polymer electrodes (CR95) and current experimental setup. Thorough solutions are needed to improve the experimental setup and protocol. There improved setup needs to be validated in a lab environment before further tests on patients in UZ Leuven. However, these action points could not be finished before the end of my PhD studies due to limited time. The suggestions for improvements are listed:

- First, if the cables can be attached firmly with the elastic bands and with no extra part hanging around the head, the inductive loops can be reduced. Applying cables with shielding can also diminish the interferences. The ideal scenario would be combining the shielded cables (connecting the active front-end to the back-end PCBs) with a wireless system. The wireless system also provides higher use comfort since the subjects are able to move more freely. However, the recording device in UZ Leuven is not a wireless system and is not compatible with the shielded cables.
- Second, it is know that dry electrodes are sensitive to motion artifacts due to lack of gel at the interference of skin/electrode. The conductive ions in the gel of wet electrodes reduce the ion concentration change resulted from the motions. Some researchers claim that the impedance and motion artifact are correlated [190, 191]. Therefore, signal processing might can reduce these motion artifacts [69]. However, developing the algorithms to remove the motion artifacts in biopotential measurements is still in the phase of experimental research.
- Third, implementing driven right leg (DRL) electrode decreases the effect of the coupled capacitance between subject and earth ground. In DRL circuit, the common mode interference signals, mostly the power line interferences, are inverted and are sent back to the subject via the DRL electrode. However, this feature is not available on the recording device we used.

Conclusions

Polymer electrodes with material composition number 95 (CR95) together with elastic bands are not optimal for the clinical EEG monitoring on children with epilepsy in UZ Leuven. During half of the recording period, signals are disturbed by power line interferences, motion artifacts and electrostatic interferences. Test setup and protocol need

to be further optimized in a lab environment for the improvement of signal quality of recorded signals. After that, more clinical validations using the improved experimental setup are needed to evaluate user comfort of the fixation device and signal quality for clinical interpretation.

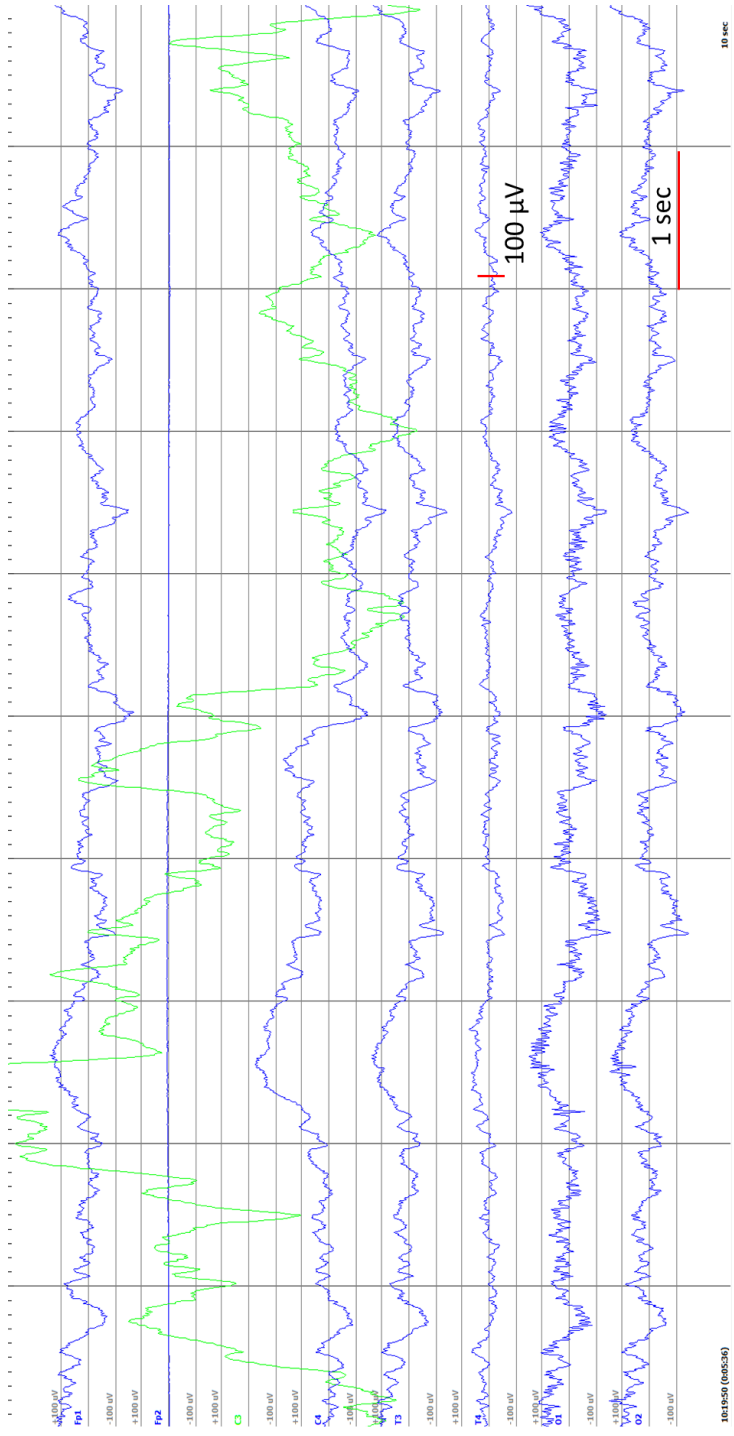

Figure 5.34: The 10-second segment of signals with good signal quality recorded from patient 1. The signals are filtered by 50 Hz notch filter and 0.1 Hz to 45 Hz 4th order Chebyshev bandpass filter.

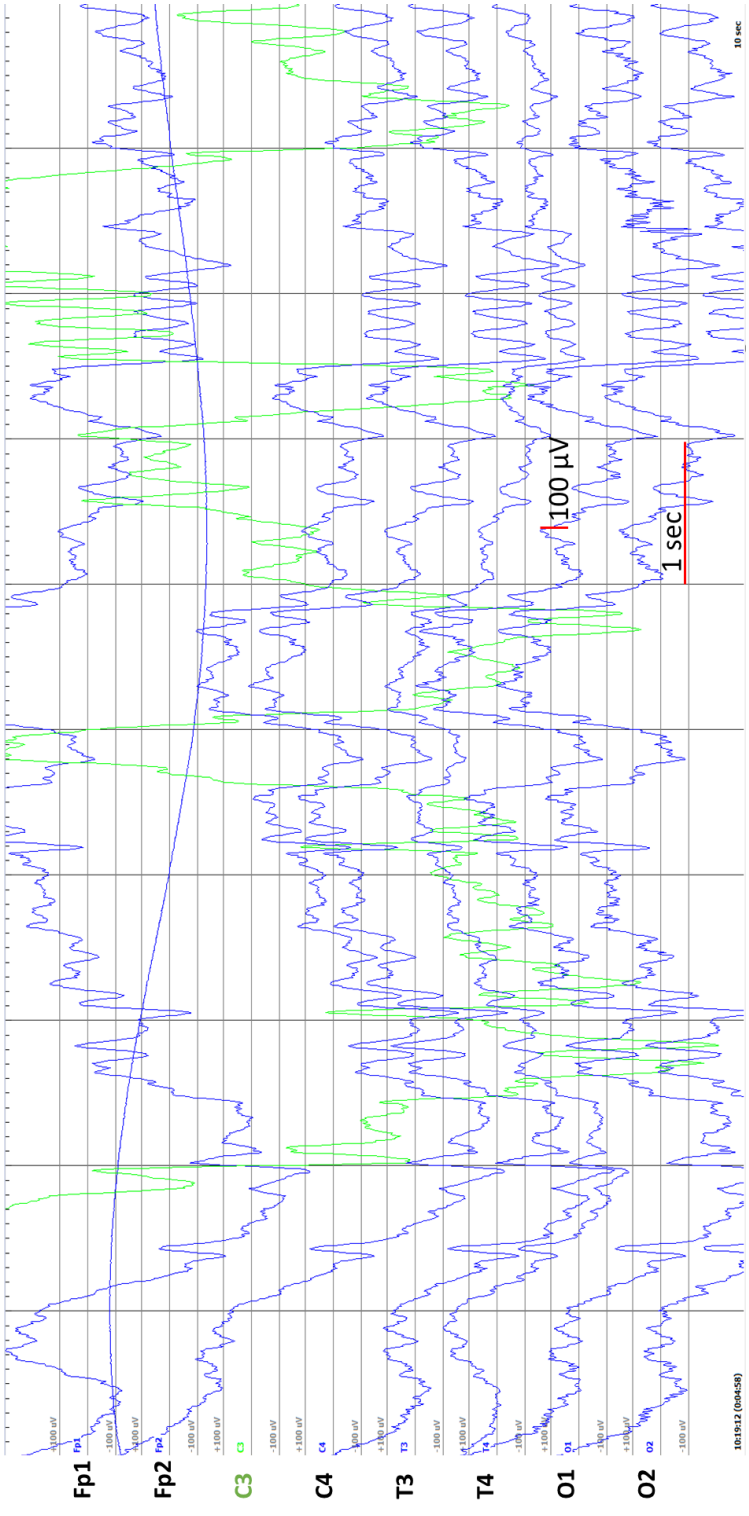

Figure 5.35: The 10-second segment of signals with bad signal quality recorded from patient 1. The signals are filtered by 50 Hz notch filter and 0.1 Hz to 45 Hz 4th order Chebyshev bandpass filter.

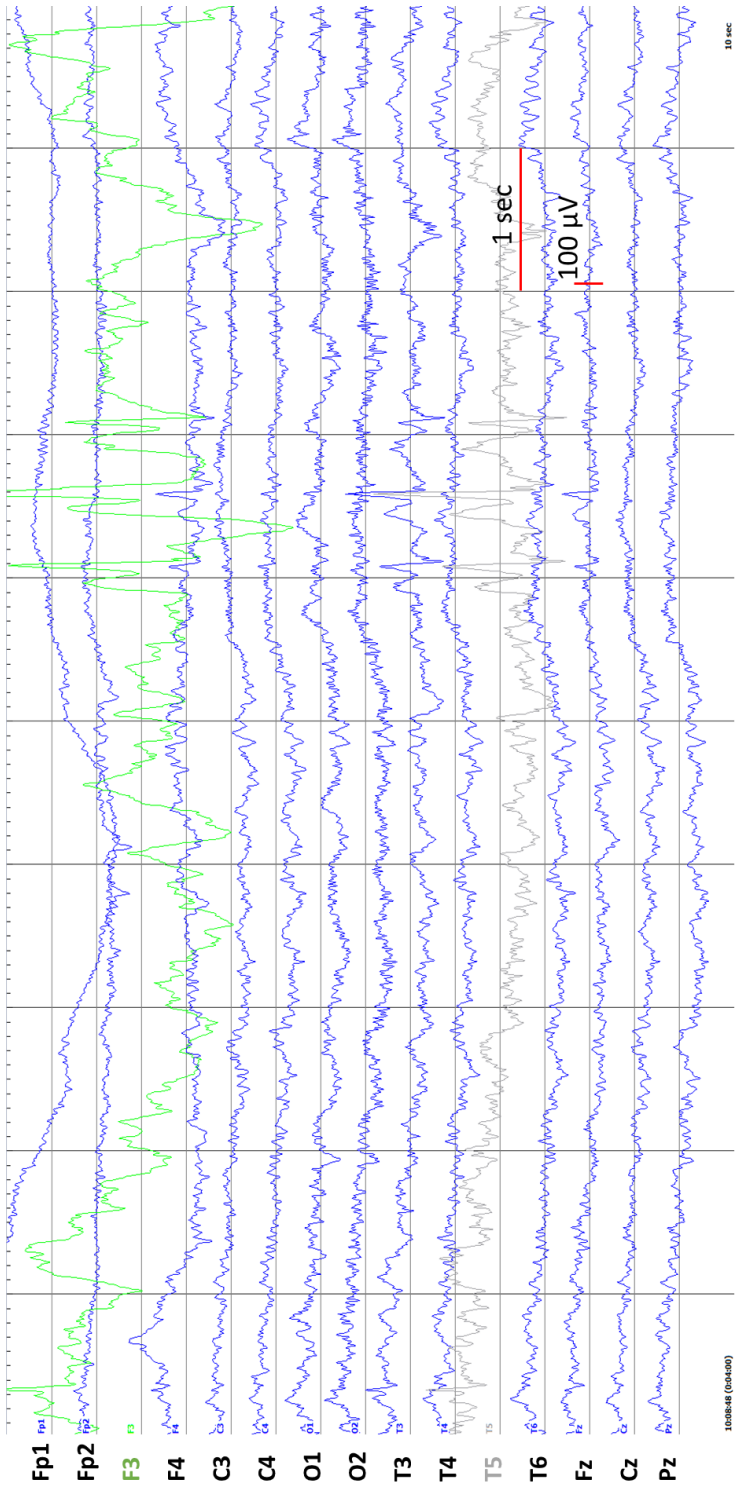

Figure 5.36: The 10-second segment of signals with good signal quality recorded from patient 2. The signals are filtered by 50 Hz notch filter and 0.1 Hz to 45 Hz 4th order Chebyshev bandpass filter.

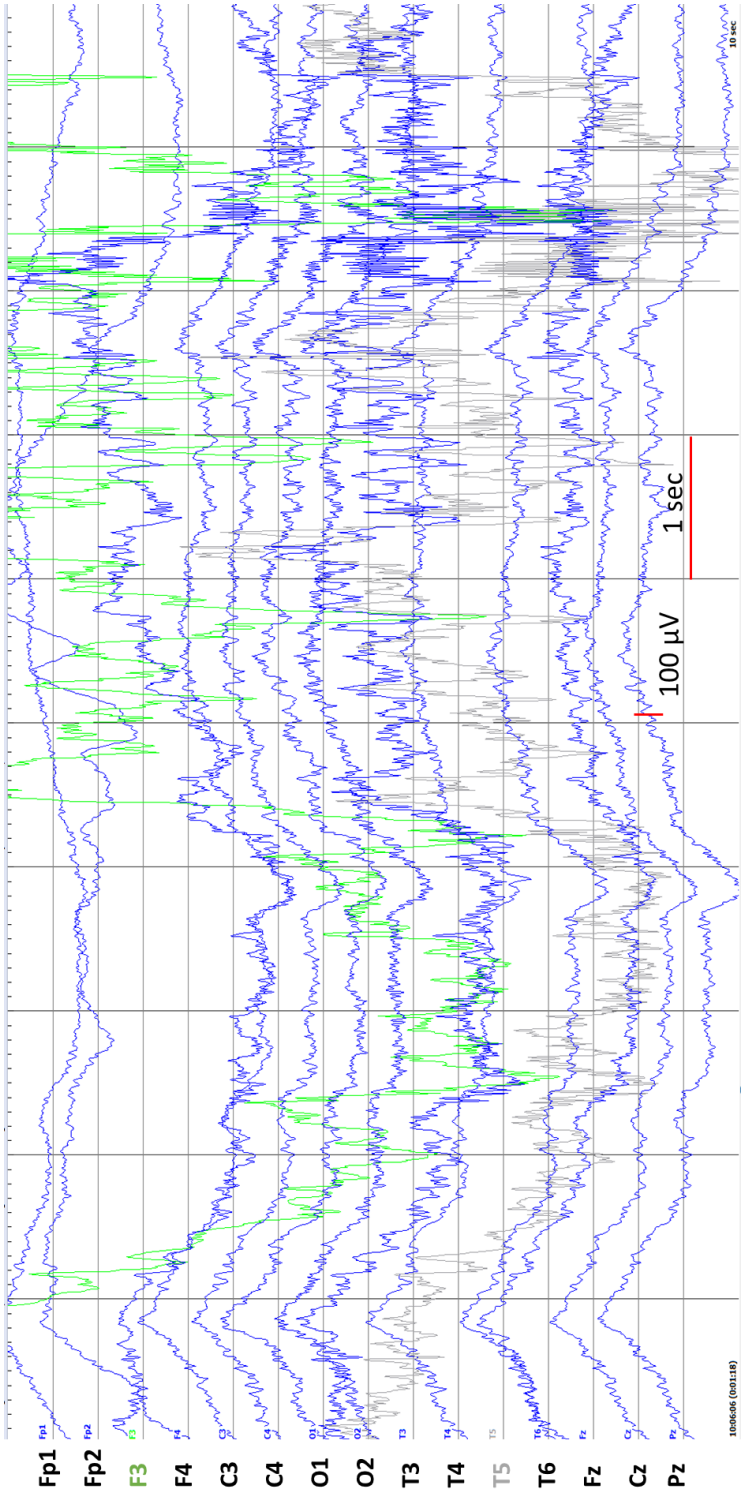

Figure 5.37: The 10-second segment of signals with bad signal quality recorded from patient 2. The signals are filtered by 50 Hz notch filter and 0.1 Hz to 45 Hz 4th order Chebyshev bandpass filter.

5.6 EEG measurement using imec's system

After testing dry electrodes using commercial available EEG systems, also the EEG recording system developed in imec is applied for dry electrode evaluation. The system includes active front-end and back-end PCBs as shown in Figure 5.38. It has eight signal channels and one reference channel. The imec active front-end PCB is connected with the recording system via an 8-wire cable. Different from the recording amplifier used in UZ Gent and UZ Leuven, the chipset can record the impedance of electrode and skin during the EEG measurements by injecting a 5nA, 1024 Hz square wave current signal through the channel and ground electrodes.

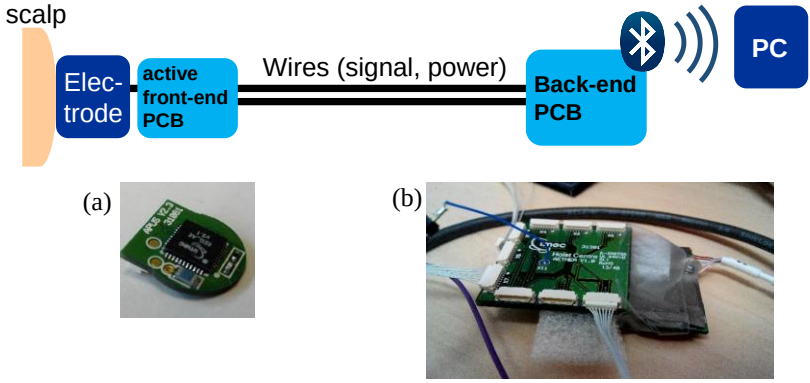

Figure 5.38: (a) The active front-end PCB (AFE v3.1) and (b) the back-end PCB (v2.3 r2) were used for the EEG monitoring in imec. Up to eight pieces of active front-end PCB can be connected to the back-end PCB.

5.6.1 Materials and protocols

Goal

4 different types of dry electrodes are evaluated. They are gel filled rigid AgCl electrode, 2 polymer electrodes with different material compositions and polymer electrode with AgCl coating.

Electrodes locations

Elastic bands were used to mount the electrodes on the locations shown in Figure 5.39. First, all wet electrodes were mounted on the scalp and recording was started. The two dry electrodes were mounted after the recording software was started in order to record the impedance variation of the dry electrodes.

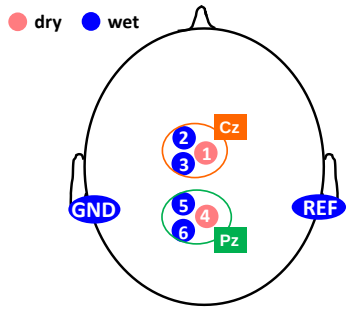

Figure 5.39: Electrode locations for tests using imec's EEG recording system.

Electrodes materials

<table>
<tr><td>Signals</td><td>5 types of dry electrodes:
<table>
<tr><th>Electrode type</th><th>Label</th><th>Picture</th></tr>
<tr><td>AgCl electrode with rigid pins</td><td>AgCl_rigid</td><td>  </td></tr>
<tr><td>Polymer dry electrode made of material composition number 95</td><td>CR95</td><td>  </td></tr>
<tr><td>Polymer dry electrode made of material composition number 64</td><td>CR64</td><td>  </td></tr>
<tr><td>Polymer dry electrode made of material composition number 64 coated with AgCl</td><td>CR64_AgCl</td><td>  </td></tr>
</table>
Wet electrode:
<table>
<tr><td>AgCl cup electrode filled with Ten20 conductive gel</td><td>wet</td><td>  </td></tr>
</table></td></tr>
<tr><td>GND & REF</td><td>Wet electrode:  </td></tr>
</table>

Table 5.5: Labels and pictures of the electrodes used in the tests using imec's EEG recording system.

All the polymer dry electrodes applied in this study are electrodes with 5 mm pin length and 13 mm total diameter. These five electrodes are abbreviated (see 'label' in Table 5.5) to be easily identified further in the text. Electrodes serving as signal or reference electrode are connected with the active front-end PCBs (as shown in Figure 5.38a). The AgCl_rigid

and wet electrodes are connected with the PCBs by short conductive wires while polymer dry electrodes were connected with the PCBs using 3D printed holders.

Protocol

This protocol and informed consent form of this evaluation are approved by the ethical committee of Holst center, imec-NL (document number: ME-15-WATS-TIP2-261). 11 adult volunteers, including 9 men and 2 women, participated in this measurement. The monitoring was taking place in a meeting room and the subjects were asked to sit comfortably on a chair and avoid movements and talking during the monitoring.

The recording consisted of the following 4 sessions:

(1) 5 minutes of electrode stabilization;

(2) 1 minute of eyes open ('session EO')

(3) 1 minute of eyes closed ('session EO')

(4) 1 minute of steady state visually evoked potential (SSVEP) stimulation displayed on a computer screen. The stimulation consists of a square object flickering at a frequency of 8 Hz rendered by Matlab. ('session SS')

After these tasks, the two dry electrodes were replaced by the next type of dry electrode. Then the tasks were repeated. The recording of using each type of dry electrode took around 10 to 15 minutes and the total recording time on one subject is around 1 hour. Among the four types of dry electrodes, CR64 electrodes were always the last one to apply. The order of the other three types of electrodes was randomized to reduce a potential bias in the user comfort evaluation performed by the subjects after all recordings.

Signal analysis

Apart from the SNR, correlation and coherence analysis, other parameters such as impedance and PSD of 50 Hz signals are determined to evaluate signal quality of the 4 types of dry electrodes. The results are discussed in 5.6.2.

5.6.2 Summary of important results

Table 5.6 is a summary of the analysis results carried out to compare the signals of 4 different types of electrodes. Important conclusions are summarized in this section. The detailed data analysis for all electrodes and the results can be found in Appendix III.

		Low quality → High quality	AgCl_rigid	CR95 §	CR64 §	CR64_AgCl
(1) User comfort*	Figure 6.7	uncomfortable – – → + + comfortable	–	+	+ +	+
(2) Setup time**	Figure 5.40, App.12	long – – → + + short	– / +	+	+ +	+
(3) Impedance magnitude	Figure App. 13-16	high – – → + + low	+	–	–	– / +
(4) PSD of 50 Hz signals	Figure App. 17	high – – → + + low	+	–	– –	+ +
(5) SNR ratio	Figure App. 18	|1-SNR ratio| > 0.3 – – → + + |1-SNR ratio| < 0.1	+ +	– / +	–	+ +
(6) Correlation	Figure App. 19	Eyes open: correlation ± STD at Cz correlation ± STD at Pz	0.89 ± 0.16 0.82 ± 0.13	0.73 ± 0.14 0.56 ± 0.24	0.73 ± 0.33 0.51 ± 0.39	0.86 ± 0.14 0.82 ± 0.13
(7) Coherence: 1-20 Hz	Figure App. 20	Eyes open: coherence ± STD at Cz coherence ± STD at Pz	0.90 ± 0.04 0.79 ± 0.10	0.68 ± 0.12 0.46 ± 0.25	0.69 ± 0.27 0.49 ± 0.34	0.82 ± 0.11 0.74 ± 0.15
(8) Coherence: 8-13 Hz	Figure App. 21	coherence ± STD at Cz coherence ± STD at Pz	0.96 ± 0.01 0.89 ± 0.12	0.87 ± 0.08 0.77 ± 0.19	0.81 ± 0.23 0.63 ± 0.29	0.93 ± 0.06 0.91 ± 0.03
(9) Correlation of impedance & PSD of 50 Hz signals	Table App. 3-10	No correlation –/+ → + + ~ 1	– / +	+ +	+ +	– / +
(10) Correlation of impedance mismatch & correlation coefficient	Table App. 11	~ -1 – – → –/+ No correlation	– / +	–	– –	– / +

Detail signal analysis can be found in Appendix III with the corresponding numbers: Figures and Tables labelled with 'App.' can be found in Appendix III.

§ The signals are recorded immediately after the polymer dry electrodes are mounted on the scalp. The obtained signals are from low quality since they are recorded immediately after mounting, hence before the stabilization was finished.

* the results of user comfort are discussed in Chapter 6, section 6.4

** might be different depending on the experimenter who mounts the electrodes

Table 5.6: Summary of the analysis results of the signals recorded using 5 types of dry electrodes using imec EEG system.

(1) *User comfort*

The user comfort of each electrode is evaluated by each participant. It is found that the polymer dry electrodes are more comfortable than the AgCl_rigid electrode. Detail results will be discussed in Chapter 6, section 6.4.

(2) *Setup time*

The setup time of an electrode is defined as the time needed to mount the electrode on the scalp and manipulate it until the experimenter considers the electrode/skin contact is good hence the impedance of the electrode can be recorded and starts decreasing due to stabilization. For the AgCl_rigid electrode, the setup time was the longest due to the shortest pins (2mm) of this electrode. In general, the setup time of an electrode at Pz location is longer than one at Cz location. This might be because most people have more hair at the Pz location. In addition, it is more difficult to mount electrodes at Pz location using the elastic bands (sometimes on that location the bands pressed in a non-perpendicular way on the electrodes).

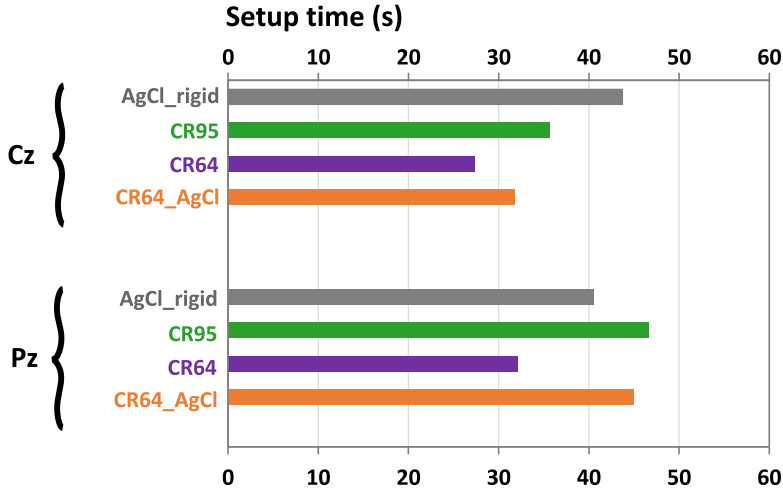

Figure 5.40: The average setup time of each type of dry electrodes at Cz (dry1) location and Pz (dry4) location on 11 subjects.

(3) *Impedance magnitude and Impedance slope*

It is found that CR95 and CR64 show the highest impedance among the 5 types of electrodes. Their impedance is ~10 times higher than that of wet electrodes. Their impedance is too high so ~25% of the impedance recorded by CR95 and CR64 reaches the saturation value of the impedance recording software. Coating AgCl on CR64 reduces the impedance of the CR64 electrodes. Comparing the impedance of electrodes at Cz and Pz positions, the ones at Pz have a slightly higher impedance. This again might be due to the larger amount of hair at the Pz location. Comparing the impedance recorded in eyes open (EO), eyes closed (EC) and SSVEP (SS) sessions, the impedance of almost all types of electrodes decreases with time (stabilization effect).

Besides the impedance magnitude, the stabilization time (time to reach a constant impedance value) is also an important criterion to evaluate an electrode. A stabilized electrode has an impedance magnitude showing only a small variation with time, which is expressed by a small impedance slope in this test. An electrode with fast stabilization time is preferred because it can record accurate signals in a short time after it is mounted on the scalp. By calculating the impedance slope of each electrode, it is found that CR95 and CR64 electrodes are not stabilized at the end of the recording sessions in this test (15 minutes). The impedance slopes of CR95 and CR64 are still around 200 Ω/s at the end of the recording while the impedance slope of wet electrodes is smaller than 10 Ω/s already in the beginning of the recording. Due to the limited recording time (15 mins) using each type of electrode in this protocol, the total stabilization time of the electrodes cann't be determined in this test, a longer recording time would be needed in future tests. If a longer EEG recording is carried out and motion artifacts cann't be avoided during the recording, the stabilization time of the polymer electrodes might even be longer because a change in the electrode-skin contact due to motion requires re-stabilization of the electrode. This is similar to the longer stabilization time of the OCP for polymer electrode without AgCl discussed in section 3.2.1.

In the following discussions, the signals of CR95 and CR64 used for further analysis are those recorded before the polymer dry electrodes are stabilized. Thus, the evaluations are 'worse cases' since the impedance was not minimal. Better results can be foreseen if the dry signals are recorded after the electrodes are stabilized.

(4) *PSD of 50 Hz signals*

It is know that an electrode with higher impedance is more prone to interferences, especially by the 50 Hz signals from the power lines. Although such 50 Hz signals in the recorded data can be easily filtered out by signal processing (see section 4.3.1), computing the PSD of 50 Hz can be an approach to suggest the electrode/skin contact quality. It is not surprising to find that signals recorded by CR95 and CR64 have stronger 50 Hz signals. Not expected is that the PSD of 50 Hz signals recorded by wet electrodes at Cz location is comparable high to that to CR95 and CR64. This might be caused by the fact that the wet electrodes are connected to the active PCBs through wires with ~2 cm length while the polymer electrodes are connected with the active PCBs via 2 layers of conductive copper tapes as shown in section 5.6.1. The exposed wires of wet electrodes might pick up the 50 Hz signals.

(5) *SNR ratio*

It is discussed that the SNR of EEG signals can only be compared when the signals are recorded on the same subjects and even better during the same period, hence simultaneous testing of all the types of electrodes on more or less the same location. Obviously, this is not possible for 6 types electrodes. Therefore, a relative 'SNR ratio' instead of the SNR itself is used to evaluate the electrodes. The 'SNR ratio' of each type of electrode is calculated by dividing the SNR of dry electrode by the SNR of its adjacent wet electrodes. It is found that the SNR ratio of CR64 is lower, while AgCl_rigid and CR64_AgCl show similar SNR ratios.

(6) *Correlation*

The correlation of two closely located wet electrodes is 0.85-0.9. This is considered as the highest correlation of the signals recorded from two close electrodes since the wet electrodes

are the gold standards. The correlation of AgCl_rigid and CR64_AgCl and their adjacent wet electrodes is similar to that of two wet electrodes. The signals recorded by CR95 and CR64 correlate less good with the wet electrodes. As discussed in the 'impedance slope' section, the interfaces of CR95 and CR64 were not stabilized during the 15 minutes recording period, which causes non-ideal electrode behavior. It is also found that the correlation during eyes closed sessions is clearly higher than when eyes open for all types of electrodes. This is because as long as both dry and wet electrodes are capable to record strong amplitude alpha waves generated when eyes are closed, the correlation of the two signals increases, as discussed in Figure 4.4 graph (5b).

(7) *Coherence of 1-20 Hz and* (8) *Coherence of 8-13 Hz*

When comparing both 1-20 Hz and 8-13 Hz coherence values for the various electrodes, results are very similar to the correlation values: the coherence of CR95 and CR64 is the lowest among all types of electrodes. Their low coherence is due to the baseline drift of the recorded signals, see Figure 5.41. When comparing the raw data and corresponding PSD recorded by a CR64 electrode and a wet electrode next to it, it can be seen that CR64 electrode suffers from more severe baseline drift than the wet electrode. Comparing the coherence of 1-20 Hz and 8-13 Hz, it is shown that the values of 8-13 Hz of all electrodes are higher than 1-20 Hz. This can again be explained by the low frequency signals (baseline drift) picked up by the electrodes. Remark also here that the polymer electrodes were not fully stabilized hence their results are not optimal. Further, is stated before, the baseline drifts are not problematic for clinical evaluation of the signals and can be filtered out easily by dedicated software.

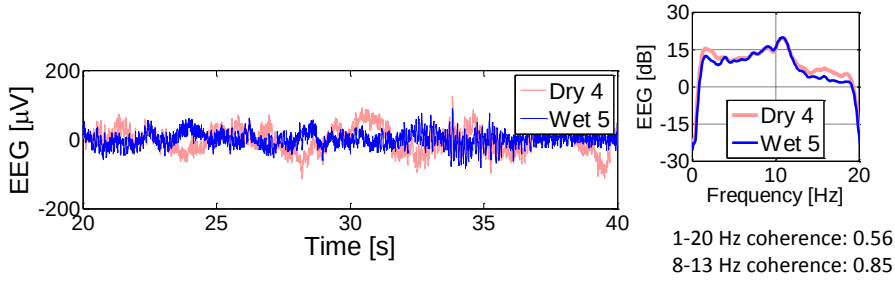

Figure 5.41: The signals acquired by polymer dry electrode (CR64) contain more baseline drift than that by wet electrode. Therefore, the correlation and coherence of the signals recorded by the dry electrode and the ones by wet electrode are low.

(9) *Correlation of impedance magnitude and the PSD of 50 Hz signals*

Although in theory electrodes with higher impedance are more prone to 50 Hz signals interferences, this is not always observed in the data recorded by the various types of electrodes on the same subject. It is assumed that the amplitude of power line signals does not varies significantly during the recording on one subject using certain type of electrode. When investigating the impedance value and the PSD of 50 Hz signals of a certain electrode recorded on one participant, it is found that the impedance magnitudes correlate well with the PSD of 50 Hz signals using CR95 and CR64 electrodes on almost all participants. However, the impedance is not correlated with the PSD of 50 Hz signals when investigating

the data in between different participants. This is because the interferences from power lines vary with time and affect differently on each participant.

For future test, it would be interesting to investigate the variation of 50 Hz signals over time using one type of electrode on one subject, in order to understand the time variation of the power line interferences. Turning on and off the electronic devices around the subjects during the measurement is also a method to study the interferences change in the recordings.

(10) *Correlation of impedance mismatch and correlation coefficient of two adjacent electrodes*

Good recording amplifiers have higher common-mode rejection ratio (CMRR) rejecting the common interferences recorded from two electrodes. Large impedance mismatch in between 2 electrodes reduces the performance of such a common-mode rejection and hence this reduces the quality of the recorded signals. This situation occurs when a dry signal electrode is combined with a wet electrode as reference. It is shown that the larger the impedance differences are between a CR64 electrode and its adjacent wet electrode, the lower is the correlation coefficient of their signals.

5.6.3 Limitations of using polymer electrodes and imec system

Goal

In the discussion in section 5.5.2, the main issues during the monitoring are electromagnetic fields generated by the power lines which disturb the signals, the motion artifacts and the bad grounding of the patients. The impacts of these disturbances on the signals using the imec recording system are studied using **4** difference types of dry **ground** electrodes. These ground electrodes are AgCl cup electrode, gel filled AgCl cup electrode, AgCl coated polymer electrode and polymer dry electrode.

Electrodes locations and types

The locations of the electrodes are shown in Figure 5.42.

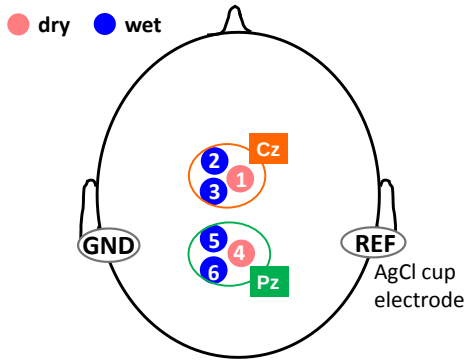

Figure 5.42: Electrode locations for tests using imec's EEG recording system.

The types of the electrodes are listed in Table 5.7:

Signals	Dry	CR95	
	Wet	AgCl cup electrode filled with conductive gel	
REF	AgCl cup electrode		
GND	AgCl cup electrode		
	AgCl cup electrode filled in conductive gel		
	AgCl coated coin-shaped CR64 electrode		
	coin-shaped CR95 electrode		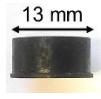

Table 5.7: The types of electrodes used in this test.

Protocol

To reproduce the disturbances shown in the patient recording in UZ Leuven which were expected to be related with the change of electromagnetic fields, motion artifacts and limited grounding of the patient, the following tasks are carried out:

(1) To change the distribution of the electromagnetic field around the electrodes:
- The experimenter walks around the subject sitting on a chair without movements and then walks away and toward the subject.
- The experimenter waves one hand around the electrodes

(2) To generate motion artifacts, the subject grinds the teeth and turns the head.

(3) To change the grounding of the subject, the subject taps the feet, first gently and then with more force.

Results and discussions

It is found that all these actions disturb both the signals recorded by wet and dry electrodes in all the recordings. The same cables connecting the active electrodes to the back-end chip and the same elastic bands mounting the electrodes on the scalp are used in this measurement and in the patient tests in UZ Leuven, in an attempt to create a similar sensitivity to electromagnetic fields disturbances and motion artifacts. In the three tasks,

the signals with the least disturbances are those applying AgCl cup with gel (wet) as ground electrode. All other types of electrodes with higher and less stable impedance than the wet electrode result in a larger and more unstable voltage on the human body coming from the ground leakage currents. This suggests that a low impedance ground electrode (such as a wet electrode) is needed for high quality recordings using dry signal electrodes.

5.6.4 Conclusion of using polymer electrodes with imec's EEG system

EEG signals can be recorded using polymer dry electrodes with imec's EEG system. However, in line with previous conclusions when using clinical EEG recording systems at UZ Gent and UZ Leuven, the signals recorded by polymer dry electrodes using imec's EEG system also contain baseline drift resulting lower signal quality comparing to the electrodes coated with AgCl. However the baseline drift can be removed by signal filtering. The permanent impedance evaluation during recording -not possible on the clinical systems- reveals that the dry polymer electrodes are not stabilized during the 15-minute recording period. Their signal quality might increase if the signals are recorded for a longer period.

5.7 Conclusions of EEG monitoring using polymer electrodes

According the EEG signals recorded using polymer electrodes with material compositions number 64 and 95, it is found that they contain more baseline drift than the conventional wet electrodes. The baseline drift becomes gentler with time, which suggests that the interface of polymer dry electrodes and skin need time to become stable. To improve the signals when using dry electrodes, using low impedance ground electrode, such as wet electrode, is desired to have less disturbances. Another approach is using a reference electrode from the same type (hence also dry electrode) to have better CMRR hence a better signal. Furthermore, coating AgCl on the polymer electrodes increases the signal quality compared to the pure dry polymer electrodes. Even though the signals recorded by polymer electrodes contain some baseline drift, the signals recorded on healthy participants and epilepsy patients in UZ Gent (data discussed in section 5.4) and recorded on healthy participants in UZ Leuven (data discussed in section 5.5.1) are evaluated by experienced medical staff and are considered from good quality, enabling a correct clinical evaluation. Regarding the recording on children with epilepsy in UZ Leuven, improvements of both the experimental set up and the protocol are needed to avoid interferences from environment and reduce motion artifacts.

Chapter 6.
User Comfort and Skin Biocompatibility

To evaluate the biocompability of polymer electrodes, in vitro cytotoxicity tests according to ISO 10993-5—(Part 5: Tests for in vitro cytotoxicity) and to USP-based test protocols were carried out as discussed in section 6.1.

Most researchers developing dry electrodes do not include a skin biocompatibility evaluation in their publication. Some papers discuss the visual observation of skin condition before and after electrode contact, as an intuitive method to evaluate the biocompatibility of their electrodes, but none of them involves a systematic skin condition evaluation by a dermatologist. The skin biocompatibility results published in these papers are presented by showing the pictures of skin after electrode/skin contact. [45] shows the pressure marks on the scalp of a neonate after wearing an EEG electrode cap for 1 hour to introduce the motivation of developing textile electrodes for EEG recording. [51, 54] show the pictures of skin condition after 7 days of flat PDMS electrodes/ skin contact to conclude the developed electrodes do not cause any adverse effects, such as erythema or urticarial. [192, 193] show the pictures of skin to compare the pressure marks left after removing conventional wet and their dry electrodes with micro pins.

Next to the cytotoxicity tests performed at Toxikon, we performed also this first order and intuitive method to evaluate electrode/skin biocompatibility by visual skin evaluation before and after electrode/skin contact. In particular, the skin conditions after short-term (less than 2 hours) and long-term (over 60 hours) electrode/skin contact were observed. The results are shown in section 6.2 and section 6.3, respectively. In section 6.4, the user comfort of the polymer electrodes together with the elastic bands during the EEG measurements evaluated by the participants are discussed.

6.1 Biocompatibility of the polymer electrodes

Besides the mechanical and electrical evaluation tests (Chapter 3), the biological response evaluation of biopotential electrodes also needs to be carried out according to the standard "ANSI/AAMI EC12:2000 Disposable ECG electrodes". The evaluation includes cytotoxicity, sensitization, irritation, and intracutaneous reactivity. The polymer material containing ~45% of carbon was tested for cytotoxicity. This material was chosen for being the optimized one, and hence selected to be applied in ECG and EEG monitoring. For this polymer composition, cytotoxicity is determined by testing the polymer material after molding, since the molding process might influence the chemical/physical properties of the material. Two cytotoxicity tests were performed: (1) in vitro cytotoxicity tests according to ISO 10993-5—(Part 5: Tests for in vitro cytotoxicity); and (2) USP-based tests (36- NF31:2013<87>, Biological Reactivity Test, In Vitro). Both test results show that this material is non-cytotoxic. The tests were performed by Toxikon Europe (Leuven, Belgium), an accredited analytical test lab assisting in medical device development, product safety, and regulatory compliance [69]. Once the final composition of the polymer material is fixed for use in a final electrode, more tests will be performed such as skin sensitization and intracutaneous reactivity.

6.2 Short term polymer electrode/skin contact

In this thesis, most of the impedance measurements on the forearm, as well as the ECG and EEG measurements lasted less than 2 hours. The skin condition of short term exposure of the forearm skin to our polymer electrode is discussed in section 6.2.1 while short term contact between polymer electrodes and the scalp is evaluated in section 6.2.2.

6.2.1 Forearm skin condition after impedance measurements

During the impedance measurements, both electrodes with pins of 2 mm and 5 mm length were applied. These electrodes were placed on the skin with sufficient pressure to ensure low contact impedance, and the skin was evaluated after 30 min and 1 h of electrode contact. No pain nor discomfort was reported, and only a shallow impression on the skin was seen (see Figure 6.1c,d and Figure 6.2c,d).

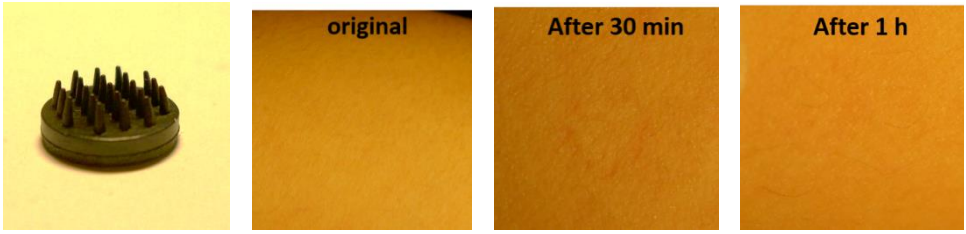

Figure 6.1: Skin condition after 1-hour use of polymer electrodes on forearm. (a) electrode with pins of 2 mm length. (b)Skin condition before and (c) (d) after contacting with the short pin electrode.

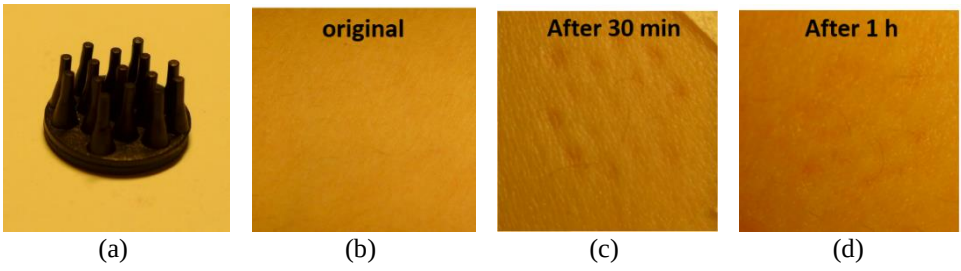

Figure 6.2: Skin condition after 1-hour use of polymer electrodes on forearm. (a) electrode with pins of 5 mm length. (b) Skin condition before and (c) (d) after contacting with the long pin electrode.

6.2.2 Scalp skin condition after EEG measurements

During the EEG monitoring, the electrodes with pins of 5 mm length shown in Figure 6.3a were mounted using elastic bands. 30 minutes after applying a polymer electrode on one of the participants, a shallow impression can be seen in Figure 6.3b. Since pressure on the electrodes is varying between subjects (identical elastic bands were used to mount the electrodes on all the adult participants, having a different head size and shape) different skin impression depths are visible after the measurements. So the user comfort is not only

determined by the electrodes, but is also strongly influenced by the system used to keep the electrode in place on the scalp.

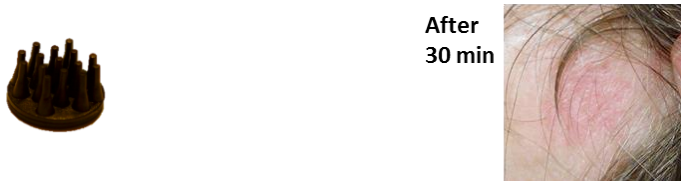

(a) (b)

Figure 6.3: (a) Electrode with pins of 5 mm length is used for EEG measurements. (b) Scalp skin condition after 30-min of electrode/skin contact.

6.3 Long term polymer electrode/skin contact

Dedicated experiments were performed to evaluate skin irritation using polymer electrodes for long-term. Coin-shaped electrodes, and electrodes with pins of 2 mm and 5mm length are used in these experiments.

6.3.1 Skin condition after coin-shaped electrode/skin contact

A **6-day** long-term test was performed using a coin-shaped electrode mounted on the upper arm skin using a non-breathable sticker. No major irritation or discomfort was reported for the total duration of the measurement, although some itching was observed, probably related to perspiration, since the non-breathable sticker precluded any ventilation. Further, some minor erythema (a painless and shallow pressure mark) was observed after 6 days of electrode contact, see Figure 6.4.

Figure 6.4: Skin condition 6 days after polymer electrodes contacting the forearm skin.

6.3.2 Skin condition after pin-shaped electrode/skin contact

Since the pin-shaped electrodes are used in most ECG and EEG measurements, the skin condition after long-term pin-shaped polymer electrode/skin contact is observed as well. For the first experiment, a polymer electrode with pins of 2 mm length attached to the chest skin for **3 days** using a breathable sticker, see Figure 6.5b. After three days of intense electrode/skin contact, a shallow impression was seen, as shown in Figure 6.5c. Although the pins of the polymer electrodes are designed with rounded edges to optimize for user comfort, these 2 mm pins remain rather sharp (compared to the 5 mm ones) resulting in a longer period for the impression to fade compared to the electrodes with 5mm pins (Figure 6.2a). The

impression was hardly seen 3 days after the removal of the electrode, see Figure 6.5f. This observation is another proof that pin-shaped polymer electrodes are not optimal for skin without any hair. The first reason discussed in section 4.3.1 is that the small contact surfaces of pin-shaped electrodes easily result in motion artifacts. The second reason is shown here that pin-shaped electrodes cause impressions on non-hairy skin.

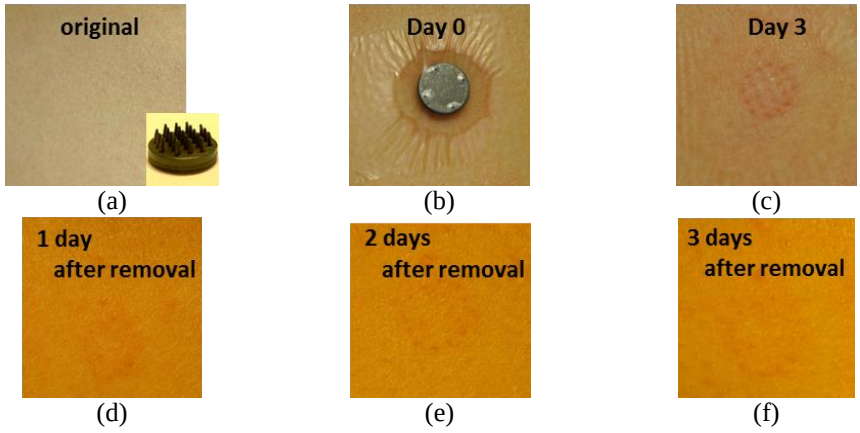

Figure 6.5: The skin condition (a) before contacting the electrode; (b) immediately after contacting the electrode; (c) 3 days after contacting the electrode; (d) 1 day after the electrode was removed; (e) 2 days after the electrode was removed and (f) 3 days after the electrode was removed.

The second experiment was contacting a polymer electrode with pins of 5 mm length and the forearm skin for **60 h** using an elastic band. No itching or pain was reported, although the subject was clearly observing the pressure of the electrode, described as very minor discomfort. Slight erythema was found after 10 h and ~35 h, on the spots where the pins touched the skin, see Figure 6.6b,c. These marks are due to a rather high pressure from the bandage used for fixation. Even the elastic bandage showed pressure marks, as visible in Figure 6.6. The slight erythema found after 60 h was similar to that of after 35 h. After removing the electrode, the pressing mark faded fast, and was hardly visible anymore after 4 h, as shown in Figure 6.6d.

Figure 6.6: (a) An electrode contacted the forearm skin for 60 h. Skin condition (b) after 10 h of electrode/skin contact; (c) after 35 h of electrode/skin contact; (d) 4 h after the electrode was removed.

These results show that both coin-shaped and pin-shaped electrodes do not cause important irritation nor skin damage. Fixing the pin-shaped electrode by a tight sticker or elastic bandage is not ideal: the localized high pressure causes slight erythema. Obviously the sticker

and elastic bands used in this thesis are for evaluation purpose only. In order to fix the electrodes at the same location during the entire measurement (few days up to 1 week), slightly more pressure than sufficient is given by the sticker or elastic bandage. The results show in Figure 6.4, Figure 6.5 and Figure 6.6 are false negative results comparing to the results using a dedicated ECG device or EEG headset with a pressure not much higher than required for good contact.

6.4 User comfort during and after EEG monitoring

Over 20 participants experienced the elastic bands (Figure 5.4a) in combination with the dry electrodes on their scalps during EEG measurements. They did not feel important discomfort during the tests. Few subjects had large heads, so the elastic bands were too short and caused important pressure. They reported discomfort from the setup after using it for about 30 minutes.

After the EEG monitoring using imec's EEG recording system discussed in section 5.6, each participant was asked to give a score to each type of dry electrode regarding its comfortability. The questionnaire can be found in Appendix IV. Scale 1 indicates the electrode is very uncomfortable while scale 5 indicates no discomfort is observed from the electrode. The average score given by the 11 participants and the standard deviation of the scores are shown in Figure 6.7.It is found that AgCl_rigid is the least comfortable. All other polymer dry electrodes get similar scores. 4 of the 11 participates report that they only feel the discomfort at the beginning 1 or 2 minutes after placing the dry electrodes on the skin. After that, they get used to the pressure from the electrodes and the elastic bands.

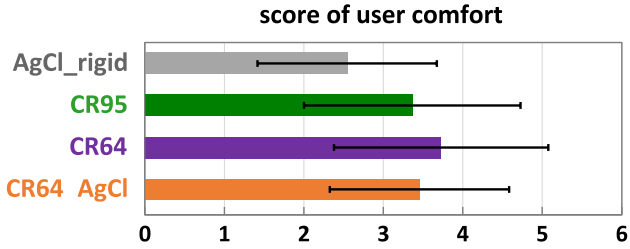

Figure 6.7: Scores regarding user comfort of each type of dry electrodes evaluated by the subjects after the EEG measurements using imec's EEG system.

After the measurements, all participants reported that removing the polymer dry electrodes causes no messed up hair and is faster and more convenient comparing to that of wet electrodes (bridge electrodes and cup electrodes filled with conductive gel).

6.5 Conclusion

The polymer electrodes used for ECG and EEG measurements in this thesis are non-cytotoxic. Pin-shaped polymer dry electrodes themselves cause shallow pressure marks after 30 minutes application on the skin. No participants report any discomfort of the skin contacted the polymer electrodes during and after the impedance, ECG and EEG measurements. Besides,

the pressure marks can be hardly seen 1 hour after the electrodes are removed. Contacting the polymer electrodes with the skin over 3 days results in slightly deeper pressure marks, but those marks are mainly caused by the high local pressure from the non-ideal fixation tape or bandage.

Few subjects with larger heads experience discomfort from the pin-shaped polymer electrodes 30 minutes after starting the EEG measurements due to the pressure from one-size elastic bands. All the subjects report that removing the polymer electrodes is faster and does not mass up the hair after the EEG monitoring.

Chapter 7.
Conclusions and Outlook

7.1 Summary of main contributions

The originality of this PhD research project and my contributions to the research field of dry electrodes for biopotential measurements are summarized in this section.

In Chapter 2, fabrication and characterization of EPDM-based polymer dry electrodes for ECG and EEG monitoring is reported. These dry, conductive and flexible polymer electrodes overcome some of the disadvantages of existing electrodes:

- Compared to rigid metal electrodes: flexibility and user comfort, an expected benefit
- Compared to previously reported polymer electrodes with conductive coating: abrasion resistance.

This has been achieved thanks to the inherent material choice and the use of conductive additives, such as stainless steel fibers, carbon and CNT in order to reduce the electrode/skin impedance hence improve the signal quality of the recorded biopotentials. Various shapes of polymer electrodes have been fabricated by compression molding and are fit to be mounted in different recording devices.

In the first part of Chapter 3 (until section 3.3), the electrical properties of the polymer electrodes containing with various additives have been characterized using open circuit potential, cyclic voltammetry and impedance measurements. For comparison, the impedance of conventional industry-standard wet ECG electrodes is also being measured. We investigated the variation of the impedance of wet electrodes on the same subject but on different days. The day-to-day variations of skin conditions and of ambient humidity result in an impedance variation and this complicates accurate comparisons. For that reason, we resorted to phantoms in order to characterize the impedance of the polymer electrodes in a more consistent way. The approach involves three phases of impedance characterization: (1) material impedance is measured by placing the cylindrical-shaped electrodes back to back; (2) pin-shaped polymer electrodes impedance is measured on phantoms and (3) pin-shaped polymer electrodes impedance is measured on human skin. In order to compare the impedance of electrodes with different contact area, we attempted to normalize the impedance values during the impedance comparison. For area normalization of the impedance of a pin-shaped electrode we used the base area of the electrode, which is the area occupied by the electrode during biopotential measurement, instead of the contact area of the pins. Furthermore, the influence of various skin pretreatments, such as skin abrasion and skin hydration, on the polymer electrode/skin impedance has been investigated. The impedance of polymer electrodes with various pin numbers has been studied. These impedance values are used as inputs in the equivalent circuit of an electrode/skin model. The variation of each component in the equivalent circuit model before and after skin pretreatments has been investigated.

In the second part of Chapter 3 (in section 3.4), the mechanical properties of the polymer electrodes with various additives and different shapes are characterized using compression tests. The elastic modulus of the polymer materials are determined by the load-displacement curves recorded in compression tests. The same technique is used to investigate the compliance of the pin-shaped polymer electrodes. The measured compliance of the pin-

shaped electrodes is compared with the predicted compliance calculated using the elastic modulus of materials and the geometric factors of the electrodes. In addition, the viscoelastic properties of polymer electrodes are characterized using stress relaxation during compression tests. While these results were not surprising, they can serve as a reference when next generations of dry electrodes are being created.

In Chapter 4 and 5, the polymer electrodes are combined with imec's ultra-low-power ECG recording amplifier for conducting ECG and EEG measurements. The polymer electrodes together with active circuits are technically compatible with the clinical EEG recording amplifiers. The EEG measurements using active polymer electrodes on healthy subjects and on epilepsy patients are performed in UZ Gent and UZ Leuven. The ECG and EEG signals recorded using polymer electrodes are compared with those recorded using conventional wet electrodes in terms of the similarity of waveform and spectrum and the ability of recorded the signals we are interested in, such as alpha waves. The results are encouraging but proper fixation of the dry electrode and arrangement of the cabling remain important to avoid interferences of the electromagnetic fields of powerlines on the cables as a consequence of motion artifacts and cable movements.

In Chapter 6, the skin condition after short-term and long-term electrode/skin contact is observed and recorded. Short-term electrode-skin contact was less than 2 hours, which is typically after impedance and biopotential measurements performed in this thesis. Long-term means approximately 1 week of electrode/skin contact. Besides optically observing the skin condition, the user comfort of the polymer electrodes has been evaluated using a user questionnaire.

7.2 Conclusions

In this section, the main conclusions of this thesis are summarized. To investigate whether the EPDM-based polymer dry electrodes are in fact promising substitutes of conventional wet electrodes (for biopotential measurement applications), dry electrode characterization tests based on criteria of high quality electrodes are carried out and compared with the results obtained on wet electrodes. These requirements include short half-cell potential (E_{hc}) stabilization time, low overpotential, low impedance, high signal quality, proper electrode/skin contact, and a less tangible one i.e. high user comfort.

The basic polymer used for the dry electrodes contains various conductive additives such as carbon and stainless steel fibers (SS), as well as additives for the adjustment of mechanical properties. Furthermore, various electrode shapes are produced for ECG vs EEG use (Chapter 2). The material composition and electrode shape are optimized based on tests evaluating the electrical and mechanical properties in Chapter 3.

As to the electrical properties of polymer dry electrodes (Chapter 3, section 3.1 to section 3.3), their E_{hc} stabilization time during open circuit potential test is long (~ 1 hour) because the electrode/skin interface is sensitive to ion redistribution that ought to take place when the interface is disturbed. Moreover, polymer electrodes behave like a polarizable electrode, resulting from a lack of molecules in the polymer material that are able to exchange

electrons with the Cl^- ions from the body. This reduces the efficiency of converting ionic current in the body into electric current in the electrode. Regarding the additives, SS and carbon nanotubes (CNT) are added in the first few batches of polymer electrodes. However, later it was decided not to use these conductive additives because increasing the quantity or size of SS fibers for decreasing the impedance of electrode damages the mold tool during electrode fabrication. Furthermore, CNT is controversial regarding biocompatibility and could not be cleared for testing on people. Hence, the impedance evaluations are focused on carbon containing polymer electrodes. The impedance of the electrodes decreases with an increase in carbon content. The impedance of electrodes containing ~49% of carbon is still 10 times higher than that of conventional wet electrodes on the human forearm skin. The higher impedance requires the use of amplifiers that can accommodate the resulting electrode offset voltage. Only small variations are observed when comparing the impedance of polymer electrodes with different pin numbers measured on the forearm. Larger impedance variations are to be expected when applying these electrodes on hairy skin but such comparison was not conducted so far.

During the impedance measurements, the influence of skin pretreatments on the polymer dry electrodes' impedance has been studied. Skin pretreatment such as applying abrasive gel/lotion or stimulating sweat hydrates the stratum corneum layer is reflected by a reduction in the electrode/skin impedance. However, this impedance reduction does not remain for a long time and it was observed that during a 30-minute to 1-hour measurement period, the impedance increases essentially because the conductive fluid (i.e. gel, lotion, sweat) evaporates or is absorbed by the deeper skin layers.

Apart from the evaluation of the electrical properties of carbon containing polymer electrodes, the mechanical properties of the carbon containing polymer electrodes are tested using compression tests. As expected, the elastic modulus of the polymer electrodes increases with rising carbon content. Hard polymers with high elastic modulus are not preferred both from a fabrication perspective and from a user comfort perspective. The compression tests show that the polymer electrodes with shorter, thicker and more pins can sustain more force (e.g. pressure from the fixation devices in EEG monitoring) without electrode-shape deformation. The compliance of the pin-shaped electrodes can also be predicted rather well using the elastic moduli of the polymer materials and the shapes of the electrodes. The design of the shape of electrodes should also provide proper electrode/skin contact and high user comfort. Based on the results of the electrical properties and the mechanical properties (Chapter 3), polymer electrodes were selected and subsequently used for further ECG and EEG measurements. The polymer electrodes with 2 mm pin length are used for ECG monitoring while the ones with 5 mm pin length are used for EEG monitoring (The detailed compositions and the shapes of electrodes can be found in section 0).

In Chapter 4, the ECG signals recorded using polymer dry electrodes are compared with those recorded by wet electrodes. It is seen that polymer dry electrodes pick up more power line interference, but these 50Hz signals can be filtered out. The correlation of signals recorded using wet and dry electrodes when the subjects are stationary is ~0.99. When the subjects move, both wet-electrode and dry-electrode based ECG signals are disturbed. The wet-electrode based ECG signals settle faster than the dry-electrode based ones which results

in a low correlation between the two signals (<0.5) in case of movement by the subject. This indicates that the comfort resulting from flexible dry electrodes comes with a price and motion-artifact detection and removal are critical for polymer dry electrodes. Apart from the ECG signals recorded on the chest, ECG signals recorded by polymer electrodes at the lower abdominal area are also investigated. The R peaks and T waves in the signals recorded from both body locations can easily be detected. During these ECG measurements, it is observed that pin-shaped electrodes are more sensitive to motion artifacts due to smaller and less constant electrode/skin contact area. Therefore, polymer electrodes without pins are more suitable for recording high-quality ECG signals and electrodes with 2-mm pin length are only necessary in the presence of abundant hair in order to have proper electrode/skin contact.

Our polymer dry electrodes have also used to record biopotential signals with smaller amplitude such as EEG signals. In that case, the electrodes are paired with active circuitry (either created with off-the-shelf components or with imec's active electrode readout circuits). EEG signals recorded by polymer dry electrodes and adjacent wet electrodes show slightly lower correlation and coherence than a pair of adjacent wet electrodes. This is mainly related to larger baseline drift, higher motion-artifact sensitivity and higher susceptibility to power line interference of dry polymer electrodes. This sensitivity to baseline drift and motion artifacts is inherent to dry electrodes and caused by the rearrangement process of the conductive ions at the double layer structure of the electrode/skin interface. If a subject is stationary, the baseline drift of the dry signals decreases significantly with time. However, when the equilibrium state of this electrode/skin interface is disturbed by motion, the rearrangement of conductive ions at the electrode/skin interface causes artifacts. It is found in Chapter 5 that polymer electrodes with AgCl coating reduce the time needed for electrode/skin interface stabilization. In addition, we found that using a ground electrode with low impedance (e.g. a wet electrode), reduces the power-line interference. Furthermore, using identical electrodes as reference and channel electrodes results in a better CMRR and hence a lower susceptibility to interference and better overall signal quality. Besides the purely mathematical analysis/comparison of the recorded EEG signals, the signal quality of these data was inspected by medical staff. Although most of the dry signals have been recorded (Chapter 5) *before* the polymer electrodes are stabilized (i.e. they contain baseline drift), specialists concluded that the dry signals without severe motion artifacts are useful for a valid clinical interpretation. In contrast, when the signals of interest are found at the same frequency band of the baseline drift (< 1 or 2 Hz), the EEG signals may be misinterpreted.

While optimization of the electrical and mechanical properties ensures overall high quality signals, user comfort is also an important criterion and Chapter 6 discusses user comfort. Clearly, the electrode material used for ECG and EEG measurements is non-cytotoxic. Pin-shaped polymer dry electrodes cause shallow pressure marks after 30 minutes of application on the skin. These marks disappear in less than 1 hour, and no participant reported any skin discomfort during and after the tests carried out to evaluate the impedance, ECG, and EEG signal acquisition. In addition, no skin irritation is found after several days of wearing polymer electrodes/skin contact. As to the user comfort of polymer electrodes mounted on the head for EEG monitoring, a few participants mentioned discomfort due to the tight mounting mechanism (relative to their larger head-size). Lastly, all participants report that

polymer electrodes are easier to be placed and removed compared to conventional wet electrodes.

In summary, the polymer dry electrodes show high user comfort and adequate signal quality during ECG and EEG monitoring. Combining polymer dry electrodes with proper fixation systems (headsets) and suitable recording devices (for signal condition), they may become a an alternative to currently used dry metal electrodes and may in certain conditions be a future alternative to conventional wet electrodes.

7.3 Outlook

In this thesis, and in spite of all progress made, it is found that polymer dry electrodes inherently exhibit a longer stabilization time and still feature a higher impedance, and are consequently also more sensitive to motion artifacts compared to wet electrodes. To further improve the signal quality and usability of polymer dry electrodes for biopotential measurements, the following topics can and should be investigated.

Further improvement of the Electrical properties of the polymer dry electrodes

The polymer dry electrodes used in this thesis do not contain ions that can easily exchange electrons with the Cl^- ions in the body. This results in an unstable electrode/skin interface, hence baseline drift or motion artifacts are more likely to be present in the signals recorded using polymer dry electrodes. Therefore, mixing polymer material with additives that can exchange electrons with Cl^- ions might lower the E_{hc} and result in a faster stabilization time [194]. In addition, increasing the Cl^- content in the polymer material makes the polymer electrodes less sensitive to the concentration changes of Cl^- ions near the electrodes, rendering them less sensitive to motion.

Another approach to shorten the stabilization time and reduce the electrode-tissue impedance is coating AgCl on the flexible polymer electrodes. However, it is found that a rigid AgCl coating layer flakes off after the electrodes are used on ~15 subjects. Therefore, improving the adhesion of the AgCl coating layer to the polymer material is necessary for increasing the usability of AgCl-coated polymer electrodes.

In this thesis, the impedance, ECG and EEG monitoring using polymer dry electrodes are mostly recorded *before* the polymer electrodes are stabilized. To increase the accuracy of the dry signals, it is necessary to start the recording only after the polymer dry electrodes have been stabilized. The stabilization time of the polymer dry electrodes can be evaluated by analyzing the impedance variation with time. Based on the impedance results shown in section 5.6.2, a longer measurement, preferably a couple of hours, is needed to evaluate the stabilization of polymer dry electrodes. During the long-term measurements, motion artifacts are evident, which might require extra re-stabilization of the polymer dry electrodes. However, research has been carried out to investigate the correlation between the motion artifacts in biopotential signals and impedance variation [190]. Recording the biopotential signals simultaneously with the impedance and analyzing their correlation might facilitate algorithm development for artifact reduction or cancellation in the recorded signals.

Another variable during the long-term impedance measurement is the change in environmental conditions, such as variation in ambient temperature, humidity and ventilation. It is found in section 3.2.5 that (as expected) the impedance decreases when the subject sweats. Therefore, controlling the environmental conditions reduces variables during measurement of impedance for stabilization time investigations.

Some of the dry electrodes presented in literature degrade during the period of use for biopotential measurements [61]. This can occur because their metal coating layers or additives degrade (e.g. oxidize) over time, thereby reducing the quality of the electrodes. Systematically studying the impedance of the polymer electrodes after multiple use cycles will reveal the stability and reusability of the material.

Further improvement of the Mechanical properties of the polymer dry electrodes

User comfort is always the result of both the polymer electrodes themselves and their fixation device. In this thesis, we did not use a mechanical headset but merely used elastic bands for fixation of the electrodes. This is only meaningful in early research. A better device for electrode fixation, which ensures good electrode/skin contact while maintaining user comfort, has to be employed or designed and constructed. It can feature springs on the electrodes to absorb some force from the device or with adjustable straps to fit all head-sizes. The force needed for good electrode/skin contact can be optimized by measuring the impedance of polymer dry electrodes when applying different pressure on the electrodes. Parallel ongoing work at imec has recently resulted in mechanical headsets that are now in used in clinical studies.

During the EEG measurements discussed in Chapter 5, only one shape of polymer dry electrodes was available, and some of the lower-quality signals might be related to the electrode shape not being suitable given the subject's hairstyle. When an optimal fixation device is available in the future, improved shapes of electrodes on subjects with different hairstyles need be investigated.

Extensive Electrode validation: EEG monitoring

Together with an optimal electrode fixation device, the cabling needs to be properly arranged to reduce electromagnetic disturbance. A wireless EEG recording system not only reduces the power line interferences inherent to cables but also provides subjects with the freedom to move. Combining this with shielded cables and a driven right leg circuit will further reduce environmental effects.

In Chapter 5, steady-state visually evoked potential (SSVEP) tests have been attempted but were unsuccessful due to the non-optimal visual stimuli. SSVEP can be used to evaluate the quality of EEG signals if the frequency of the stimuli and test conditions are well controlled. Besides the signal analysis techniques mentioned in Chapter 5, an event-related potential (ERP) test can also be carried out for further evaluation. ERP measures the brain response which is the direct result of a specific sensory, cognitive, or motor event. imec has previously created SSVEP and ERP based systems with rigid AgCl based dry electrods. If polymer dry electrodes show good results during SSVEP and ERP tests, they will be attractive for brain computer interface (BCI) applications.

Extensive Usability and user comfort studies

It is currently not clear whether the optimum use case for these electrodes is single or multiple use. For certain applications each electrode may have to be used many times before it can be replaced. For such application scenarios, a procedure for cleaning or even sterilizing the polymer electrodes needs to be investigated. Furthermore, the influence of these processes on material properties will need to be evaluated to ensure electrode reusability.

With respect to skin irritation caused by the polymer material, a systematic evaluation of the skin condition during 1-week polymer electrode/skin contact on a larger population will provide more statistics on long-term user comfort. A pin-shaped polymer electrode is not ideal for such long-term tests, as discussed in section 6.3.2. A flat electrode with rounded edge and a sufficiently large area to avoid irritation would be ideal. Recording the level of erythema (if there is any) using a color reference card is an established approach to evaluate the skin condition. The test protocol and the clinical tests have to be created and supervised by a dermatologist.

To extend the usability of polymer dry electrodes for recording EEG signals during daily life, the fixation device should not only provide sufficient mechanical support, but should also have an elegant appearance. A device that does not impede social interaction would be desirable. This is a human-centered design challenge and task which will be critical for acceptance in ambulatory conditions.

There is clearly still work ahead before this technology can become a product. Nevertheless, this PhD research has shown the attractiveness of conducting polymer dry electrodes and has made a number of steps forward towards practically useful soft polymer electrodes

Appendix I

In section 3.4.1, the nano-indentation test is one of the techniques to determine the elastic modulus of the polymer materials. Although it has been discussed in section 3.4.1 that nano-indentation tests are not suitable to measure the hardness and elastic modulus of our polymer materials, the protocol and the results which have been performed and recorded are reported here as a reference for future studies of using nano-indentations on similar materials.

Nano-indentation tests were performed on 13-mm diameter and 5-mm high test buttons with various carbon contents as shown in Figure App. 1a. The tests were carried out using a nano indenter XP system (MTS Systems Corporation), equipped with a standard three-sided pyramid diamond indenter tip (Berkovich). During the measurements of our rubber samples, the tool's maximum displacement of 20 μm and a constant strain rate of 0.05 s^{-1} are used. The nano-indentation tests are carried out on one sample of each material. For each material, multiple measurements (8 to 13) are performed. From the experimentally obtained load-displacement curves, 3 important quantities could be measured: the maximum load P_{max}, the maximum displacement h_{max}, and the elastic unloading stiffness S, defined as the slope of the unloading curve's upper portion during the initial stages of unloading (also called the contact stiffness) as shown in Equation App. 1 [148, 195]. An example of load-displacement curve and the 3 quantities can be found in Figure App. 1b.

$$S = \left(\frac{dP}{dh}\right)_{P_{max}} \qquad \textit{Equation App. 1}$$

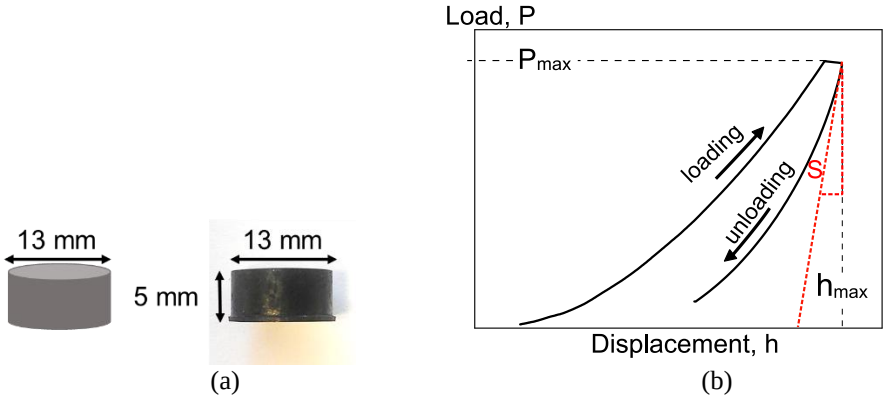

Figure App. 1: (a) Test buttons with various materials were used in nano-indentation tests. (b) The hardness and elastic moduli were defined by the load-displacement curve of the nano-indentation test.

As introduced in [148, 195], the hardness (H) and elastic modulus (E) were calculated based on their relationship to the contact area (A) and measured contact stiffness (S), as indicated in Equation App. 2 and Equation App. 3:

Equation App. 2

$$H = \frac{P_{max}}{A}$$

where P_{max} is the maximum applied force and contact area (A) is the projected contact area of the indenter with the sample surface, which is determined from the indenter tip shape calibration, as described in [150].

$$S = \beta \frac{2}{\sqrt{\pi}} \sqrt{A} \left[\frac{1 - \nu^2}{E} + \frac{1 - {\nu_i}^2}{E_i} \right]^{-1}$$

Equation App. 3

where β=1.034 is the geometry correction factor of a Berkovich indenter [149], ν is the poisson's ratio of the sample which is not determined in this thesis, so a value widely used for rubber materials is used: ν = 0.5. E_i (1140 GPa) and ν_i (0.07) are the elastic constants of the diamond indenter tip. The contact area (A) is the same as in *Equation App. 2*.

The hardness is determined by Equation App. 2 using the same principle as used in other indentation tests: dividing the applied force by the area of impression. One of the advantages of using the nano indenter XP system is that the instant hardness is calculated by the software of the indentation tool during the entire loading process [196]. However, the maximum applied force and the projected contact area are commonly used to determine the hardness. The continuous stiffness measurement (CSM) technique is also involved in the nano indenter XP system, so the contact stiffness (S) during the loading protion of an indentation test can be measured [196]. The measured contact stiffness was used to obtained the elactic modulus of test sample using Equation App. 3.

The hardness and elastic moduli of the test buttons with various amount of carbon content are shown in Figure App. 2. It is shown that both hardness and elastic modulus increase with the increasing of carbon content. However, the indent depth used in the measurements is not suitable for our polymer test button with a rough surface and a skin. Furthermore, the parameters used to calculate the elastic modulus based on the nano-indentation tests, are values derived for hard materials, they are less suitable for our softer polymer materials. Due to this, the obtained elastic moduli have to be considered as 'relative' E-values, only to be used to compare various rubbers. Therefore, the elastic moduli of various test buttons with different materials are characterized using the compression tests discussed in section 3.4.1 in this thesis.

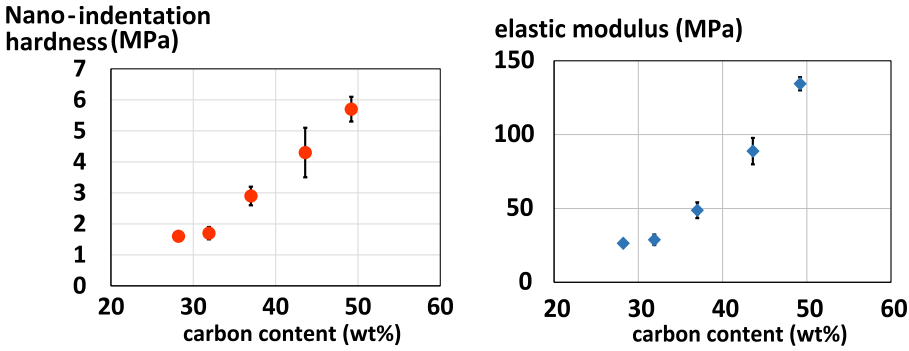

Figure App. 2: The hardness in MPa unit and elastic moduli of test buttons with various amounts of carbon content.

Appendix II

In Section 5.5.1, the polymer dry electrodes for EEG measurements are evaluated using the commercial recording system in UZ Leuven. A full description of the experimental work including results and discussion are shown in this section (Appendix II).

Electrodes types and locations

During all the recordings, signals from six channel electrodes were evaluated. The locations of the electrodes for the various tests are shown in Table App. 1. Test 1 is mounting the GND and REF electrodes behind the earlobes. Test 2 is mounting the GND and REF in frontal region. In each test, two test conditions are included: dry GND and REF, and wet GND and REF. Dry electrodes are polymer electrodes with material composition number 95 combined with the our own active circuit (see section 5.1 and Figure 5.2).

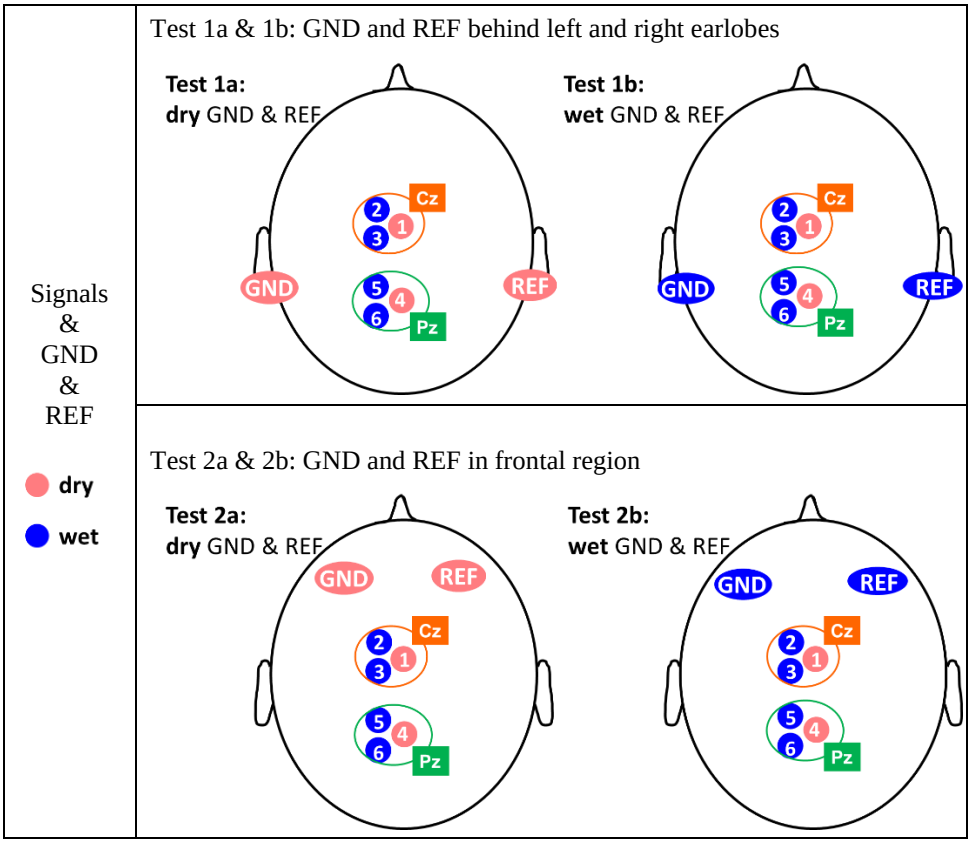

Table App. 1: Electrode types and locations for various test conditions using the EEG recording device in UZ Leuven.

Always, wet electrodes were mounted closed to the dry electrodes to allow signal comparison, which is performed by calculating the SNR, correlation and coherence of two

adjacent electrodes. The two wet electrodes were placed on the left of a dry electrode forming a triangle in order to account the spatial variability of the EEG signals. They were not placed below the dry one because the ones closer to occipital area (the wet ones) would acquire stronger alpha waves. The triangle electrode location should result in a correct comparison between the two wet ones and a pair of wet and dry ones.

Protocol

During the monitoring, the subjects repeated the open/close eyes tasks for three or four time periods. This test protocol has been approved upfront by the ethical committee of UZ Gent.

Signal analysis

- SNR when eyes closed
- Correlation and coherence of two adjacent wet electrodes and of a pair of wet and dry electrodes

Results and discussions

Test 1a & 1b: GND and REF behind left and right earlobes

The signal spectra for the recordings when the subject closed his eyes are shown in Figure App. 3. Very clear alpha waves are seen. The spectra of wet2 and wet3 are very similar and that of wet5 and wet6 are rather similar, although a slightly higher alpha peak is visible in wet6, this proves that the small difference in electrode location will not cause important changes in the signals. Also signal dry1 in both tests, and dry4 in Test 1a, are producing very similar signals as their neighboring wet electrodes, proving that these dry electrodes give high quality recording. There is however a disadvantage of the dry electrodes clearly visible in the graphs: the high intensity of signals of low frequency is typical for baseline drift. In Test 1a, the reference electrode suffers from baseline drift, hence all signal electrodes show this high intensity of low frequency signals. In Test 1b, the wet REF electrode is fine, but dry4 suffers from baseline drift.

When calculating the SNR for the signals of Tests 1a and 1b, the baseline drift becomes even more visible. Since the low frequency signal components are defined as ‘noise’ in SNR calculations, a lower SNR is calculated when baseline drift is present. The SNRs of all the recordings are shown in Figure App. 4. Each data point in the figure represents the SNR value of that recording session, hence 3 SNRs per signal electrode for this Test 1. Without surprise, the SNR of the signals recorded in Test 1a is low because of the baseline drifts of the dry REF electrode. In Test 1b, all wet electrodes show high SNR except dry4, again due to baseline drift. In Test 1b, the SNR of wet6 is slightly higher than that of wet5, which might be related to the wet6 location: stronger alpha waves are present in the occipital region (hence larger alpha peak in wet6 signal, as already seen in Figure App. 3).

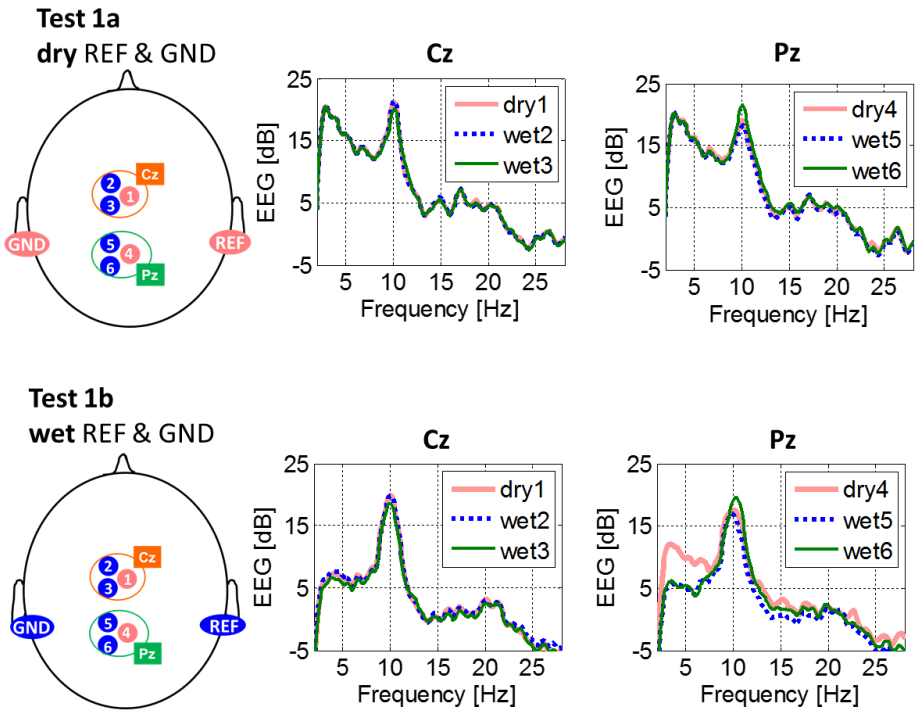

Figure App. 3: The PSD of the signals recorded in Test 1a and Test 1b.

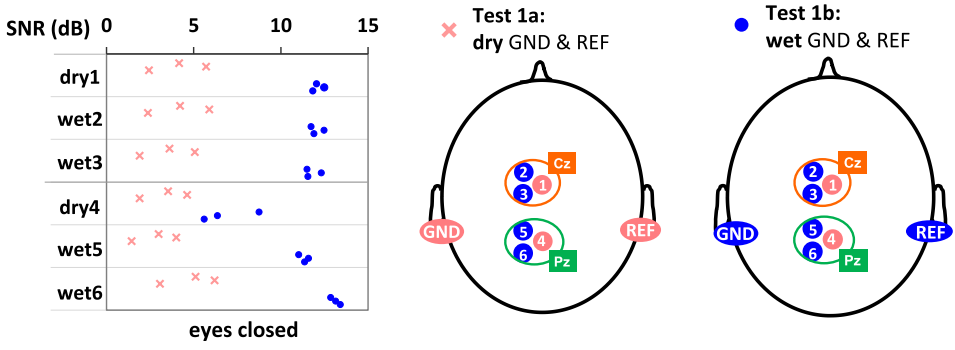

Figure App. 4: SNR of the signals recorded by wet and dry electrodes when placing the ground and reference electrodes behind the earlobes (Test 1a and Test 1b). Each data points represent the SNR of each recording sessions.

With regard to the similarity of the signals recorded by adjacent electrodes, the correlation and coherence of the 2-30 Hz frequency range are calculated – see Figure App. 5 and Figure App. 6, respectively. The two figures show that applying dry REF and GND electrodes results in a higher correlation and coherence of all pairs of electrodes compared to applying wet REF and GND electrodes. However, it is not correct to conclude that the

signal quality of applying dry REF and GND is better than that of wet ones, as discussed in session 4.2. This is because such high correlation and coherence are mainly the result of the common low frequency signals picked up by the dry REF signals.

Therefore, it is better to evaluate the signal quality of polymer dry electrodes using the signals recorded with wet REF and GND electrodes. For this electrode configuration, the correlation and coherence of electrodes near the Pz location are lower than those near the Cz location. The lower correlation and coherence of dry4_wet5 and dry4_wet6 resulted from the baseline drift discussed in Figure App. 3. The lower correlation and coherence of wet5_wet6 might have resulted from the larger amount of hair at the Pz location. Another explanation is that the variability of the signals recorded at Pz is larger when the electrodes are located as shown in Test 1b.

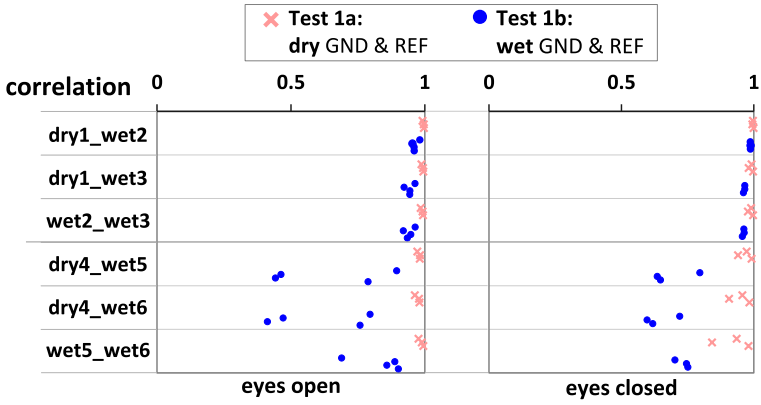

Figure App. 5: Correlation of a pair of electrodes when placing the ground and reference electrodes behind the earlobes. Each data point represents the correlation of each recording session.

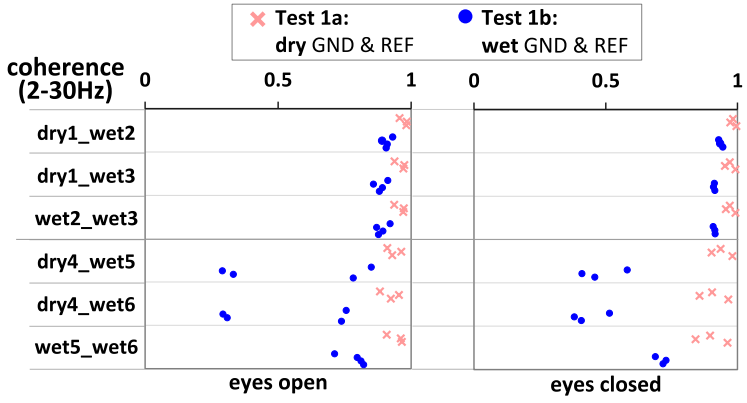

Figure App. 6: Coherence at the 2-30 Hz frequency range of a pair of electrodes when placing the ground and reference electrodes behind the earlobes. Each data point represents the coherence of each recording session.

Test 2a and 2b: GND and REF in the frontal region

The SNR of the signals recorded when eyes are closed is shown in Figure App. 7. The SNR of Test 2 is lower than that of Test 1. This might be due to the fact that the subject in Test 2 is different from the one in Test 1. Another explanation is that the REF electrode in the frontal region records weaker alpha waves than behind the earlobes. In addition, the SNR of signals recorded using dry GND and REF electrodes is lower than when using wet ones. This again resulted from the baseline drift of the signal recorded by the dry REF electrode discussed in section 5.5.1.

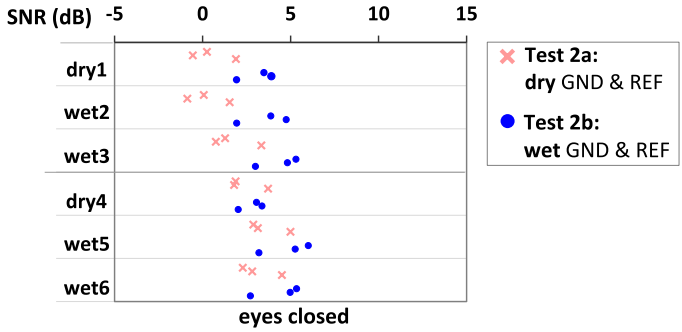

Figure App. 7: SNR of the signals recorded by wet and dry electrodes when placing the ground and reference electrodes in the frontal region. Each data point represents the correlation of each recording session.

The results of correlation and coherence analysis are shown in Figure App. 8 and Figure App. 9, respectively. Only the signals recorded using wet GND and REF electrodes are discussed because the baseline drift recorded by the dry REF electrode influences the results recorded using dry GND and REF electrodes. The correlation and coherence of the signals recorded at the Cz region in Test 2 are lower than those in Test 1; this might have been caused by the higher sensitivity of the frontal REF electrode to the variation between electrodes at the Cz region. Regarding the signals recorded from the Pz region, the correlation and coherence of dry4_wet5 and dry4_wet6 are again lower than those of wet5_wet6.

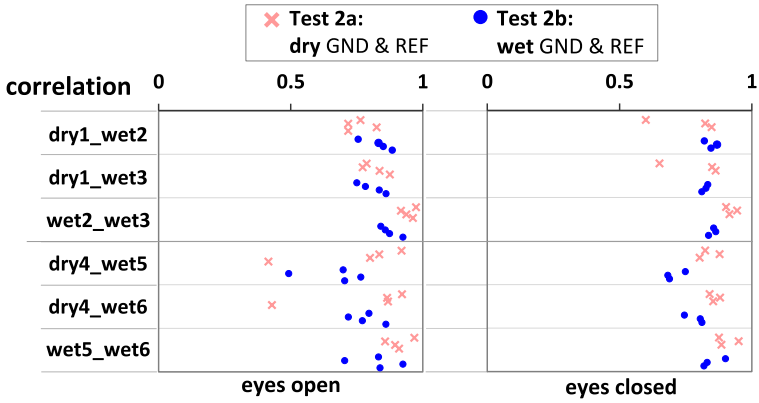

Figure App. 8: Correlation of a pair of electrodes when placing the ground and reference electrodes in the frontal region. Each data point represents the correlation of each recording session.

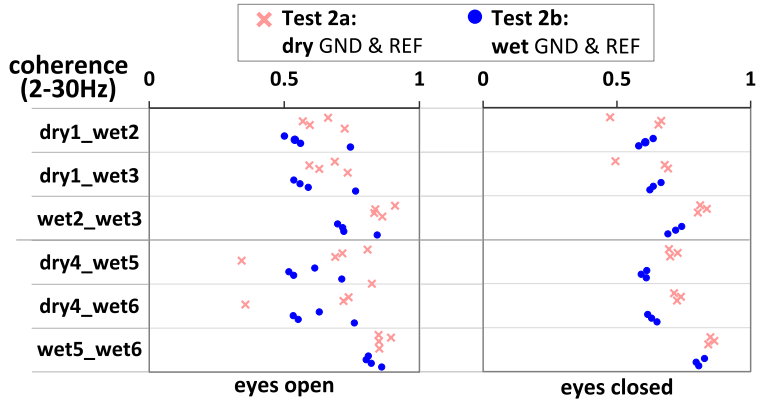

Figure App. 9: Coherence at the 2-30 Hz frequency range of a pair of electrodes when placing the ground and reference electrodes in the frontal region. Each data point represents the correlation of each recording session.

Appendix III

The evaluations of polymer dry electrodes for EEG measurements are carried out using imec's EEG system. The important results are discussed in section 5.6.2. Detailed data analysis for all electrodes and the results can be found in Appendix III.

Goal

4 different types of dry electrodes are evaluated. They are gel filled rigid AgCl electrode, 2 polymer electrodes with different material compositions and polymer electrode with AgCl coating.

Electrodes locations

Elastic bands were used to mount the electrodes on the locations shown in Figure App. 10. First, all wet electrodes were mounted on the scalp and recording was started. The two dry electrodes were mounted after the recording software was started in order to record the impedance variation of the dry electrodes.

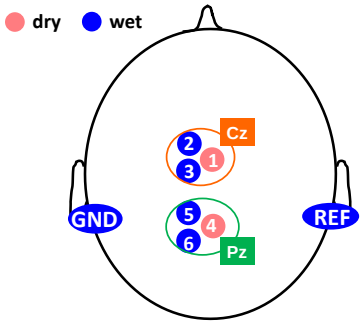

Figure App. 10: Electrode locations for tests using imec's EEG recording system.

Electrodes materials

<table>
<tr><td>Signals</td><td>5 types of dry electrodes:
<table>
<tr><th>Electrode type</th><th>Label</th><th>Picture</th></tr>
<tr><td>AgCl electrode with rigid pins</td><td>AgCl_rigid</td><td>  </td></tr>
<tr><td>Polymer dry electrode made of material composition number 95</td><td>CR95</td><td>  </td></tr>
<tr><td>Polymer dry electrode made of material composition number 64</td><td>CR64</td><td>  </td></tr>
<tr><td>Polymer dry electrode made of material composition number 64 coated with AgCl</td><td>CR64_AgCl</td><td>  </td></tr>
</table>
Wet electrode:
<table>
<tr><td>AgCl cup electrode filled with Ten20 conductive gel</td><td>wet</td><td>  </td></tr>
</table></td></tr>
<tr><td>GND & REF</td><td>Wet electrode:  </td></tr>
</table>

Table App. 2: Labels and pictures of the electrodes used in the tests using imec's EEG recording system.

All the polymer dry electrodes applied in this study are electrodes with 5 mm pin length and 13 mm total diameter. These five electrodes are abbreviated (see 'label' in Table App. 2) to be easily identified further in the text. Electrodes serving as signal or reference electrode are connected with the active front-end PCBs (as shown in Figure 5.38a). The AgCl_rigid and wet electrodes are connected with the PCBs by short conductive wires while polymer dry electrodes were connected with the PCBs using 3D printed holders.

Protocol

This protocol and informed consent form of this evaluation are approved by the ethical committee of Holst center, imec-NL (document number: ME-15-WATS-TIP2-261). 11 adult volunteers, including 9 men and 2 women, participated in this measurement. The monitoring was taking place in a meeting room and the subjects were asked to sit comfortably on a chair and avoid movements and talking during the monitoring.

The recording consisted of the following 4 sessions:

(1) 5 minutes of electrode stabilization;

(2) 1 minute of eyes open (‘session EO’)

(3) 1 minute of eyes closed (‘session EO’)

(4) 1 minute of steady state visually evoked potential (SSVEP) stimulation displayed on a computer screen. The stimulation consists of a square object flickering at a frequency of 8 Hz rendered by Matlab. (‘session SS’)

After these tasks, the two dry electrodes were replaced by the next type of dry electrode. Then the tasks were repeated. The recording of using each type of dry electrode took around 10 to 15 minutes and the total recording time on one subject is around 1 hour. Among the five types of dry electrodes, CR64 electrodes were always the last one to apply. The order of the other three types of electrodes was randomized to reduce a potential bias in the user comfort evaluation performed by the subjects after all recordings.

Results and discussions

(1) User comfort

The results of user comfort of all types of electrodes are discussed in section 6.4.

(2) *Setup time*

Data analysis

In each recording, the researcher started the recording before placing the dry electrodes on the Cz and Pz locations. The researcher always placed the electrode on Cz first, then on Pz. As soon as the impedance value of the dry electrode could be read and started to decrease, the time was defined as the setup time of that electrode. The setup time of the Pz electrode shown here was the moment when the setup of both Cz and Pz electrodes were both completed. For example, in the scenario of Figure App. 11, the settling time of the Cz electrode (Dry1) is 45 s while that of both Cz and Pz electrode (Dry4) is 85 s.

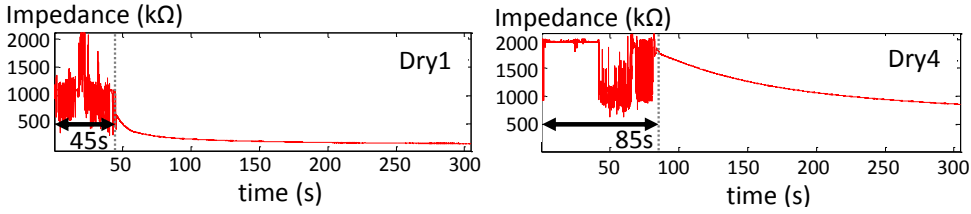

Figure App. 11: The setup time of the dry electrodes was defined as the moment in which the impedance value was able to be recorded and started to decrease.

The setup time of each type of dry electrode is shown in Figure App. 12. AgCl_rigid electrode recorded the longest setup time due to its pins which were the shortest (2mm). In order to get good AgCl_rigid/skin contact, more efforts were needed to move the hair apart from the Cz and Pz locations. The setup time of CR64 at the Pz location (dry4) was the shortest; however, this did not imply that it was the easiest for setting up the CR64 electrodes. The impedance value of CR64 on some subjects was saturated, so the experimenter tried to adjust the electrodes several times before the impedance value became meaningful. The data shown

here is the setup time of the 1st manipulation. In general, the setup time of Pz (dry4) electrodes was longer than that of Cz (dry1) electrode. This might have come about because most people have more hair at the Pz location than at the Cz location. Besides, this might also be explained by the limitation of using the elastic bands as a fixation device. The elastic band above Cz was almost always giving sufficient and perpendicular force to the electrodes. The elastic band above Pz did not always give sufficient force because it did not always provide a perpendicular force to the electrode. It took a longer time to find the location where the elastic band provided a perpendicular force to the scalp.

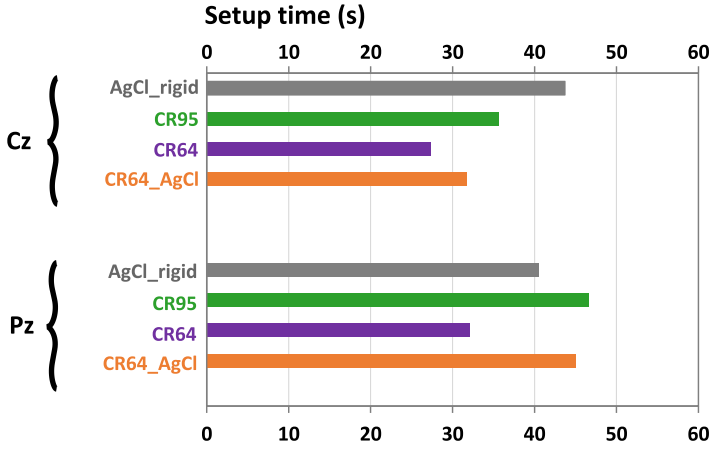

Figure App. 12: The average setup time of each type of dry electrodes at Cz (dry1) location and Pz (dry4) location on 11 subjects.

(3) *Impedance magnitude*

Data analysis

The impedance magnitude of each electrode was recorded during the EEG monitoring. Saturated and abnormally small data caused by the limitation of the recording device is removed before the analysis.

Figure App. 13 shows the impedance magnitude of each type of dry electrode at the Cz and Pz locations. The impedance of wet electrodes was plotted in the same figure. The impedance of the wet electrode at Cz represents the average impedance of wet2 and wet3 electrodes, while impedance at Pz represents the average impedance of wet5 and wet6 electrodes (as the locations shown in Figure App. 10). The dots in Figure App. 13 indicate the mean value of each type of electrode. The number next to each box represents the number of datasets removed when plotting this figure. The dataset was removed from AgCl_rigid at Cz because the data was abnormally small. All other datasets were removed due to saturation. Figure App. 13 shows that CR95 and CR64 had the highest impedance among all types of dry electrodes. Besides, it also shows that the high impedance of CR95 and CR64 electrodes caused saturation more often than other types of electrodes according to the number of removed datasets. Therefore, the actual impedance magnitudes of CR95 and CR64 were

higher than the value shown in Figure App. 13. This issue got worse when placing these two types of electrodes at the Pz location. This might have come about because there was more hair at the Pz location than at the Cz location for most subjects. The bigger amount of hair at the Pz location might also explain the larger variation in CR95 and CR64 electrodes at the Pz location. Polymer dry electrodes with surface modification resulted in lower impedance. CR64 with AgCl coating layer had a lower impedance than CR64.

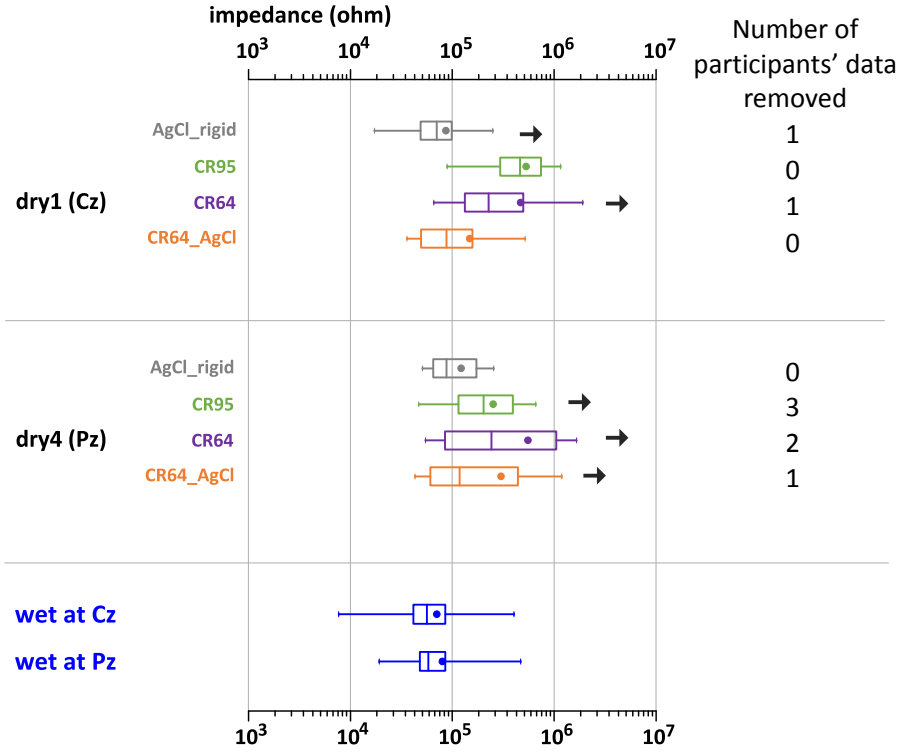

Figure App. 13: Magnitude of impedance for each type of electrode. The dots show the mean value of the impedance. The lines in the box mean the median, the upper lines in the boxes mean the 75th percentile, and the lower lines of the boxes mean the 25th percentile. The upper and lower caps mean the maximum and minimum value. The number next to each box represents the number of datasets removed when plotting this figure. The dataset is removed from AgCl_rigid at Cz because the data is abnormally small. All other datasets are removed due to saturation.

The impedance for each type of dry electrode during each recording session (EO, EC, SS) was recorded, and the average impedance of each type of dry electrode is shown in Figure App. 14.

The order of the tasks that the subjects performed was always EO, EC, then SS, so the impedance values of these sessions reveal the impedance variation with time. It is shown that the impedance of almost every type of dry electrode decreased during the recordings. This trend is clearly observed in the data of CR64, CR64_AgCl, and CR95 at the Pz location. This might have been caused by sweat generated from the skin and which started to build ionic

conductive channels after the polymer dry electrodes were mounted. The slope of the impedance variation will be discussed in the next session.

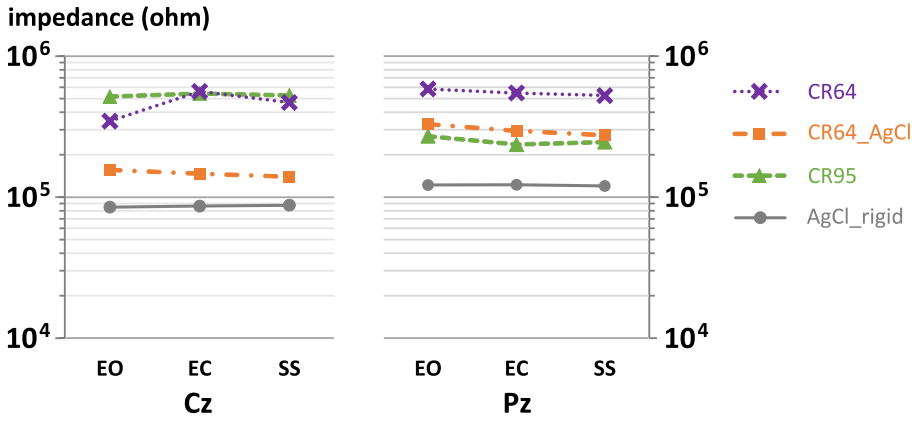

Figure App. 14: Magnitude of impedance for each type of electrode during each recording session: eyes open (EO), eyes closed (EC) and SSVEP (SS). The impedance at Cz and Pz locations is plotted separately.

Impedance slope

Data analysis

To calculate the impedance slope, the average impedance of the electrode at the last minute of the recording and that at the first minute of the recording were computed. Then the magnitude of impedance of the last minute was deducted from that at the first minute. Lastly, the deducted impedance value was divided by the time of the recording, resulting in the impedance slope. The impedance slope shown in this session is in ohm/s.

Figure App. 15 shows the impedance slope of each type of dry electrode at the Cz and Pz locations. When analyzing the impedance slope, the dataset with abnormally small and saturated impedance value was removed as mentioned in the 'impedance magnitude' session. It is found that the impedance of wet electrode and AgCl_rigid decreased slowly during the recordings. In contrast, the impedance of CR95 and CR64 decreased significantly during the recordings. The impedance of AgCl coated CR64 electrode also decreased with time. Even though the impedance of CR95, CR64 and CR64_AgCl electrodes decreased faster than the rest of the electrodes, the magnitude of impedance did not reach that of wet or AgCl_rigid electrodes during the 10-15 minute recording periods.

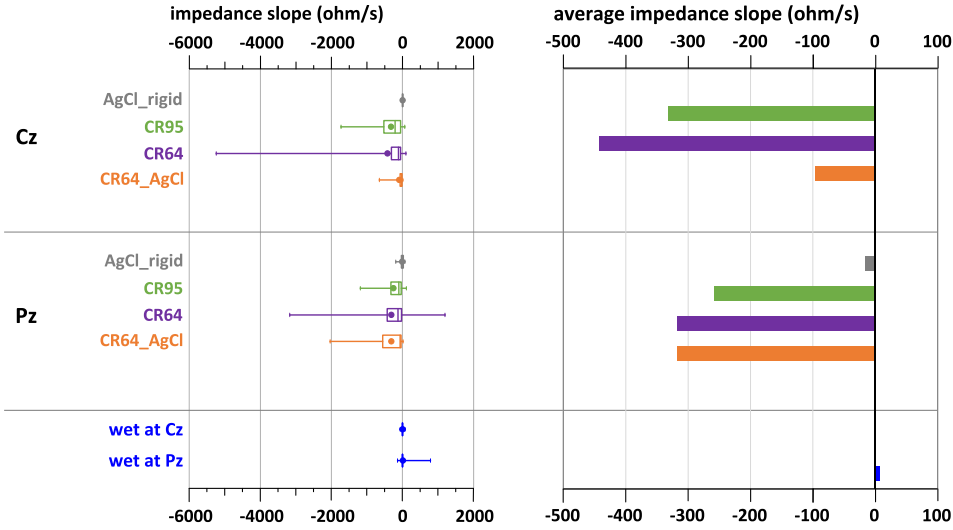

Figure App. 15: Impedance slope of each electrode at the Cz and Pz locations. The box and whisker chart indicates the same statistical values as described in Figure App. 13. To compare the impedance slope of the electrodes, the average value of impedance slope is shown in the plot to the right.

The slope of the impedance variation of every type of electrode became gentler with time. This trend can be found in the impedance slope by comparing the data of each recording session, see Figure App. 16. The impedance slope of EO sessions is the steepest, while that of SS sessions is the gentlest. The impedance of AgCl_rigid became stabilized during the three recording sessions, while the impedance of the other electrodes kept decreasing. Due to the limited recording time for each participant, the impedance variation of CR64 or CR95 along with a longer time, namely several hours, is unknown in this evaluation.

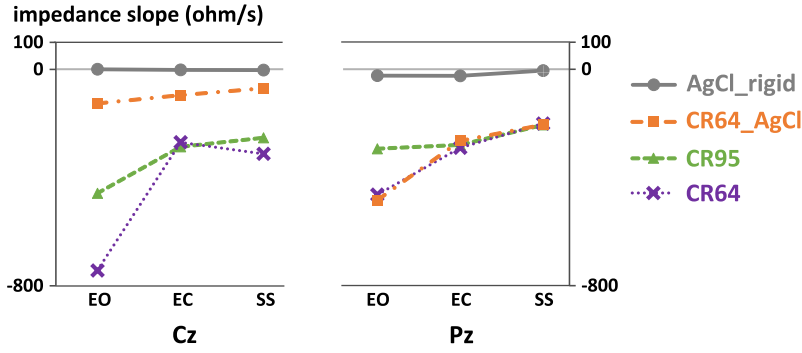

Figure App. 16: Impedance slope of each type of electrode during each recording session: eyes open (EO), eyes closed (EC) and SSVEP (SS). The impedance slope at the Cz and Pz locations is plotted separately.

(4) *PSD of 50 Hz signals*

Data analysis

It is known that an electrode with higher impedance is more prone to disturbances. In other words, the signal of these electrodes contains stronger 50 Hz signals. Although the 50 Hz signals can be filtered out by data post processing, the power spectral density (PSD) of the raw signals recorded by each type of dry electrode is calculated as a parameter to evaluate the signal quality. The calculation is introduced in session 5.3.2. The PSD shown in this session is in dB unit.

Figure App. 17a shows the PSD of the 50 Hz signal recorded for each type of dry electrode. The standard deviation of the 50 Hz signals' PSD can be found in Figure App. 17b. It is found that CR95 and CR64 electrodes pick up more 50 Hz signals than other electrodes. AgCl_rigid and CR64_AgCl electrodes pick up less 50 Hz signals than the wet ones. That these electrodes show a lower PSD of 50 Hz might not imply that they have better electrode/skin contact compared to wet electrodes. This result could be caused by the fact that the PCBs of wet electrode were connected with the AgCl cup electrode through a short wire while the PCBs of polymer dry electrode were connected directly to the input of the back side of polymer electrodes (see session 5.6.1). Another possible explanation might be that the 50 Hz signals picked up by CR64_AgCl are a better match for that picked up by the reference electrode, so the common-mode rejection ratio (CMRR) in the recording system shows a better performance.

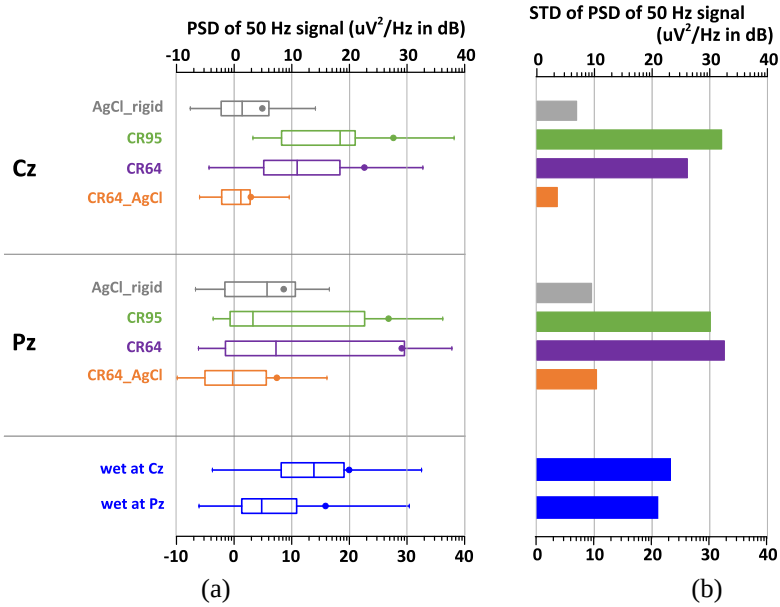

Figure App. 17: (a) PSD of the 50 Hz signals of the EEG signals acquired using each electrode at the Cz and Pz locations. The box and whisker chart indicates the same statistical values as described in Figure App. 13. (b) The standard deviation (STD) of the PSD of 50 Hz signals recorded by each type of electrode.

When observing the PSD of 50 Hz signals with time, the value of the signals recorded by most electrodes remains similar, except for the value of CR64 electrodes which clearly decreases during the recordings.

Signals filtering

All the results discussed above are based on the data of individual electrodes and the raw data recorded by them. Before analyzing the signal to noise ratio (SNR) when eyes closed and SSVEP, as well as correlation and coherence of the signals, they were filtered by the filters mentioned in section 5.3.1. However, a 1-20 Hz bandpass filter was applied instead of the 2-30 Hz one used for the data acquired at UZ Gent. This is because almost all signals recorded by the imec system contain noise distributed at 20-26 Hz, which is generated from the Bluetooth transceiver. The aim of the evaluation using the imec system is to validate the compatibility of the polymer dry electrodes and imec recording system and to compare the signal quality, especially focusing on the baseline drift (low frequency signals) for all types of dry electrodes. Therefore, analyzing the signals in the 1-20 Hz frequency range is sufficient.

(5) *SNR ratio*

Data analysis

In this evaluation, the intensity of the alpha waves recorded by each type of dry electrode is compared using SNR calculation. The definition of SNR is slightly different from the one introduced in session 5.3.3. All signals in this evaluation are filtered by the 1-20 Hz notch filter. Therefore, signals distributing at 1-8 Hz and 13-20 Hz are defined as noise during the SNR calculation. The SNR value in dB is shown in Figure App. 18a.

It is found that the SNR of the signals recorded at Pz location is higher than that at Cz location. This is because electrodes around Pz are closer to the origin of alpha waves, occipital region. The SNR of the signals recorded by CR64 electrodes is the lowest. This indicates CR64 is less capable to record the alpha waves or its signal is disturbed by more noises. According to the EEG spectrum shown in Figure 5.41, the second reason can better explain the results. The SNR of CR64_AgCl is slightly higher than that of wet electrodes.

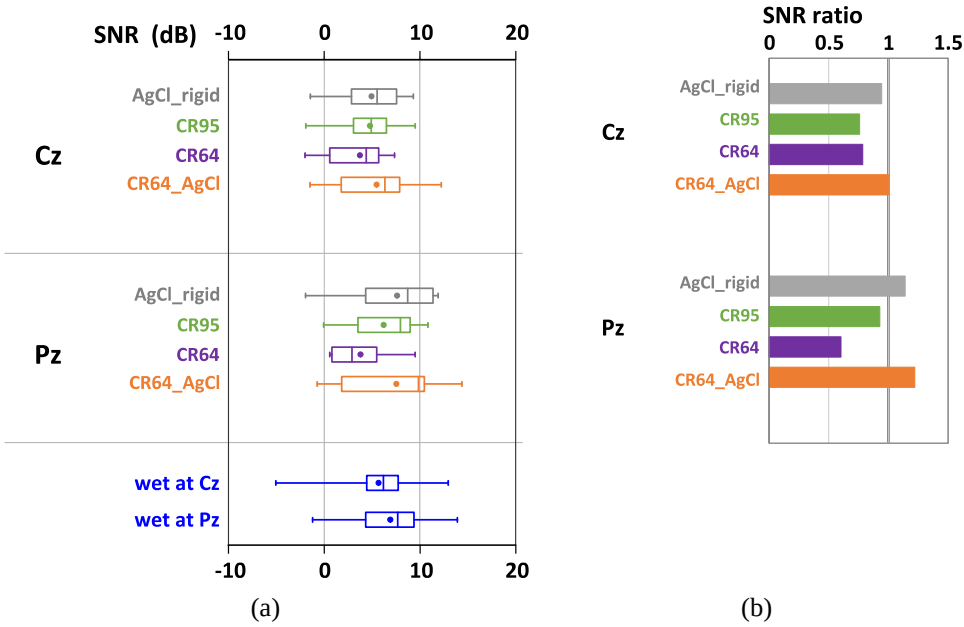

Figure App. 18: (a) SNR of EEG signals recorded when subjects closed their eyes; (b) the SNR ratio of the EEG signals recorded by each type of dry electrode to the SNR of that recorded by their two adjacent wet electrodes.

The intensity of the alpha waves varies with time and with person (discussed in session 5.4.2 and session 5.4.3). Therefore, the SNR of the signals recorded by dry electrodes in each recording was compared with the SNR of signals recorded by their adjacent wet electrodes in order to eliminate the variations in alpha wave intensity with time. The SNR ratio is calculated by having the SNR of dry electrodes divided by that of wet electrodes, as shown in Figure App. 18b. It is shown that the SNR of CR64's signals is much lower than that of the adjacent wet electrodes. This confirms that the signals recorded by CR64 represent the lowest signal quality. In addition, the bigger amount of hair at the Pz location (where the alpha waves are stronger than Cz) increases the difficulty for CR64 electrodes to pick up the signals.

SNR ratio during SSVEP

During the SSVEP recordings, 8 Hz square stimuli were rendered in a window. However, many limitations surfaced during the measurements. First, although the subjects were asked to look at the stimuli during the recordings, it was hard to identify if they focused on the stimuli during the entire recordings. Moreover, the stimuli were located in the center of a laptop screen, and occupied only a third of the screen, resulting in a small region as focus. A full-size window was not used because it was found visually that the frequency of the stimuli was not constant. Second, whether the size and frequency of the stimuli were sufficient to arouse the responses of every subject was uncertain. Third, it was difficult to render exact 8 Hz stimuli and to have it confirmed. During the signal analysis using the SNR calculation shown in section 5.3.3, stronger 6-10 Hz signals are only observed in the recordings on a few

subjects during the SSVEP. Due to the limitations of the setup and the preliminary results, the SNR during SSVEP is not discussed in this thesis.

(6) *Correlation*

Data analysis

During correlation analysis, not only were the signals of one dry electrode and one of the adjacent wet electrodes analyzed, but so were the signals of one dry electrode and the average signal of two adjacent wet electrodes. In addition, the correlation of the two adjacent wet electrodes was analyzed. Since the wet electrodes are considered to be the gold standard, the correlation of the signals recorded from the two adjacent wet electrodes is considered as the highest correlation of the two electrodes in a short distance. The labels in the figures shown in this session indicate which two signals are being compared. For example, in Figure App. 19, dry1_gel2 shows the correlation of signals recorded from dry1 and gel2 electrodes (the electrodes' locations are indicated in Figure 5.39). The dry1_gel2gel3 means the correlation of dry1 and the averaged signals of gel2 and gel3. Gel2_gel3 means the correlation of signals recorded from gel2 and gel3 electrodes. There are five bars shown in the wet2_wet3 category. They indicate the correlation of wet2 and wet3 electrodes during the recordings using each type of dry electrode, that is, the correlation at different times.

The correlation value of a pair of electrodes when subjects open and close their eyes is shown in Figure App. 19. It is found that the correlation of dry and wet electrodes at the Pz location is lower than that at the Cz location. The correlation of two wet electrodes shows this difference as well. This might be caused by the bigger amount of hair at the Pz location as well as the difficulty of settling both wet and dry electrodes at the back of the heads using elastic bands. Another reason might be that spatial variability can be better recorded by the electrodes at the Pz region in our setup [197].

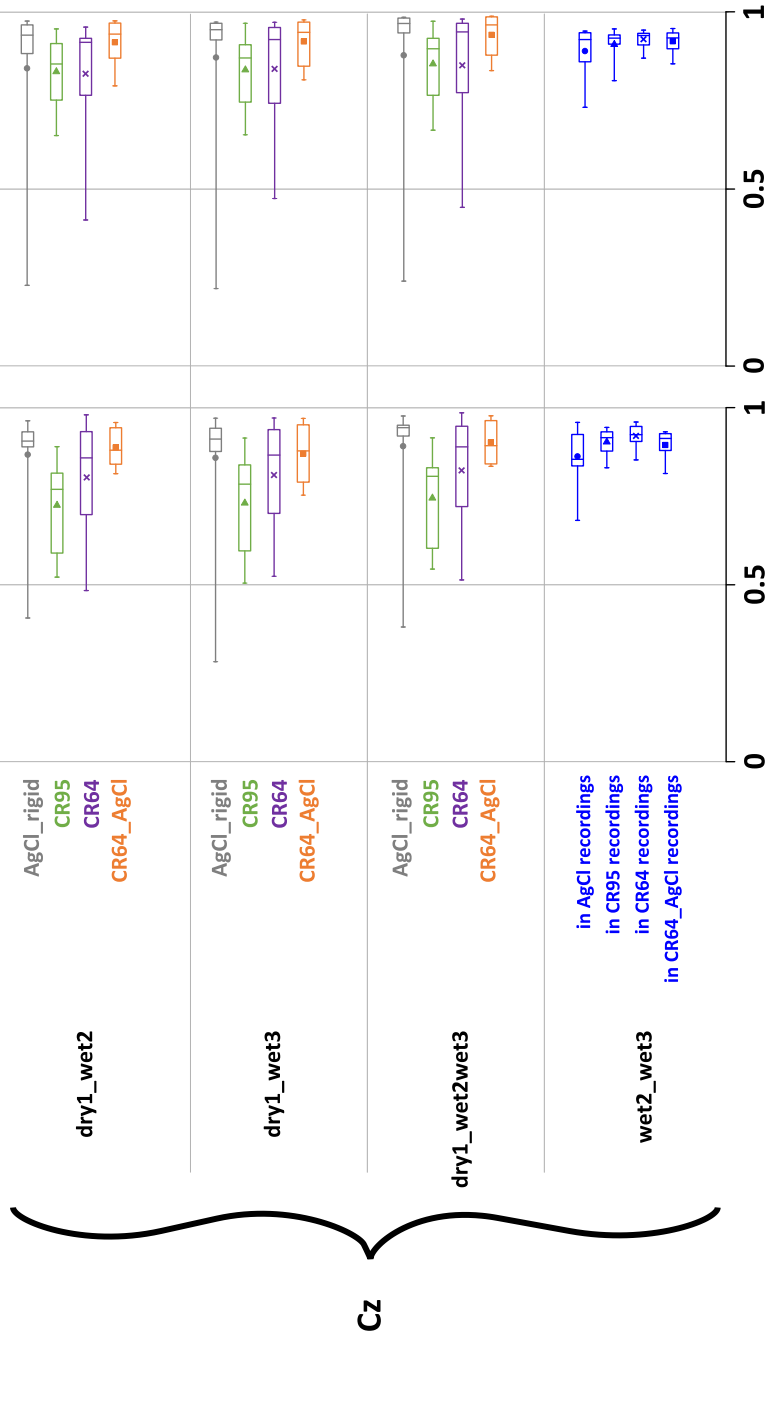

This figure continues on next page.

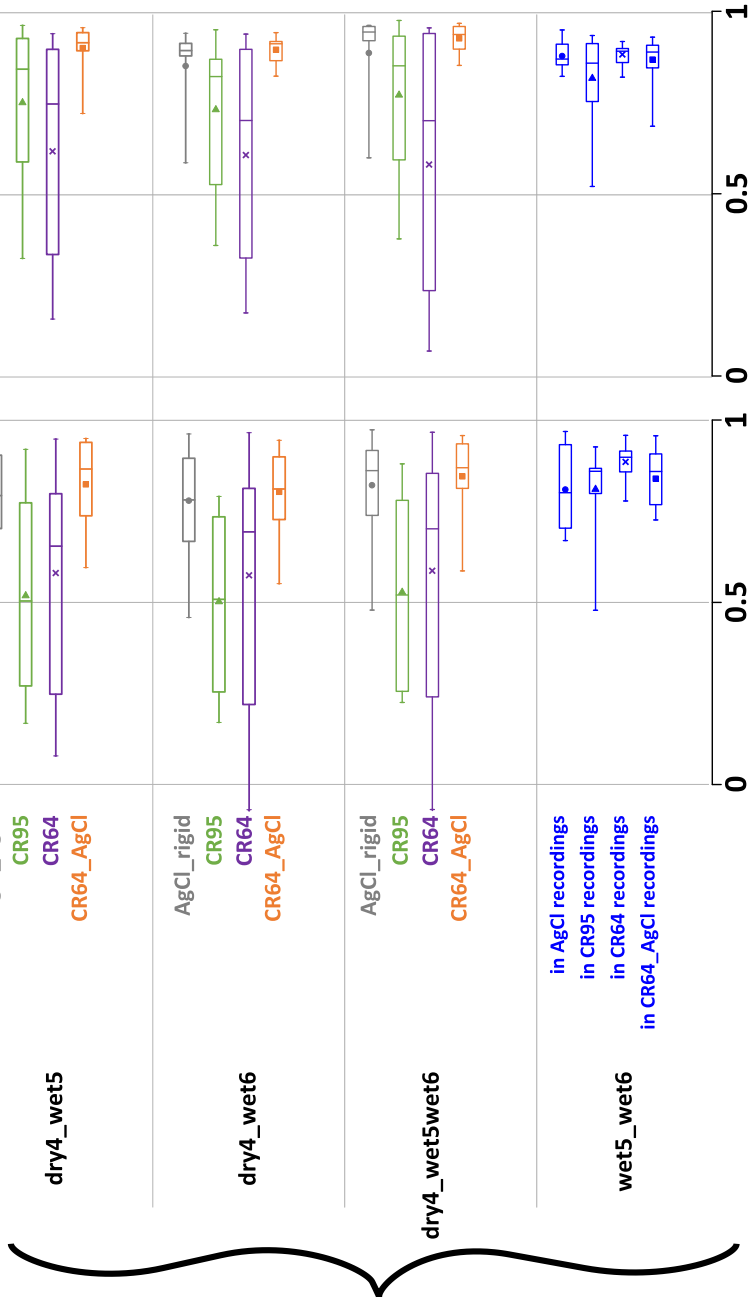

Figure App. 19: Correlation of EEG signals of a pair of electrodes when subjects opened and closed their eyes.

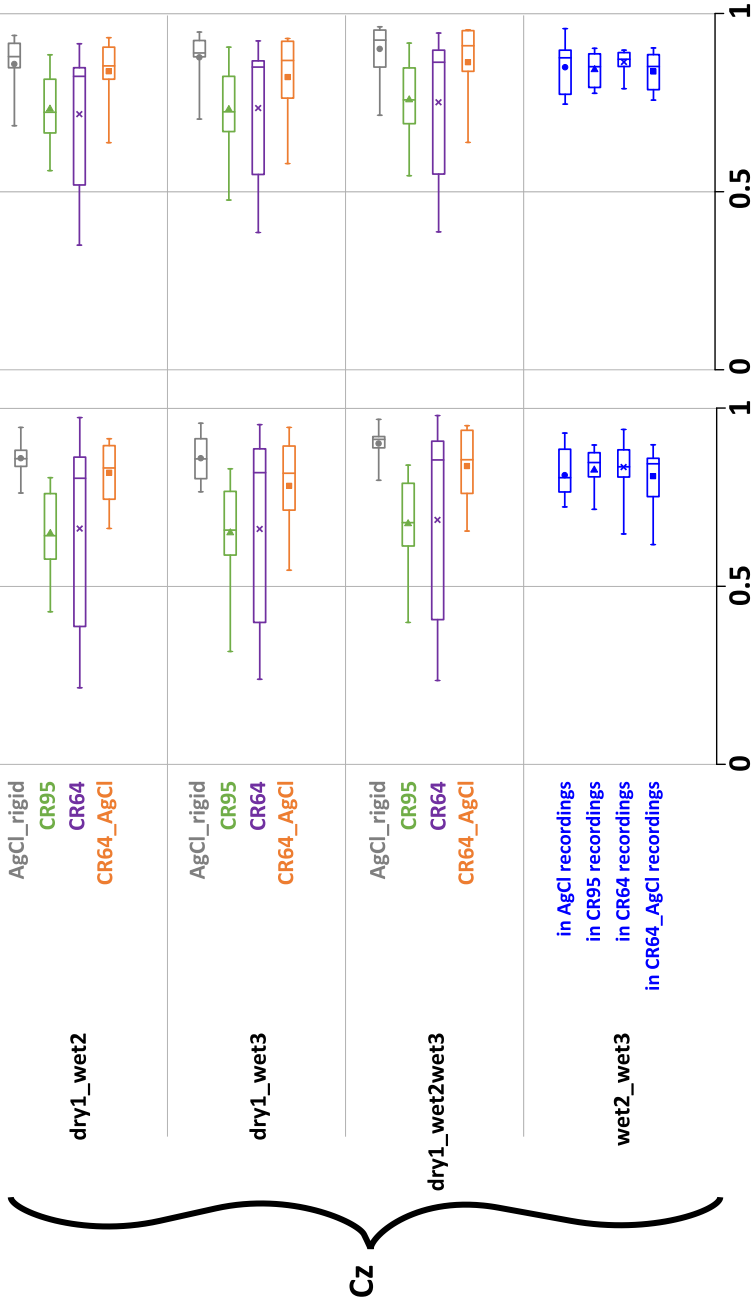

This figure continues on next page.

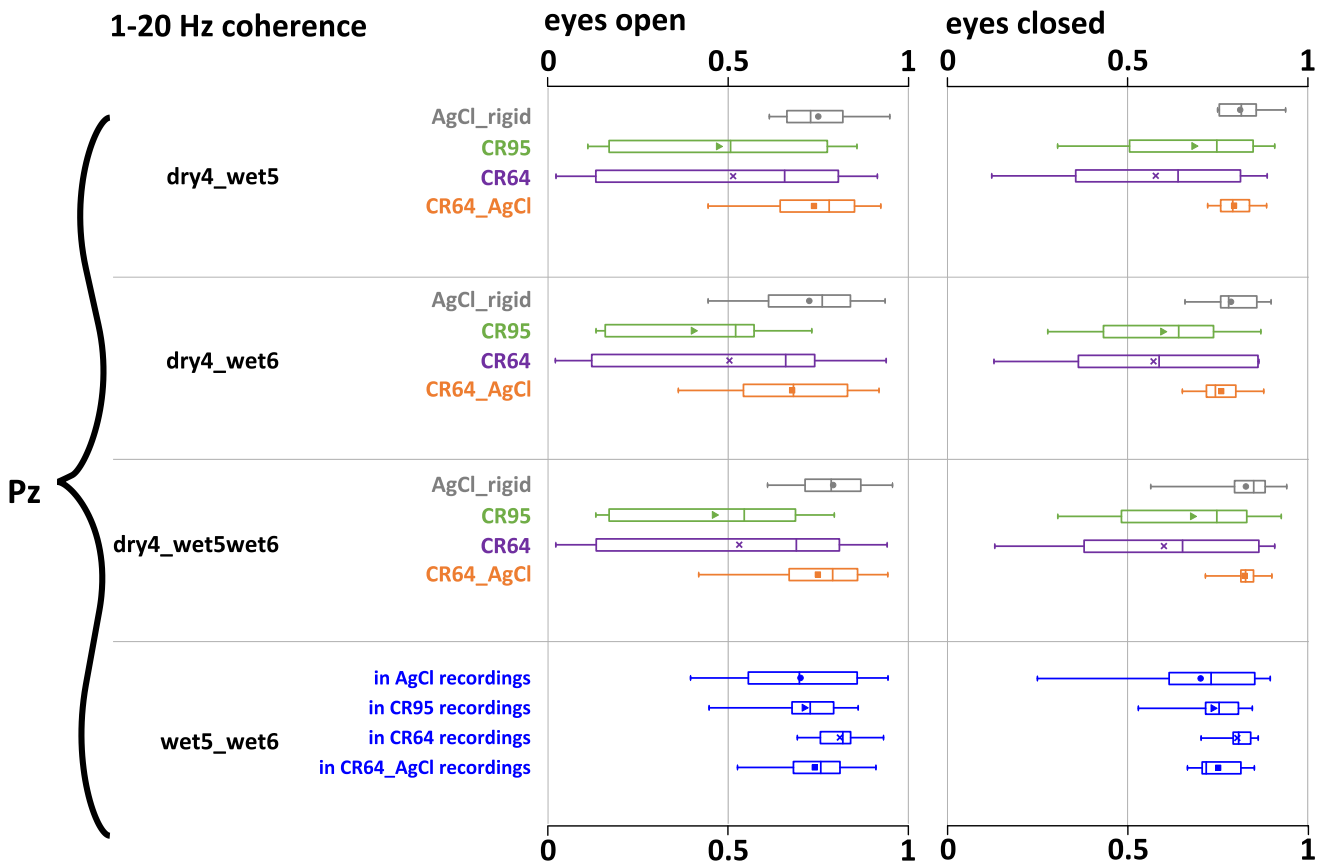

Figure App. 20: Coherence of EEG signals at frequency range of 1-20 Hz, also called overall coherence. The compared signals are acquired by a pair of electrodes when subjects opened and closed their eyes.

When comparing various types of dry electrodes, the signals of CR64 and CR95 correlated the least with the signals of their adjacent wet electrodes. Besides, the variation in the correlation between these two types of dry electrode and wet electrode is the biggest. Signals acquired by CR64_AgCl and their adjacent wet electrode show a high correlation. In addition, the variation in value is small. The correlation of the recorded signals increases when the eyes of the subjects are closed. This is because strong amplitude alpha waves dominate the EEG signals when the eyes are closed. As long as both dry and wet electrodes are capable of recording these strong amplitude alpha waves, the correlation of their signals is high. In contrast, there is no dominant signal when the eyes are open. If the signal of dry electrodes is disturbed by noise, the correlation between the signals recorded by dry and wet electrodes decreases.

(7) *Coherence of 1-20 Hz and* (8) *Coherence of 8-13 Hz*

Data analysis

> The coherence of the signals recorded by a pair of electrodes is calculated using the parameters introduced in section 5.3.5. Both 1-20 Hz coherence and 8-13 Hz coherence are analyzed. The labels used in this session are the same as those in the 'correlation' session.

Figure App. 20 shows the coherence between a pair of dry and wet electrodes on the one hand and a pair of wet electrodes on the other when the eyes of subjects are open and closed. The results are very similar to the value of correlation. The signals recorded at the Pz location show lower coherence. The coherence of signals recorded by polymer dry electrodes (CR64 and CR95) and their adjacent wet electrodes is low. Besides, the value varies over a wide range. The coherence of signals recorded by CR64_AgCl and its adjacent wet electrodes is the highest among all types of dry electrodes.

Low correlation and coherence of CR64 and wet electrodes are due to the low frequency signals picked up by the CR64 electrodes. These low frequency signals can be easily identified by observing the raw EEG signals recorded by CR64 and their PSD, as shown in Figure 5.41.

When investigating the recordings of eyes-closed sessions, 8-13 Hz coherence is calculated and shown in Figure App. 21. The coherence values of all types of electrodes are higher compared to that of the overall coherence. This proves again that the interferences are signals distributed in a frequency range outside of 8-13 Hz. It is found that the alpha coherence of CR64_AgCl is higher than that of their adjacent wet electrodes. One possible explanation is that the vertical distance between wet and dry electrodes is closer than that between two wet electrodes. This is because the alpha waves are generated from the occipital region of the brain and the intensity of alpha waves decreases along with distance to the occipital region. The order from the furthest to the closest vertical distance of electrodes at the Pz location to the occipital region is wet5, dry4 and then wet6. Therefore, the intensity of alpha waves picked up by wet5 and wet6 shows a larger variation than that picked up by dry4 and wet5 or dry4 and wet6.

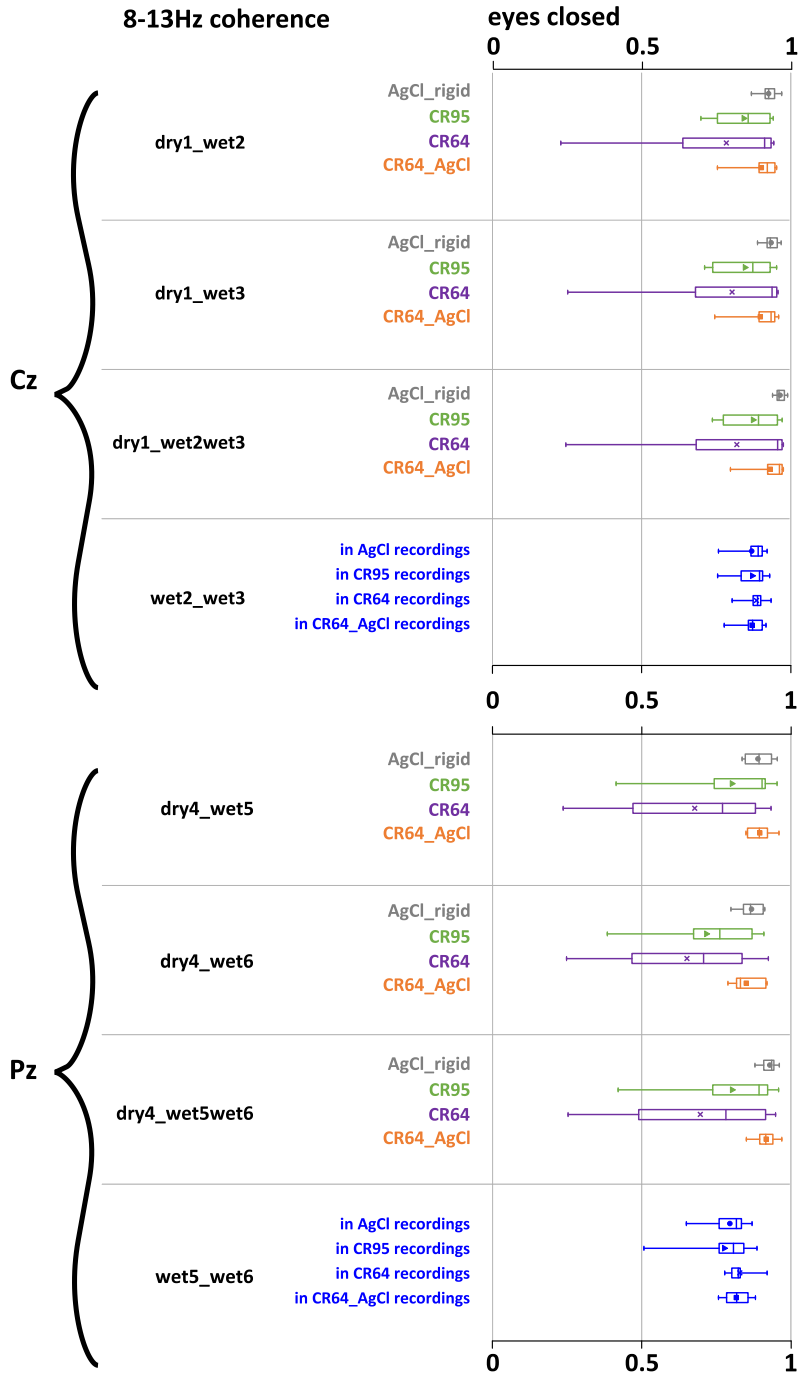

Figure App. 21: Coherence of EEG signals at frequency range of 8-13 Hz. The compared signals were acquired by a pair of electrodes when subjects closed their eyes.

Possibility of using PSD of 50 Hz signals and correlation coefficient of the signals to eliminate motion artifacts in the signals

It has been proven that motion artifacts, which resulted from skin deformation and electrode movements in the recorded signals, correlate with the impedance of the electrode/skin interface [198]. Adaptive filtering methods are established to eliminate these artifacts in the recorded signals based on the magnitude of the impedance [190, 199]. If the PSD of 50 Hz signals and the correlation coefficient of the signals are also correlated with the magnitude of impedance, these parameters could be applied in the algorithms for motion artifact reduction as well.

(9) *Correlation of magnitude of impedance and the PSD of 50 Hz signals*

The correlation between the magnitude of impedance and power spectrum of 50 Hz signals is analyzed by means of four approaches.

(i) Signals recorded in EO, EC and SS sessions using dry1 (Cz) and dry4 (Pz) electrodes on individual subjects:

One example of this correlation analysis is that the correlation coefficient for applying CR95 electrodes on subject 3 indicates the correlation between the six impedance values and the six PSD values shown in Table App. 3. All other values shown in Table App. 4 are computed using the corresponding impedance data and PSD data.

A positive correlation can be found when using CR64 electrodes on almost all subjects. This suggests that when applying CR64 electrodes, the individual electrode's magnitude of impedance can be used to estimate the PSD of its 50 Hz signals. No consistent correlation is found when using other types of electrodes.

Recording session	electrode	Impedance magnitude (ohm)	PSD of 50 Hz signals (uV^2/Hz)
EO	dry1	4.57E+05	159.72
	dry4	1.56E+05	0.66
EC	dry1	4.69E+05	140.72
	dry4	1.03E+05	0.43
SS	dry1	4.65E+05	146.07
	dry4	9.84E+04	0.44

Table App. 3: The data used to calculate the correlation coefficient when using CR95 electrodes at both Cz and Pz locations on subject 3.

	S3	S4	S5	S6	S7	S8	S9	S10	S11	S12	S13
AgCl_rigid	0.90	0.01	0.99	-0.65	-0.40	0.32	0.98	0.98	-0.73	0.96	1.00
CR95	0.99	0.92	0.99	-0.79	1.00	-0.83	-0.88	0.81	1.00	-0.83	0.99
CR64	0.99	-0.57	1.00	0.97	1.00	0.87	0.98	0.96	0.73	0.71	0.94
CR64_AgCl	0.99	-0.55	0.94	-0.90	-0.90	-0.70	1.00	-0.81	-0.08	0.26	0.97

Table App. 4: Correlation coefficients of the electrodes' magnitude of impedance and the PSD of its 50 Hz signals.

(ii) Signals recorded in EO, EC and SS sessions using dry1 (Cz) electrodes on individual subjects:

One example of this analysis is that the correlation coefficient of subject 3 when using the CR95 electrode indicates a correlation between the three impedance values and three PSD values shown in Table App. 5. All other values shown in Table App. 6 are computed using the corresponding impedance data and PSD data.

When applying CR95 electrodes at the Cz location, a positive correlation can be found between the magnitude of impedance and the PSD of 50 Hz signals.

Recording session	electrode	Impedance magnitude (ohm)	PSD of 50 Hz signals (uV^2/Hz)
EO	dry1	4.57E+05	159.72
EC	dry1	4.69E+05	140.72
SS	dry1	4.65E+05	146.07

Table App. 5: The data used to calculate the correlation coefficient when using CR95 electrodes at the Cz location on subject 3.

	S3	S4	S5	S6	S7	S8	S9	S10	S11	S12	S13
AgCl_rigid	-1.00	0.84	-0.94	NaN	0.10	1.00	-0.96	-0.97	-0.92	-0.69	-0.72
CR95	-1.00*	0.94	0.98	0.95	0.96	0.89	0.97	0.99	0.99	1.00*	0.99
CR64	0.95	-0.44	-1.00*	-0.31	0.96	0.98	1.00	-0.79	-0.36	-0.93	0.98
CR64_AgCl	0.31	-0.60	0.99	0.75	0.90	-0.70	-1.00*	-0.55	0.87	0.16	0.76

Table App. 6: Correlation coefficients of the electrodes' magnitude of impedance and the PSD of its 50 Hz signals. The asterisk next to the number indicates that the p-value of the magnitude of impedance and the power spectrum of 50 Hz signals is smaller than 0.05.

(iii) Signals recorded in EO, EC and SS sessions using dry4 (Pz) electrodes on individual subjects:

One example of this analysis is that the correlation coefficient of subject 3 (when using the CR95 electrode) indicates a correlation of the three impedance values and three power spectrum values, as shown in Table App. 7. All other values shown in Table App. 8 are computed using the corresponding impedance data and PSD data.

When applying CR95 or CR64 at the Pz location, positive correlations between the magnitude of impedance and the PSD of 50 Hz signals are found. This indicates that when the impedance decreases with time (highest impedance during the EO recording and lowest impedance during the SS recording), the PSD of 50 Hz signals also decreases.

Recording session	electrode	Impedance magnitude (ohm)	PSD of 50 Hz signals (uV^2/Hz)
EO	dry4	1.56E+05	0.66
EC	dry4	1.03E+05	0.43
SS	dry4	9.84E+04	0.44

Table App. 7: The data used to calculate the correlation coefficient when using CR95 electrodes at the Pz location on subject 3.

	S3	S4	S5	S6	S7	S8	S9	S10	S11	S12	S13
AgCl_rigid	-0.59	0.99	0.93	-0.65	0.03	-1.00	0.11	0.44	-0.15	0.58	0.97
CR95	0.99	1.00*	0.99	0.88	0.92	0.95	0.96	0.98	0.96	0.99	0.99
CR64	1.00*	0.92	0.98	1.00	0.83	0.75	1.00*	-0.69	0.40	0.42	0.97
CR64_AgCl	0.99	-0.70	1.00*	0.33	-0.40	NA	0.93	0.43	0.15	-0.48	0.89

Table App. 8: Correlation coefficients of the electrodes' magnitude of impedance and the PSD of its 50 Hz signals. The asterisk next to the number indicates that the p-value of the magnitude of impedance and the power spectrum of 50 Hz signals is smaller than 0.05. The negative correlation of CR64 on S10 results from the saturated impedance values.

(iv) Average data recorded in EO, EC and SS sessions using both dry1 and dry4 electrodes between subjects:

In Table App. 9, an example of the average impedance's correlation coefficient of EO, EC and SS sessions and the PSD of 50 Hz signals when using CR64_AgCl electrodes at the Pz location on all subjects is calculated. The values in Table App. 10 are computed using the corresponding data, as introduced in the example.

A high positive correlation is only found when using CR64_AgCl electrodes at the Pz location. This implies that the magnitude of impedance of the electrode/skin could not be used to estimate the PSD of 50 Hz signals recorded by that electrode among subjects. This is because the interference of 50 Hz signals from the environment is not constant in all the recordings on different subjects.

	S3	S4	S5	S6	S7	S8	S9	S10	S11	S12	S13
Average Impedance at Pz (kohm)	737.67	73.47	447.67	49.40	108.00	NA	1072.67	50.03	127.00	61.73	267.33
Average PSD of 50Hz signals (uV^2/Hz)	11.54	1.60	5.09	0.44	0.26	0.37	37.82	0.11	0.47	1.64	1.13

Table App. 9: The data used to calculate the correlation coefficient when using CR64_AgCl electrodes at the Pz location.

	Cz	Pz
AgCl_rigid	0.23	0.03
CR95	0.58	0.12
CR64	0.63*	0.57
CR64_AgCl	0.69*	0.92*

Table App. 10: The correlation coefficients of the magnitude of impedance and PSD of 50 Hz signals between subjects. The asterisk next to the number indicates that the p-value of the magnitude of impedance and the power spectrum of 50 Hz signals is smaller than 0.05.

(10) *Correlation of impedance mismatch and correlation coefficient of two adjacent electrodes*

Most recording amplifiers reject common interferences (e.g. the 50 Hz power line interferences) from the two input signals. If the interferences contained in those two signals

are not exactly the same (e.g. different amplitudes), only part of the common interferences is cancelled, resulting in interferences remaining in the recorded signals. The impedance mismatch between the dry electrodes and reference electrode is one of the reasons that the interferences still remain in the recorded signals. Since all the signals are recorded with respect to the same reference electrodes, the influence of the two adjacent signal electrodes' impedance mismatch on the similarity of their signals is investigated. The correlation coefficient is close to -1 if and when a large impedance mismatch reduces the similarity of the signals. The impedance mismatch in this calculation means the absolute value of the impedance difference between a dry electrode and its adjacent wet electrodes. These results can be found in Table App. 11.

It is found that when applying CR64 electrodes among all subjects, the correlation coefficient of the signals correlates with the difference in impedance. This correlation can also be found in the data recorded using CR95 electrodes at the Pz location. In other words, the impedance mismatch between CR95 and CR64 on the one hand and wet electrodes on the other results in the waveform or phase differences in the recorded signals.

The magnitudes of impedance between two wet electrodes vary as well. The results of the same calculations carried out using data of two adjacent wet electrodes show no correlation. This is because the impedance variation between two wet electrodes is smaller than that between a dry and wet electrode. Moreover, the similar electrode/skin interface of the wet signal electrode and that of the wet reference electrode might acquire similar interferences, which can easily be rejected by the recording amplifier.

	Cz		Pz	
	dry1_gel2	**dry1_gel3**	**dry4_gel5**	**dry4_gel6**
AgCl_rigid	0.08	0.22	0.38	0.25
CR95	0.00	0.03	-0.64*	-0.51*
CR64	-0.82*	-0.81*	-0.83*	-0.79*
CR64_AgCl	-0.46	-0.31	-0.66	-0.41

Table App. 11: The correlation coefficients of the difference between the magnitudes of impedance and the correlation coefficients of a pair of electrodes. The asterisk next to the number indicates that the p-value of the impedance mismatch and the correlation coefficient of two adjacent electrodes is smaller than 0.05.

Appendix IV

Section 5.6 is mentioning the test protocol and the questionnaire used to evaluate the comfortability of each type of electrode after the EEG monitoring using imec's EEG recording system. The protocol consists of the following: AgCl_rigid, CR95 and CR64_AgCl were the first 3 types of electrodes placed on the scalp, but the order of them was randomized. The 4th type of electrode was CR64 and the 5th type of electrode was CR64_gylcerol. The participants were only informed regarding the number of the types of electrodes, they received no information about the location or order in which each type of electrode was placed. Hence the participants were evaluating the user comfort of each electrode without having any idea about the type of electrode they were evaluating.

According to your experiences, please grade the user comfort of each type of **electrode**.

Types of electrodes	User comfort					remarks
	1 Very uncomfortable	2	3 I can feel the pressure from electrodes, but I can bear it	4	5 Do not feel any uncomfortable	
1						
2						
3						
4						
5						

Other remarks (regarding the elastic bands, the setup):

Bibliography

[1] G. Buzsáki, C. A. Anastassiou, and C. Koch, "The origin of extracellular fields and currents — EEG, ECoG, LFP and spikes," *Nat Rev Neurosci,* vol. 13, no. 6, pp. 407-420, 06//print, 2012.

[2] T. Kirschstein, and R. Köhling, "What is the Source of the EEG?," *Clinical EEG and Neuroscience,* vol. 40, no. 3, pp. 146-149, 2009.

[3] F. L. da Silva, "EEG: Origin and Measurement," *EEG - fMRI: Physiological Basis, Technique, and Applications*, C. Mulert and L. Lemieux, eds., pp. 19-38, Berlin, Heidelberg: Springer Berlin Heidelberg, 2010.

[4] I. Khurana, "Cardiovascular system," *Textbook of medical physiology*, pp. 241-389: Elsevier, 2006.

[5] M. Lopez-Gordo, D. Sanchez-Morillo, and F. Valle, "Dry EEG Electrodes," *Sensors,* vol. 14, no. 7, pp. 12847-12870, 2014.

[6] J. G. Webster, and J. W. Clark, *Medical Instrumentation: Application and Design*: Wiley, 2008.

[7] E. J. Berbari, "Principles of electrocardiography," *The Biomedical Engineering Handbook*, pp. 13-1 - 13-10, 2000.

[8] H.-J. Yoo, and C. Van Hoof, *Bio-Medical CMOS ICs*, 1 ed.: Boston, MA : Springer US, 2011.

[9] B. B. Winter, and J. G. Webster, "Reductionl of Interference Due to Common Mode Voltage in Biopotential Amplifiers," *IEEE Transactions on Biomedical Engineering,* vol. BME-30, no. 1, pp. 58-62, 1983.

[10] A. C. Metting van Rijn, A. Peper, and C. A. Grimbergen, "High-quality recording of bioelectric events. Part 1. Interference reduction, theory and practice," *Med Biol Eng Comput,* vol. 28, no. 5, pp. 389-97, Sep, 1990.

[11] E. Huigen, *Noise in biopotential recording using surface electrodes*, University of Amsterdam, Section Medical Physics, 2000.

[12] M. R. Neuman, "Biopotential amplifiers," *Medical instrumentation: application and design*, pp. 316-318, 1998.

[13] R. F. Yazicioglu, C. V. Hoof, and R. Puers, *Biopotential Readout Circuits for Portable Acquisition Systems*: Springer Publishing Company, Incorporated, 2008.

[14] S. Patel, H. Park, P. Bonato, L. Chan, and M. Rodgers, “A review of wearable sensors and systems with application in rehabilitation,” *Journal of NeuroEngineering and Rehabilitation (JNER),* vol. 9, no. 1, pp. 21, 2012.

[15] M. Chan, D. Estève, J.-Y. Fourniols, C. Escriba, and E. Campo, “Smart wearable systems: Current status and future challenges,” *Artificial Intelligence in Medicine*, vol. 56, no. 3, pp. 137-156, 2012.

[16] P. van Mierlo, M. Papadopoulou, E. Carrette, P. Boon, S. Vandenberghe, K. Vonck, and D. Marinazzo, “Functional brain connectivity from EEG in epilepsy: Seizure prediction and epileptogenic focus localization,” *Prog Neurobiol,* vol. 121c, pp. 19-35, Oct, 2014.

[17] S. Sur, and V. K. Sinha, “Event-related potential: An overview,” *Industrial Psychiatry Journal,* vol. 18, no. 1, pp. 70-73, Jan-Jun, 2009.

[18] L. F. Nicolas-Alonso, and J. Gomez-Gil, “Brain Computer Interfaces, a Review,” *Sensors,* vol. 12, no. 2, pp. 1211-1279, 2012.

[19] S. Amiri, A. Rabbi, L. Azinfar, and R. Fazel-Rezai, "A Review of P300, SSVEP, and Hybrid P300/SSVEP Brain- Computer Interface Systems," *Brain-Computer Interface Systems - Recent Progress and Future Prospects*, 2013.

[20] T. von Zglinicki, M. Lindberg, G. M. Roomans, and B. Forslind, “Water and ion distribution profiles in human skin,” *Acta Derm Venereol,* vol. 73, no. 5, pp. 340-3, Oct, 1993.

[21] N. Meziane, J. G. Webster, M. Attari, and A. J. Nimunkar, “Dry electrodes for electrocardiography,” *Physiological Measurement,* vol. 34, no. 9, pp. R47-R69, Sep, 2013.

[22] Y. M. Chi, J. Tzyy-Ping, and G. Cauwenberghs, “Dry-Contact and Noncontact Biopotential Electrodes: Methodological Review,” *IEEE Reviews in Biomedical Engineering,* vol. 3, no. 1, pp. 106-119, Dec., 2010.

[23] J. S. Lee, J. Heo, W. K. Lee, Y. G. Lim, Y. H. Kim, and K. S. Park, “Flexible capacitive electrodes for minimizing motion artifacts in ambulatory electrocardiograms,” *Sensors (Basel),* vol. 14, no. 8, pp. 14732-43, 2014.

[24] J. Ottenbacher, and S. Heuer, "Motion artefacts in capacitively coupled ECG electrodes." pp. 1059-1062.

[25] J. M. Lee, F. Pearce, A. D. Hibbs, R. Matthews, and C. Morrissette, "Evaluation of a capacitively-coupled, non-contact (through clothing) electrode or ECG monitoring and life signs detection for the objective force warfighter," *Combat Casualty Care in Ground Based Tactical Situations: Trauma Technology and Emergency Medical Procedures*, DTIC Document, 2004, pp. 25-1 - 25-10.

[26] G. Ruffini, S. Dunne, L. Fuentemilla, C. Grau, E. Farres, J. Marco-Pallares, P. C. P. Watts, and S. R. P. Silva, “First human trials of a dry electrophysiology sensor using a carbon nanotube array interface,” *Sensors and Actuators A: Physical*, vol. 144, no. 2, pp. 275-279, 2008.

[27] L.-S. Hsu, S.-W. Tung, C.-H. Kuo, and Y.-J. Yang, “Developing Barbed Microtip-Based Electrode Arrays for Biopotential Measurement,” *Sensors*, vol. 14, no. 7, pp. 12370-12386, 2014.

[28] W. C. Ng, H. L. Seet, K. S. Lee, N. Ning, W. X. Tai, M. Sutedja, J. Y. H. Fuh, and X. P. Li, “Micro-spike EEG electrode and the vacuum-casting technology for mass production,” *Journal of Materials Processing Tech.*, vol. 209, no. 9, pp. 4434-4438, 2009.

[29] M. Arai, Y. Nishinaka, and N. Miki, “Electroencephalogram measurement using polymer-based dry microneedle electrode,” *Japanese Journal of Applied Physics*, vol. 54, no. 6S1, pp. 06FP14, 2015.

[30] T. C. Ferree, P. Luu, G. S. Russell, and D. M. Tucker, “Scalp electrode impedance, infection risk, and EEG data quality,” *Clinical Neurophysiology*, vol. 112, no. 3, pp. 536-544, 2001.

[31] T. Torfs, Y. H. Chen, H. Kim, and R. F. Yazicioglu, “Noncontact ECG recording system with real time capacitance measurement for motion artifact reduction,” *IEEE Trans Biomed Circuits Syst*, vol. 8, no. 5, pp. 617-25, Oct, 2014.

[32] "Emotiv User Maunal: Headset and software setup for your Emotiv EPOC neuroheadset," 05 AUG., 2015; https://emotiv.zendesk.com/hc/en-us/articles/201222455-Where-can-I-find-a-user-manual-.

[33] A. R. Mota, L. Duarte, D. Rodrigues, A. C. Martins, A. V. Machado, F. Vaz, P. Fiedler, J. Haueisen, J. M. Nóbrega, and C. Fonseca, “Development of a quasi-dry electrode for EEG recording,” *Sensors and Actuators A: Physical*, vol. 199, pp. 310-317, 9/1/, 2013.

[34] S. Radevski, H. Hata, and K. Matsumoto, "Real-time monitoring of neural state in assessing and improving software developers' productivity," *Proceedings of the Eighth International Workshop on Cooperative and Human Aspects of Software Engineering*, IEEE Press, 2015, pp. 93-96.

[35] P. Roy, S. Oh, P. Shyamkumar, M. Ramasamy, R. E. Harbaugh, and V. K. Varadan, “Nanotextile Bio-sensors for Mobile Wireless Wearable Health Monitoring of Neurological and Cardiovascular Disorders,” *Journal of ISSS*, vol. 3, no. 1, pp. 28-77, 2014.

[36] A. Fleury, M. Sugar, and T. Chau, “E-textiles in Clinical Rehabilitation: A Scoping Review,” *Electronics*, vol. 4, no. 1, pp. 173, 2015.

[37] P. Shyamkumar, P. Rai, S. Oh, M. Ramasamy, R. Harbaugh, and V. Varadan, "Wearable Wireless Cardiovascular Monitoring Using Textile-Based Nanosensor and Nanomaterial Systems," *Electronics*, vol. 3, no. 3, pp. 504-520, 2014.

[38] Z. Liu, and X. Liu, "Progress on Fabric Electrodes Used in Biological Signal Acquisition," *Journal of Minerals and Materials Characterization and Engineering*, vol. 3, no. 03, pp. 204, 2015.

[39] C. R. Merritt, "Electronic textile-based sensors and systems for long-term health monitoring," Electrical Engineering and Biomedical Engineering, North Carolina State University, Raleigh, North Carolina, 2008.

[40] B. Taji, S. Shirmohammadi, V. Groza, and M. Bolie, "An ECG monitoring system using conductive fabric," *Medical Measurements and Applications Proceedings (MeMeA), 2013 IEEE International Symposium*, IEEE, 2013, pp. 309-314.

[41] M. K. Yapici, T. Alkhidir, Y. A. Samad, and K. Liao, "Graphene-clad textile electrodes for electrocardiogram monitoring," *Sensors and Actuators B: Chemical*, 2015, pp. 1469-1474.

[42] G. Paul, R. Torah, S. Beeby, and J. Tudor, "The development of screen printed conductive networks on textiles for biopotential monitoring applications," *Sensors and Actuators A: Physical*, vol. 206, pp. 35-41, 2/1/, 2014.

[43] G. Paul, R. Torah, S. Beeby, and J. Tudor, "Novel active electrodes for ECG monitoring on woven textiles fabricated by screen and stencil printing," *Sensors and Actuators A: Physical*, vol. 221, no. 0, pp. 60-66, 1/1/, 2015.

[44] S. Nishimura, Y. Tomita, and T. Horiuchi, "Clinical application of an active electrode using an operational amplifier," *Biomedical Engineering, IEEE Transactions on*, vol. 39, no. 10, pp. 1096-1099, 1992.

[45] J. Löfhede, F. Seoane, and M. Thordstein, "Textile Electrodes for EEG Recording — A Pilot Study," *Sensors*, vol. 12, no. 12, pp. 16907, 2012.

[46] D.-H. Kim, N. Lu, R. Ma, Y.-S. Kim, R.-H. Kim, S. Wang, J. Wu, S. M. Won, H. Tao, and A. Islam, "Epidermal electronics," *Science*, vol. 333, no. 6044, pp. 838-843, 2011.

[47] J. J. Norton, D. S. Lee, J. W. Lee, W. Lee, O. Kwon, P. Won, S. Y. Jung, H. Cheng, J. W. Jeong, A. Akce, S. Umunna, I. Na, Y. H. Kwon, X. Q. Wang, Z. Liu, U. Paik, Y. Huang, T. Bretl, W. H. Yeo, and J. A. Rogers, "Soft, curved electrode systems capable of integration on the auricle as a persistent brain-computer interface," *Proc Natl Acad Sci U S A*, vol. 112, no. 13, pp. 3920-5, Mar 31, 2015.

[48] S. M. Lee, H. J. Byeon, J. H. Lee, D. H. Baek, K. H. Lee, J. S. Hong, and S.-H. Lee, "Self-adhesive epidermal carbon nanotube electronics for tether-free long-term

continuous recording of biosignals," *Scientific Reports,* vol. 4, pp. 6074, 08/15/online, 2014.

[49] D. Ko, C. Lee, E.-J. Lee, S.-H. Lee, and K.-Y. Jung, "A dry and flexible electrode for continuous-EEG monitoring using silver balls based polydimethylsiloxane (PDMS)," *Biomedical Engineering Letters,* vol. 2, no. 1, pp. 18-23, 2012/03/01, 2012.

[50] P. Leleux, J.-M. Badier, J. Rivnay, C. Bénar, T. Hervé, P. Chauvel, and G. G. Malliaras, "Conducting Polymer Electrodes for Electroencephalography," *Advanced Healthcare Materials,* vol. 3, no. 4, pp. 490-493, 2014.

[51] J.-Y. Baek, J.-H. An, J.-M. Choi, K.-S. Park, and S.-H. Lee, "Flexible polymeric dry electrodes for the long-term monitoring of ECG," *Sensors and Actuators A: Physical,* vol. 143, no. 2, pp. 423-429, 5/16/, 2008.

[52] C.-Y. Chen, C.-L. Chang, T.-F. Chien, and C.-H. Luo, "Flexible PDMS electrode for one-point wearable wireless bio-potential acquisition," *Sensors and Actuators A: Physical,* vol. 203, pp. 20-28, 12/1/, 2013.

[53] L. Chin-Teng, L. Lun-De, L. Yu-Hang, I. J. Wang, L. Bor-Shyh, and C. Jyh-Yeong, "Novel Dry Polymer Foam Electrodes for Long-Term EEG Measurement," *Biomedical Engineering, IEEE Transactions on,* vol. 58, no. 5, pp. 1200-1207, 2011.

[54] J. H. Lee, S. M. Lee, H. J. Byeon, J. S. Hong, K. S. Park, and S.-H. Lee, "CNT/PDMS-based canal-typed ear electrodes for inconspicuous EEG recording," *Journal of Neural Engineering,* vol. 11, no. 4, pp. 046014, 2014.

[55] P. Salvo, R. Raedt, E. Carrette, D. Schaubroeck, J. Vanfleteren, and L. Cardon, "A 3D printed dry electrode for ECG/EEG recording," *Sensors and Actuators A: Physical,* vol. 174, pp. 96-102, 2012.

[56] P. Fiedler, J. Haueisen, D. Jannek, S. Griebel, L. Zentner, F. Vaz, and C. Fonseca, "Comparison of three types of dry electrodes for electroencephalography," *Acta Imeko,* vol. 3, no. 3, pp. 33-37, 2014.

[57] P. Fiedler, P. Pedrosa, S. Griebel, C. Fonseca, F. Vaz, E. Supriyanto, F. Zanow, and J. Haueisen, "Novel Multipin Electrode Cap System for Dry Electroencephalography," *Brain Topography,* pp. 1-10, 2015/05/22, 2015.

[58] C. Grozea, C. D. Voinescu, and S. Fazli, "Bristle-sensors--low-cost flexible passive dry EEG electrodes for neurofeedback and BCI applications," *J Neural Eng,* vol. 8, no. 2, pp. 025008, Apr, 2011.

[59] L.-D. Liao, I. J. Wang, S.-F. Chen, J.-Y. Chang, and C.-T. Lin, "Design, Fabrication and Experimental Validation of a Novel Dry-Contact Sensor for Measuring Electroencephalography Signals without Skin Preparation," *Sensors,* vol. 11, no. 6, pp. 5819-5834, Jun, 2011.

[60] W. D. Hairston, K. W. Whitaker, A. J. Ries, J. M. Vettel, J. C. Bradford, S. E. Kerick, and K. McDowell, "Usability of four commercially-oriented EEG systems," *Journal of neural engineering*, vol. 11, no. 4, pp. 46018-46018, 2014.

[61] Y.-H. Yu, S.-W. Lu, L.-D. Liao, and C.-T. Lin, "Design, Fabrication, and Experimental Validation of Novel Flexible Silicon-Based Dry Sensors for Electroencephalography Signal Measurements," *Translational Engineering in Health and Medicine, IEEE Journal of*, vol. 2, 2014.

[62] M. Di Rienzo, V. Racca, F. Rizzo, B. Bordoni, G. Parati, P. Castiglioni, P. Meriggi, and M. Ferratini, "Evaluation of a textile-based wearable system for the electrocardiogram monitoring in cardiac patients," *Europace*, vol. 15, no. 4, pp. 607-612, 2013-04-01, 2013.

[63] "Comparison of consumer brain–computer interfaces," Aug. 12, 2015; https://en.wikipedia.org/wiki/Comparison_of_consumer_brain%E2%80%93computer_interfaces.

[64] L. Mayaud, M. Congedo, A. Van Laghenhove, D. Orlikowski, M. Figère, E. Azabou, and F. Cheliout-Heraut, "A comparison of recording modalities of P300 event-related potentials (ERP) for brain-computer interface (BCI) paradigm," *Neurophysiologie Clinique/Clinical Neurophysiology*, vol. 43, no. 4, pp. 217-227, 10//, 2013.

[65] M. Duvinage, T. Castermans, M. Petieau, T. Hoellinger, G. Cheron, and T. Dutoit, "Performance of the Emotiv Epoc headset for P300-based applications," *Biomed Eng Online*, vol. 12, pp. 56, 2013.

[66] C. Guger, G. Krausz, B. Z. Allison, and G. Edlinger, "Comparison of dry and gel based electrodes for P300 brain–computer interfaces," *Frontiers in neuroscience*, vol. 6, pp. 60, 2012.

[67] F. Nijboer, B. van de Laar, S. Gerritsen, A. Nijholt, and M. Poel, "Usability of Three Electroencephalogram Headsets for Brain–Computer Interfaces: A Within Subject Comparison," *Interacting with Computers*, pp. iwv023, 2015.

[68] K. McDowell, C.-T. Lin, K. S. Oie, T.-P. Jung, S. Gordon, K. W. Whitaker, S.-Y. Li, S.-W. Lu, and W. D. Hairston, "Real- World Neuroimaging Technologies," *Access, IEEE*, vol. 1, pp. 131-149, 2013.

[69] P. Reis, F. Hebenstreit, F. Gabsteiger, V. von Tscharner, and M. Lochmann, "Methodological aspects of EEG and Body dynamics measurements during motion," *Frontiers in Human Neuroscience*, vol. 8, no. 156, pp. 1-19, 2014-March-24, 2014.

[70] P. Reis, "Questions regarding paper titled 'Methodological aspects of EEG and body dynamics measurements during motion'," Y.-H. Chen, ed., 2016.

[71] D. Callan, G. Durantin, and C. Terzibas, “Classification of Single-Trial Auditory Events Using Dry-Wireless EEG During Real and Motion Simulated Flight,” *Frontiers in Systems Neuroscience*, vol. 9, no. 11, 2015-February-17, 2015.

[72] D. Collado-Mateo, J. C. Adsuar, P. R. Olivares, R. Cano-Plasencia, and N. Gusi, “Using a dry electrode EEG device during balance tasks in healthy young-adult males: Test–retest reliability analysis,” *Somatosensory & Motor Research*, vol. 32, no. 4, pp. 219-226, 2015/10/02, 2015.

[73] T. S. Grummett, R. E. Leibbrandt, T. W. Lewis, D. DeLosAngeles, D. M. W. Powers, J. O. Willoughby, K. J. Pope, and S. P. Fitzgibbon, “Measurement of neural signals from inexpensive, wireless and dry EEG systems,” *Physiological Measurement*, vol. 36, no. 7, pp. 1469, 2015.

[74] H. F. Posada-Quintero, B. A. Reyes, K. Burnham, J. Pennace, and K. H. Chon, “Low Impedance Carbon Adhesive Electrodes with Long Shelf Life,” *Annals of Biomedical Engineering*, vol. 43, no. 10, pp. 2374-2382, 2015.

[75] T. Shigemitsu, T. Nagata, G. Matsumoto, and S. Tsukahara, “Electrical properties of the carbon fibre electrode and its application,” *Medical and Biological Engineering and Computing*, vol. 18, no. 3, pp. 359-362, 1980/05/01, 1980.

[76] C. J. De Luca, R. S. Le Fever, and F. B. Stulen, “Pasteless electrode for clinical use,” *Medical and Biological Engineering and Computing*, vol. 17, no. 3, pp. 387-390, 1979/05/01, 1979.

[77] N. Meziane, S. Yang, M. Shokoueinejad, J. G. Webster, M. Attari, and H. Eren, “Simultaneous comparison of 1 gel with 4 dry electrode types for electrocardiography,” *Physiological Measurement*, vol. 36, no. 3, pp. 513-529, 2015.

[78] L. Rattfält, “Smartware electrodes for ECG measurements: Design, evaluation and signal processing,” Department of Biomedical Engineering, Linköping University, Linköping, 2013.

[79] K. Awara, R. Kitai, M. Isozaki, H. Neishi, K. Kikuta, N. Fushisato, and A. Kawamoto, “Thin-film electroencephalographic electrodes using multi-walled carbon nanotubes are effective for neurosurgery,” *Biomed Eng Online*, vol. 13, pp. 166, 2014.

[80] E. Huigen, A. Peper, and C. A. Grimbergen, “Investigation into the origin of the noise of surface electrodes,” *Medical and Biological Engineering and Computing*, vol. 40, no. 3, pp. 332-338, 2002/05/01, 2002.

[81] M. R. Neuman, "Biopotential Electrodes," *Medical Instrumentation: Application and Design*, J. G. Webster, ed., pp. 189-240, United States of America: John Wiley & Sons, 2008.

[82] E. McAdams, "Biomedical electrodes for biopotential monitoring and electrostimulation," *Bio-Medical CMOS ICs*, pp. 31-124: Springer, 2011.

[83] K. J. Vetter, *Electrochemical kinetics: theoretical aspects*: Elsevier, 2013.

[84] C. H. Hamann, A. Hamnett, and W. Vielstich, "Electrode Potentials and Double-Layer Structure at Phase Boundaries," *Electrochemistry*, pp. 77-155, Germany: Wiley-VCH, 2007.

[85] H. Von Helmholtz, "Studies of electric boundary layers," *Wied. Ann*, vol. 7, pp. 337-382, 1879.

[86] G. Gouy, "Sur la fonction électrocapillaire," *Ann. Phys.(Paris)*, vol. 7, no. 9, pp. 129-184, 1917.

[87] O. Stern, "Zur theorie der elektrolytischen doppelschicht," *Zeitschrift für Elektrochemie und angewandte physikalische Chemie*, vol. 30, no. 21-22, pp. 508-516, 1924.

[88] D. C. Grahame, "The electrical double layer and the theory of electrocapillarity," *Chemical reviews*, vol. 41, no. 3, pp. 441-501, 1947.

[89] J. M. Bockris, M. Devanathan, and K. Muller, "On the structure of charged interfaces," *Proceedings of the Royal Society of London A: Mathematical, Physical and Engineering Sciences*, 1356, The Royal Society, 1963, pp. 55-79.

[90] H. Wang, and L. Pilon, "Accurate Simulations of Electric Double Layer Capacitance of Ultramicroelectrodes," *The Journal of Physical Chemistry C*, vol. 115, no. 33, pp. 16711-16719, 2011/08/25, 2011.

[91] L. L. Zhang, and X. S. Zhao, "Carbon-based materials as supercapacitor electrodes," *Chemical Society Reviews*, vol. 38, no. 9, pp. 2520-2531, 2009.

[92] L. Pilon, H. Wang, and A. d'Entremont, "Recent Advances in Continuum Modeling of Interfacial and Transport Phenomena in Electric Double Layer Capacitors," *Journal of The Electrochemical Society*, vol. 162, no. 5, pp. A5158-A5178, 2015.

[93] S. Srinivasan, "Electrode/electrolyte interfaces: Structure and kinetics of charge transfer," *Fuel Cells*, pp. 27-92: Springer, 2006.

[94] J. O. M. Bockris, and A. K. N. Reddy, "The Basic Electrodic Equation: The Butler-Volmer Equation," *Modern electrochemistry*, pp. 862-909, United States of America: Plenum Publishing Coporation, 1970.

[95] A. J. Bard, L. R. Faulkner, J. Leddy, and C. G. Zoski, "Formal Potential," *Electrochemical methods: fundamentals and applications*, pp. 52-53: Wiley New York, 2001.

[96] J.-L. Burgot, "Activities and Activity Coefficients," *Ionic Equilibria in Analytical Chemistry*, pp. 37-48: Springer, 2012.

[97] G. J. Janz, and D. J. Ives, "Silver, silver chloride electrodes," *Annals of the New york Academy of Sciences*, vol. 148, no. 1, pp. 210-221, 1968.

[98] N. Sato, "Equilibrium Potential of Electrode Reactions," *Electrochemistry at metal and semiconductor electrodes*, pp. 206-210: Elsevier, 1998.

[99] W. Gao, Z. Li, and N. M. Sammes, "Ag-ion conductors," *An introduction to electronic materials for engineers*, pp. 383-384: World Scientific, 2011.

[100] H. Mehrer, "Ionic Crystals," *Diffusion in solids: fundamentals, methods, materials, diffusion-controlled processes*, pp. 468-469: Springer Science & Business Media, 2007.

[101] A. J. Bard, L. R. Faulkner, J. Leddy, and C. G. Zoski, "Electrochemical Potentials," *Electrochemical methods: fundamentals and applications*, pp. 61-62: Wiley New York, 2001.

[102] N. Sato, "Electric Double Layer at Solid/Aqueous Solution Interfaces," *Electrochemistry at metal and semiconductor electrodes*, pp. 127-132 Elsevier, 1998.

[103] P. Pedrosa, E. Alves, N. P. Barradas, P. Fiedler, J. Haueisen, F. Vaz, and C. Fonseca, "TiNx coated polycarbonate for bio-electrode applications," *Corrosion Science*, vol. 56, pp. 49-57, Mar, 2012.

[104] W. Feder, "Silver- silver chloride electrode as a nonpolarizable bioelectorde," *Journal of applied physiology*, vol. 18, no. 2, pp. 397-401, 1963.

[105] A. Baars. "IVIUM Soft maunal 2010 color," 23 Oct., 2015; http://www.ivium.nl/filez/documents/Manual_2010.pdf.

[106] O. G. Martinsen, and S. Grimnes, "Electrodics and AC Phenomena," *Bioimpedance and bioelectricity basics*, pp. 41-55: Academic press, 2011.

[107] H. Sohmyung, K. Chul, Y. M. Chi, A. Akinin, C. Maier, A. Ueno, and G. Cauwenberghs, "Integrated Circuits and Electrode Interfaces for Noninvasive Physiological Monitoring," *Biomedical Engineering, IEEE Transactions on*, vol. 61, no. 5, pp. 1522-1537, 2014.

[108] S. Grimnes, "Impedance measurement of individual skin surface electrodes," *Med Biol Eng Comput*, vol. 21, no. 6, pp. 750-5, Nov, 1983.

[109] L. A. Geddes, "Historical evolution of circuit models for the electrode-electrolyte interface," *Annals of Biomedical Engineering*, vol. 25, no. 1, pp. 1-14, 1997/01/01, 1997.

[110] L. Shen, V. X. Afonso, J. G. Webster, and W. J. Tompkins, “The electrode system in impedance-based ventilation measurement,” *Biomedical Engineering, IEEE Transactions on,* vol. 39, no. 11, pp. 1130-1141, 1992.

[111] F. Vanlerberghe, M. De Volder, M. Op de Beeck, J. Penders, D. Reynaerts, R. Puers, and C. Van Hoof, "2-scale topography dry electrode for biopotential measurements," *2011 33rd Annual International Conference of the IEEE Engineering in Medicine and Biology Society*, IEEE, 2011, pp. 1892-1895.

[112] A. A. Athawale, and A. M. Joshi, “Studies on electrically conductive composites of ethylene propylene diene monomer rubber and steel fibers,” *Journal of Applied Polymer Science,* vol. 120, no. 5, pp. 3036-3041, 2011.

[113] R. N. Rothon, "The use of fillers in polymers," *Particulate fillers for polymers*, pp. 21-23: iSmithers Rapra Publishing, 2001.

[114] D. Prutchi, and M. Norris, *Design and Development of Medical Electronic Instrumentation: A Practical Perspective of the Design, Construction, and Test of Medical Devices*: John Wiley & Sons, Inc., 2005.

[115] E. McAdams, "The Skin’s Parallel Resistance, RSP," *Bio-Medical CMOS ICs*, p. 58: Springer, 2011.

[116] P. Tallgren, S. Vanhatalo, K. Kaila, and J. Voipio, “Evaluation of commercially available electrodes and gels for recording of slow EEG potentials,” *Clinical Neurophysiology,* vol. 116, no. 4, pp. 799-806, Apr, 2005.

[117] T. Niederhauser, A. Haeberlin, T. Marisa, M. Jungo, J. Goette, M. Jacomet, R. Abacherli, and R. Vogel, “Electrodes for Long-Term Esophageal Electrocardiography,” *IEEE Transactions on Biomedical Engineering,* vol. 60, no. 9, pp. 2576-2584, 2013.

[118] J. Rosell, J. Colominas, P. Riu, R. Pallas-Areny, and J. G. Webster, “Skin impedance from 1 Hz to 1 MHz,” *IEEE Trans Biomed Eng,* vol. 35, no. 8, pp. 649 - 651, 1988.

[119] A. S. Berson, and H. V. Pipberger, “Skin-electrode impedance problems in electrocardiography,” *American Heart Journal,* vol. 76, no. 4, pp. 514-525, 1968.

[120] E. Alanen, J. Nuutinen, K. Nicklén, T. Lahtinen, and J. Mönkkönen, “Measurement of hydration in the stratum corneum with the MoistureMeter and comparison with the Corneometer,” *Skin Research and Technology,* vol. 10, no. 1, pp. 32-37, 2004.

[121] B. A. Taheri, R. T. Knight, and R. L. Smith, “A dry electrode for EEG recording,” *Electroencephalography and Clinical Neurophysiology,* vol. 90, no. 5, pp. 376-383, May, 1994.

[122] S. Björklund, T. Ruzgas, A. Nowacka, I. Dahi, D. Topgaard, E. Sparr, and J. Engblom, “Skin Membrane Electrical Impedance Properties under the Influence of

a Varying Water Gradient," *Biophysical Journal*, vol. 104, no. 12, pp. 2639-2650, 6/18/, 2013.

[123] R. R. Warner, M. C. Myers, and D. A. Taylor, "Electron Probe Analysis of Human Skin: Determination of the Water Concentration Profile," *Journal of Investigative Dermatology*, vol. 90, no. 2, pp. 218-224, 1988/02/01, 1988.

[124] J. W. Fluhr, R. Darlenski, and C. Surber, "Glycerol and the skin: holistic approach to its origin and functions," *British Journal of Dermatology*, vol. 159, no. 1, pp. 23-34, 2008.

[125] C. L. Silva, D. Topgaard, V. Kocherbitov, J. J. S. Sousa, A. A. C. C. Pais, and E. Sparr, "Stratum corneum hydration: Phase transformations and mobility in stratum corneum, extracted lipids and isolated corneocytes," *Biochimica et Biophysica Acta (BBA) - Biomembranes*, vol. 1768, no. 11, pp. 2647-2659, 11//, 2007.

[126] S. Bjorklund, J. M. Andersson, Q. D. Pham, A. Nowacka, D. Topgaard, and E. Sparr, "Stratum corneum molecular mobility in the presence of natural moisturizers," *Soft Matter*, vol. 10, no. 25, pp. 4535-46, Jul 7, 2014.

[127] J. Hadgraft, and M. E. Lane, "Transepidermal water loss and skin site: A hypothesis," *International Journal of Pharmaceutics*, vol. 373, no. 1–2, pp. 1-3, 5/21/, 2009.

[128] C. D. Oster. "Proper skin prep helps ensure ECG trace quality," 21 MAR, 2016; http://multimedia.3m.com/mws/media/358372O/proper-skin-prep-ecg-trace-quality-white-paper.pdf.

[129] "Improving ECG quality," 21 MAR, 2016; http://www.mysupplies.philips.com/Documents/lit/453564119681.pdf.

[130] F. Minow. "Minimizing impedances and using the right electrolyte gel saves time and makes research more effective," May 13, 2016; http://www.brainproducts.com/files/public/products/brochures_material/pr_articles/1303_ECG-Gel.pdf.

[131] O. G. Martinsen, and S. Grimnes, *Bioimpedance and bioelectricity basics*: Academic press, 2011.

[132] Z. B. Vosika, G. M. Lazovic, G. N. Misevic, and J. B. Simic-Krstic, "Fractional Calculus Model of Electrical Impedance Applied to Human Skin," *PLoS ONE*, vol. 8, no. 4, pp. e59483, 2013.

[133] J. P. Reilly, and H. Antoni, *Electrical stimulation and electropathology*: Cambridge University Press, 1992.

[134] S. J. Luck, *An introduction to the event-related potential technique*: MIT press, 2014.

[135] K. Vonck, "Disadvantage of sweat in EEG measurements," Y.-H. Chen, ed., 2016.

[136] R. Dozio, A. Baba, C. Assambo, and M. J. Burke, "Time Based Measurement of the Impedance of the Skin-Electrode Interface for Dry Electrode ECG Recording," *Engineering in Medicine and Biology Society, 2007. EMBS 2007. 29th Annual International Conference of the IEEE*, 2007, pp. 5001-5004.

[137] C. Assambo, and M. J. Burke, "Low-Frequency Response and the Skin-Electrode Interface in Dry-Electrode Electrocardiography," *Advances in Electrocardiograms - Methods and Analysis*, R. M. Millis, ed., pp. 23-52: InTech Open Access Publisher, 2012.

[138] S. Iskander-Rizk, "Dry Electrode-Skin Contact Impedance Evaluation for Reliable EEG Measurements ", Biomedical Engineering, Delft University of Technology Delft, 2013.

[139] "sebaceous gland: human skin cross section " 22 MAR, 2016; http://kids.britannica.com/comptons/art-120217.

[140] J. Jossinet, and E. McAdams, "Hydrogel Electrodes In Biosignal Recording," *Engineering in Medicine and Biology Society, 1990., Proceedings of the Twelfth Annual International Conference of the IEEE*, IEEE, 1990, pp. 1490-1491.

[141] J. Rösler, H. Harders, and M. Baeker, "Elasticity," *Mechanical behaviour of engineering materials: metals, ceramics, polymers, and composites*, pp. 31-62: Springer Science & Business Media, 2007.

[142] R. Brown, "Short Term Stress — Strain Properties," *Physical testing of rubber*, pp. 109-172: Springer US, 2006.

[143] "Rubber Hardness," 18 AUG., 2016; http://www.npl.co.uk/science-technology/mass-and-force/hardness/rubber-hardness.

[144] A. N. Gent, "On the relation between indentation hardness and Young's modulus," *Rubber Chemistry and Technology*, vol. 31, no. 4, pp. 896-906, 1958.

[145] "British Standard 903 Methods of testing vulcanised rubber Part 19 (1950) and Part A7 (1957)," 1950, 1957.

[146] B. Lautrup, "Hooke's law," *Physics of continuous matter : exotic and everyday phenomena in the macroscopic world*, pp. 125-134: CRC press, 2011.

[147] M. C. Boyce, and E. M. Arruda, "Constitutive models of rubber elasticity: a review," *Rubber chemistry and technology*, vol. 73, no. 3, pp. 504-523, 2000.

[148] W. C. Oliver, and G. M. Pharr, "Measurement of hardness and elastic modulus by instrumented indentation: Advances in understanding and refinements to methodology," *Journal of materials research*, vol. 19, no. 01, pp. 3-20, 2004.

[149] A. C. Fischer-Cripps, "Contact Mechanics," *Nanoindentation*, pp. 1-20: Springer New York, 2011.

[150] K. Vanstreels, and A. M. Urbanowicz, "Nanoindentation study of thin plasma enhanced chemical vapor deposition SiCOH low-k films modified in He/H 2 downstream plasma," *Journal of Vacuum Science & Technology B: Microelectronics and Nanometer Structures*, vol. 28, no. 1, pp. 173-179, 2010.

[151] R. Brown, "Conditioning and Test Atmospheres," *Physical Testing of Rubber*, pp. 51-62: Springer US, 2006.

[152] V. M. Litvinov, R. A. Orza, M. Klüppel, M. van Duin, and P. C. M. M. Magusin, "Rubber–Filler Interactions and Network Structure in Relation to Stress–Strain Behavior of Vulcanized, Carbon Black Filled EPDM," *Macromolecules*, vol. 44, no. 12, pp. 4887-4900, 2011/06/28, 2011.

[153] V. M. Litvinov, and P. A. M. Steeman, "EPDM−Carbon Black Interactions and the Reinforcement Mechanisms, As Studied by Low-Resolution 1H NMR," *Macromolecules*, vol. 32, no. 25, pp. 8476-8490, 1999/12/01, 1999.

[154] P. Ghosh, and A. Chakrabarti, "Conducting carbon black filled EPDM vulcanizates: assessment of dependence of physical and mechanical properties and conducting character on variation of filler loading," *European Polymer Journal*, vol. 36, no. 5, pp. 1043-1054, 5/1/, 2000.

[155] H. Tan, and A. I. Isayev, "Comparative study of silica-, nanoclay- and carbon black-filled EPDM rubbers," *Journal of Applied Polymer Science*, vol. 109, no. 2, pp. 767-774, 2008.

[156] S. N. Lawandy, S. F. Halim, and N. A. Darwish, "Structure aggregation of carbon black in ethylene-propylene diene polymer," *Express Polymer Letters*, vol. 3, no. 3, pp. 152-158, 2009.

[157] S. He, Y. Lin, L. Chen, S. Cao, J. Lin, and X. Du, "Improvement in thermal conductivity and mechanical properties of ethylene-propylene-diene monomer rubber by expanded graphite," *Polymer Composites*, 2015.

[158] W. C. Lee, M. Zhang, and A. F. Mak, "Regional differences in pain threshold and tolerance of the transtibial residual limb: including the effects of age and interface material," *Archives of physical medicine and rehabilitation*, vol. 86, no. 4, pp. 641-649, 2005.

[159] S. Byström, C. Hall, T. Welander, and Å. Kilbom, "Clinical disorders and pressure-pain threshold of the forearm and hand among automobile assembly line workers," *Journal of Hand Surgery (British and European Volume)*, vol. 20, no. 6, pp. 782-790, 1995.

[160] N. Özkaya, M. Nordin, D. Goldsheyder, and D. Leger, "Mechanical Properties of Biological Tissues," *Fundamentals of Biomechanics*, pp. 221-236: Springer, 2012.

[161] J. Vincent, "Basic Elasticity and Viscoelasticity," *Structural Biomaterials*, pp. 1-28, 2012.

[162] L. Gargallo, and D. Radic, "Viscoelastic Behaviour of Polymers," *Physicochemical Behavior and Supramolecular Organization of Polymers*, pp. 43-162 Springer Science & Business Media, 2009.

[163] T. A. Osswald, "Mechanical Behavior of Polymers," *Understanding polymer processing: processes and governing equations*, pp. 29-54: Carl Hanser Verlag GmbH Co KG, 2015.

[164] R. Brown, "Creep, Relaxation and Set," *Physical testing of rubber*, pp. 200-213: Springer Science & Business Media, 2006.

[165] B. Song, and W. Chen, "One-Dimensional Dynamic Compressive Behavior of EPDM Rubber," *Journal of Engineering Materials and Technology,* vol. 125, no. 3, pp. 294-301, 2003.

[166] A. S. Khan, and O. Lopez-Pamies, "Time and temperature dependent response and relaxation of a soft polymer," *International Journal of Plasticity,* vol. 18, no. 10, pp. 1359-1372, 2002.

[167] J. C. Shaw, "Correlation and coherence analysis of the EEG: A selective tutorial review," *International Journal of Psychophysiology,* vol. 1, no. 3, pp. 255-266, 1984/03/01, 1984.

[168] M. A. Guevara, and M. Corsi-Cabrera, "EEG coherence or EEG correlation?," *International Journal of Psychophysiology,* vol. 23, no. 3, pp. 145-153, 10//, 1996.

[169] B. R. Eggins, "Skin contact electrodes for medical applications," *Analyst,* vol. 118, no. 4, pp. 439-442, 1993.

[170] N. Thakor, "Building Brain Machine Interfaces–Neuroprosthetic Control with Electrocorticographic Signals," *Newsletter,* vol. 2015, 2015.

[171] M. Jorfi, J. L. Skousen, C. Weder, and J. R. Capadona, "Progress towards biocompatible intracortical microelectrodes for neural interfacing applications," *Journal of Neural Engineering,* vol. 12, no. 1, pp. 011001, 2015.

[172] Y.-J. Huang, C.-Y. Wu, A. M. K. Wong, and B.-S. Lin, "Novel Active Comb-Shaped Dry Electrode for EEG Measurement in Hairy Site," *Biomedical Engineering, IEEE Transactions on,* vol. 62, no. 1, pp. 256-263, 2015.

[173] A. Searle, and L. Kirkup, "A direct comparison of wet, dry and insulating bioelectric recording electrodes," *Physiological Measurement*, vol. 21, no. 2, pp. 271-283, May, 2000.

[174] C. Fonseca, J. P. S. Cunha, R. E. Martins, V. M. Ferreira, J. P. M. de Sa, M. A. Barbosa, and A. M. da Silva, "A Novel Dry Active Electrode for EEG Recording," *Biomedical Engineering, IEEE Transactions on*, vol. 54, no. 1, pp. 162-165, 2007.

[175] J. R. Wolpaw, N. Birbaumer, D. J. McFarland, G. Pfurtscheller, and T. M. Vaughan, "Brain–computer interfaces for communication and control," *Clinical neurophysiology*, vol. 113, no. 6, pp. 767-791, 2002.

[176] "Active Electrode Building Guide," 07 11 2014, 2014; http://users.dcc.uchile.cl/~peortega/ae/.

[177] S. Patki, B. Grundlehner, A. Verwegen, S. Mitra, J. Xu, A. Matsumoto, R. F. Yazicioglu, and J. Penders, "Wireless EEG system with real time impedance monitoring and active electrodes," *Biomedical Circuits and Systems Conference (BioCAS), 2012 IEEE*, 2012, pp. 108-111.

[178] J. L. Blom, and M. Anneveldt, "An electrode cap tested," *Electroencephalography and Clinical Neurophysiology*, vol. 54, no. 5, pp. 591-594, 1982.

[179] M. Teplan, "Fundamentals of EEG measurement," *Measurement science review*, vol. 2, no. 2, pp. 1-11, 2002.

[180] "Headcaps of BIOSEMI," 30 Sep., 2015; http://www.biosemi.com/headcap.htm.

[181] "EEG cap of NR Sign Inc.," 30 Sep., 2015; http://www.nrsign.com/eeg/eeg-accessories/.

[182] W. J. Ray, and H. W. Cole, "EEG alpha activity reflects attentional demands, and beta activity reflects emotional and cognitive processes," *Science*, vol. 228, no. 4700, pp. 750-752, 1985.

[183] A. M. Tautan, W. Serdijn, V. Mihajlovic, B. Grundlehner, and J. Penders, "Framework for evaluating EEG signal quality of dry electrode recordings," *Biomedical Circuits and Systems Conference (BioCAS), 2013 IEEE*, 2013, pp. 186-189.

[184] D. J. Acunzo, G. MacKenzie, and M. C. W. van Rossum, "Systematic biases in early ERP and ERF components as a result of high-pass filtering," *Journal of Neuroscience Methods*, vol. 209, no. 1, pp. 212-218, Jul 30, 2012.

[185] W. Young. "Working with Cranky Op-Amps," 15 Dec., 2015; http://tangentsoft.net/audio/hs-opamp.html.

[186] "Proper Design Techniques Solve High-Speed Op-Amp Stability Problems," 15 Dec., 2015; http://electronicdesign.com/analog/proper-design-techniques-solve-high-speed-op-amp-stability-problems.

[187] A. Garcés Correa, L. Orosco, P. Diez, and E. Laciar, "Automatic detection of epileptic seizures in long-term EEG records," *Computers in Biology and Medicine*, vol. 57, pp. 66-73, 2/1/, 2015.

[188] "Guideline twelve: guidelines for long-term monitoring for epilepsy," *Journal of clinical neurophysiology: official publication of the American Electroencephalographic Society*, vol. 25, no. 3, pp. 170, 2008.

[189] A. B. Usakli, "Improvement of EEG signal acquisition: an electrical aspect for state of the art of front end," *Intell. Neuroscience*, vol. 2010, pp. 2-2, 2010.

[190] A. Bertrand, V. Mihajlovic, B. Grundlehner, C. Van Hoof, and M. Moonen, "Motion artifact reduction in EEG recordings using multi-channel contact impedance measurements," *Biomedical Circuits and Systems Conference (BioCAS), 2013 IEEE*, IEEE, 2013, pp. 258-261.

[191] A. Comert, and J. Hyttinen, "Impedance spectroscopy of changes in skin-electrode impedance induced by motion," *BioMedical Engineering OnLine*, vol. 13, no. 1, pp. 149, 2014.

[192] M. Kim, T. Kim, D. Kim, and W. Chung, "Curved Microneedle Array-Based sEMG Electrode for Robust Long-Term Measurements and High Selectivity," *Sensors*, vol. 15, no. 7, pp. 16265, 2015.

[193] J. R. Schofield, "Electrocardiogram Signal Quality Comparison Between A Dry Electrode and A Standard Wet Electrode over a Period of Extended Wear," Cleveland State University, 2012.

[194] W. J. Dunseath Jr., *Non-polarizable dry biomedical electrode*, United States 5003978,to Technology 21, Inc. (Durham, NC), 1991.

[195] W. C. Oliver, and G. M. Pharr, "An improved technique for determining hardness and elastic modulus using load and displacement sensing indentation experiments," *Journal of Materials Research*, vol. 7, no. 06, pp. 1564-1583, 1992.

[196] "Manual of The Nano Indenter XP " 18 AUG., 2016; http://www.msm.cam.ac.uk/mechtest/docs/XP%20User's%20Manual.pdf.

[197] F. PLUM, "Handbook of Electroencephalography and Clinical Neurophysiology," *Archives of Neurology*, vol. 26, no. 6, pp. 556-556, 1972.

[198] A. Cömert, "The Assessment and Reduction of Motion Artifact in Dry Contact Biopotential Electrodes," *Tampereen teknillinen yliopisto. Julkaisu-Tampere University of Technology. Publication; 1319*, 2015.

[199] D. Buxi, K. Sunyoung, N. van Helleputte, M. Altini, J. Wijsman, R. F. Yazicioglu, J. Penders, and C. Van Hoof, "Correlation Between Electrode-Tissue Impedance and Motion Artifact in Biopotential Recordings," *Sensors Journal, IEEE,* vol. 12, no. 12, pp. 3373-3383, 2012.

Curriculum vitae

Yun-Hsuan Chen was born in Taipei, Taiwan. She received her BSc. degree in material science and engineering from the National Tsing Hua University, Hsinchu, Taiwan in 2008. She then completed her MSc. degree following the Erasmus Mundus Master Course named "Molecular nano- and bio-photonics for telecommunications and biotechnologies (MONABIPHOT)" from Ecole Normale Supérieure de Cachan, Cachan, France, and Universidad Complutense de Madrid, Madrid, Spain, in 2011. Since 2011, she joined imec and worked towards her Ph.D degree at imec/KULeuven, Leuven, Belgium, under the guidance of Prof. Chris Van Hoof and Dr. Maaike Op de Beeck. Her research focuses on dry electrodes for high quality bio-potential measurements.

Scientific publications

Journal contributions

1. **Y. H. Chen**, M. Op de Beeck, L. Vanderheyden, E. Carrette, V. Mihajlovic, K. Vanstreels, B. Grundlehner, S. Gadeyne, P. Boon, and C. Van Hoof, "Soft, Comfortable Polymer Dry Electrodes for High Quality ECG and EEG Recording," *Sensors*, vol. 14, no. 12, pp. 23758-23780, Dec, 2014.

2. T. Torfs, **Y. H. Chen**, H. Kim, and R. F. Yazicioglu, "Noncontact ECG recording system with real time capacitance measurement for motion artifact reduction," *IEEE Trans Biomed Circuits Syst*, vol. 8, no. 5, pp. 617-25, Oct, 2014

Conference contributions

1. **Y. Chen**, M. Op de Beeck, L. Vanderheyden, E. Carrette, V. Mihajlovic, B. Grundlehner, S. Gadeyne, P. Boon, and C. Van Hoof, "Soft, Comfortable Polymer Dry Electrodes for high Quality ECG and EEG Recording," in *Proceedings of the 1st Int. Electron. Conf. Sens. Appl.*, 1–16 June 2014; Sciforum Electronic Conference Series, Vol. 1, 2014 , g014; doi:10.3390/ecsa-1-g014

   This paper received the best paper award of the conference.

2. **Y. H. Chen**, M. Op de Beeck, L. Vanderheyden, K. Vanstreels, H. Vandormael, and C. Van Hoof, "Soft conductive polymer dry electrodes for high-quality and comfortable ECG/EEG measurements," in *Advances in Science and Technology*, 2014, pp. 102-107

3. **Y.-H. Chen**, M. Op de Beeck, E. Carrette, L. Vanderheyden, B. Grundlehner, V. Mihajlovic, et al., "Polymer-based dry electrodes for high user comfort ECG/EEG measurements," in *Proceedings of Smart Systems Integration (SSI), 8, Vienna,* 2014, pp. 329-336.

4. **Y. H. Chen**, M. Op de Beeck, L. Vanderheyden, V. Mihajlovic, B. Grundlehner, and C. Van Hoof, "Comb-shaped polymer-based Dry electrodes for EEG/ECG measurements with high user comfort," in *Engineering in Medicine and Biology Society (EMBC), 35th Annual International Conference of the IEEE*, 2013, pp. 551-554

5. **Y.-H. Chen**, M. Op de Beeck, L. Vanderheyden, and C. Van Hoof, "Comparison of various polymer-based dry electrodes for high quality EEG/ECG measurements," in *Proceedings of Smart Systems Integration Conference (SSI), Amsterdam, the Netherlands*, 2013.

6. M. Op de Beeck, **Y.-H. Chen**, L. Vanderheyden, S. Gadeyne, E. Carrette, B. Bonte, S. Dehollander, K. Vonck, T. Vervust, A. Oostra, C. Van Hoof, and P. Boon, "Soft conductive polymer dry electrodes embedded in a comfortable headset for high-quality and user-friendly EEG measurements performed in a non-clinical setting," in *Biomedica*, Genk, 2015.

7. A.-M. Tautan, V. Mihajlovic, **Y.-H. Chen**, B. Grundlehner, J. Penders, and W. Serdijn, "Signal Quality in Dry Electrode EEG and the Relation to Skin-Electrode Contact Impedance Magnitude," in *Proceedings of the 7th International Conference on Biomedical Electronics and Devices, Angers, Loire Valley, France*, 2014, pp. 3-6.

FACULTY OF ENGINEERING SCIENCE
DEPARTMENT OF ELECTRICAL ENGINEERING
MICAS DIVISION
Kasteelpark Arenberg 10
B-3001 HEVERLEE, BELGIUM
Yun-Hsuan.Chen@imec.be